Edge Trimming of CFRP- Surface Roughness Measurement and Prediction

Author: Nicolas Duboust

September 2018

A thesis submitted in partial fulfilment of the requirements of a postgraduate degree

**The University of Sheffield
Faculty of Engineering
Department of Mechanical Engineering**

Thesis

Abstract

Use of carbon fibre composites has been increasing in the aerospace industry. However, there is still a need for finishing operations by conventional machining in the manufacturing of composite parts. Composites have a very different machinability to metals and can suffer from a number of surface defects during machining. The fibres are also highly abrasive and can cause rapid tool wear which in turn leads to increased likelihood of machining defects. This project has focussed on the machined surface quality developed during machining using new surface inspection techniques and additional surface roughness parameters. It is important to be able to accurately measure the surface roughness in order to ensure the integrity of in service components and quantify surface damage from machining. The aim of this project is to develop new numerical modelling techniques for the edge trimming of carbon fibre reinforced plastic (CFRP), and develop methods for the prediction of surface roughness. Different experimental techniques have been used to analyse post-machining damage, including scanning electron microscopy (SEM), computed tomography scanning (CT) and a focus variation system for measuring surface roughness. CFRP specimens have been edge trimmed using a poly crystalline diamond (PCD) cutting tool, and compared for different machining parameters, tool wear and material fibre orientations. Cutting forces were recorded and the surface quality was inspected using the optical focus variation method. Regression models from experimental data have been combined with finite element (FE) models to create a surface roughness prediction tool which includes the effects of tool wear. Areal surface roughness S_a measurements were taken using the optical system and the advantages of the system have been compared with conventional stylus roughness measurement methods. Experimental data was used to validate 3D and 2D FE milling models using MSC Marc. New FE models were developed using adaptive re-meshing, and user subroutine to control the cutting tool movement and simulation idle time. Progressive levels of tool wear have been implemented in the 2D model by using cutting edge

radius measurements from experiment. FE and experimental results show that tool wear and material fibre orientation have a significant effect on the cutting forces and surface roughness. Regression models showed that the surface roughness was most affected by tool wear, feed rate and cutting speed. A reasonable comparison has been found between FE and experiment and the FE models were capable of predicting the effects of tool wear due to cutting edge rounding. 3D models were found to better predict thrust forces than 2D FE model. The optical system was found to be useful technique for measuring surface roughness of machined fibrous composite surfaces and is more reliable than conventional roughness measurements. New strategies for roughness measurement have been recommended.

Confidentiality Statement

This work is protected by copyright and other intellectual property rights. The information in this document was created by the author at the University of Sheffield. The information in this document is proprietary and confidential to Rolls-Royce and is available to authorised recipients only – copying and onward distribution is prohibited other than for the purpose for which it was made available. This thesis should not be reproduced or extensively quoted without the expressed permission of the author.

This thesis has been reviewed by Rolls-Royce and some confidential information has been removed. The thesis will be published online with a 1 year embargo and an inspection of this work by third parties before the embargo period requires the expressed admission by the author and Rolls-Royce. Confidentiality of the information contained within the thesis should not be revealed as a result of the thesis examination until the thesis has become part of the public domain. Specific information on material lay-up, application and material sourcing has been removed from the thesis for confidentiality reasons.

Acknowledgements

Table of Contents

List of Figures

List of Tables

List of Nomenclature

E	Young's Modulus in each principle direction (Pa)
$E1_t$	Tensile modulus in principle fibre direction (Pa)
$E1_t$	Compressive modulus in principle fibre direction (Pa)
E_r	Edge Radius (µm)
F_r	Feed Rate (mm/min)
F_x	Feed force (N)
F_y	Thrust force (N)
G	Shear modulus (Pa)
P-value	Probability value. Statistical significance of null hypothesis.
R_a	Arithmetic Mean Roughness (µm)
RPM	Cutting Speed in (rev/min)
R-Sq	Coefficient of determination which describes the statistical significance of a parameter.
R-Sq (adj)	Adjusted coefficient of determination which describes the significance of a parameter and is adjusted for the number of predictor terms in the model.
S	Shear Strength (Pa)
S_a	Areal Arithmetic Mean Roughness (µm)
S-value	Residual standard error and is used to find the sample variance of each of the populations of data from the fitted regression line
υ	Poisson's ratio
X_t	Tensile failure strength in fibre principle direction (Pa)
X_c	Compressive failure strength in fibre principle direction (Pa)
Y_t	Tensile failure strength in fibre transverse principle direction (Pa)
Y_c	Compressive failure strength in fibre transverse principle direction (Pa)
ε	Strain in each principle direction
σ	Stress in each principle direction (Pa)

List of Abbreviations

CFRP   (Carbon Fibre Reinforced Plastic)

FRPs   (Fibre Reinforced Plastics)

PCD   (Poly Crystalline Diamond)

CVD   (Chemical Vapour Deposition)

CT   (Computed Tomography Scan)

SEM   (Scanning Electron Microscopy)

FE   (Finite Element)

FEM   (Finite Element Modelling)

FEA   (Finite Element Analysis)

CER   (Cutting Edge Rounding)

Chapter 1
Introduction

1.1 Engineering Context

Carbon fibre reinforced polymers (CFRPs) have high strength-weight properties and a great potential for weight saving and efficiency improvements in the aerospace industry. As well as weight saving, FRPs also have desirable properties including superior corrosion resistance, fatigue resistance and a high stiffness. As a result there has been a growing use of fibre composites in the aerospace industry in recent years and drive for development of manufacturing processes.

Although in industry near-net shape production of composite components is desirable, the conventional machining of composites such as drilling, milling and trimming is still often necessary for joining parts and finish machining. During machining, carbon fibres have been shown to be highly abrasive and can cause rapid cutting tool wear [1],[2]. Cutting tool wear can cause an increased prevalence of surface defects and can potentially lead to the damage of the machined workpiece, or a decrease in the material mechanical properties. In machining CFRP it has been shown that surface damage defects during machining can occur, including delamination, fibre pull-out, un-cut fibres, matrix cracking and matrix burning [3]. There has been shown to be a correlation between surface profile and mechanical performance [4]. The strength and fatigue life of in-service components in the aerospace industry is critical to component performance. Therefore understanding the surface topography and defects caused during machining is essential for manufacturing these components. In the aerospace industry there are tight tolerances and a strict control of surface damage caused during machining is a requirement for component manufacture. Also, in industry it is expensive and wasteful to scrap

damaged material from the manufacturing process and efforts should be made to avoid this.

Due to the increased usage of carbon fibre in industry there is a necessity to understand the fundamental aspects of FRP machining, chip mechanisms and the surface damage types caused during machining. It has been shown in the literature review that standard methods for measuring roughness using a stylus have a number of problems [5]. The accurate measurement of surface damage is important in machining and is an area which requires further research for composite surfaces. This project will assess defects from machining on a composite edge trimmed surface and assess characterisation methods and metrics of machined composite surfaces.

This project is sponsored by Rolls-Royce which is currently developing new composite carbon fibre components for their aircraft engines. During their manufacturing processes an edge trimming machining process is required after curing to obtain the correct geometry and allow part assembly. However, due to the non-homogeneous structure and anisotropic material properties of fibre composites- (which are made up of an epoxy matrix and fibre), they have a very different machinability to metals. Carbon fibre machining is a complex process and it has been found by industry that tool wear and surface quality are a problematic issue during the edge trimming process. It has also been found that there are problems with accurately assessing surface roughness on a machined composite surface. Rolls-Royce is therefore interested in understanding how different process parameters will affect the surface damage caused during machining and improving roughness measurement methods. A greater knowledge of the machining process, and how the machining process parameters will affect the surface quality generated during machining, is therefore of interest to both industry and academia. Machining process parameters including feed rate and cutting speed, tool geometry and tool wear,

material type and material fibre orientation, can have an effect on machining forces and the generated surface quality. Understanding how these parameters affect the machining process will lead to more consistent manufacturing of composite comparts, ultimately making components both safer and cheaper to produce. Being able to accurately measure and predict surface roughness and understand or reduce the damage from machining is consequently the research topic of this project.

The literature review has shown problems with standard stylus methods for characterising surface profile of machined composite surfaces. It has also been found in the published literature that there is a need for more research into FE methods for the milling of composite materials and surface damage prediction during machining. Currently the large majority of research using FE has focussed on orthogonal and 2D machining simulations, with some recent research using 3D models for the drilling CFRP [6]. However, it has been found there is a need for development of more advanced FE models for the milling process. An important development, which will be introduced in this research, is to use FE to predict the effects of tool wear and changing cutting edge radius on a CFRP edge trimming process. Hence, from the literature review and requirements from industry the main aims of this research will be to develop surface characterisation methods and predictive tools for quantifying surface profile and machining damage on a machined composite surface. Experimental methods including optical focus variation, CT scanning and SEM will be use to characterise surface damage on different fibre orientations. Developments in surface characterisation methods will then be applied to create a tool for predicting surface roughness using a combination of novel FE models and regression equations obtained from experiment. This research will therefore improve surface roughness characterisation and measurement method, especially of a non-homogeneous multidirectional laminate, and develop

predictive tools to assess the effects of machining parameters on machined surface quality. These developments will be useful to industrial manufacturers of composite components and researchers alike.

1.2 Project Overview

Due to the requirement from industry and associated findings from the literature review, this project has focussed on an edge trimming process of Carbon Fibre Reinforced Plastic using industrially appropriate PCD cutting tools. Initially, surface profile of machined composite surfaces will be assessed using experimental techniques on different fibre orientations. Optical focus variation tool will be used to implement new roughness measurement strategy and better surface characterisation. Then, the improved roughness measurement quantification strategy will be implemented with novel FE methods, for a CFRP edge trimming process, and consequently will be used to predict roughness and assess the effects of tool wear on machined surface quality.

The first section of work stems from the findings in the literature that there are problems with current surface roughness measurement methods for machined composite surfaces. As a result, new optical surface characterisation techniques will be evaluated for roughness measurement in this research using an optical non-contact Alicona focus variation system. The implementation of improved techniques for surface roughness calculation in this project will be used to quantify machining damage and increase the accuracy of measurements, also allowing realisation of the effects of increased tool wear on the surface quality. Additionally, thorough assessment of damage mechanisms and surface damage will be made using additional roughness parameters, SEM imaging and CT scanning. The aims of the current research project will increase the understanding of the complex cutting mechanisms, and surface quality, which is caused during CFRP machining, with the use of new surface analysis techniques on different fibre orientations. Consequently, an improvement in the

understanding of the failure mechanisms and machining damage in a composite edge trimming process will allow improved characterisation of surfaces and will be required to develop further predictive tools and FE models.

Experimental edge trimming tests will be conducted using a 3-flute zero helix PCD milling tool. An edge trimming process has been chosen over an end milling process due to having a consistent chip thickness and therefore being more appropriate for comparing with FE models than an end milling, while still being applied for use in industry. Cutting forces will be measured from experiments using a dynamometer, while machining multidirectional and unidirectional laminates at different fibre orientations, cutting speed, feed rate and various degrees of tool wear. An assessment of different machining parameter effects on surface quality will be quantified and the experimental machining tests will then be compared with novel 2D and 3D FE simulations to validate modelling methods, to assess the effects of tool wear and predict surface roughness.

In the Experimental tests surface analysis techniques will be used to assess the cutting mechanism and surface quality depending upon material fibre orientation. SEM micrographs and CT scans will be applied upon different layers of a machined multidirectional surface, which has different fibre orientation plies, to analyse cutting mechanism and surface and subsurface damage respectively. The suitability and advantages of the optical system for roughness measurements for machined composite surfaces will be evaluated along with applying additional roughness parameters, including S_a, skewness and kurtosis. Additional roughness parameters have been applied to give a more thorough characterisation of surface damage types on each of the different laminate layers of a multidirectional laminate.

New FE (Finite Element) modelling methods will be developed for a composite edge trimming process using implicit finite element software MSC Marc. Numerical modelling is a useful tool which can be used to reduce the need for costly and time consuming experimental trials and has been applied by previous researchers to machining problems [7],[8][9]. The object of these models is to be able to accurately predict the machining process, which can be used to analyse effects of changes in machining parameters, workpiece properties, predict surface damage, and changes due to tool geometry and wear. The prediction of roughness in a composite machining process has been found to be limited in the literature. Methods which make use of numerical modelling tools to predict roughness and the effects of tool wear on composite machining are in need of development. Development of new methods to predict roughness using numerical modelling can increase the understanding of the damage mechanisms in composite machining.

In this research, measured surface roughness from experimental tests will be used to generate regression equations to calculate the effects of input machining parameters on surface quality. The regression equations and FE simulations will then be applied in combination to make predictions of the surface roughness. The aim of the developed models is to allow the assessment of the effects of changes in tool wear by cutting edge rounding and other machining process parameters on the cutting forces and hence make a prediction for the changes in surface roughness. These models will be useful to industry because they will allow a better prediction of the effects of machining on surface quality and damage while reducing the need for many experimental tests and trials.

1.3 Layout of Sections.

A brief overview of the work in each of the sections is described:

Chapter 1 Introduction

An introduction to the CFRP machining problem is presented. The need for research into surface roughness measurement techniques and development of Finite Element modelling methods for an edge trimming process has been emphasised. An overview of the thesis experimental work and developments in FE modelling is described, and additionally the problems of cutting tool wear which can extend machining induce damage.

Chapter 2 Literature Review

The literature review firstly outlines fibre composite properties and their failure mechanisms. Secondly, the machining process for carbon fibre is described with the milling process and some current work in the literature of composite machining. The surface roughness measurement methods and theory is outlined. Then the current difficulties found in the literature with standard methods for measuring roughness of machined composite surfaces are highlighted. Finally, the current literature on FE modelling for machining of composites is assessed and the need for more research into the milling process is emphasised. The novelty of the new FE models for roughness prediction and the calculating the effects of tool wear on cutting forces is highlighted.

Chapter 3 Preliminary Assessment of Surface Roughness Measurement Methods

A preliminary set of experiments have been completed which focus on surface roughness measurement method, analysing machining damage and surface topography of machined composites. The optical focus variation system is applied for the roughness measurement of a multidirectional laminate

machined composite surface. New procedures for roughness measurement have been introduced and recommended methods are described for future researchers. The suitability of the optical method over conventional stylus measurements has been evaluated. Roughness parameters for composite surface damage characterisation have been assessed, including R_a, S_a, skewness and kurtosis. Histograms have been shown to characterise the surface profile distribution, defects and surface quality across the machined surface of different fibre orientations.

Section 3.3 takes a detailed look at the cutting mechanisms and damage types on individual fibre orientations using scanning electron microscopy (SEM) imaging. This has been compared with experimental roughness measurements and has also highlighted the advantages of using areal roughness parameters to measure surface roughness of a multidirectional composite. Visual assessment of the damage and cutting mechanism is detailed for each fibre orientation- the 135 degree fibre orientation has been found to show the highest surface damage, including pitting and fibre pull-out.

Chapter 4 Main Experiment- Edge Trimming Trials Experimental Procedure

The methodology of the first experimental trial, which is an edge trimming process on a unidirectional laminate, is outlined. Novel surface roughness measurement methods have been applied using the optical focus variation system to measure machined surface damage. A poly crystalline diamond (PCD) edge trimming tool has been used to make cuts at different levels of tool wear which will be used to compare and validate novel 2D and 3D FE models. Cutting edge rounding, resulting from tool wear, has been measured experimentally using optical system. A new method has been applied using a zero helix PCD cutting tool, (which has a consistent chip size through the workpiece thickness), to allow comparison with plane strain FE models. Cutting

forces have been recorded using a dynamometer over different fibre orientations.

The second experimental trial is outlined which is an edge trimming trial on a multidirectional laminate. The test has been created using design of experiments and ANOVA to create a regression model which will show the effects of different parameters on the output surface roughness. The effects of tool cutting edge radius, feed rate and cutting speed have been assessed and the regression model will be used as a new prediction tool for surface roughness using 3D FE models. Assessment of additional surface roughness parameters including areal parameter S_a, and skewness and kurtosis, have been applied to characterise surface damage. CT scanning has been used to assess the different damage types present on the surface and look for sub-surface delamination. The chip removal mechanism and surface appearance has been assessed on different fibre orientations.

Chapter 5 Edge Trimming Experimental Results

The experimental results from multidirectional and unidirectional edge trimming tests are shown. This includes the roughness measured on different fibre orientations and an analysis of the effect of fibre orientation on surface quality. The resulting effects of different machining parameters are presented using main effects plots. Cutting edge rounding has been measured, using the optical system to calculate edge radius, which will be used as an input for FE models. The roughness of different fibre orientations has been assessed using the optical system. Surface roughness and surface topography have been found to be significantly affected by the fibre orientation. Areal roughness parameters have been applied, and it is found that measurements made using the optical system will give a more accurate representation of the machining induced surface damage. It was therefore reasoned that optical methods of

surface roughness characterisation is more reliable than using standard profilometer methods.

Section 5.4 Results- CT Scanning of Machined Samples

Sub-surface damage, inter-laminar delamination, and maximum damage depth resulting from machining were assessed using micro CT scanning. The potential sub-surface damage due to inter-laminar delamination and crack propagation of existing voids is assessed. Edge trimmed samples were compared with un-machined samples, to find if damage is due to existing manufacturing defects, or is due to propagation of cracks from forces and damage caused during the cutting process. The presence of some internal delamination and cracks has been found in unidirectional machined samples. It is concluded that roughness measurements are adequate as a defect characterisation method where there is no apparent sub-surface damage and defects present from manufacturing in the multidirectional laminate.

Chapter 6 Multiple Linear Regression Modelling

Multiple linear regression modelling has been used to create S_a roughness predictive equations for unidirectional and multidirectional machined laminates. Statistical methods have been applied to assess the contribution of different predictor terms, including interaction terms. Stepwise method has been used to add or remove predictors, and the R-Sq, R-Sq(Adj) and histogram of residual checks was applied to check for suitability of the fit of regression equations to model data. Cutting edge radius, measured experimentally, has been included as a parameter in surface roughness predictions to calculate the contribution of tool wear on machined profile.

Chapter 7 FE Modelling of Machining

The FE models and modelling methods are outlined in this section. New 2D and 3D models, for the edge trimming process of carbon fibre machining, have been created. Models have been applied using orthotropic equivalent homogeneous material properties and a Hashin damage model for progressive composite material failure. Progressing levels of tool wear, due to changes in the surface geometry and measured cutting edge radius, have been assessed by looking at the corresponding output effect on machining forces. A user subroutine has been applied to control the cutter movement, tool-workpiece contact and the size of the time-step. Adaptive meshing is used on the workpiece and cutting tool to control element size. The elastic properties of PCD have been applied to cutter tip- while the main cutter body has rigid body constraints. Finally, output machining forces have been recorded while varying machining parameters and compared with experimental data to validate FE results.

Chapter 8 Results- FE Modelling of Composite Machining

First the results are presented for unidirectional edge trimming which has been compared with 2D and 3D FE models. 2D models have been able to show the changes in cutting forces as a consequence of tool wear. The cutting forces calculated using FE have been validated by previously obtained experimental values. The damage mechanisms calculated by the Hashin damage model have been compared on different fibre orientations.

In this section, results from 3D FE multidirectional models are presented next. Predicted values of S_a surface roughness, using novel method, have been compared with experimental measurements. The effect of increasing feed rate and cutting speed on FE calculated cutting forces has been combined with experimentally obtained regression models to make a prediction of surface roughness. The predicted change in surface roughness has been presented

due to changes in model parameters. Increasing feed and an increasing cutting edge radius have both been found to have a significant increasing effect on the S_a surface roughness. Feed rate and CER have shown an interacting effect on the roughness, whereby a combined increase of both parameters will have a significantly higher effect on resulting surface damage than changes in one parameter alone. Predicted roughness has been compared with experimentally measured roughness at additional feed rates and cutting speeds, which were outside of model limits, to find the accuracy of predictions lying outside of model range. Is it shown that accurate predictions of surface roughness have been obtained using predictor terms which are located within regression model training limits.

Chapter 9 Discussion & Outputs

An analysis of the thesis results has been presented, with a comparison of findings in the literature. The novelty, limitations and the importance to industry of current work has been discussed.

Chapter 10.0 Conclusions

A bullet summary of the findings with quantification of the results is shown. In Section 10.1 the future work is presented: improvements upon on the current work is discussed, along with proposals for new research projects into carbon fibre machining processes.

Chapter 2
Literature Review

2.1 Carbon Fibre Introduction

To understand the machining of composites, the different failure mechanisms and material properties of carbon fibre composites must be understood. Fibre reinforced polymers (FRPs) are made up of a reinforcing fibre like glass or carbon and a binding polymeric matrix material. A typical fibre volume fraction can be around 60 %. The matrix material acts as a binder for the reinforcing fibres, distributes loads and protects the fibres from external damage. The carbon fibres are generally made from a PAN (polyacrynitryl) pre-cursor by oxidizing and carbonizing at high temperatures. The fibres have a small diameter of around 5-10 μm which are then grouped together to make a tow. These tows can then be pre-impregnated with the epoxy matrix material in order to make pre-preg sheets or used in filament winding processes. Carbon fibres have a superior stiffness and strength compared to glass fibres, which makes them the preferred choice for demanding mechanical applications. For the matrix constituent, thermoset and thermoplastic are the two main categories of polymeric plastic used. Usually in high grade aerospace application epoxy resins are generally preferred.

To make the composite material, pre-preg sheets can be manufactured by wetting the sheet carbon fibre in a resin bath, and they must then be stored in refrigeration until use. In standard manufacturing methods, the pre-preg sheets can then be layered up and cut to shape on a mould surface before being vacuum bagged and autoclave cured at high temperature and pressure. The pre-preg vacuum bagging process is shown in Figure 2-1(a). Firstly, the pre-preg sheets are cut to shape layered up on a mould surface which is coated with a release agent. The pre-preg sheets are then covered with a release film and

breather layer before being covered by the vacuum bagging which is sealed around the edge with sealant tape. Finally the air is removed by vacuum pump and then the whole pre-preg layup is autoclave cured. The vacuum bagging process ensures minimal voids and consistent curing of the resin in the finished composite material. A graphical representation of a laminate is shown in Figure 2-1(b) which has four unidirectional plys layered up in different fibre orientations. The fibre orientations are 0,45,-45(135) and 90 which will be the fibre orientations used in this project. These different fibre orientations are used to give the composite stable mechanical properties in all directions and inhibit crack propagation. Generally the laminate will be layered up in a balanced or symmetric lay-up where the plys will be symmetric through the centre line. This ensures balanced mechanical properties and prevents warping of the laminate during cooling and curing due to different thermal expansion coefficients.
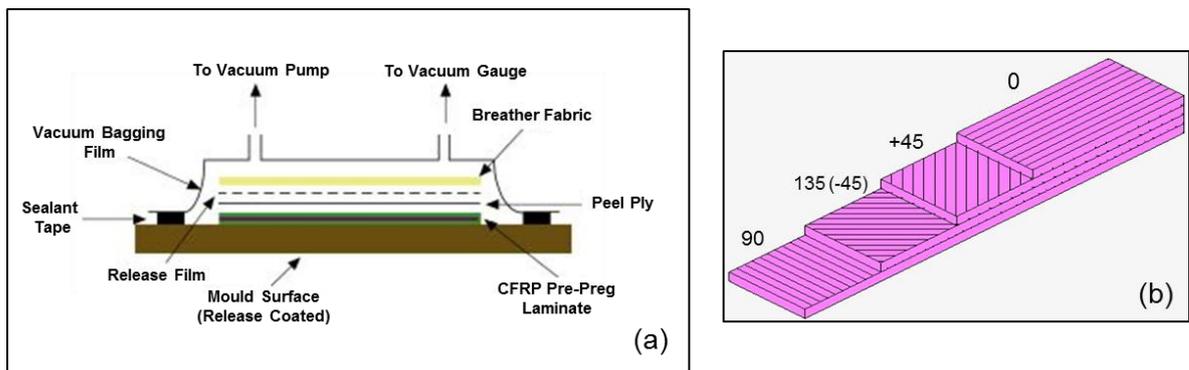
Figure 2-1- (a) Pre-preg layup and vacuum bagging.

(b) Graphic representation of a laminate with different layers and fibre orientations.

2.2 Carbon Fibre Mechanical Behaviour

This project is focusing on long chain fibrous composites, as opposed to short chain or woven composite materials. Long chain unidirectional carbon fibre composites are non-homogeneous and exhibit anisotropic material properties, this means they have directional mechanical properties. They have a different

modulus and strength in the fibre principle direction compared to the transverse fibre direction. There is a different failure mechanism compared to metals and in FRPs there is the possible accumulation of several damage modes until failure. In Figure 2-2 a number of the different modes of failure are shown. The fibres can fail in tension and in compression due to brittle fracture, the matrix can crack and be crushed and fibre pull-out and fibre-matrix de-bonding will occur at the weak interface. The damage in composites can be a sudden or progressive failure and there can be a number of different possible damage types in both the fibres and matrix. The magnitudes and types of damage will be dependent upon loading conditions and material properties. Cracks can form along the laminate boundaries in the form of inter-laminar delamination which is in the plane between the layers by de-bonding, as shown in Figure 2-3. These defects can occur quite readily due to voids between the layers during manufacture or excess resin which can lead to stress concentrations due to load transfer between different layers. Translaminar cracks, shown in Figure 2-3, are less common because the cracks do not tend to propagate through adjacent laminae due to a preferred direction for crack growth. There are different fracture characteristics of the energy for crack propagation, between the adjacent laminate boundaries, shown in Figure 2-3, and the energy is dissipated or tends to propagate along the weaker laminae boundaries [10].
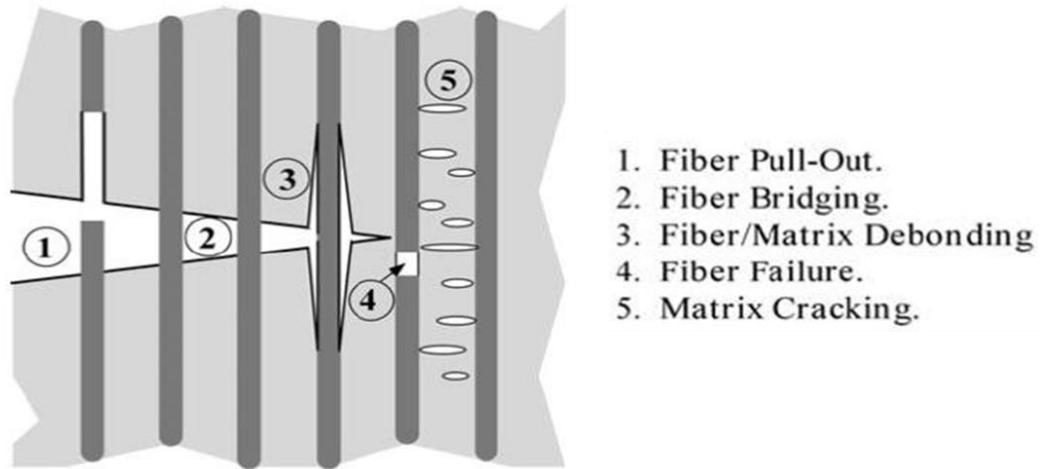
Figure 2-2 - Different failure mechanisms of laminate fibre composites. Adapted from REF [10]

1. Fiber Pull-Out.
2. Fiber Bridging.
3. Fiber/Matrix Debonding
4. Fiber Failure.
5. Matrix Cracking.
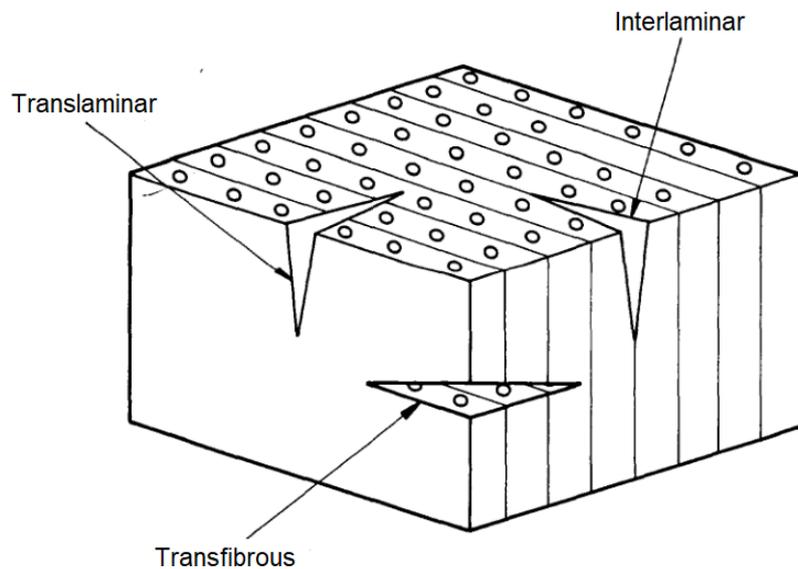
Figure 2-3 - Failure definition types [11].

In most homogeneous engineering materials cracks are generally formed due to the material, loads, geometry and boundary conditions. However in composites the interface between the fibres and matrix material can also separate by de-bonding or de-cohesion. Therefore due to the material fibre direction and the weak fibre-matrix interface there is a preferred direction for crack growth [12]. Unidirectional carbon fibre material is described as orthotropic because the elastic modulus and strength are different in fibre

18

tensile direction and transverse direction. This is due to the higher fibre strength and stiffness than that of the matrix and interface. Laminate theory is generally used to predict the elastic modulus of a combination of stacked layers on the macro level, by taking into account the stiffness of individual layers based on the modulus in each of the principle directions.

The tensile strength of a composite is mainly determined by the fibre strength, volume fraction, and amount and size of flaws which make up the fibre. This is because in reality the brittle fibre strength is dependent on thickness, and length. A longer or thicker fibre will have a higher probability of flaws and therefore a lower strength. In tension during a fibre dominated failure mode the material will have the greatest strength, which is why it is also important to have a high fibre volume fraction. The carbon fibres behave approximately elastically in tension up to their fracture strength [12].

CFRP is made up of an epoxy resin matrix, of which the properties can generally be assumed to be isotropic and of having a higher modulus and strength than thermosetting resins [3]. When a unidirectional composite is loaded in tension in the transverse fibre direction, there is a matrix dominated failure mode. The orthotropic properties of the composite mean that, in this instance it will fail at a much lower strength than in fibre dominated failure mode. During transverse loading the fibres will remain intact or unbroken and the matrix will fail due to void nucleation and crack propagation [12]. There will also be fibre-matrix de-bonding at the interface. The matrix failure will begin at weak defect points in the interface such as voids in the matrix or small fibres-resin gaps [13]. Then, from these defects, cracks will propagate along the weaker fibre-matrix interface. During matrix dominated failure such as in transverse loading, the interface fails nearly immediately after any crack begins. The transverse strength is determined mostly by the resin, but in a fibre composite transverse strength is generally slightly lower than the resin only strength.

In machining of carbon fibres there are factors which can affect the material machinability. These include the mechanical properties of the fibre and resin, the fibre volume fraction and the ply orientation. Also, other factors include the matrix glass transition temperature and the thermal conductivity of the matrix and fibres. The material failure and stiffness will be determined by the strength, stiffness of the matrix and fibre phases and also the bonding strength at the interface of the fibre-matrix. The manufacturing process and any manufacturing defects can affect the composite mechanical properties due to residual stresses, resin voids, fibre waviness and variation in fibre and matrix distribution. Therefore the lay-up, pressure and curing process is important to maintain consistent material properties.

The polymer matrix has less strength and stiffness than the reinforcement but it still plays a part in the cutting process. It has a low thermal conductivity which can affect heat build-up in the cutting zone. It also holds the fibres together and the elastic recovery or bounce back of the material can cause friction and heating in the cutting area. Heating of the polymer during machining can take it above its glass transition temperature which will affect the machining forces and surface quality. Burning of the matrix should definitely be avoided in the cutting zone. The matrix will soften or burn at temperatures during machining if the localised temperature at the tool workpiece interface becomes too high. However, carbon fibres have mechanical properties which are fairly stable up to high temperatures. The stress strain relationship of the fibres is essentially linear or stable up to 1000 °C [14],[15]. The fibres only exhibit a temperature dependant young's modulus above 1200°C where it becomes visco elastic and visco plastic above around 1600°C. This is below the temperatures which will occur during machining. So the temperature dependant properties of the matrix, which will cause softening, only need be taken into account at or above the glass transition temperature.

20

2.3 Composite Machining Introduction

Carbon fibre composites bring new challenges to machining and manufacturing. CFRP material, especially with a high fibre content and tough resin system, is highly abrasive and can cause intensive wear on cutting tools. Additionally, researchers have shown that there are a number of problems which can be found during composite machining [3]:

- Surface quality issues:
- Delamination.
- Fibre pull-out.
- Matrix Burning.
- Matrix Cracking
- Edge Burring
- Un-cut Fibres
- Tool wear:
- Edge Chipping.
- Abrasive Wear.
- Edge Rounding.
- Coating Delamination.

Early researchers investigated the machining of composites and found that unlike during metal machining a continuous chip is not produced. While machining thermoset FRPs there are dust-like or small fragmented chips produced [16]. The carbon fibres are brittle and abrasive and will have a low strain to breakage. The matrix or thermosetting plastic (usually epoxy resin), also exhibits very small plastic deformation before failure. This means that in machining carbon fibre the material is generally crushed and fractures sharply [17]. The cutting mechanism is dictated mainly by fibre fracture, de-bonding of fibre-matrix interface, and fibre cutting angle. There is very little plastic deformation [18]. Standard metal cutting tools and coatings have been shown to

produce a surface with poor quality and have a low resistance to wear when machining composites. They also have a different wear mechanism. Therefore there must be new practises and research into machining of fibre composites in order to understand the cutting mechanisms and improve surface quality as the machining differs extremely from metal cutting.

In the machining of fibre composites delamination has been found to be a problem. There are three main different types of delamination which have been characterised and are shown in Figure 2-4 and Figure 2-5. Type I and type II delamination which is shown in Figure 2-4. Type I delamination is where the fibres on the top surface have been broken and removed inwards from the machined edge [3]. Whereas in Type II delamination, the fibres protrude over the machined edge and there are fibres which have sprung back after the tool has passed without being cut. Type I/II are a combination of I and II where there is some damage inwards of the machined edge and fibres which protrude outwards [3]. Type III delaminations occur when there are cracks or debonded fibres which are partially attached lying parallel to the machined edge, as shown in Figure 2-5. The fibre orientation and machining parameters will affect the magnitude and type of delamination which occur during machining.

22
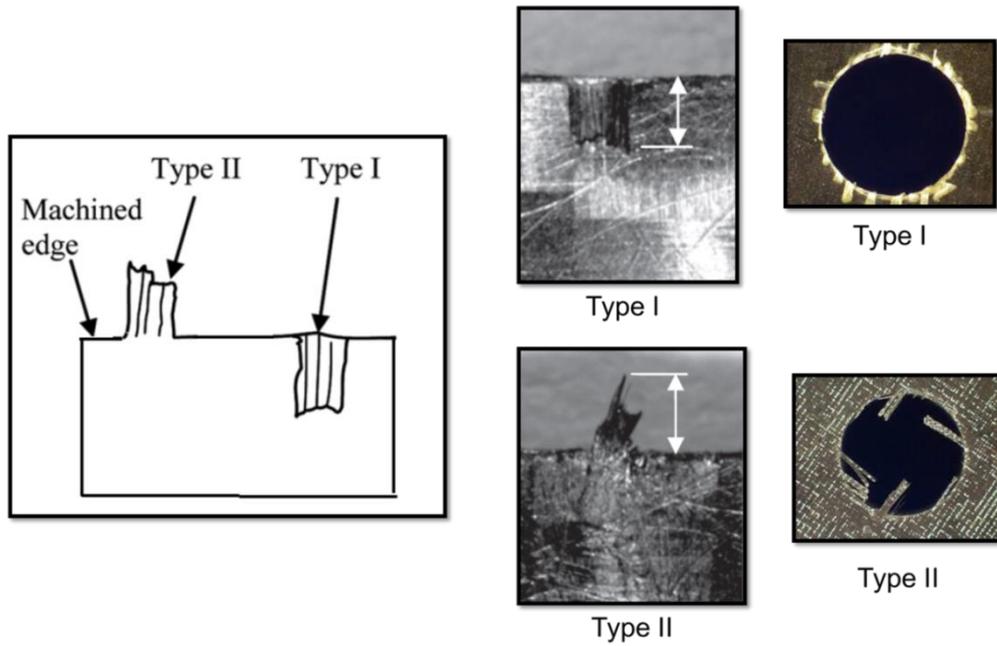
Figure 2-4- Type I and Type II delamination. Adapted from REF [3],[19]
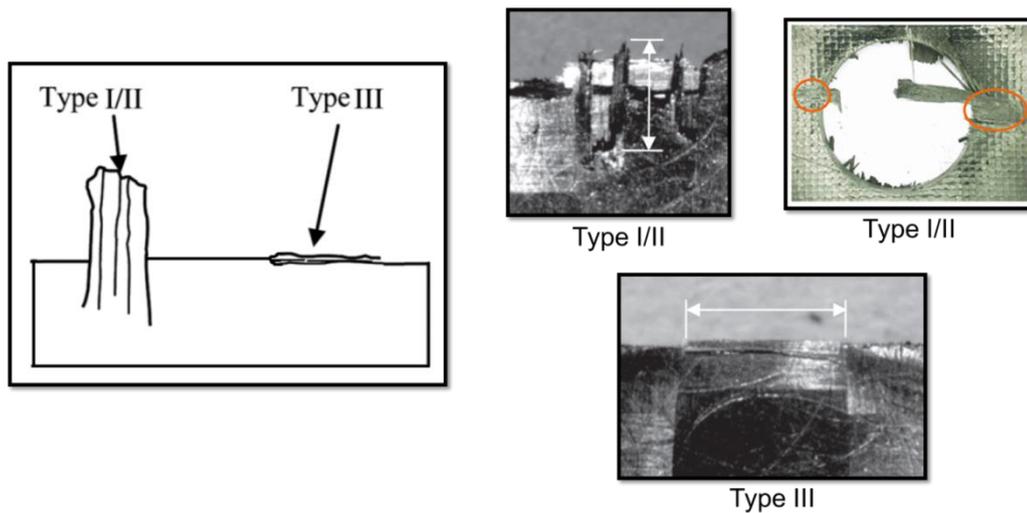
Figure 2-5- Type I/II and Type III delamination. Adapted from REF [3],[19]

It has also been found in the research that the fibre orientation in relation to the cutting direction will play a critical factor in the chip removal mechanism and surface damage [3],[20],[21]. The definition for the fibre orientations direction which will be used in this document is shown in Figure 2-6. As it can be seen the cutting mechanism varies according to the different fibre orientations. Likewise

the machining damage, surface quality and cutting forces have also been shown to vary due to the fibre orientation.
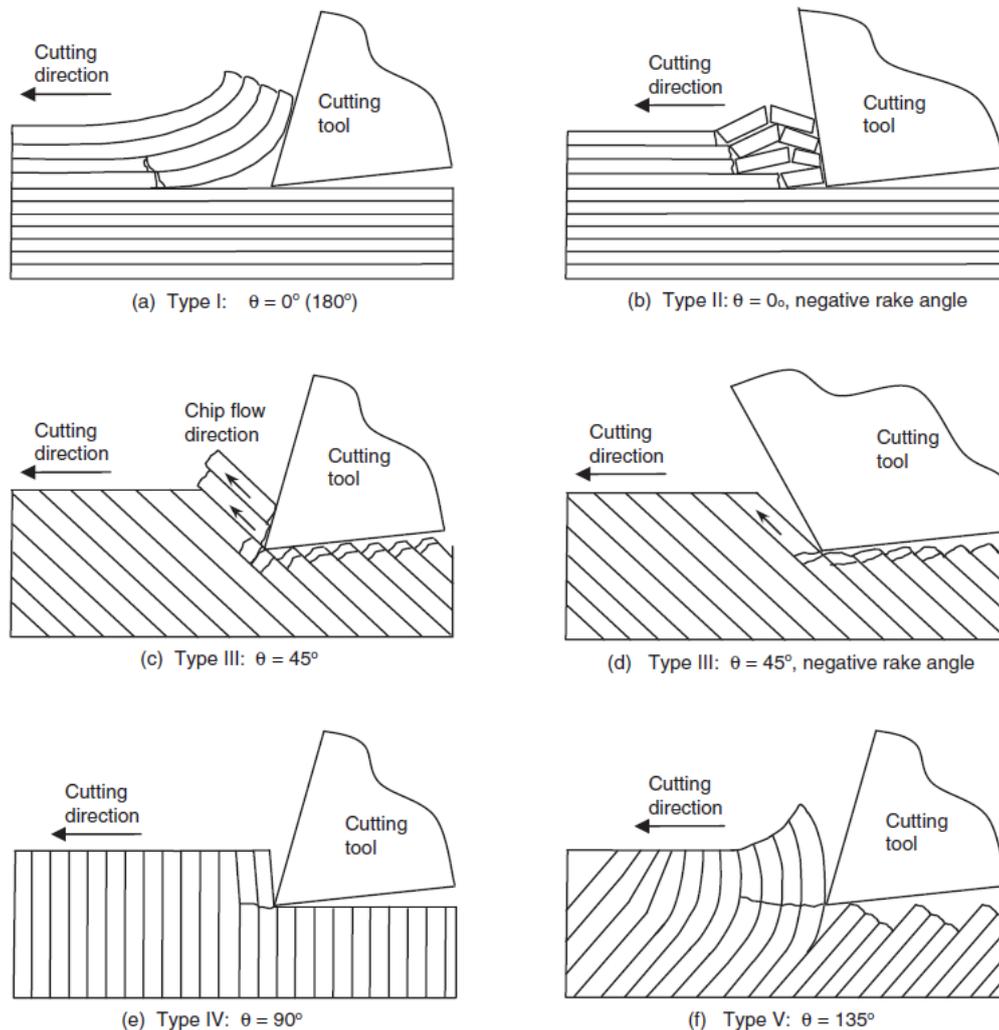
Figure 2-6 - Cutting mechanisms at different fibre orientations. Adapted from REF [3],[21].

In the 0 degree orientation the fibres are pushed upwards and then fracture on their cross section due to bending and micro buckling- Figure 2-6(a). First the fibre is debonded by de-cohesion from the fibres-matrix interface, and then the fibres are bent up like a cantilever beam [2]. A crack will propagate along the interface until eventually the small rectangular chip is removed when the fibres finally fracture. D.H. Wang et al. [21], found that the machining forces fluctuate as the fibres go through a cycle of bending in a peel fracture effect,

and this will repeat after a small rectangular fragment is removed. The de-bonding or de-cohesion will occur when the stress is greater than the physical bonding strength between the fibres and matrix interface. M. Ramulu et al. [5], found that the machined surface was left covered in clean fibres lying parallel to the surface, and the fibre orientation could be seen on SEM images.

In the 90 degree fibre orientation, the fibres are first compressed by the tool which causes them to fracture perpendicular to the fibre length. Then in order for a small particle to release, there is a secondary fracture by inter-laminar shear along the fibre matrix boundary [21]. Small fractured particles are produced and some out of plane displacement may be seen on the surface in the cutting direction. Early research by Koplev et al. [16], found that irregular sized chips were produced as opposed to small rectangular chips in the 0 degree fibre orientation. A larger overall cutting force was found while machining the 90° degree fibre orientation compared to the 0°. This is due to the fact that all the fibres must be sheared and compressed rather than in bending in the 0 degree fibre orientation.

In the 45 degree orientation the fibres are predominantly sheared by the tip of the cutting tool and then a small dust-like chip is removed when the fibres de-bond from the matrix [3]. It is also possible for individual fibres to pull out from below the machined surface [2]. The fluctuation in cutting forces was found to be less in the 45° degree orientation than the 0 degree fibre orientation.

The 135 orientation, where the fibres are facing into the path of the cutting tool has a different cutting mechanism. Here there is a combination of bending, crushing and fibre shearing. The fibres are bent and then a crack begins to propagate below the surface along the fibre-matrix boundary where there is de-bonding [20]. The fibre matrix interface is fairly weak due to the interfacial bonding strength between them. The crack will propagate and finally

the fibres will be crushed and break, leaving a damaged surface. Generally the surface roughness of the 135 degree orientation has been found to be worse than of those below 90 [16],[20].

Figure 2-7 shows cutting for a small and larger depth of cut in fibre orientations greater than 90°. Wang & Zhang [20] found that at the smaller depth of cut which is less than the fibre diameter, the end of the fibre is compressed and the surrounding matrix is fractured- Figure 2-7a. However the fibres will not always break and small protruding or un-cut fibres can be left on the material surface. In a greater depth of cut, the fibre is pushed by F1 in a direction outwards from the workpiece and the tool tries to bend the fibres. This can cause fibre matrix de-bonding and micro cracks below the machined surface, parallel to F2.
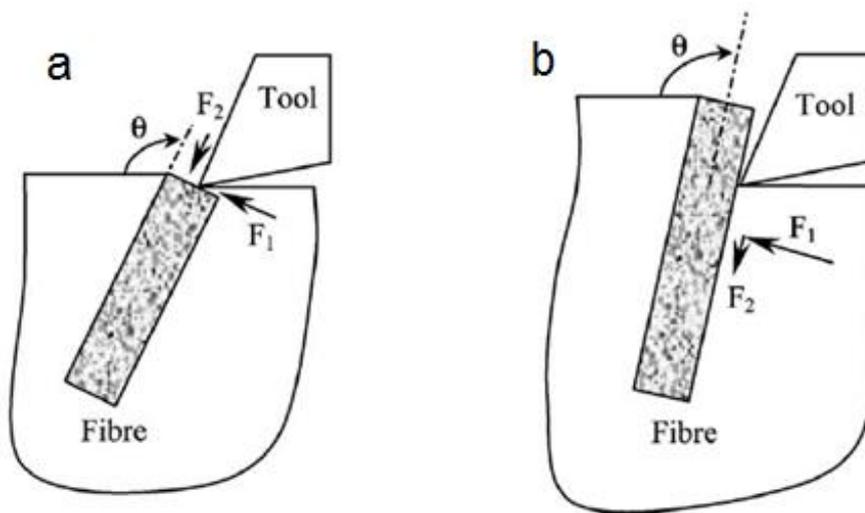
Figure 2-7 - Cutting mechanism at positive fibres orientation at small and large depth of cut. Adapted from REF [18].

2.3-1 Milling of Composite Materials

Milling is a machining process which is used heavily in industry and is used in composite manufacturing. It can be used for creating many different flat or shaped surfaces, including slots, pockets and contours [22]. In milling the

26

spindle rotates the tool about an axis and is fed into the workpiece. The milling tool usually has multiple cutting edges and the spindle axis of rotation can either be horizontal or vertical [23]. The tool has a rotational speed and a feed speed which combine to make up the feed- which is the distance the tool advances in one revolution. The cutting tool will have an axial depth of cut (a_p) and radial depth of cut (a_e). The three main types of milling are plain, face and end milling. In plain milling the cutting edge is parallel to the spindle axis and can be either parallel or inclined to the workpiece feed direction. The sides of the cutting tool are used to make the cut on the periphery of the tool. In face milling the face and sides at the bottom of the tool are used for cutting and in end milling the sides the base of the tool are used for cutting [22].

In milling the cutting mechanism will differ to that shown previously in turning. Due to the rotation of the cutting edge, a variable depth of cut is taken from the workpiece. The change in chip thickness in conventional milling is shown in Figure 2-8(a). In conventional milling the tool rotation is against, or opposite, the feed direction and the machining forces will cause the tool and workpiece to push away from each other. Whereas, in down or climb milling the tool rotation will be with the feed direction. In conventional face milling for each rotation of a single cutting edge, the un-deformed chip thickness increases to a maximum before a chip is removed, whereupon a new cutting edge will cut into the material [24],[25]. When machining fibre composites the cutting tool edge in relation to the fibre orientation will change as the tool rotates through the material shown in Figure 2-8(b). Unlike with orthogonal turning, the fibre orientation in relation to the cutting edge is not constant- Figure 2-8(b)-, and also, the chip thickness is not constant, so the machining forces will be fluctuating within each cycle of a tool cutting edge rotation. Cutting forces will increase as the chip thickness increases and then drop once the chip is removed. The depth of cut will determine the area and number of fibres being

cut, while the feed rate, cutting speed and tool geometry will determine the chip thickness [26].
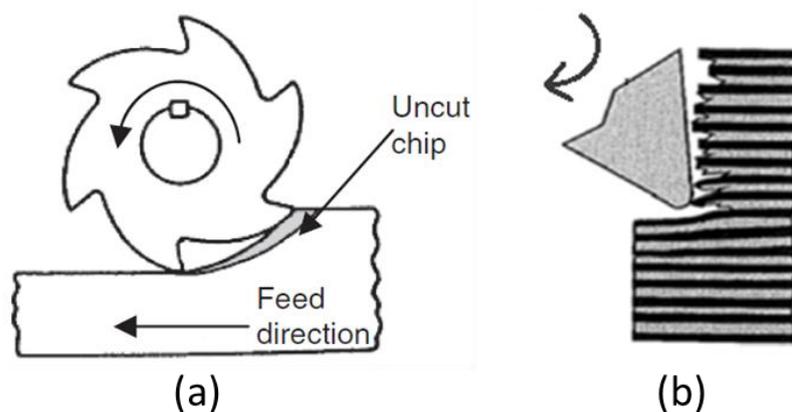
Figure 2-8 – (a) Change in chip dimensions during conventional milling [3], (b) Rotation of the cutting edge will vary against fibre orientation [26].

Karpat et al [18], created a mechanistic model using cutting force coefficients obtained from milling tests for slot milling of a CFRP laminate. The authors showed that in slot milling the tool cutting edge will vary against the material fibre orientation as the tool rotates which is adapted and shown in Figure 2-8(b) and Figure 2-9. Cutting force coefficients represent a materials resistance to machining in the radial and tangential directions. The authors found that the radial cutting forces were higher when cutting laminates at a 0 and 90 degree fibre orientation, compared to machining laminates with a 45 and 135 degree fibre orientation. However the highest tangential cutting forces were found when machining at the 135 degree fibre orientation. It was explained that the cutting forces are "due to the combined effect of the instantaneous fibre cutting angle and the instantaneous chip thickness" [18]. Delamination or un-cut fibres was found to be a product of both cutting tool wear and material fibre orientation and the delamination was found to occur most where there were maximum tangential forces.
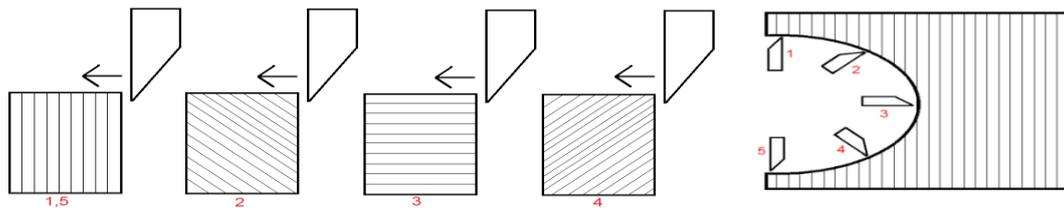
Figure 2-9- Slot milling, cutting tool edge to fibre orientation. Adapted from REF [18].

A number of researchers have performed experiments on milling of composites. Azmi et al. [26], used Taguchi analysis to find the machinability of GFRP with respect to surface roughness, tool life and machining forces. A unidirectional glass-epoxy fibre with 16 layers was end milled and 3 measurements were taken to get an average surface roughness. Flank wear was the most dominant wear mechanism by mechanical abrasion. The feed rate was found to be more dominant on roughness than cutting speed. The resultant cutting force was most significantly influenced by feed and depth of cut. Tool wear, fibre orientation, cutting forces and machining parameters will all therefore have an effect on surface quality.

Davim et al. [27], looked at the machining forces, surface roughness and delamination during end milling. The machining force was found to increase with feed rate and decrease with cutting velocity. The feed rate had the most statistical influence on the delamination factor to the workpiece and surface roughness was found to increase with feed rate and decrease with cutting speed. Mathivanan et al. [28], have also analysed the machining forces in end milling of CFRP and GFRP using ANOVA factorial design. Machining forces were found to increase approximately linearly with feed and also increased with cutting speed. The machining forces were found to be higher when machining CFRP than GFRP due to its higher stiffness and strength.

Hintze et al. [29], looked at delamination on a woven plain weave CFRP fabric with 0 and 90 degree fibres direction. They found that the woven yarn which

causes crimp or undulation in the fabric causes variation in delamination on different areas of the woven composite surface when machined. The undulation of the woven yarn was found to be more critical to the extent of delamination than changes in the different tool geometry which the authors applied. Figure 2-10 shows the different delamination found on the woven yarn with different possible delamination types. Type I/II was found to be the most dominant type of delamination.
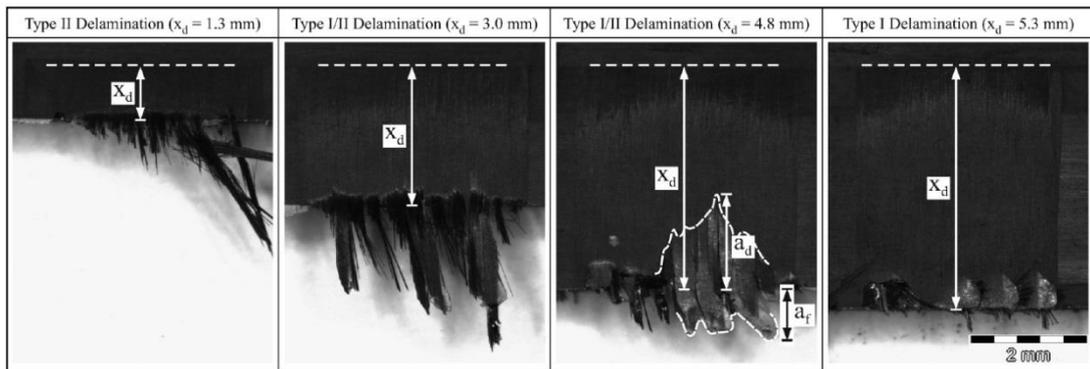
Figure 2-10- Different delamination on a machined edge of woven composite [29].

Research by Haddad et al. [4] have used three different machining processes, water jet, abrasive diamond cutter and standard burr tool. The machined surfaces were compared by using contact and non-contact roughness measurement methods. The fatigue life and mechanical properties were investigated in response to surface quality. Importantly, it was found that the type of machining process and the surface roughness after machining had an effect on mechanical performance. The inter-laminar shear strength and compressive strength decreased with an average increase in surface roughness. Therefore; minimising surface roughness and damage is of importance in the machining processes because it can affect the strength and integrity of components.

Ahmad et al. [19], looked at the machining damage in edge trimming of CFRP. They investigated surface roughness and edge delamination while machining with a burr style router. Surface roughness measurements were made by Mitutoyo profilometer. Delamination frequency and depth were found to increase with an increase in chip effective thickness. The equation for chip effective thickness is shown in Equation 1, where a_e is the radial depth of cut V_f the feed rate and V_c is the cutting speed. An increase in feed and a decrease in cutting speed will increase the chip effective thickness.

$$Chip\ effecitve\ thickness = a_{eff} = a_e\frac{V_f}{V_c} \qquad \text{Equation 1}$$

The surface roughness measured in the longitudinal direction was found to increase with chip effective thickness. Delaminations were recorded along the machined edge and it was found that type I/II were the most dominant type. Figure 2-11 shows some high levels of delamination in surface plies seen by the authors when machining with a large chip effective thickness. Ahmad et al. [30], has again reported similar findings of the effects of chip effective thickness on surface roughness.
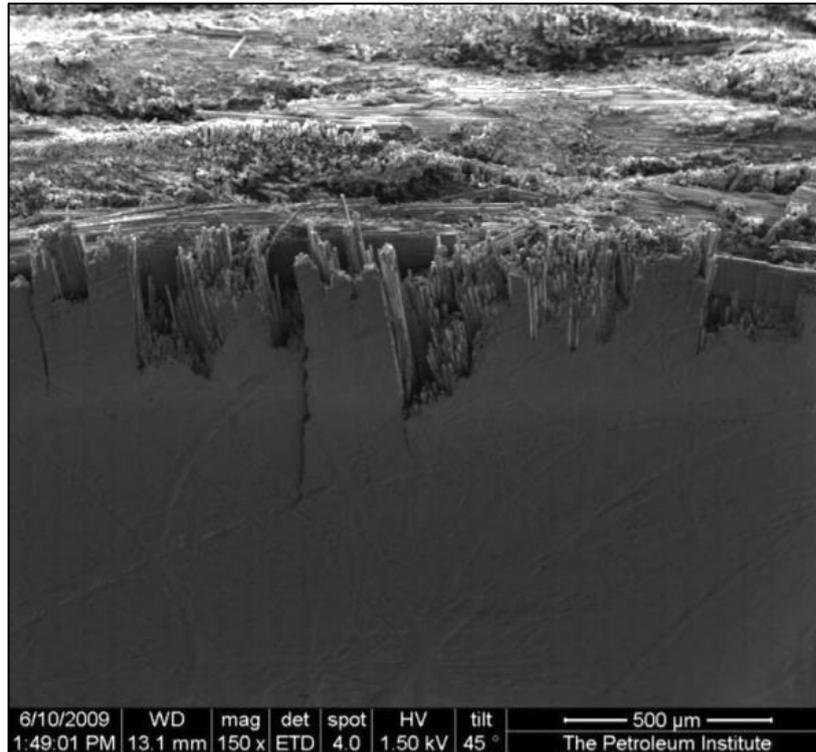
Figure 2-11- SEM image of type I/II delamination on edge machined at extreme cutting conditions [19].

2.3-2 Other Machining Processes

Drilling is a process which is widely used in composite industry to allow assembly or joining of components. However, there are strict requirements for holes in order to meet surface integrity and geometry requirements. In order to allow easy assembly, the position and diameter of the holes must be within tolerance, and also the holes must be mechanically safe. One alternative to drilled holes in composites is to adhesively bond joints. This can be advantageous because the cost and weight associated with fasteners is reduced. Bonded joints can also act as a stress distributer, as the load will be applied over a larger area and the stiffness of an epoxy adhesive could be tailored to be closer to that of the bonded materials. However bonded joints are permanent and can't be disassembled. If components need to be later inspected or replaced this would be problematic. Additionally, the lifetime of the adhesively bonded joints may be uncertain. Another potential is creating of

holes during the lay-up and curing. However, due to the distortion when cooling, the accuracy of these holes is poor [31]. For these reasons drilling of composite materials is still widely used in the aerospace industry. It has been found that there is a significant amount of research in the literature into composite drilling, and delamination at the top and bottom ply has been found to be a significant problem. This will lead to large costs in production if material must be scrapped. The thrust force has been shown to be one of the main factors contributing to delamination [3]. There can be two types of delamination:

- Peel-up which occurs on the when the top laminate plies are pulled up by the flutes and causes them to bend and separate- Figure 2-12b.
- Push-down delamination occurs as the tool approaches the exit- Figure 2-12a. The bottom layers are pushed by the vertical thrust force which causes them to bend. The inter-laminar interface is relatively weak and this bending can cause a crack to propagate along the interface and de-cohesion [3].
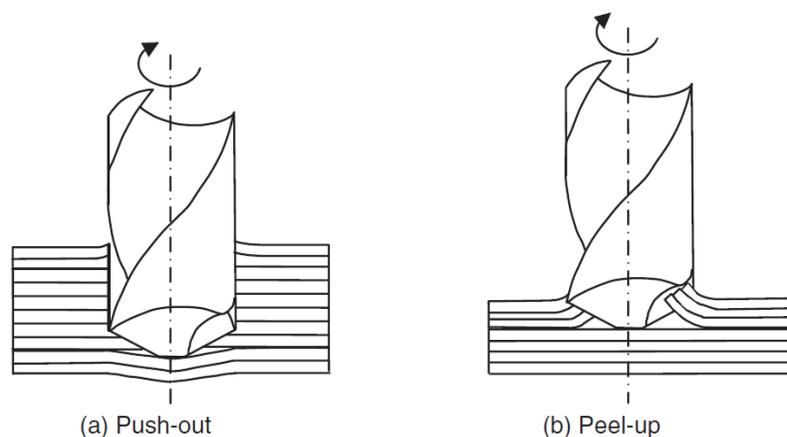
(a) Push-out   (b) Peel-up

Figure 2-12- Two types of delamination while drilling composites. (a) Push-out, (b) Peel-up. Adapted from REF [3].

The thrust force is correlated with the feed rate: if the feed rate rises there is increase in the uncut chip thickness and a corresponding increase in the thrust

force [3]. Therefore the increase in feed rate has shown to be critical cause of delamination. This effect is mainly contributing to the push-out delamination on the bottom ply. Tool wear and chisel edge size has also been shown to contribute to the thrust force which will in turn contribute to delamination [32]. One method to reduce the delamination from the thrust force is to reduce the feed rate near to the hole exit.

Wen-chou Chen [33] drilled composite holes and used X-ray to find the size of the damage by delamination. The holes were coated with tetrabiomethane before x-ray was applied. Torque and thrust force were investigated with a dynamometer to see how the onset of delamination is affected. Tool geometry, tool wear and drilling parameters effects on the delamination were also investigated. Important findings from this study were:

Delamination is most prominent when there is a high thrust force, and lowering the feed rate will reduce the torque and thrust force. "In order to improve the hole quality at the exit, the feed rate at the exit needs to be decreased during the drilling process" [33].

"The delamination becomes serious as the wear rate of the drill rises during the drilling process" [33]. Delamination increases with increasing tool flank wear as does the thrust force. The drill wear also causes delamination to be more serious at high spindle speeds.

Shyha et al. [31] used a stepped drill and twist drill with different coatings, point and helix angle. The effects of tools on delamination were discussed. The step drill was found to reduce the thrust force in the 2nd stage of drilling significantly by creating a pilot hole effect. This is because there is less chisel edge contact with the workpiece during the 2nd stage. They found that stepped drill had a longer tool life than the conventional, and that the uncoated twist drill had a longer tool life than the TiN coated. The dominant wearing

34

mechanism was found on the flank and chisel edge of the tools by chipping. Increasing the feed rate increased the thrust force, but it also lengthened the tool life.

Other problems that may occur during drilling are burning of the matrix and fibre pull out. Temperature build-up can be high while drilling due to the low thermal conductivity of the matrix. This can cause shrinkage of the hole once the tool is removed which means dimensional accuracy would not be achieved [3]. It has been found that there is a significant amount of research into drilling of FRPs materials, most of which has not been presented here. There has been significant experimental research into causes of, and strategies for, reduction in delamination, and the effects of machining parameters on tool life and delamination. It has been found that there is less research conducted into the milling process and into the surface generated during edge trimming and therefore this has been chosen as focus area.

2.4 Surface Roughness Measurement for Composite Machining

In order to assess the quality of the machined surface of components, surface roughness parameters are often calculated [5]. It is important, too, for the composite manufacturing industry be able to accurately quantify surface roughness and assess the surface damage induced by machining. This will ensure the integrity of components and reduce costs in the machining process. It is also important from an academic research point of view to be able to characterise chip formation and understand how surface damage may be affected by changing machining parameters, i.e. tool condition, tool geometry or feed rate and cutting speed.

Typically in industry, a stylus profilometer is often used to measure surface roughness. However there have been problems found in the literature with using this method for machined fibrous composites. Difficulties have been

found by Ramulu et al. [5], it was found that when measuring roughness parallel to the fibre direction, the stylus passes over multiple plies or span over multiple fibre orientations. Azmi et al. [34], have also reported that the Ra may not always reflect the machining damage or surface quality of machined fibrous composites. They pointed out two specific problems with roughness measurement carried out by profilometer: i) protruding fibres on the machined surface can affect the movement of the stylus or stick to the stylus tip, and ii) that the deviations in the roughness reading is very dependent upon measurement direction and position due to material non-homogeneity. Ahmad et al. [19] found that the surface roughness increased with chip effective thickness when measured in the longitudinal direction, however no clear trend was found when measuring in the transverse direction, which may have been due to the problems of using a profilometer roughness measurement method on non-homogenous composite surfaces.

The profilometer works by trailing a small radius diamond tipped stylus in a straight line along the specimen, as shown in Figure 2-13. A transducer then detects small deviations in profile height which can be used to calculate roughness parameters. The sample is measured with an overall evaluation length, which is split into a number of sampling lengths, which is to be performed according to British standard ISO 4288:1998. The R_a parameter is the most commonly used surface roughness parameter and is defined as the arithmetic mean roughness of the profile. First the profile must be filtered to remove the long wavelength or low frequency component, so that the high frequency roughness component is maintained. This low frequency profile waviness is removed from the profile deviation according to the British standard ISO 11562:1997 and is shown in Figure 2-14. In Figure 2-14(a) three profiles are shown, one which is the un-filtered profile measured by stylus, the second shows the profile waviness, and has the high frequency component

removed, the third is the profile roughness and has only the high frequency component. Figure 2-14(b) shows how the profile waviness is removed according to the standard, where a higher percentage of the profile with a low frequency component is removed from the measurement.

The R_a roughness parameter is then calculated as the centre line average which is the deviation of the surface profile from the centre line. The centre line is calculated to lie where the sum of the area contained (by the profile), above and below the centre line is equal. The absolute value of the peak or valley is used in the R_a parameter, so it does not distinguish between peaks or troughs but only the deviation from the centre line. Similarly, the S_a parameter is described as the arithmetic mean of the absolute of the ordinary values over a definition area, rather than along a profile line.

In measurements made using a stylus the lateral and vertical resolution of the profile measurement is determined upon the stylus edge radius. The stylus tip will never be able to get fully to the bottom of surface valleys and therefore the profile measurement will be different depending upon the size of the stylus edge radius, as shown in Figure 2-13. The lateral resolution is measured in the horizontal stylus traversing direction, and the vertical resolution is in the profile height direction.
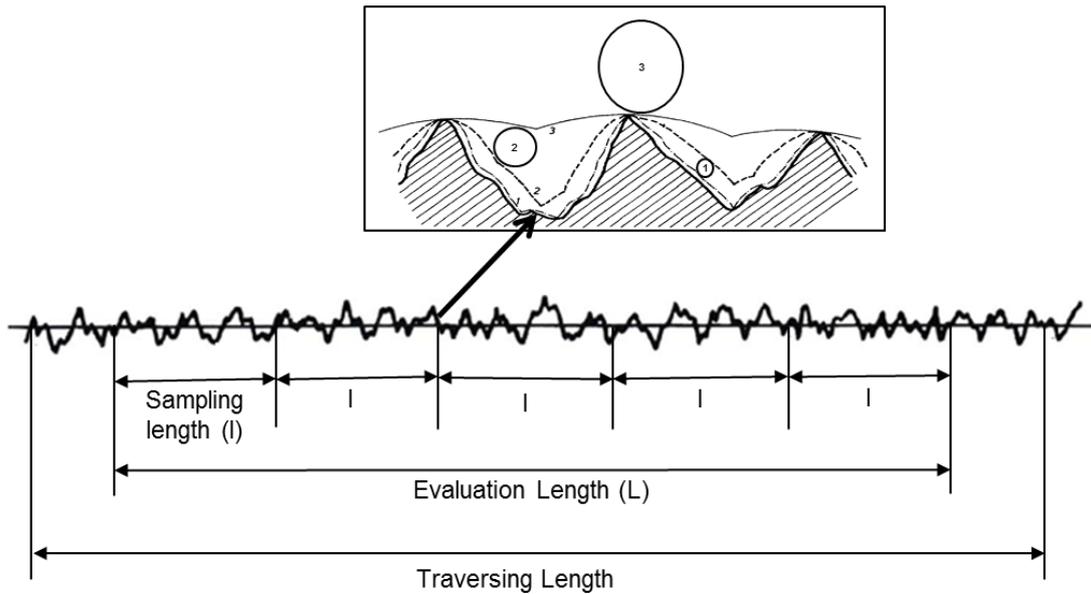
Figure 2-13- Profile evaluation length and sampling length. The stylus radius will dictate the profile vertical and lateral resolution as shown.
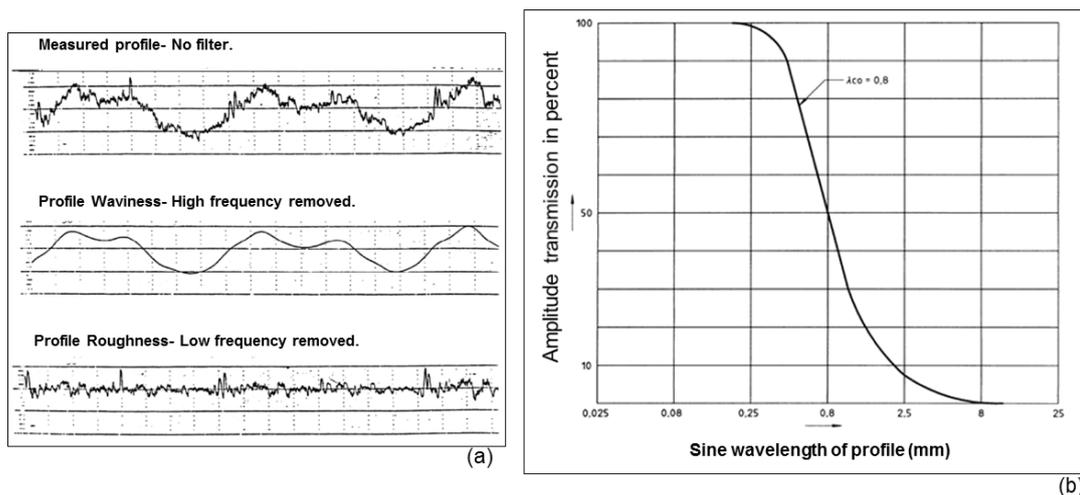
Figure 2-14- Removal of low frequency component in roughness measurement, (a) Measured profile with waviness and roughness shown, (b) Removal of profile waviness.

Ghidossi et al. [35], researched the effect of machining parameters on failure stresses and roughness. It was found that increasing the cutting speed reduced the surface roughness during edge trimming of GFRP and CFRP. A surprising result was found, that the surfaces with the highest R_a did not necessarily have the lowest failure stresses, and therefore the R_a parameter did not give a full

38

indication of damage. Slamani et al. [36], has found problems using R_a to show the extent of machining surface damage due to increasing tool wear, which they found was because of matrix burning and sticking when using a worn cutting tool.

Some recent research by Gara and Tsoumarev, [37] has created a roughness prediction equation for transverse and longitudinal roughness measurements using a theoretical equation and regression equation from experimental test. They have found that feed rate was the strongest contributing parameter to the roughness and that up milling gave a better surface finish than down milling. However, their longitudinal roughness measurements were taken using a stylus profilometer and there was little detail given of the method used to take measurements, effect of fibre orientation on roughness, or of the standard deviation in these measurements. Their regression equation took into account the effects of cutting speed and feed rate but does not include any effects of tool wear. Their tests were performed using an uncoated knurled cutting tool, which will have a very high tool wear rate when machining a composite surface, and is probable to be a contributing factor to the roughness.

Wern et al. [38], studied the surface roughness of composite drilled holes using two PCD drills and with varying feed rates. SEM was used to look at the surface and varying roughness parameters were investigated. They saw a variation in surface roughness at different points on the drilled hole due to fibre orientation shown in Figure 2-15. In the negative fibres orientation to cutting direction they observed fibres pull out which caused pitting and a rough surface. In the other directions the surface was smooth with smeared matrix and sheared fibres. They found R_t and R_z more effective than R_a at quantifying the depth of the valleys and machining damage for composite materials. The feed rate also increased the surface roughness once it went beyond 0.1778 mm/rev.
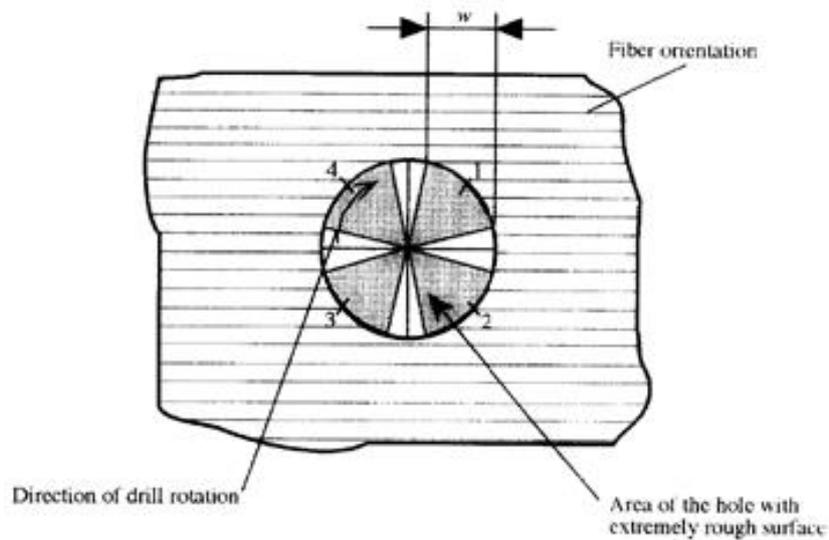
Figure 2-15 - Variation in roughness at different points on hole surface due to fibres orientation [38].

Colak and Sunar [39], have performed milling experiments on a unidirectional CFRP laminate with a PCD cutting tool to create a mechanistic model using cutting force coefficients. They have measured surface roughness using a Nanovea optical profilometer. The surface roughness was found to be highest when machining with high feed rate and low cutting speed. They, however, did not investigate the use of different roughness parameters or discuss the difficulties of measuring surface roughness of a multidirectional machined composite surface because the measurements were made on a unidirectional laminate. It has been shown by other researchers that the feed rate followed by cutting speed has the strongest dependence on surface roughness, and that increasing feed and decreasing cutting speed will generally increase roughness [40]–[42].

Nurhaniza et al. [41] have also used statistical methods and design of experiments to show the contribution of feed rate, cutting speed and depth of cut on the surface roughness but not the effects of tool wear. They have used a profilometer to measure R_a surface roughness and yet have not fully discussed the effect of fibre orientation on the surface roughness or described the

40

uncertainty in measuring surface roughness of a multidirectional laminate with this method. Other researchers have made useful contributions to the literature using design of experiments to analyse the effects of the feed rate and cutting speed on surface roughness, yet the effect of tool wear and fibre orientation has not been included [40],[42].

Kumaran et al. [43] have predicted surface roughness of water jet machined CFRP material using regression analysis. Linear surface roughness measurements (R_a) have been taken using a profilometer and visual surface profile measurement was made using a non-contact 3D surface measurement NV-2000. An assessment of the contribution of each of the test variables on surface roughness was made and regression analysis was able to show the effect of water jet parameters on surface roughness within a 95 % confidence level.

Ismail et al. [44] have drilled hemp fibre reinforced composite (HFRP) composite and used design of experiments to analyse the effects of drilling parameters, fibre aspect ratio, and drill diameter. Delamination and surface roughness were found to increase with greater fibre aspect ratio which correlated to longer length fibres. The delamination damage was lower in the HFRP than CFRP sample and surface roughness measurements were taken using mitoyoto profilometer along the drilling direction, through ply thickness.

Ismail et al. [45] have assessed surface roughness, delamination factor and chip morphology when drilling CFRP and HFRP. They have sectioned the holes and used SEM images to analyse surface quality. The SEM images showed some internal propagation of cracks, delamination and burnt epoxy resin in the CFRP material. Delamination was found to be higher in the 10mm diameter tool compared to the 5mm tool and at higher feed rates. Chip morphology showed that the CFRP chips were discontinuous but not fully dust-like, whereas the

HFRP chips were more continuous with brown ribbon like chips. This was because the CFRP has a brittle thermoset epoxy resin while there was a ductile thermoplastic polycaprolactone (PCL) resin for the HFRP.

2.4-1 Roughness Parameters

Due to the non-homogeneous structure of fibre composites, the use of S_a areal roughness parameters may be useful when applied to a machined surface. In a study by U.C Nwaogu et al. [46], the use of a commercial optical system manufactured by Alicona was applied for surface roughness measurement. They compared tactile profilometer and Alicona optical device for the roughness measurement of casting surfaces. Areal and profile surface roughness parameters were used and it was found that the areal (S_a) comparators had less variation in measurement than the profile parameters (R_a). They compared conventional R_a from profilometer measurement with the S_a parameter from Alicona focus variation system and found an agreement. It was recommended that the areal parameters (S_a) were more useful in measuring the surface of castings due to giving a better representation of a non-homogeneous surface and were also found to have a better repeatability. The use of the S_a parameter has good potential for application in composite surface roughness measurement due to the non-homogeneous structure and described unreliability of stylus measurements. The non-homogeneous structure of a fibrous composite machined surface is variable due to the different fibre orientations and cutting mechanisms on each layer. Therefore roughness measurement must be able to accurately represent this.

A relevant issue to machined surface damage detection is whether the R_a parameter (arithmetic mean roughness) can give enough information to quantify the surface quality alone. Herring et al. [47] studied different roughness parameters to assess surface finish of a CFRP mould surface manufactured by different methods. The maximum peak to valley height (R_t),

skewness (R_{sk}) and kurtosis (R_{ku}) were studied. The authors stated that a minimum of R_a, R_{sk} and R_{ku} should be calculated to give a thorough understanding of a composite surface. All of the parameters used were capable of distinguishing between the surfaces manufactured by different methods, but the Rt parameter was shown to be most sensitive to individual scratches or particles on the surface.

Recent research, by Rimpault et al. [48], has used fractal analysis of cutting force signals when CFRP trimming by end milling using a diamond coated tool. They have performed machining experiments at increasing levels of tool wear using 3 different levels of feed rate and cutting speed. Tool flank wear was measured by optical microscope according to ISO 8688-2. It was observed that there was some burning of the matrix at tool flank wear above 0.3mm, although they stated that cutting edge rounding may be a better indicator. They found that with the cutting force signal fluctuated more at lower levels of tool wear when there was a sharper milling tool due to cutting small groups of fibres, as shown in Figure 2-16.
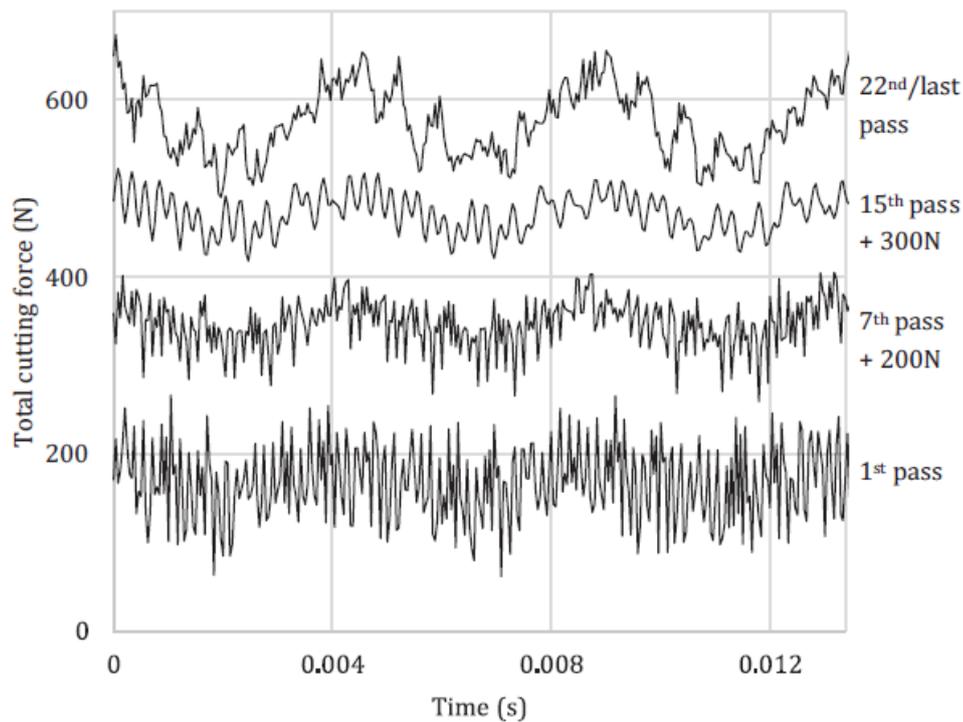
Figure 2-16- The total cutting force at different levels of tool wear, with 3 tool rotations shown [48].

Importantly they stated that- "R_a was found to be inadequate to evaluate the surface finish of fibre reinforced plastic composites." They therefore decided to use tool wear as their comparative factor vs the signal forces, and did not include roughness measurements in their analysis. Although, little detail was given as their reason for R_a being inadequate to evaluate surface quality, it may have been because of the problems of using standard stylus method. In any case, this paper again highlights the need for further research into surface analysis using different measurement techniques and possible use of additional roughness parameters to better represent surface quality of FRPs machined surface.

The skewness and kurtosis roughness parameters are explained in Figure 2-17. The skewness indicates whether a surface is characterised by peaks or valleys and is a statistical measure of the profile symmetry or height distribution. The

44

kurtosis, shown in Figure 2-17, highlights whether the surface profile has peaks and valleys which are either sharp or rounded. A profile which has a negative or low skewness will have more valleys than peaks, while a positive skewness will describe one which has more peaks. A profile which has a high kurtosis will have sharp peaks, while one with a low kurtosis will have rounded peaks. The kurtosis and skewness are not represented in the R_a parameter, and it has been shown that two unequal surfaces can have the same R_a [49]. Therefore these parameters will be investigated to see if they can give more information about a machined composite surface quality.

It has been found that the large majority of research in the literature on roughness measurement has focussed on R_a measurements made by stylus measurements. It has been shown that there are issues with this method and that additional parameters may further improve measurement accuracy and information on surface structure. A number of researchers have used design of experiments and linear regression in order to analyse the composite machining process and effects of parameters on surface roughness [37],[40],[42],[50]. It has been found that the majority of research into parameters affecting the surface roughness have focussed on the effects of feed rate, cutting speed and depth of cut. The effects of tool wear have generally not been included as a statistical contribution in regression equations for the surface roughness.
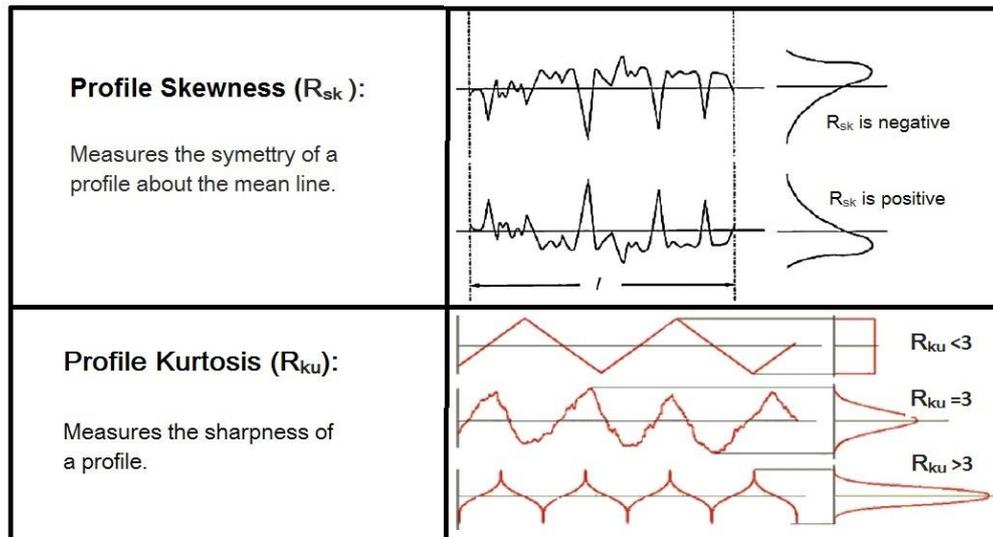
Figure 2-17- Profile skewness and kurtosis.

2.4-2 Surface Roughness Measurement Methods

A brief look at some of the different methods which can be used to measure surface roughness are described. A detailed explanation of surface texture measurements methods is described by R. Leach [51],[52]. The standard methods being contact profilometers which work by trailing a stylus tip and measuring the profile deviations. The stylus tip is usually diamond tipped and carefully manufactured with a small radius often in the region of 2-10 μm [51]. To measure surface roughness, a transducer is used to detect profile deviations on the surface and then subsequent amplification of the signal is introduced, this is followed by filtering of long wave profile spatial frequency components [51]. There are a number of errors which can be associated with stylus tip measurements, including deformation of the material by the stylus tip and skidding of the stylus tip. Additionally, the dimensions of the stylus will introduce filtering and levelling errors, and the calculation method which is applied to sample and filter the profile information will affect the obtained results. A number of these issues are detailed by R. Leach [51]. In roughness measurement, stylus devices are often used to make profile line measurements of the sample, however, it has become increasingly important in to be able to

46

take areal form and roughness measurements. As a result of being able to take areal measurements there is more capability to fully characterise surface structure and to make informed decisions about how profile form may affect in-service performance and the function of components and materials. Although it is possible to take areal roughness measurements with specialised profilometer devices, scanning times can take several hours because they must take multiple line measurements. Therefore, optical devices can become advantageous when taking areal topography and roughness measurements because the scanning time can be significantly reduced.

Other methods exist: for example non-contact methods like coherence scanning interferometry (CSI) and focus variation devices which can be used to take areal texture measurements and create surface images. CSI devices work by using white light and the localisation of interference fringes, the devices can determine topography and optical properties of the surface. This method can also be called vertical scanning white light interferometry. CSI uses two beams of light, which can interfere constructively or out of phase to give destructive interference. A low coherence light source is used which has a short coherence length and determines the ease at which a light source can interfere with itself [52]. A beam splitter is used at the objective lens to split the light, where one is directed at a reference mirror and the other light beam at the measured sample. The reflected beams from mirror and sample are recombined, and the optical path length of the two beams must be very nearly identical for interference to be seen at the detector. The detector measures the light intensity at different vertical distances to the sample and the light intensity will vary due to the interference. The light intensity can be used to find the interference maximum and therefore the sample profile heights at each pixel can be determined [52]. Surface heights are determined by finding where interference effects are most strong and the intensity data for each pixel point

is determined over successive camera frames. Commercial coherence scanning interferometers are available from a number of different manufacturers. This method has a high vertical resolution and can be used for roughness measurements of very smooth surfaces and steep flanked or rough surfaces. It is also a non-contact method which means that it will not scratch the surface and is not dictated by the edge radius of the profilometer to get into sharp grooves like with a stylus.

Chromatic confocal microscopy is another optical method which can be used to find sample profile information. The principle works by using two pinhole apertures in front of the detector and light source. The optical path length from the detector to the specimen is the same as that from the emitted light source. Then, the vertical height to the specimen can be varied, and when the profile height is not in focus then the reflected light does not pass through the detector pin hole and there is zero intensity. On the other hand, when the height of the profile is in focus, then the light does pass through the detector pin hole. The system is on a vertical scanning system and therefore image intensity can be compared with profile height at different points on the surface. The disadvantage of this system is that it requires longer scanning times than other optical methods because the co-ordinate values of each point must be obtained with the moving of the instrument mechanism. The accuracy of the instrument will depend upon the spot size of the light source.

Another method is focus variation devices which work by using the small depth of focus of an optic to take multiple images at different vertical distances from the sample. A full high resolution 3D image can be constructed which can be used to make high accuracy form and roughness measurements and can also capture colour information. The method works by searching for the best focus position of an optical element which then has a certain distance value from the sample, this process is carried out a number of times and a depth

map of the sample is created. By moving the distance of the sample to the objective lens, then the image will be in varying degrees of focus from low, to high and then to low again. Lenses with a narrow depth of field are used because they have a limited focus range [51]. A CCD sensor is used to detect image focus by using contrast information at isolated points on the image. The standard deviation of the contrast between pixels can be used to detect image focus. The contrast between grey values of pixels in an isolated region will have a low standard deviation when the focus is very low. In reverse, when there is focussed image then there will be a high standard deviation of the contrast between neighbouring pixels [51]. The position of maximum focus must then be calculated by finding the peak point in the focus curve.

Focus variation can capture information from very rough surfaces and steep flanks with a high vertical resolution. However, it does have difficulty measuring on very smooth or highly reflective surfaces. Some of its main applications are topographical measurements and form and roughness measurements of machined surfaces and cutting tools. A focus variation method has been applied in the current study using commercial system manufactured by Alicona. This method has been used because of its ability to perform high accuracy areal roughness measurements and give colour information. It can be used to take areal scans of relatively large dimensions, which will be tested to see if it proves advantageous when applied on a non-homogeneous composite surface. It has also been applied to perform cutting edge radius measurements to quantify tool wear.

2.5 Cutting Tools for Composite Machining

The challenges of machining composites have also lead to the development of new cutting tools. During machining the cutting tools are under intense localised pressure, high temperatures and friction. Due to the strong abrasive wear of carbon fibres early researchers of machining found insufficient wear

resistance of standard cutting tools such as, high speed steel, cemented carbide and existing nitrogen and carbon based coatings [2],[53]. These tools were also shown to leave a surface with a poor surface quality [54],[55]. It has been shown that the initial tool geometry and tool wear will play a critical role in surface roughness, edge delamination and burring [3]. It is necessary to have a sharp cutting edge to be able to cleanly shear and cut fibres and reduce delamination or un-cut fibres. Tool wear will lead to a decrease in the surface quality, therefore tools with a good wear resistance are required. The superior qualities of PCD and diamond coated tools, plus an improvement in their manufacturing methods has led to these becoming increasingly used in composite machining. These tools have very high hardness and have an increased tool life over more standard tooling.

Initial tool geometry and tool wear have been shown in the literature to play a critical role in surface roughness, edge delamination and burring. J. Zhang et al. [54], looked at the performance of CVD coated tools compared to standard WC-CO tools, (tungsten-carbide with cobalt binder), and they found that the CVD tools had a superior wear resistance and produced more holes with a higher hole quality. The first diamond coated tools were researched yet these had insufficient layer adhesion and suffered from coating delamination [53]. However an improvement in the adhesion of the diamond coating by new manufacturing methods has led to these tools becoming increasingly viable for high quality carbon fibre machining. The benefits include tool life in excess of 10 times that of uncoated tools [56]. Diamond coating is deposited onto the base tool geometry in a thin layer by chemical vapour deposition (CVD) or physical vapour deposition (PVD). This is done in a vacuum chamber at high temperature and pressure, where carbon gas is introduced to form a pure crystalline diamond structure on the tool surface. High concentrations of hydrogen gas are used in the chamber in order to stabilise the bonding of

50

diamond and prevent the generation of unwanted graphite films [57]. Typically diamond coating of thickness of around 5 microns is formed on the surface [55]. The diamond coating has the advantage that it can be deposited onto complex base tool geometry, but the coating will still increase the cutting edge radius on the tool. The cutting edge radius and the roughness of the diamond coating will generally be higher than that of PCD tools which have been ground to a smooth finish [58].

 PCD tools are another alternative to diamond coated tools for composite machining and they utilise the superior material properties of diamond. PCD tools have a measurable increased tool life to that of standard grain size diamond coated tools [58]. These tools can also be manufactured with a sharp cutting edge by grinding or laser cutting, and the PCD edge is resistant to abrasive wear. The PCD is manufactured by sintering together diamond powder at high temperature and pressure to create a disordered diamond crystal. Usually it manufactured by sintering the powder with cobalt binder onto a backing disk or stud with a cobalt binder to create a thin layer [59]. The disks can be around 60mm diameter and 1.7-4.6mm thickness [60]. The diamond crystal can then be cut by electro discharge machining into segments, and then must be ground or laser cut in order to create the required geometry which can be used for a cutting tool edge. The segments are generally soldered or brazed onto the cutting tool base in order to create a cutting edge. Figure 2-18 shows a PCD disk on a tungsten carbide backing which is then cut into segments and can form part of the tool [61].
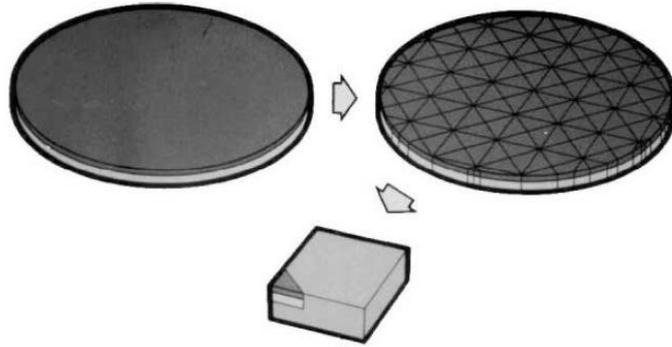
Figure 2-18 – PCD disk which is then cut into segments before brazing onto tool [61].

P.S Sreejith et al. [62] evaluated PCD tool performance while machining of carbon composites. They looked at machining temperatures and cutting pressure. It was found that during machining the tool will experience thermal and mechanical stresses, and that the matrix and fibre exhibit quite different mechanical and thermal properties. During composite machining there is a non-continuous chip produced, and because the material has non-homogeneous directional properties, there will be a variation in dynamic loading during the machining process. They found that the PCD edge will wear due to abrasion but also there is low cycle fatigue due to dynamic load fluctuation and edge chipping. As well as abrasion some of the wear was attributed to spalling by the mechanical load fluctuation and fatigue. In spalling, small flakes or chunks of material will be broken off by crack propagation.

Faraz et al. [63], have assessed the cutting edge rounding (CER) as a wear indicator in machining of CFRPs using drilling. They stated that the tool wear is due to an evenly distributed abrasive wear along the length of the cutting edge in the machining of CFRPs. Fibre abrasion was given as the dominant wear mechanism and the cutting edge rounding is a useful indication of tool bluntness or sharpness due to wear. Hole delamination was quantitatively

52

assessed along with drilling forces. A strong correlation was seen between thrust forces and hole exit/entry delamination with measured cutting edge rounding. Linear regression equations were used to show the effect of CER and thrust force on delamination. CER is also explained to be a useful analysis parameter to use for tool wear analysis because at new tool condition with zero wear there will be a non-zero edge radius. Therefore cutting edge rounding is a purely quantitative parameter intrinsic of current tool geometry unlike with flank wear (V_B) measurement, which measures loss of material.

Diamond coated and PCD tools have a low coefficient of friction, and in addition they also have good chemical and thermal stability at high temperatures. PCD tools have a relatively stable hardness at high cutting pressure and temperature, which is due to the superior properties of the diamond [62]. Generally PCD tools have an increased tool life compared to that of standard grain size diamond coated tools [58]. However PCD can cost as much as 3-5 times that of diamond coated tools and 6-10 times that of uncoated carbide [56]. In this research the use of PCD and diamond coated tools has therefore been applied and the effects of tool wear have been realised as having an important effect on surface quality.

2.6 CT Scanning for Sub-Surface Damage Inspection

As well as surface damage in the form of delamination and surface roughness, it is also possible that there is damage below the machined subsurface. Therefore experimental methods and non-destructive techniques are required which can show the machining damage or manufacturing defects which may lie below the surface of fibre composites. For example, many damage types like delamination, micro-cracks and fibre breaks could be present, or manufacturing defects like excessive voids, fibre waviness and inclusions. Sub-surface damage caused by machining could adversely affect the material strength and integrity of components or give rise to unexpected failures.

Therefore there is a need for techniques which can show the machining damage or manufacturing defects below the surface of fibre composites which will not be seen by optical microscope or SEM images.

X-Ray micro tomography or (micro- CT) is a technique which has been used in order to assess fibre composites using specialist equipment. The specimen is radiographed many times around a rotated axis which allows a 3 dimensional internal image of the component to be generated [64]. The variation in the intensity of unabsorbed radiation is seen as shades of grey on the radiograph. The rotation of the axis must be used because cracks which do not have a significant depth in the beam direction will not be seen in the image. High resolution images of the specimen sub-surface damage can be seen, giving full through thickness damage indication. The matrix and carbon fibre have low absorption of the X-ray therefore good contrast could be difficult to obtain. In some instances penetrant liquids with high absorption have been used to increase contrast and crack definition, but the cracks must pass through the surface. The penetrant liquid is applied onto the surface to look for cracks which propagate into the material.

P. Shilling et Al. [65] used a SkyScan 1072 desktop X-ray micro scanner to analyse damage in graphite and glass fibre composites with and without penetration dye. It was found that the size of voids could be determined in the glass fibre without dye. However in the carbon fibre the micro cracks could not be resolved well without the use of dye penetrant which increased the visibility. The use of the dye was found to give good resolution to the cracks but it was reliant on the connectivity of the cracks. Figure 2-19 shows the comparison between images from CT with and without dye penetrant and an optical microscope image taken of a cross-section.

54
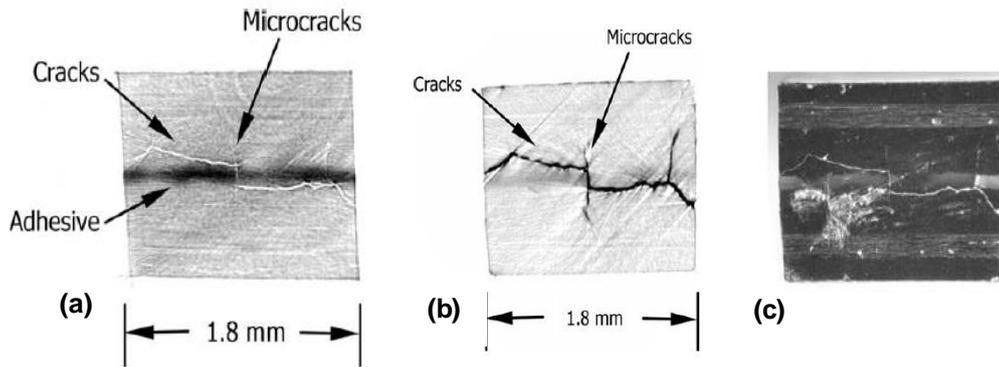
Figure 2-19- Comparison of images taken of a carbon fibre specimen by Micro-CT scan (with and without dye penetrant) and optical microscope.
(a) CT image section without dye penetrant,
(b) CT image section with dye penetrant, (c) Optical microscope. Adapted from REF [65].

P. Wright et al. [66] used the synchrotron radiation computed tomography (SRCT) which can achieve very high resolution down to 0.3 μm to analyse damage in CFRP material. A multidirectional notched laminate was loaded in tension and the inter-laminar cracks and delamination and also fibre breakage can be analysed. The intensity spectrum of the absorption of the different phases of the material including cracks can be used to create a greyscale image. Figure 2-20 and Figure 2-21 show two different image cross-sections taken from the SRCT images. A high resolution image is shown which shows inter-laminar cracks and fibre breakage present in the material. The authors reported that this was the first study to look in such detail at a fibre composite using SRCT image but it was not applied to machined specimens.
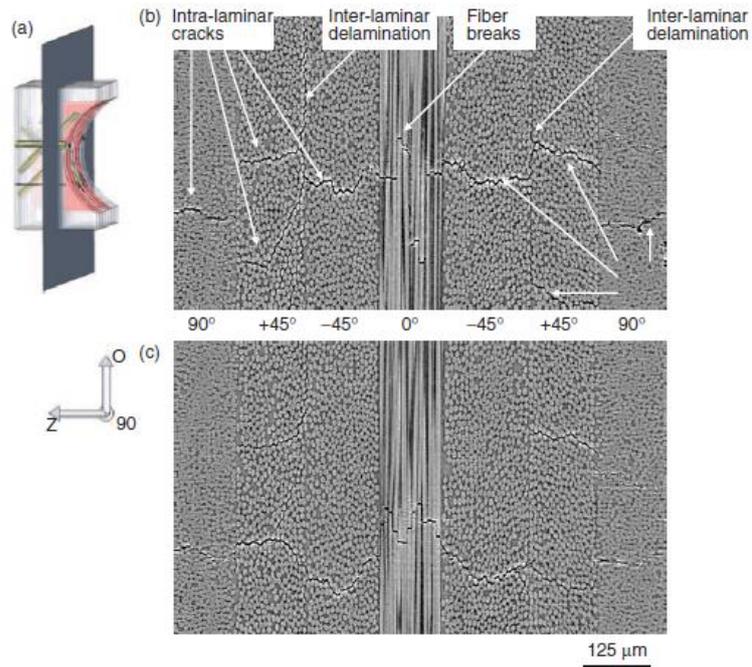
Figure 2-20- Two cross section images taken by SRCT ahead of crack notch. Showing Inter-laminar delamination and intra-laminar cracks [66].
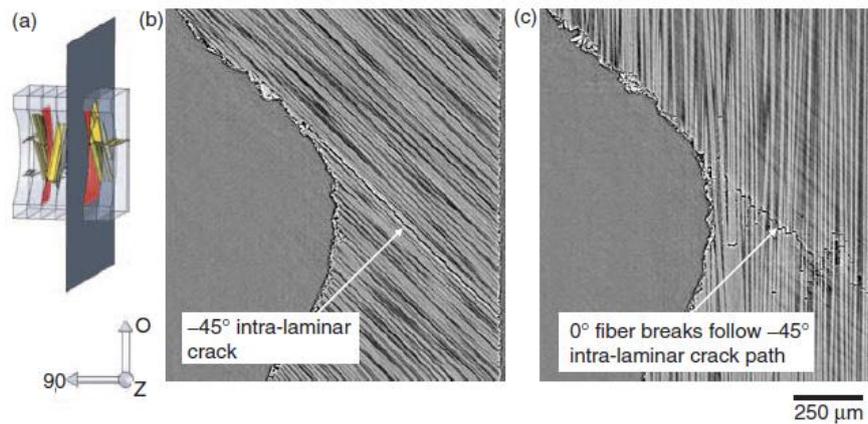
Figure 2-21 - Cross sections taken by SRCT through 45 and 0 degree ply. Showing crack paths through the material [66].

V.A Phadnis et AL. [6] used a CT scan to find drill entry and exit delamination to validate a 3D drilling FE model. The 3D Micro-CT scan had the advantage of being able to see the delamination area at the entry and exit. A code was developed in Matlab in order to quantify the delamination size from the 3D scans, using the delamination factor which is based on the delamination area.

The 3D CT scan is shown in Figure 2-22 which shows the different grey scale for the hole delaminated areas, however the damage must be correctly distinguished from the hole delamination and undamaged areas.
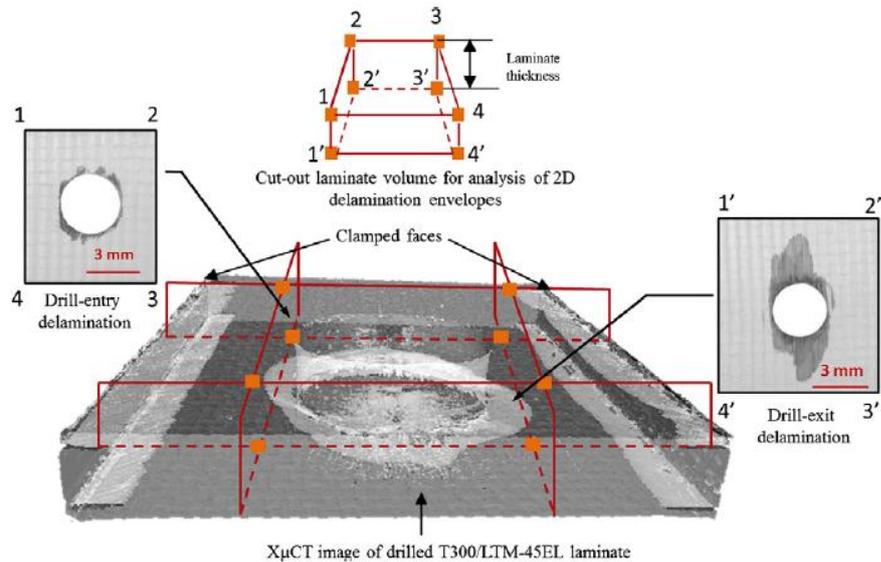
Figure 2-22 - CT scan of drill entry and exit delamination [6].

Some other researchers have used CT scan to analyse drilling delamination, including Tsao & Hocheng. [67], who used C-Scan and CT scan to analyse the delamination due to drilling from various drill bits. They found the C-Scan and CT scan both performed similarly for this application and were able to image the delamination area. There is however a need for application and research of CT scanning technique to the milling process, which will be useful to understand how the milling process may affect the subsurface which cannot be seen by standard technique. The milling process differs significantly from drilling and the damage may be more difficult to observe if it is not contained mainly to the top and bottom laminate layers as delamination. CT scanning can be applied to look for subsurface damage, including inter-laminar delamination and matrix cracking. CT scanning may also be able to expose manufacturing defects, or damage which is caused by machining, that would not be revealed by using surface imaging methods.

2.7 Finite Element Modelling for Composite Machining

The use of finite element or numerical modelling to analyse the machining process has growing interest because it can reduce costs during expensive machining trials. There has therefore been progression of FE methods from initial machining of metallic materials and then developing of models to be applied for the machining of fibre composites. Early researchers into FE modelling for composite machining have developed 2D methods for orthogonal turning. A number of models currently contained in the literature have used orthogonal machining, and two different methods have generally been used in this approach. The first is the Equivalent Homogeneous Material (EHM) approach: the composite material is modelled as an orthotropic material in a single phase [9],[8],[68]. Here the material will have modulus and failure properties in the two principle directions depending upon the matrix and fibre properties, and plane stress or plane strain conditions. The second approach is a micro-mechanics approach where the fibres are modelled in separate phases, with an interface or cohesive elements between them to replicate the fibre-matrix bonding and de-cohesion [69],[70],[71]. Here, the elastic properties and separate failure modes of the two parts must be modelled with a separation criterion at the fibre-matrix interface, cohesive elements have often been used to allow separation. It can then be possible to see stress, strain and damage variation throughout the two phases of the material- matrix and fibre. Figure 2-23 shows a multiphase approach looking at the effects of using different rake angle tools.
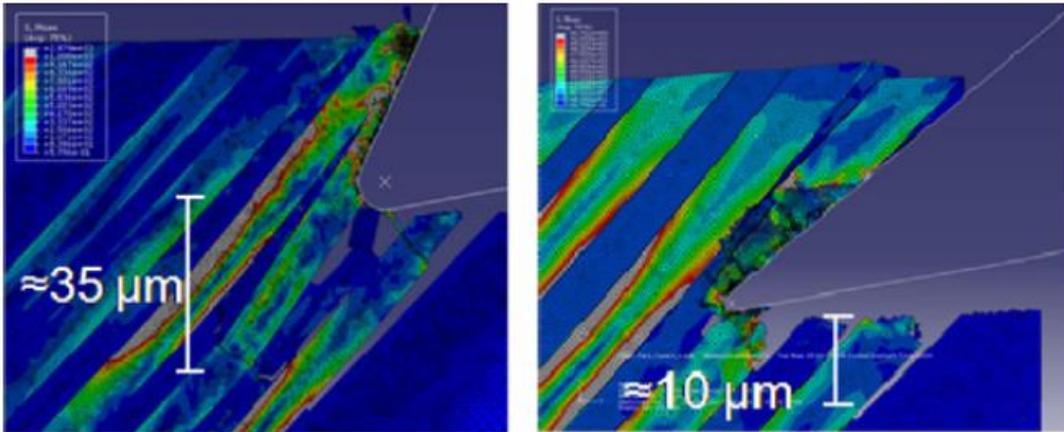
Figure 2-23 - Finite element model of composite machining to simulate use of a new high rake angle tool [71].

Some authors have also looked at 3D approaches to modelling: Santiuste et al. [72] compared a 2D and 3D orthogonal cutting model for machining of carbon long fibre composite with an EHM model – Figure 2-24. The 3D model can be used to model both unidirectional and quasi-isotropic laminates with variations in stacking sequence, or fibre orientation, and look at out of plane effects on machining. In contrast, 2D models can only be used to model unidirectional laminates and use plain strain or plane stress assumptions.
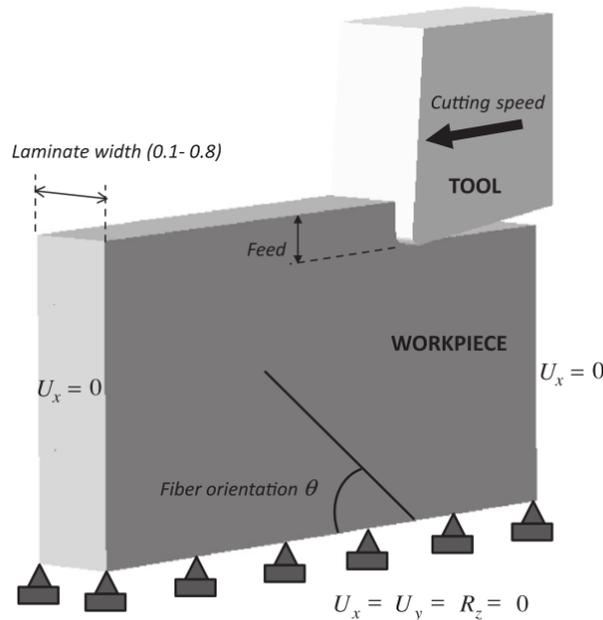
Figure 2-24 – 3D EHM model of orthogonal turning [72].

Some recent orthogonal machining research by Xu and Mansori [73],[74] has looked into machining of CFRP/Titanium stack. Cutting Speed, feed rate, friction coefficient, and material fibre orientations have been selected as input parameters for the model. They achieved a good comparison between FE model and experiment and they found different chip morphologies between titanium and the CFRP. In the CFRP there was small dust-like chips, while in the titanium there were continuous and serrated chips. They also looked into a simulated R_a by selecting 100 sampling nodes along the cutting length of 1mm. The machined surface R_a of the titanium was found to be lower than that of the CFRP. The CFRP surface was found to be more influenced by friction factor than titanium. However, the R_a value was dictated by the mesh size and therefore it is an estimated value. They also analysed the interface damage between the composite titanium bond interface using cohesive elements.

 Gao et al. [75] have performed experimental milling test and orthogonal FE simulation of multidirectional CFRP laminates at four different fibre orientations. Diamond coated and cemented carbide tool were used for machining, with SEM and stylus measurements to assess surface quality and roughness respectively. They used a 3-D micro mechanical model with ABAQUS/Explicit where the matrix and fibre have been modelled as separate phases. They introduced a thermomechanical model based on heat production produced by coulomb frictional law, where a different friction coefficient has been applied at different fibre orientations. In this model they have compared orthogonal FE model with experimental milling model where there is not orthogonal cutting in machining by milling. They have analysed cutting forces versus fibre orientation angle and surface roughness versus fibre orientations. The different cutting mechanism found in their simulations according to fibre orientation is shown in Figure 2-25. They have also analysed the contribution of different machining parameters on the surface roughness using ANOVA and

found that fibre orientation, cutting speed and depth of cut had the most significant effects on roughness. A slight decrease in roughness was found with increasing cutting speed, while an increased depth of cut lead to a higher roughness.
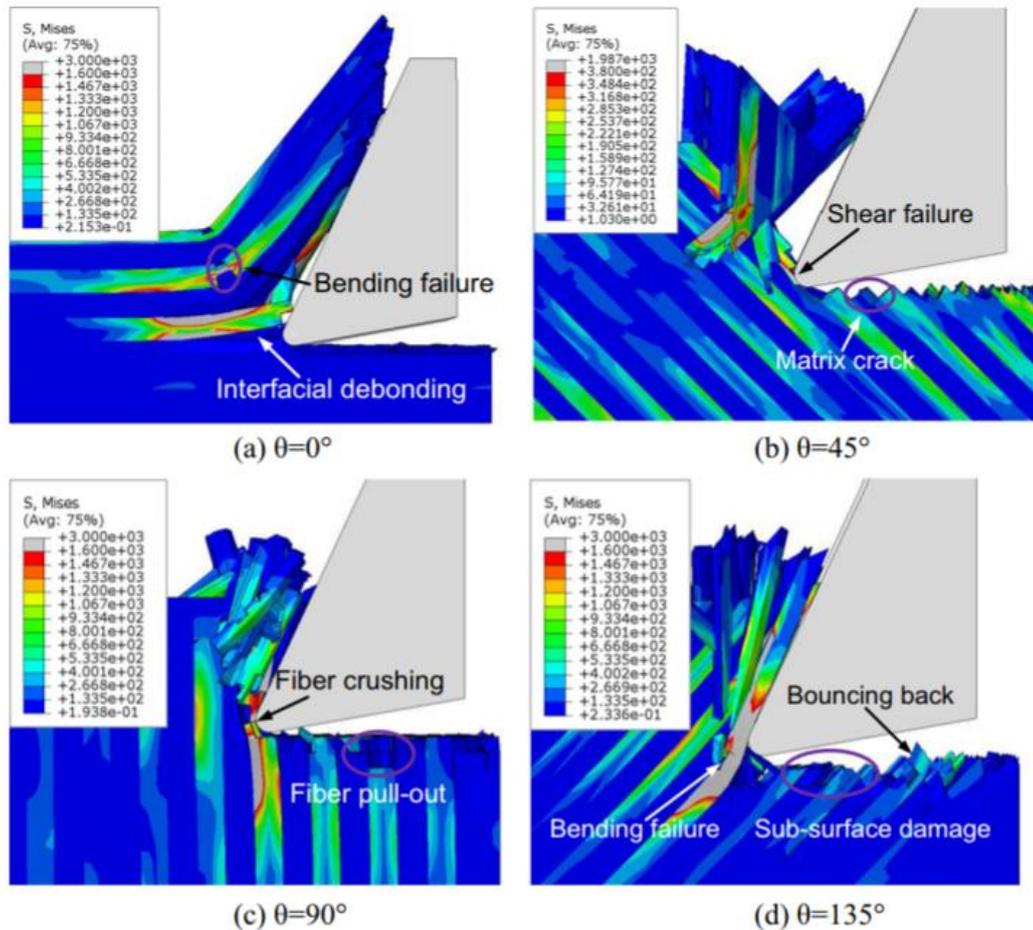
Figure 2-25- Cutting mechanism on different fibre orientations in micro-mechanical orthogonal cutting model. Adapted from REF [75].

These methods have developed FE methods for the composite machining process although they are limited to orthogonal machining process which cannot be applied to the milling or drilling process. As milling and drilling are extensively used in industry both in composites and metallic manufacturing, it is therefore of high importance to improve finite element capabilities in this area.

Some more recent research into the drilling of composites has been performed by V.A Phadnis et al. [6]. The authors analysed drilling of CFRP using a 3D finite element model, and the Hashin's criteria is used to model fibre failure in compression or tension, while Puck's criterion is used for the matrix failure. The model is shown in Figure 2-26. The model used to predict the torque and thrust forces as a method to optimize drilling parameters in order to reduce delamination. A recommendation of low feed rates and high cutting speed was recommended to reduce drilling delamination. They used Abaqus Explicit with user subroutine in order to create material failure models.
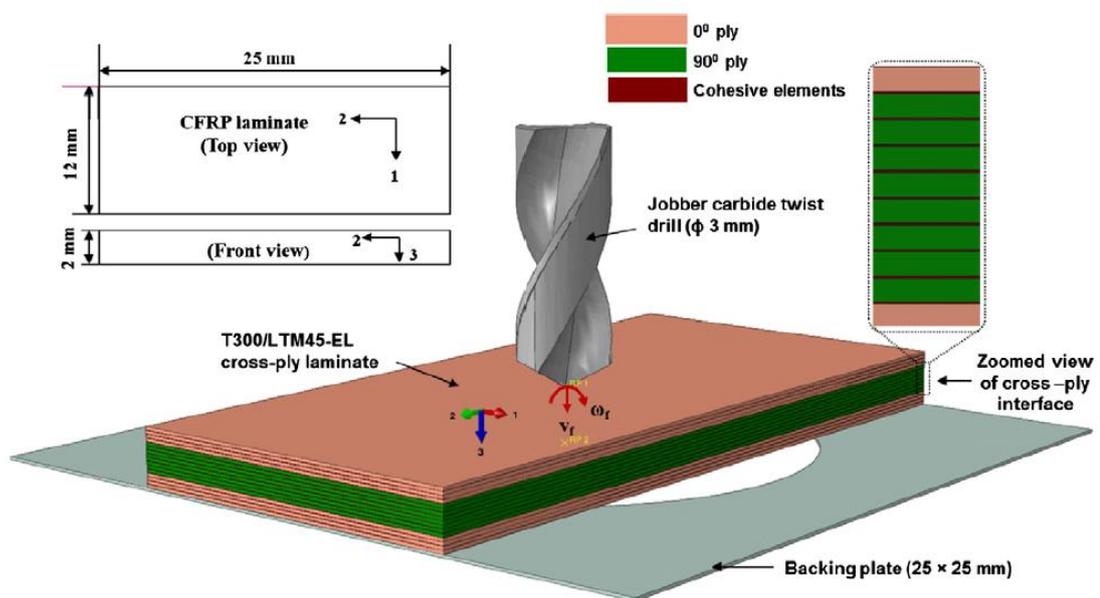
Figure 2-26- Drilling CFRP laminate 3D model [6].

From the literature review it has been found that there is a lack of research contained in the literature to date for the simulation of milling fibre composite materials. A 2015 review by Kahwash et al. [76], focussed on different processes for modelling of fibrous composite machining did not show any current literature for the milling of FRP composites. As milling is a commonly used process in industry it is therefore of importance to further research into FE methods for predicting the milling of composite materials.

2.8 Discussion- Literature Review

From the findings in the literature review and the proposed direction supported by Rolls-Royce, it was decided to focus on the experimental milling process. Although drilling has been found to be a commonly used process in industry, Rolls-Royce uses an edge trimming process during their manufacturing and was therefore interested in furthering research into the surface damage caused during machining. It has also been found that the experimental research contained in the literature into drilling is more comprehensive than milling and therefore research into the complex milling process of fibrous composites is a requirement. Consequently, this project has focussed machining surface damage, roughness measurements methods and improving the capabilities of modelling for edge trimming using novel 3D and 2D FE simulations.

From the literature review, it has been found that it is important to be able to predict and accurately measure surface roughness during a machining process. It is a requirement to be able to accurately measure roughness to ensure the in-service integrity of components, understand and quantify machining induced surface defects, and ensure an efficient and cost effective machining process for industrial applications. Therefore in this project new methods to improve surface damage characterisation will be developed. The use of the Alicona focus variation optical system will be investigated to improve the accuracy of machined composite surface roughness measurements. New roughness measurement strategies will be applied to expansively quantify damage and cutting mechanism of a machined surface at different fibre orientations. Additional roughness parameters including areal roughness parameter S_a, will be studied to give a more thorough and accurate description of machining damage of a multidirectional laminate. Skewness (R_{sk}), and kurtosis (R_{ku}) roughness parameters will be also be applied to a machined

composite surface to assess surface defects and characterise surface topography across different fibre orientations.

It has been found in the literature that methods for the prediction of surface roughness in composite machining are few. Also that predicting the effects of tool wear using finite element simulation in an edge trimming process has not been thoroughly researched for a carbon fibre composite. The literature has shown that tool wear will have a critical effect on surface quality and delamination, and that there is a requirement for development of new cutting tools for composite machining. The effects of tool wear on machined surface quality will be assessed in this work using cutting edge rounding to quantify edge condition from experiment.

A flow diagram of the issues which have been found from the literature are shown in Figure 2-27. The diagram also shows the proposed project outline. The project has started with the initial question of assessing damage from a composite machining process. From this, the diagram outlines the initial generation of improved characterisation methods for surface roughness measurement with additional roughness parameter assessment. The research flow diagram requires an improved characterisation method for roughness evaluation which will then be applied in experiments to develop a new roughness prediction strategy. The strategy will combine FE and regression equations which will be validated by machining experiment. The regression equations will be trained and developed using experimental data including the effects of tool wear, feed rate, cutting speed and cutting forces and further show how they will affect the generated surface roughness.

Project Plan

Surface Defects Assessment:
Machined Composite Surfaces.
(Assumption: Find CFRP
Machining Defects)

Issues: Stylus Measurements
Roughness Parameters
Roughness Prediction
FE Modelling of CFRP Milling

Define Problem:
Surface roughness measurement
of machined composite surfaces.
(Milling, Edge Trimming)

1. Non-homogeneous surface.
2. Variation in damage with
   fibre orientation.
3. Stylus Measurements.

Literature   Review

Method

Measurement Solution

Metrics: Roughness Parameters

Surface   Analysis

Effects of Material
Non-homogeneity on
Machining Defects &
Cutting Mechanism

Apply Solution:
Improved Characterisation of
Surface Damage

Accurate Assessment of Machining
Parameter Effects on Surface Quality
& Machining Defects.

(Tool Wear, Feed Rate, Cutting Speed)

CT-scanning

Experimental   Analysis

Model Validation

Experimental Data
Inputs: Edge Rounding
Feed Rate
Cutting Speed
Outputs: Roughness (Sa)
Cutting Forces (N)

Virtual: FE Modelling
Cutting Forces Assessments

Predictive   Tools

Chip Formation
(Fibre Orientation Effects)

Virtual: Cutting Forces

Regression Model
(Model Training)

Experiment:
Outputs: Roughness (Sa)
(Validation)

Indirect Roughness Prediction
$Sa, R_{sk} R_{ku}$

Effect of Changes in CER
(Tool Ageing)

Figure 2-27- Flow diagram of project requirements.

The project will be split initially into a development section where a baseline set of initial experimental tests will be performed to assess machining damage and improve upon experimental methods for roughness measurement. The findings from this test will be used in the following experimental tests, and following this, roughness measurement methods will be applied to generate new roughness prediction tools. Experimental milling tests using a PCD tool will be performed to generate different roughness samples, these will then be measured using a new optical measurement strategy, and the samples used to generate regression equations for the surface roughness. Consequently, a combination of regression equations and FE methods will be used to generate new prediction tools and allow assessment of how the surface roughness will be affected by changes in machining parameters and tool wear. Novel finite element models will be developed using a user subroutine to control the cutting tool movement and adaptive meshing of the CFRP workpiece is applied. The experimentally obtained regression equations for the surface roughness and the developed FE models, will be used to generate a new method for predicting surface roughness in a CFRP edge trimming process. The projects aim is to generate a method for predicting surface roughness and this method will be able to assess the effects of increasing tool wear and different machining parameters on the surface quality. Combined with the developed new roughness measurement strategies this project will improve the understanding of damage and defects in a composite machining process and can be applied to improve the efficiency of machining and the integrity of machined components.

Finally, the literature has also shown that CT scanning can be successfully used for damage detection in fibre composites, including carbon fibre. However, most CT scanning in the composite machining literature has been applied to

look at the exit delamination of drilled holes. CT scans will hence be applied to look at defects in a machined subsurface from milling and to see if there is internal damage which is not apparent from optical images, surface roughness measurements and SEM scans. The occurrence of subsurface delamination and matrix cracking will be assessed using a CT scanner. It will also be a useful assessment because it will indicate if roughness measurement alone can make an evaluation of machining damage or if other measurement strategies need to be applied to ensure safe in-service components. SEM images and CT scanning will be applied to multidirectional and unidirectional laminates to assess the effects of fibre orientation on the machined surface quality, the cutting mechanism and the damage depth. Therefore this research project aims to take a comprehensive look at the machined surface and surface roughness generated in an edge trimming process with the use of new predictive methods and optical surface assessment.

Chapter 3
Preliminary Assessment of Surface Roughness Measurement Methods

3.1 Evaluation of Optical Based Alicona Technique

From the literature review it has been highlighted that there are problems with the current stylus methods for characterising surface roughness. Therefore it was decided that the first part of this project would make a thorough assessment of surface quality, surface damage and surface roughness measurement methodology. The following section will assess roughness measurement methods and make a detailed characterisation of surface damage on unidirectional and multidirectional composites at different fibre orientations and machining parameters, using the optical focus variation system and SEM imaging.

An initial set of experiments have been performed to focus on machined surface characterisation, and techniques for the surface roughness measurement of a machined multidirectional laminate. This is used as a benchmarking study to assess roughness measurement methodology and characterise machined surface quality using different roughness parameters. It has been shown in the literature review that there are reliability issues with current standard roughness measurement technique using the stylus method. Therefore the Alicona focus-variation optical system has been evaluated in order to measure surface roughness and the potential advantages of this system have been discussed. The use of areal roughness parameters (S_a) and other roughness parameters including skewness and kurtosis have been assessed to give a more thorough description of the surface damage and machining defects. The skewness and kurtosis has been analysed on the machined surface of different fibre orientations to give a thorough analysis of

cutting mechanism and surface quality on each fibre orientation and therefore quantify surface damage across a non-homogeneous surface structure. SEM micrographs of machined surface have been applied to investigate cutting mechanism and damage types across each different fibre orientations. The effects of cutting parameters feed rate and cutting speed have been assessed on surface quality. The suitability of using the Alicona focus variation system for roughness measurement over conventional stylus measurement has then been discussed.

3.1-1 Experimental Set Up

Machining was performed on CMS Ares 5-axis Machine Tool. The CFRP machined laminate has a 0/-45/90/45 stacking sequence, with a full thickness of 4.1 mm and 22 plies, shown in Figure 3-1b. The fibre orientation definition is shown previously in Figure 2-6. The composite is a commercially available CFRP with epoxy resin as matrix binder, and is manufactured by pre-preg lay-up and autoclave curing. The cuts were performed with full tool holder diameter width of cut, i.e. a_e= 25 mm, and an axial depth of cut of a_p= 4.1 mm, shown in Table 3-1. A 52 mm length of cut was applied. A poly crystalline diamond (PCD) tipped insert manufactured by Sandvik was used and it was held using a 25 mm diameter tool holder which is described in

Table 3-2. The cutting tool is shown in Figure 3-1a. A single insert was used with one cutting edge on the tool. Four levels of feed per tooth and cutting speed were applied as shown in Table 3-1.

Table 3-1- Cutting test parameters.

Feed per Tooth (mm)	Feed (mm/min)	Cutting Speed (mm/min)	ap (mm)	ae (mm)
0.025	17.75	85	4.1	25
0.04	28.41	175	-	-
0.06	42.61	225	-	-
0.075	53.26	285	-	-

Table 3-2- Insert and tool holder properties

Insert Holder	Make	Sandvik Coromant
	Serial no.	SC6320156
	Helix Angle	0°
	No. of Flutes	4
	Tool Diameter	25 mm
	Material	Solid Carbide
	Cutting Direction	Right Hand
Insert	Make	Sandvik Coromant
	Serial no.	R390-11T304E-P4-NL CD10
	Clearance Angle – AN	21°
	Rake Angle	21°
	Insert Width – W1	6.8 mm
	Cutting Edge Effective Length – LE	11 mm
	Major Cutting Edge Angle	90°
	No. of Inserts	1
	Cutting Material	PCD brazed to WC
	Corner Radius – RE	0.4 mm
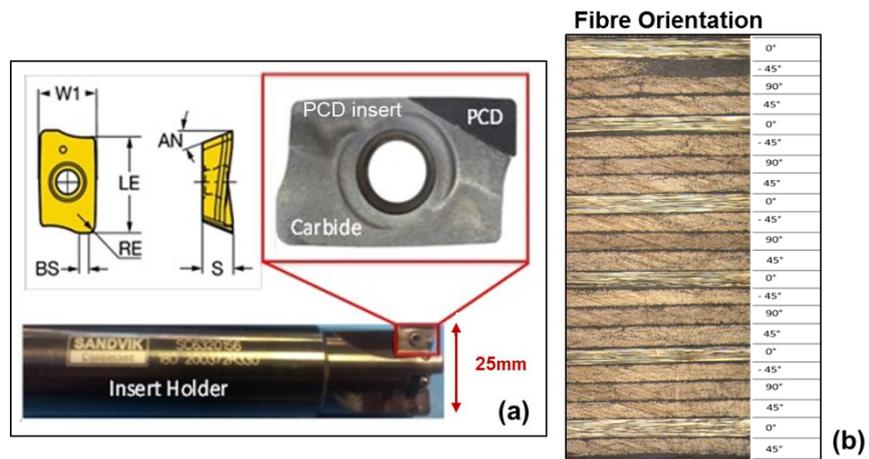
Figure 3-1- (a) PCD insert and 25 mm diameter tool holder,
(b) CFRP material fibre orientation lay-up and stacking sequence.

The workpiece and fixture used in the setup is shown in Figure 3-2. The workpiece is clamped by holes onto the fixture and there is a full-slot machined through the workpiece.
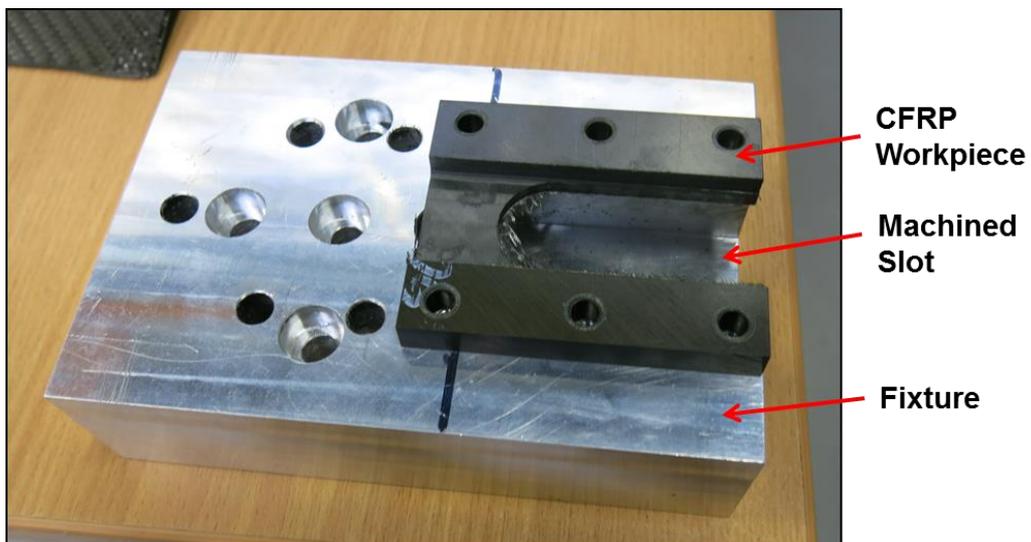
Figure 3-2-Experimental setup of machined slot, workpiece and fixture.

3.1-2 Roughness Measurements

Surface profile measurements have been taken in this study using optical scans with a commercial optical system which is manufactured by Alicona. The system can be used to create three dimensional surface images which capture

72

colour and topographical information. The system works by focus-variation, using the limited depth of field of an optic and optical sharpness to take multiple images at progressing vertical distances from the sample. A full high resolution 3D image is created and the profile height information can be used to calculate form or roughness parameters. An image of the Alicona "InfiniteFocusSL" system is shown in Figure 3-3(a), with a schematic diagram in Figure 3-3(b). The optical system allows the analysis of different roughness parameters including areal surface roughness parameters like S_a. The system operation is detailed by R. Danzl et al. [77] and [78]. The capability of the system to attain comparable roughness measurements with a calibrated stylus device is described. Roughness measurements are made using a standard roughness specimen.

As shown previously in the literature there are reliability issues with using conventional stylus measurements for the measurement of machined composite surfaces. It has been found that the use of surface areal parameters can be useful for composite surfaces due to the non-homogeneous structure and variation in damage across the surface. This will be discussed. The author has published journal paper on the application of this system for the machining of composite materials and detailed the advantages of this system over standard profilometer measurements. The use of alternative roughness parameters like S_a, skewness (R_{sk}) and kurtosis (R_{ku}) are also described [79]. The results of this paper are summarised in this experimental section.
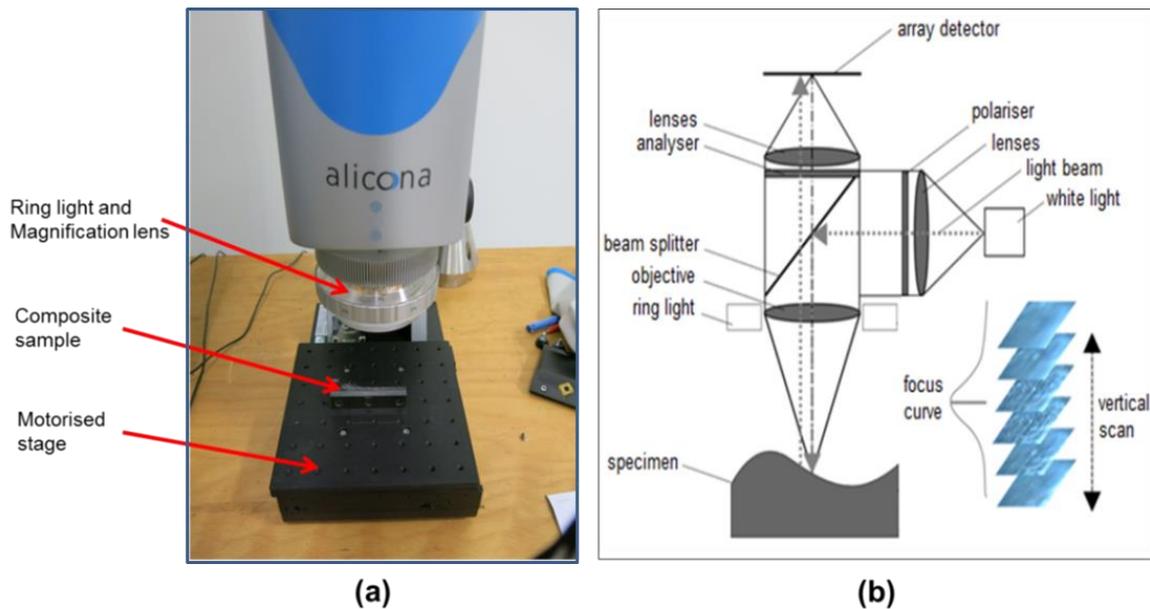
Figure 3-3- (a) Alicona system and composite sample,
(b) Schematic diagram of system.

3.1-3 Measurement Method

Surface texture measurements were taken using the optical system from the side of the slot in conventional or climb milling. It is known that conventional or climb milling on either side of the slot result in a different cutting mechanism and therefore surface qualities. All of the texture measurements were taken from the side of the slot which is in conventional milling and is the intended machined surface to be left on the part. Also, to be consistent, all of the measurements were taken from the same side and in the same position. The focus variation surface scans for roughness measurements were taken in the centre of the machined sample surface in the through thickness and machined length directions. A scan size of 2mm by 2mm was applied as shown in Figure 3-4. Subsequent roughness measurements of the individual layers of the laminate and of different fibre orientations have been calculated. The suitability of using transverse or longitudinal roughness measurements will be assessed- where transverse measurements lie perpendicular to the machining feed direction and through the laminate thickness. R_a, skewness and kurtosis

74

roughness parameters have been calculated for individual fibre orientations to assess variability in surface structure and cutting mechanism on each layer.
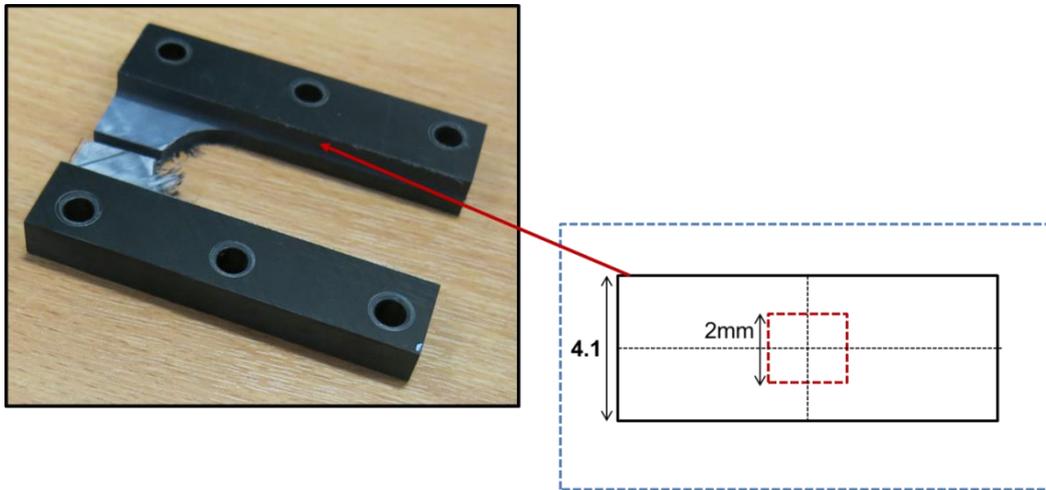
Figure 3-4- Position of optical scans for roughness measurements on sample.

3.2 Surface Damage Characterisation

An optical scan taken using the focus variation system is shown in Figure 3-5 of the multidirectional laminate. The surface texture can be visualised from the optical image. In Figure 3-5 is shown a close up of the profile where some pitts and smooth layers can be seen. The image shows that there is a variation in profile texture on different layers of the laminate. The surface scans are a three dimensional high resolution surface image which contains profile height information and can subsequently be used to calculate surface roughness parameters. The surface roughness parameters R_a, skewness and kurtosis are calculated.
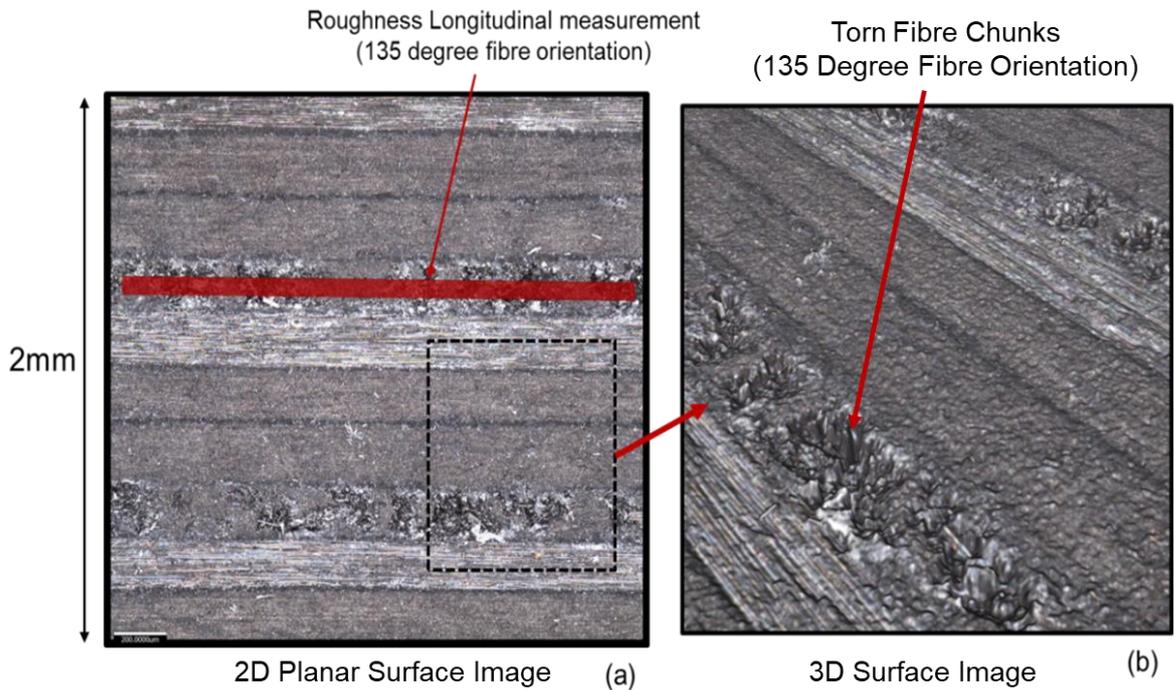
Figure 3-5- Optical focus variation surface scan of machined surface.
(a) 2D planar view of machined surface (2mm by 2mm). (Position shown in Figure 3-4).
(b) 3D Profile Texture Image.

The optical system allows the measurement of roughness along a defined path on the material, and therefore individual fibre orientations or ply layers can be measured- which is shown in Figure 3-6. The system was used to take roughness measurements across each of the 4 different fibre orientations- 0, 45, 90 and 135 degrees. As can be seen in Figure 3-6 there is a large difference in maximum profile height when the 0 degree- Figure 3-6b is compared with the transverse measurement- Figure 3-6c. This means that the position and direction of travel when taking roughness measurements must be consistent and accurate in order to achieve reliable measurements.
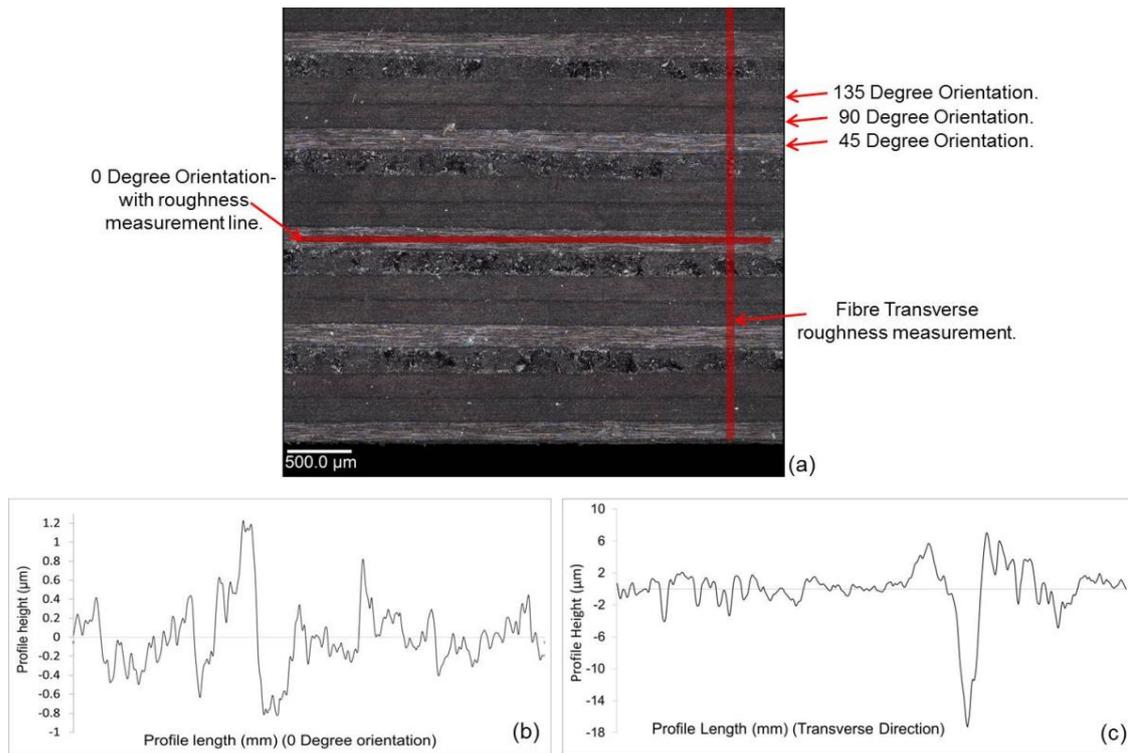
Figure 3-6-
(a) 3D surface structure images of multidirectional laminate measured by optical system. Red line shows the user selected roughness measurement path in transverse direction and a 0 degree laminate.
(b) Profile path for 0 degree fibre orientation,
(c) Profile path for transverse direction.

The optical system has been applied to take surface roughness measurements parallel to the fibre orientation. This is because of the significant difficulty in measuring by the stylus when measuring parallel to the fibre depending upon the position or angle of the stylus, as reported in the literature [5], [34]. Consequently, it very difficult to know which individual laminate layer or fibre orientation is being measured because they cannot be seen by naked eye and importantly they each have a slightly varying ply thickness, due to variation in material consolidation and thermoplastic matrix dense regions. The literature has shown, that the stylus path may not lie in parallel with the fibres or pass over multiple orientations, and therefore gives a variable and unreliable result [34]. Ramulu et Al. [5] has reported that stylus measurements made in the

longitudinal direction of a multidirectional laminate "appeared to be random." Importantly, their work has presented that it was possible to achieve accurate roughness measurements parallel to the fibre direction in a unidirectional laminate but not for a multidirectional laminate. Their roughness measurement results, of the multidirectional laminate, in the longitudinal direction were not deemed acceptable to present for this reason. Subsequently, it has been decided that the optical device is more suitable for measuring individual ply layers of a multidirectional laminate, and therefore the results for the surface roughness were obtained using the optical method to select individual plys. In addition it was rationalised that the stylus is not fully dependable to make roughness measurements of a multidirectional laminate in the longitudinal direction due to material non-homogeneity and fibre orientation effects.

Figure 3-7 shows an optical focus variation image of multidirectional machined surface which highlights the different surface damage on each of the fibre orientations. The position of the scan is a 2 by 2 mm image, which is perpendicular to the machined surface in the centre of the sample, as shown in Figure 3-7. The optical profile scan shows that on the machined surface the fibres lie parallel to the surface in the 0 degree fibre orientation. The surface is quite reflective and appears light in colour, and the 0 degree orientation surface is dominated by predominantly fibres. The chips are removed by fibre bending and de-cohesion between the matrix and fibre boundary. The fibres which lie on the surface appear to show little matrix material adhering to their exterior. In the 45 and 90 degree fibre orientation sheared fibre ends and epoxy matrix can be seen- the surface is relatively smooth. On the other hand, the profile of the 135 degree fibre orientation is significantly more damaged then the other three and is characterised by torn fibres and removed chunks of material. Fibres have been crushed and fractured and lie out of plane from their original orientation. The bending and crushing cutting mechanism causes

a significantly worse surface damage on this fibre orientation compared to the others. Furthering from the assessments made in these images, roughness measurements will be compared across each of the fibre orientations and a detailed analysis of cutting mechanism on each fibre orientation will be assessed using optical SEM images.
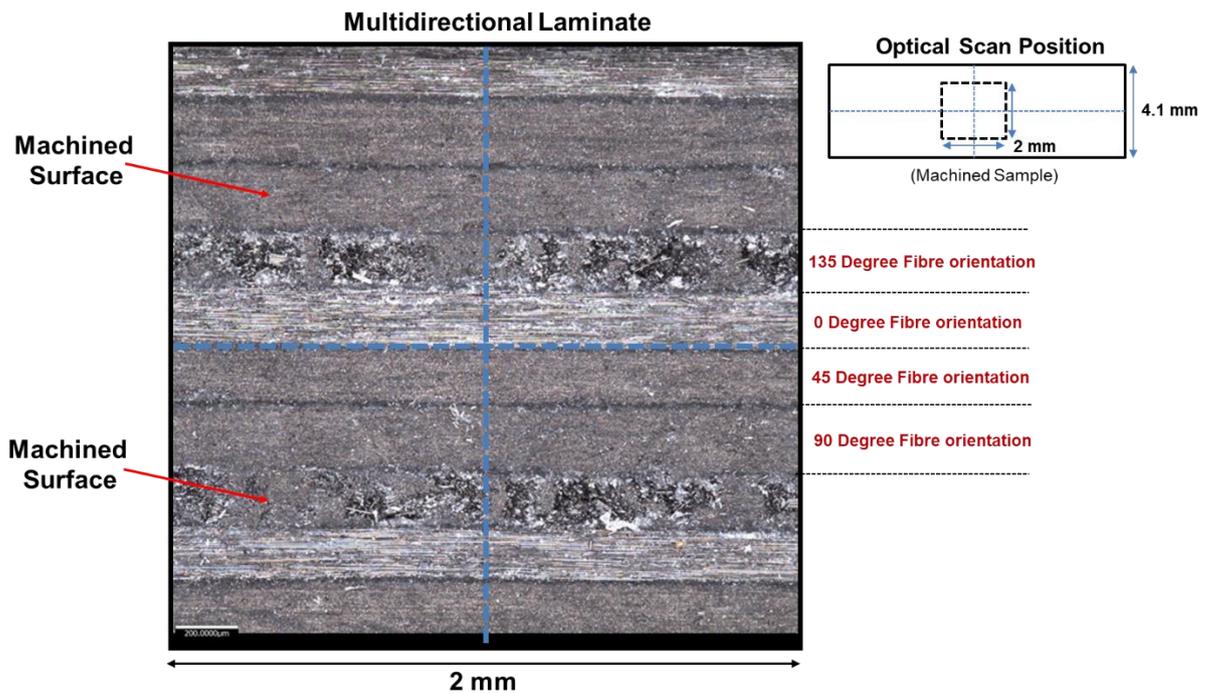
Figure 3-7- Optical surface measurement highlighting different surface damage on each fibre orientation. The image shows the edge machined surface profile.

Average R_a roughness was measured using the optical system and selected for each individual fibre orientation which is shown in Figure 3-8. A large variation in calculated roughness of the machined surface on each fibre orientation across one laminate was found, and the 135 degree fibre orientation had the significantly highest roughness. The 135 degree fibre orientation was critically found to have a roughness which is near to a factor of 10 times higher than the 45 degree. This effect can only be explained by the different cutting mechanism which is a product of the fibre orientation in relation to machining direction, as the laminate layers have the same material make-up, and because

79

the whole surface is machined with the same parameters. A detailed close up of the different surface structure is shown next to the graph in Figure 3-8 for each of the fibre orientations taken by SEM image. It is therefore realised that all of the fibre orientations should be included in order to take reliable roughness measurements, and that the 135 degree orientation will be critical in determining the highest surface roughness and machining defects. The standard deviation in the measurements was also highest on the 135 degree fibre orientation, as shown in Figure 3-8, due to the larger variation in surface structure and damage. The difference in profile across different fibre orientations means that changing the stacking sequences or laminate lay-up will cause a completely different machined surface profile. Therefore roughness measurements must be representative of the whole laminate layers in order to achieve an accurate measurement. Consequently, it was found that when using the stylus there is a high likelihood of the surface roughness being under-represented if the 135 orientation is not proportionally included in the overall roughness measurements. Therefore a potential uncertainty in using stylus method for measurement of a multidirectional surface is a consequence of this result.
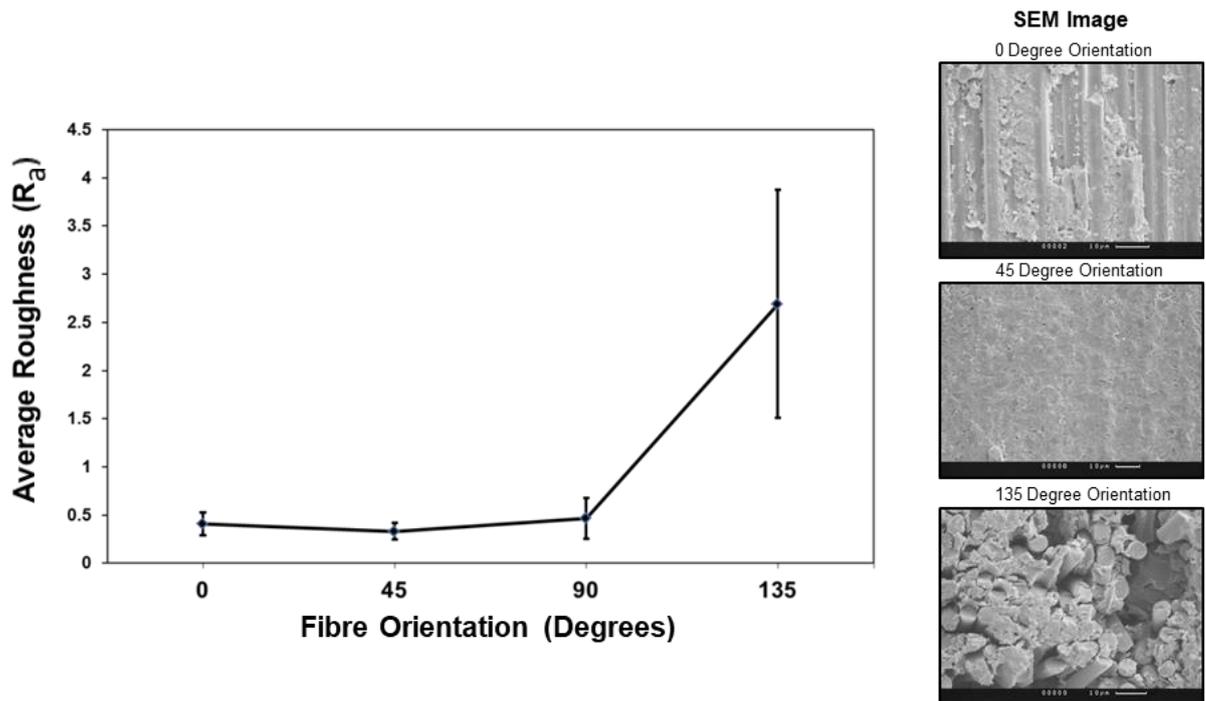
Figure 3-8- Average roughness vs fibre orientation on multidirectional laminate, with error bars shown as standard deviation using optical technique. SEM images of fibre orientation machined surface are shown for reference.

3.2-1 Parameter Effects of Feed rate and Cutting Speed on Surface Roughness

The cutting tests were performed at different cutting speeds and feed rates, and the significance of these effects of these parameters was assessed. Graphs and statistical methods have been applied to find the effect on the surface roughness.

In Figure 3-9-Figure 3-12 the roughness across the 0, 45, 90 and 135 degree fibre orientation is shown versus increasing feed rate for each of the 4 different applied cutting speeds. A fairly similar trend was seen across the data for the 0, 45 and 90 degree orientations in each of the applied feed rates and cutting speeds. However, the 135 degree fibre orientation showed some slightly different trends with cutting speed, there was also a higher scatter or standard deviation in the measured values along with a higher magnitude in roughness. The higher standard deviation can be explained by the different cutting

mechanism and a surface profile which has more variation in structure due to pits and torn fibre chunks. The 0, 45 and 90 all showed a highest roughness with a cutting speed of 225 m/s and a generally increasing roughness with feed per tooth.

It can be confirmed that increasing the feed rate caused an increase in surface roughness across all of the cutting speeds applied. The main effects plot for feed rate and cutting speed across all fibre orientations is shown in Figure 3-13. Minitab software was used to calculate and display the main effects plot [80]. A main effects shows the mean response from the input factors on the output response. In this case the two factors were cutting speed and feed rate and their corresponding output effect on R_a. Figure 3-13shows that there was a mean increase in the surface roughness due to a higher feed rate.   In machining, there is an increase in effective chip thickness when the feed rate is increased with larger chips and torn fibres being removed. This effect can explain the increase in roughness. Ahmad and Shahid. [30] have shown that decreasing the equivalent chip thickness is strongly correlated with lowering surface roughness. The chip effective thickness is a geometric function of the feed speed and cutting speed, and therefore in order to get the best surface quality, the feed rate and cutting speed parameters will both have a jointly contributing effect. Also, a component of the increase in roughness with increasing feed can always be attributed due to the ideal roughness which is a function of the square of the feed and tool nose radius.

Statistics was applied to test data using regression modelling and showed that feed rate had a stronger contribution on increasing the roughness than the cutting speed did. A P value of 0.03 was found for the feed rate which indicated that the parameter has a statistically significant effect on the roughness. An interesting result was found, which was that the feed rate had a most significant effect on the 135 degree fibre orientation. This result tells us

82

that increased levels of machining damage from an increased feed rate will be most likely have the strongest effect of increasing machining damage on the 135 fibre orientation compared to the others.

In Figure 3-13 it is illustrated that increasing the cutting speed from 85 to 225 (m/s) caused a mean increase in R_a surface roughness, but at the highest cutting speed of 285 (m/s), there was a mean decrease. Increasing the cutting speed will cause a decrease in un-cut chip thickness and it has been reported that the cutting mechanism may change to a "mechanical wrenching" [81]. An increase in cutting speed can also affect the temperature at the tool workpiece interface. There will be less time for energy dissipation for each rotation of the cutting tool and therefore an increase in tool workpiece temperature as it heats due to friction. This will cause a thermal softening of the matrix and a reduction in its stiffness. The matrix would then hold the fibres together less strongly and there can be a corresponding change in cutting forces. There can also be smearing of the matrix on the surface which can affect the subsequent surface roughness measurements.
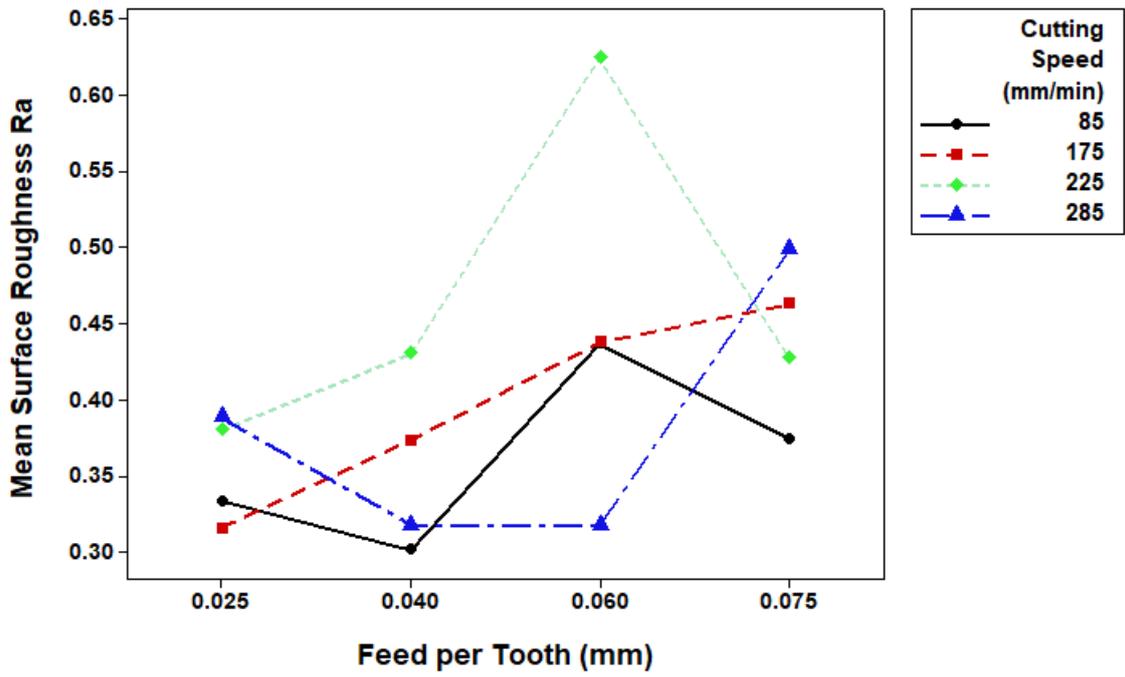
Figure 3-9- Mean R_a Surface roughness for 0 degree fibre orientation, against feed rate grouped at each cutting speed.
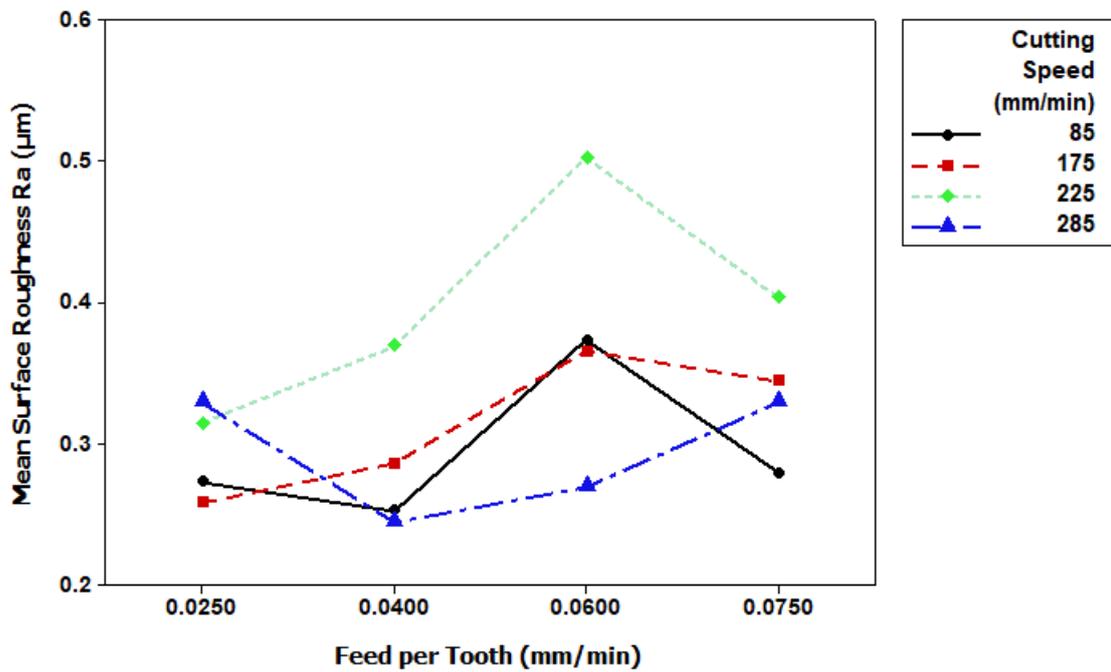
Figure 3-10- Mean R_a surface roughness for 45 degree fibre orientation, against feed rate grouped by cutting speed.
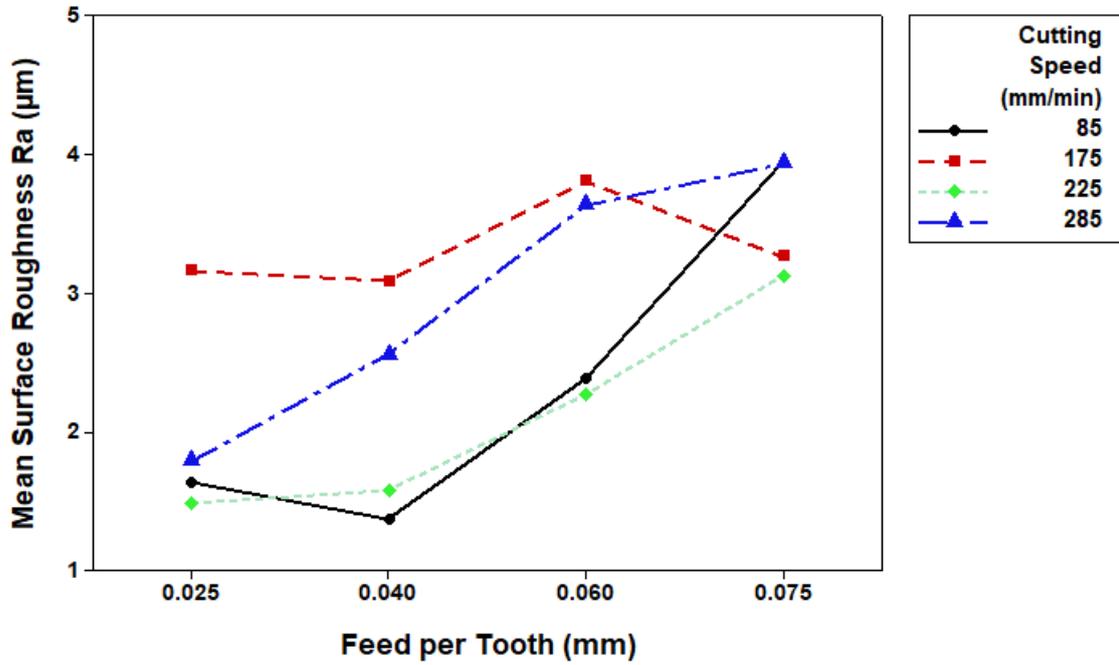
Figure 3-11- Mean R_a surface roughness for 90 degree fibre orientation, against feed rate grouped at each cutting speed.
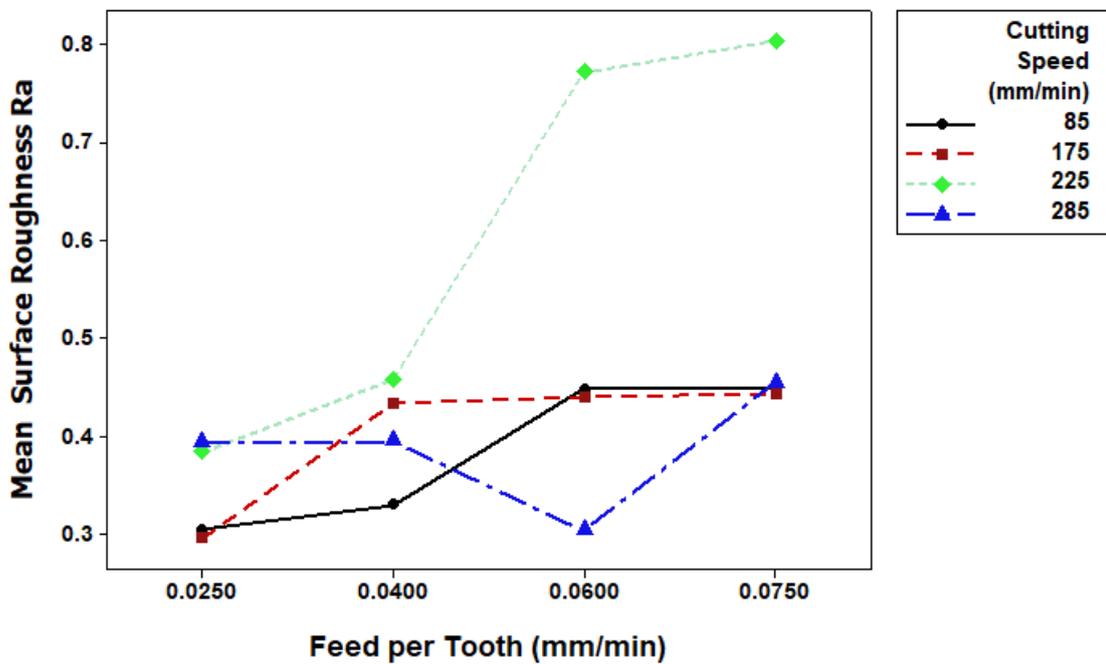
Figure 3-12- Mean Ra surface roughness for 135 degree fibre orientation, against feed rate grouped at each cutting speed.
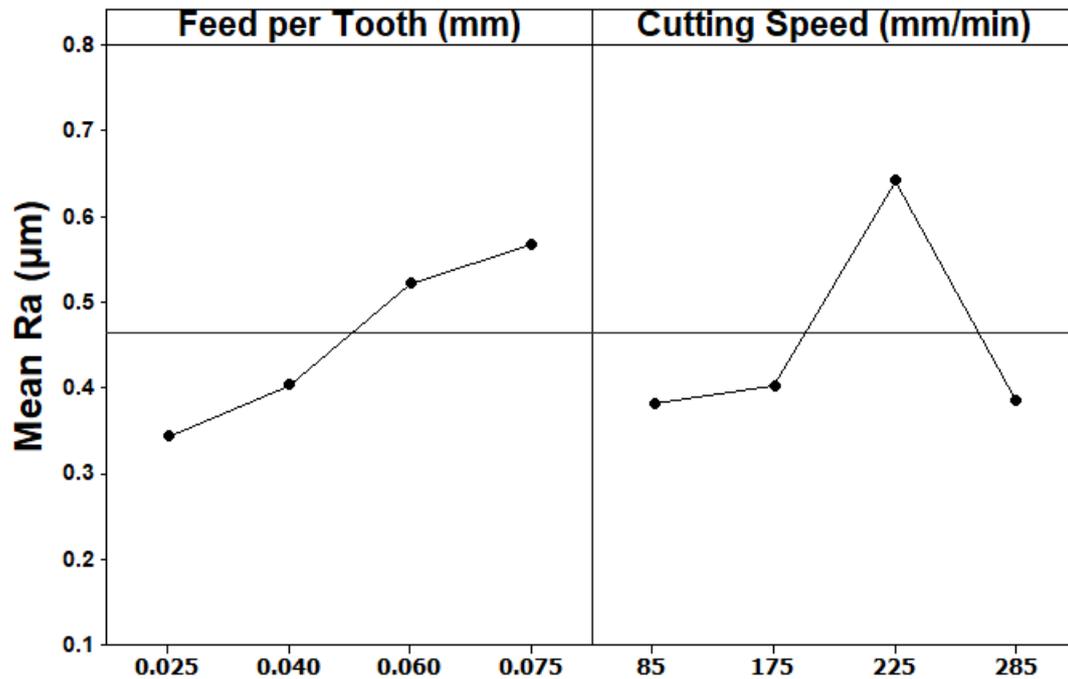
Figure 3-13- Main Effects for mean roughness for 90 degree fibre orientation, against feed rate and each cutting speed. Shown for multidirectional laminate and optical technique.

3.2-2 Profile Histograms, Skewness & Kurtosis Measurements

Skewness and kurtosis parameters have been calculated to assess the surface damage and see if they can give more thorough information of surface structure and machining defects than only using the R_a or S_a parameters. The outputs of these parameters are not represented in the R_a mean roughness parameter, and it is also possible for two different surfaces profiles to have the same R_a value [49]. The parameters were calculated from the same positions as the R_a measurements. Histograms of each of the different fibre orientations have also been represented graphically. The histograms are used to show the percentage of height values of the surface profile above or below the mean profile line. They are useful to give information about the height distribution of a profile and thus can give more information about the surface texture. The aim was to see if the additional parameters and histograms can give more quantitative information about surface defects and surface profile of a

86

machined composite surface. The surface structure was also assessed on each different fibre orientation.

The average skewness and kurtosis for the 0, 45, 90 and 135 degree fibre orientations are shown in Table 3-3. It was found that the skewness was positive in all fibre orientations except the 135, which had a negative skewness. In the histogram shown in Figure 3-14, there is a large tail in the negative direction. This negative skewness characterises a surface with more valleys than hills and tells us that the surface is full of deep cracks and voids of removed material. The cutting mechanism causes fibre pull-out and chunks of torn or bent fibres to be removed from the surface. The 45 and 90 degree fibre orientations had a positive skewness and therefore have more hills than valleys. This can be explained by the smoother surface which has less cracks protruding below the machined layer, there are sheared fibres protruding from the surface. The zero degree fibre orientation also has a positive skewness due a lack of deep cracks or voids. The surface is characterised by fibres which lie parallel to the surface and some which have been bent and fractured. The histogram in Figure 3-16 for the 45 degree fibre orientation shows a lack of tails in the negative direction, which indicates that there are minimal cracks propagating into the surface, or sub-surface damage. The skewness was therefore found to be a useful indicator in giving information about the machining damage on a surface. It can indicate whether the surface is made up of protruding fibres (positive skewness), which was found to be typical of the 90 and 45 degree fibre orientations, or made of torn fibres, pits and fibre-pull out (negative skewness), which was found to be typical of the 135 degree fibre orientation. The 135 degree orientation was therefore found to have a higher degree of machining damage and sub-surface machining damage which correlates with the higher roughness seen and negative skewness.

Fibre orientation (⁰)	Average skewness (Rsk)	Average kurtosis (Rku)	Multidirectional laminate. Mean R_a (µm)	Multidirectional Laminate. Mean Rt (µm)
0	1.55	13.73	0.4	4.7
45	1.68	13.01	0.3	2.9
90	1.48	15	0.5	4.9
135	(-)1.25	9.25	2.7	38.4
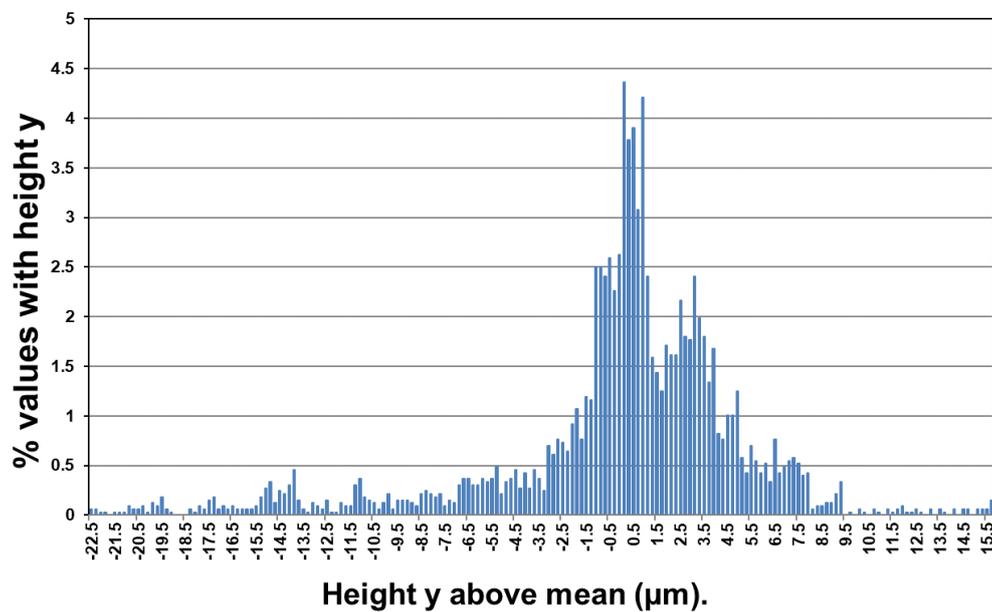
Figure 3-14- The 135 degree fibre orientation histogram on multidirectional laminate using optical system.

The kurtosis was also analysed to further indicate surface damage. The kurtosis is a measure of the peak sharpness. It was found that the 90 degree fibre orientation had the highest kurtosis. This tells us that the 90 degree fibre orientation had the sharpest peaks and it is hypothesised that this is due to sharp protruding fibre ends and un-cut fibres which have been sheared at different lengths. The histogram for the 90 degree fibre orientation has a lack of tails in the negative or positive direction- Figure 3-15. This indicates that the

88

surface is fairly regular, however there are a small number of points in the positive direction lying away from the mean which were caused by protruding un-cut fibres. Some of the fibres will be sheared at different lengths and therefore protrude from the surface. All of the fibre orientations have a relatively high kurtosis, suggesting that there is a profile made up of quite sharp peaks and valleys of either deep cracks or protruding fibres. The surface which has the lowest kurtosis is the 135 degree fibre orientation, as shown in Table 3-3.This is explained due to this profile having more surface machining damage with large rounded pits and valleys caused by chunks of torn material, whereas, the other fibre orientations have sharper protruding fibres- (above the machined surface).
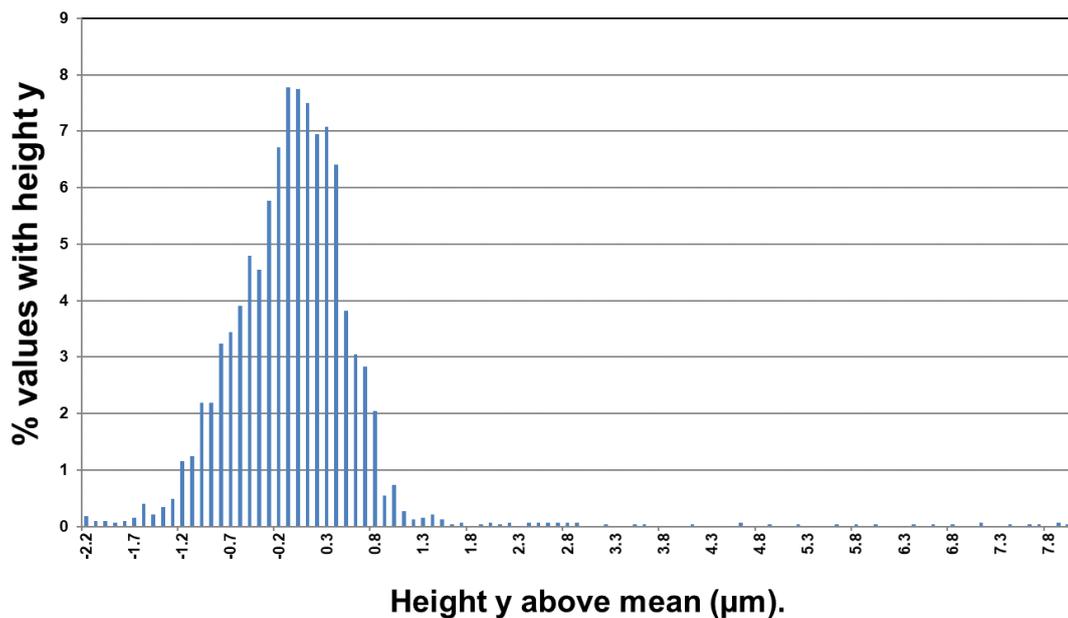
Figure 3-15- The 90 degree fibre orientation histogram on multidirectional laminate using optical system.

The skewness was found to be a useful parameter, due to its ability to distinguish between surfaces with mostly cracks and voids or having protruding and un-cut fibres. The optical system was used to analyse these parameters due to its ability to measure one layer of the mutli-directional laminate and

therefore accurately quantify roughness parameters of different fibre orientations. This would not have been possible to accurately measure using a standard stylus measurement.
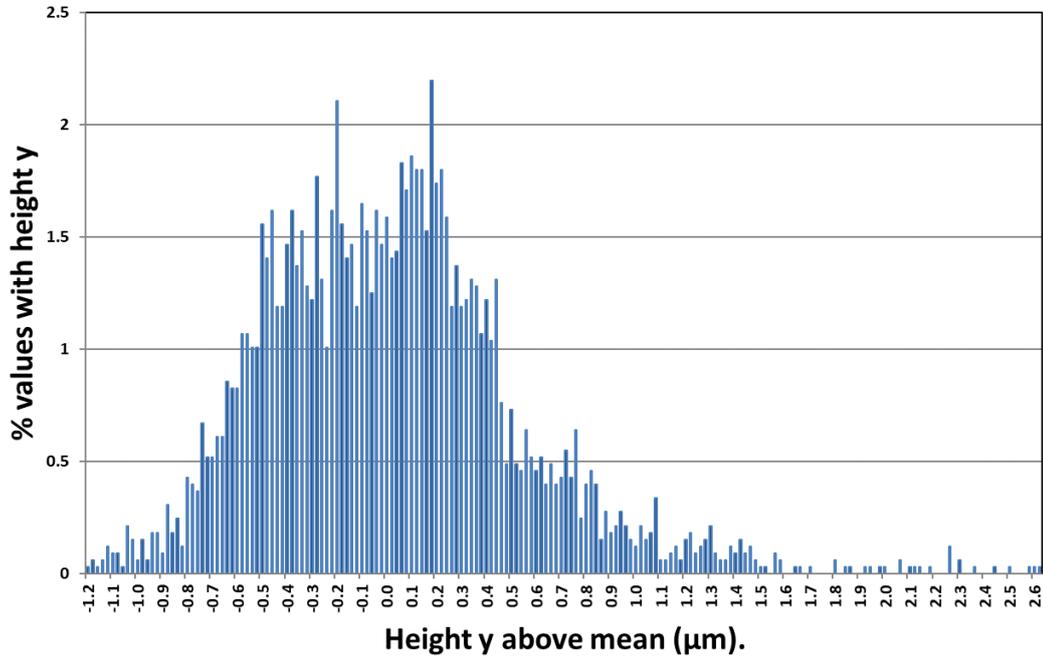
Figure 3-16- The 45 degree fibre orientation histogram on multidirectional laminate using optical system.

3.2-3 Summary of Surface Roughness Measurements

The stylus system has been compared against measurements made using Alicona focus variation based optical system. The focus variation system was found to give more reliable measurements and was capable of accurately extracting surface profile information of an individual ply layer. The stylus method has been shown in literature to find a wide variation in calculated surface roughness value of a "random" nature when applied to measurement path lying parallel to the fibre orientation in a multidirectional laminate [5]. Therefore the optical based system was applied and was shown to be a useful technology for measuring different individual surface plys. The surface roughness was found to be highest on the 135 degree fibre orientation which was characterised by pits and torn fibres and it is concluded that this will have a

consequence for applying accurate and representative measurements of the whole surface profile of a multidirectional laminate. It has been shown by other researchers that the R_a parameter alone may not sufficient to characterise machining damage of non-homogeneous surface [46]. Therefore, skewness and kurtosis parameters were used effectively to characterise additional information of surface machining damage on different fibre orientations. The skewness parameter was able to indicate the presence of larger torn chunks, pits and a surface characterised by large valleys. The kurtosis parameter was able to indicate the presence of un-cut fibres protruding from the surface, especially on the 90 degree fibre orientation. The aim of this section was to assess and develop methods for surface roughness of a composite surface. The new methods for measuring roughness of a machined composite surface have been applied using the optical system and shown improvements upon standard stylus methods. This method has been applied using additional parameters and on individual fibre orientations. The optical based system will consequently be applied to the next section of work to further characterise machined composite surfaces and in conjunction with developing a new method for accurately predicting surface roughness. In the next section S_a areal roughness parameters will be applied on a multidirectional surface due to the inherently found fluctuation variation in surface structure and machining defects on different fibre orientations.

3.3 Surface Analysis using SEM Micrographs

3.3-1 Analysis of Cutting Mechanism and Surface Damage on Fibre Orientations

Micrographs of the surface of the machined samples were taken using scanning electron microscope (SEM) images from the previous test. The SEM micrographs have been taken of a machined multidirectional composite in order to understand the cutting mechanism and characterise the surface damage types due to machining. Thorough characterisation of surface topography and damage mechanisms have been identified in relation to the different material fibre orientations. SEM micrographs are shown from Figure 3-17 to Figure 3-23 of different machined surfaces and fibre orientations. The aim of these SEM micrographs is to assess how machining damage is related to material fibre orientation and to find if these images correlate with the previously measured surface roughness.

Figure 3-17 shows the variation in surface structure and machining damage of different laminate layers on a multidirectional laminate. The 0, 90 and 135 degree fibre orientations are shown and it can be seen that there is a significant variation in the quality and appearance of the surface structure across each of the different layers, (even though they have been machined with the same machining conditions and have the same material properties). The fibre orientation therefore has a significantly strong effect on surface and sub-surface quality, machining damage and cutting mechanism, as confirmed previously by roughness measurements and literature.
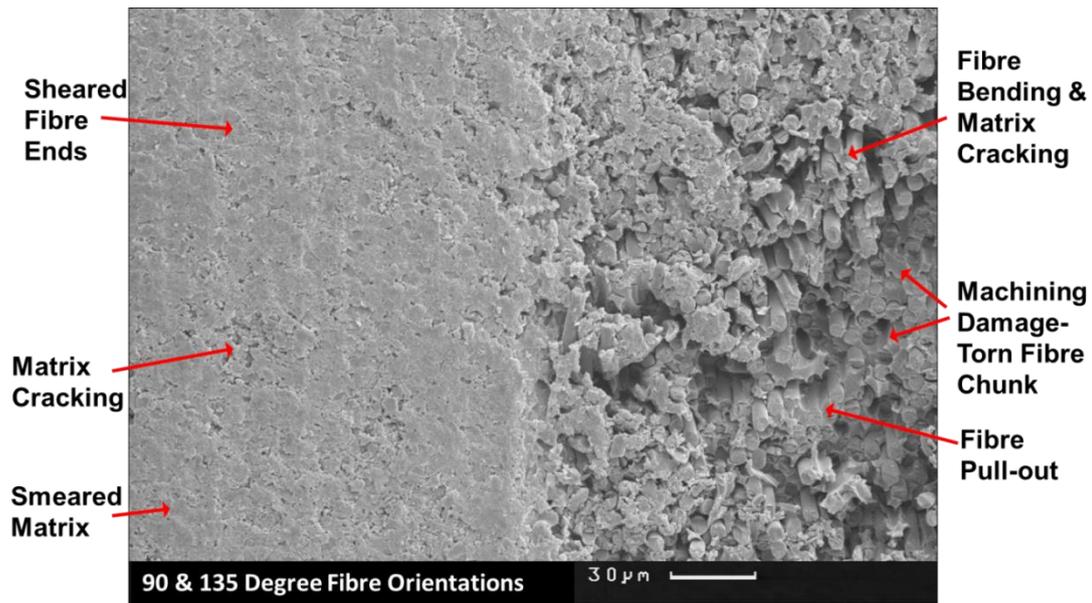
Figure 3-17- SEM image of 90 and 135 degree ply.
(These tests were performed at a cutting speed of 175 mm/min and feed of
0.075 mm/rev on multidirectional laminate.)

In Figure 3-19 and Figure 3-21, the 0 and 45 degree fibre orientations have been found to be relatively smooth, unlike the 135 degree which has large chunks of material removed and torn fibres. The visual appearance of the surfaces and damage which can be seen on each of the fibre orientations correlates with the magnitude of the roughness measurements made previously in Figure 3-8. That is the 135 degree fibre orientation has the highest roughness measured roughness and most visual damage.

The cutting mechanism in the 135 degree fibre orientation is caused by bending of the fibres leading to a primary fracture and this will propagate below the machined surface along the interface of matrix and fibre. The tool will push through the material causing the fibres to break in a combination of bending fibre shearing and fracture [9]. The matrix material is crushed and cracked causing de-cohesion from the fibres and cracks in the material. There are torn fibres below the machined surface, and the surface profile shows a greater damage depth than seen in the other fibre orientations. The deep

93

valleys and torn-fibres were described by the negative skewness which was measured on the 135 degree fibre orientation. The SEM micrographs of the 135 degree fibre orientation show fibres which have been bent out of plane and fractured left lying on the surface- Figure 3-17, Figure 3-18 and Figure 3-20. A bouncing back effect, (where the fibres spring back after the tool has passed), was suggested in the literature for composite machining by Wang and Zang [20]. It would be expected that this effect would be exaggerated in the machining of the 135 degree fibre orientation due to the large amount of bending and buckling of fibres which can be seen. The un-cut and bent fibres will spring back after the cutting tool has pushed past leaving a damaged and uneven surface.
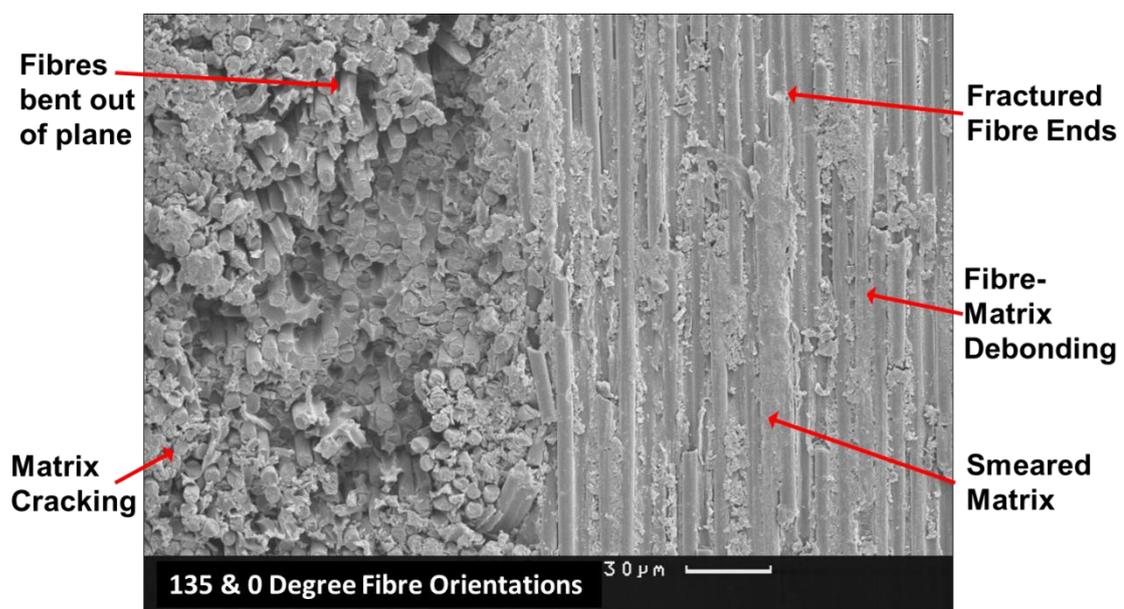
Figure 3-18- SEM image of 135 and 0 degree ply.
(These tests were performed at a cutting speed of 175 mm/min and feed of 0.075 mm/rev on multidirectional laminate.)

Looking at Figure 3-18 and Figure 3-19 for machining of the 0 degree fibre orientation there is a bending and fracture cutting mechanism causing chip removal. Depicted in the SEM micrographs there is little visible damage which propagates below the surface. The fibres are bent and crushed causing them to

de-bond along the interface, followed by fibre fracture. This finding is in agreement with work by Wang and Zang. [20], and Wang et al. [21]. Fibres can be seen lying on the surface in their original orientation, with little damage, and some fractured fibre ends can be seen. Most of the matrix appears to have been removed from the fibre surface by de-cohesion. In Figure 3-23, the beginnings of a fibre being bent and one being fractured can be clearly seen, depicting the fibre bending and fracture cutting mechanism. Some dust, and cut fragments of matrix and fibre can also be seen lying on the surface. The surface appeared shinier than in the other fibre orientations, especially in the optical focus variation images, due to reflection of the light from the fibre side surface.
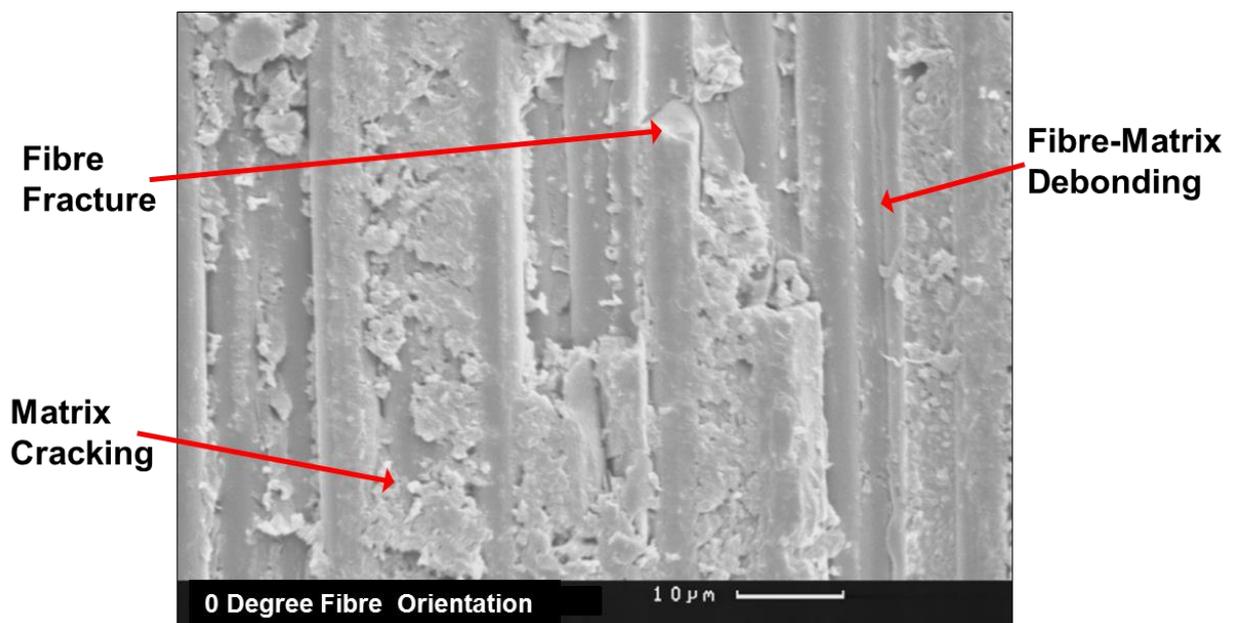
Figure 3-19- The 0 Degree fibre orientation SEM image.
(These tests were performed at a cutting speed of 175 mm/min and feed of 0.075 mm/rev on multidirectional laminate.)

The 90 degree fibre orientation is presented in Figure 3-17. On this fibre orientation the surface is visually smoother than the 135 degree fibre orientation. The roughness of the 90 degree fibre orientation was found to be slightly higher than measured on the 0 and 45 fibre orientations. The surface

appears smoother than the 135 degree fibre orientation and a fibre shearing and cutting mechanism is proposed in accordance with findings in the literature [3]. Cut fibre ends can be seen lying perpendicular to the surface and some of the surface appears to be covered in smeared matrix. The variation in profile height is caused by fibres sheared at different lengths, causing protruding fibre ends. These protruding fibre ends explain why the 90 degree fibre orientation had the highest kurtosis and sharp peaks.
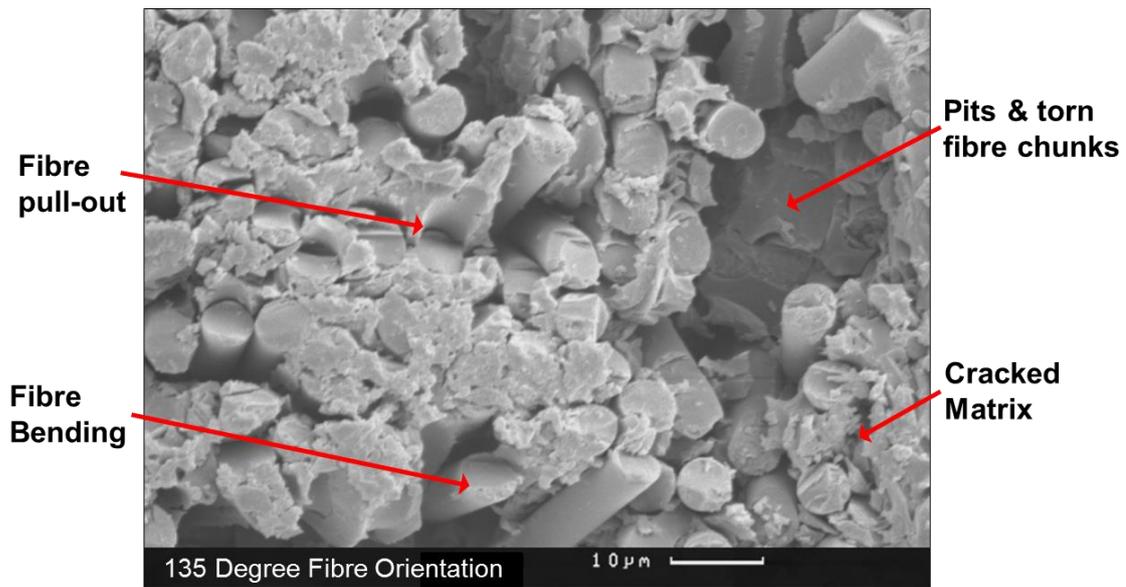
Figure 3-20- The 135 Degree fibre orientation SEM image.
(These tests were performed at a cutting speed of 175 mm/min and feed of 0.075 mm/rev on multidirectional laminate.)

The 45 degree fibre orientation surface is, in appearance, most similar to the 90 degree fibre orientation. It is covered in sheared fibre ends and smeared matrix as shown in Figure 3-21. The surface looks very smooth and it is hard to distinguish any individual fibres, unlike on the other fibre orientations. This surface was found to have the lowest roughness and no cracks can be seen propagating below the machined surface. It is suggested that most of the fibres are being sheared and cut cleanly on their cross section without being bent. A strong fibre tension dominated failure mode has been found along with a high resultant cutting force [82]. The authors contrasted this to a weaker

96

matrix dominated failure mode in the 135 degree fibre orientation and lower cutting forces.

In Figure 3-22 it can be seen that the different fibre orientations have a different profile height across the machined surface. These micrographs are taken from experimental test on the multidirectional laminate machined with the tool manufactured by SGS. The material is a The 90 degree fibre orientation had a profile which sits higher than the 0 degree and 135 degree. This suggests that where there is a bending type cutting mechanism, (found in the 135 and 0 degree fibre orientation), then the profile height will be lower than when there is a shearing cutting mechanism, as in the 90 and 45 degree fibre orientations. In Figure 3-17, it can clearly be seen that there is more subsurface damage in the 135 degree fibre orientation, and there are large chunks of fibres removed.
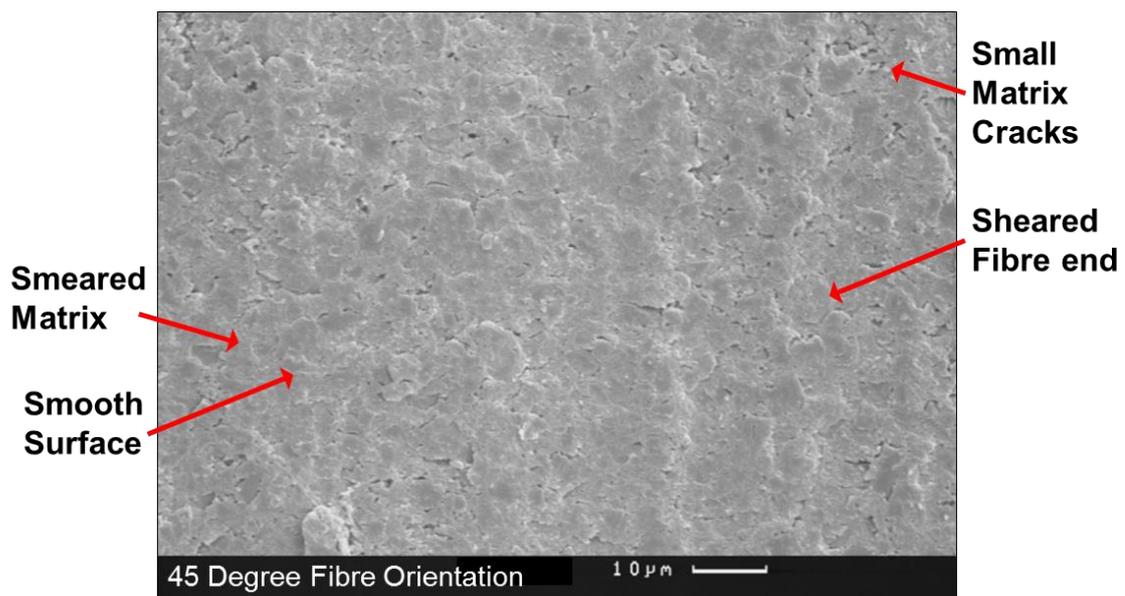
Figure 3-21- The 45 Degree fibre orientation SEM image.
(These tests were performed at a cutting speed of 175 mm/min and feed of 0.075 mm/rev on multidirectional laminate.)
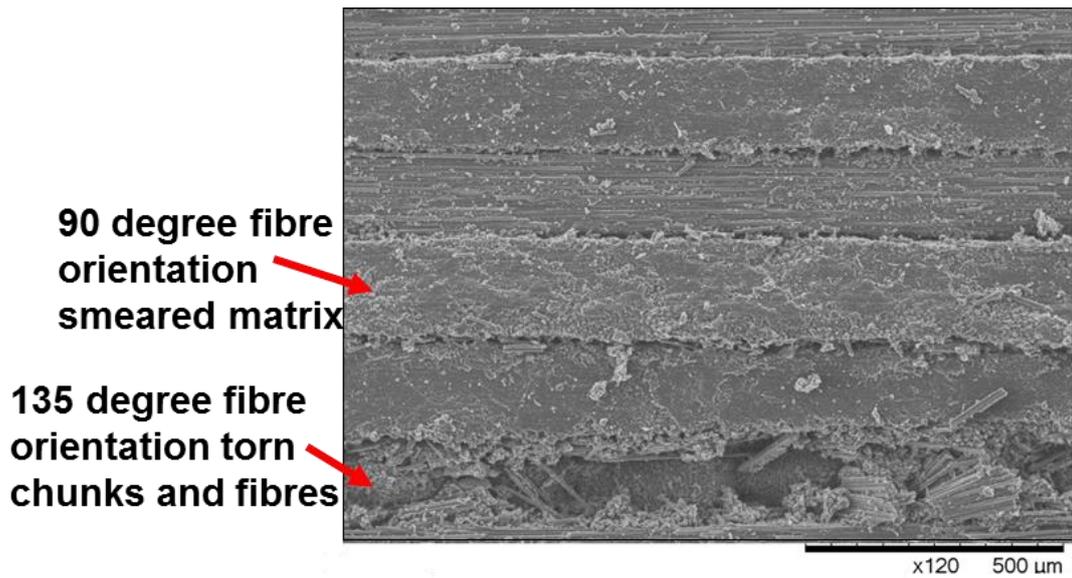
Figure 3-22- Multidirectional laminate, experimental test 2, worn cutting tool. (These tests are on multidirectional laminate, SGS tool, Feed 1200 mm/min, 7000RPM)
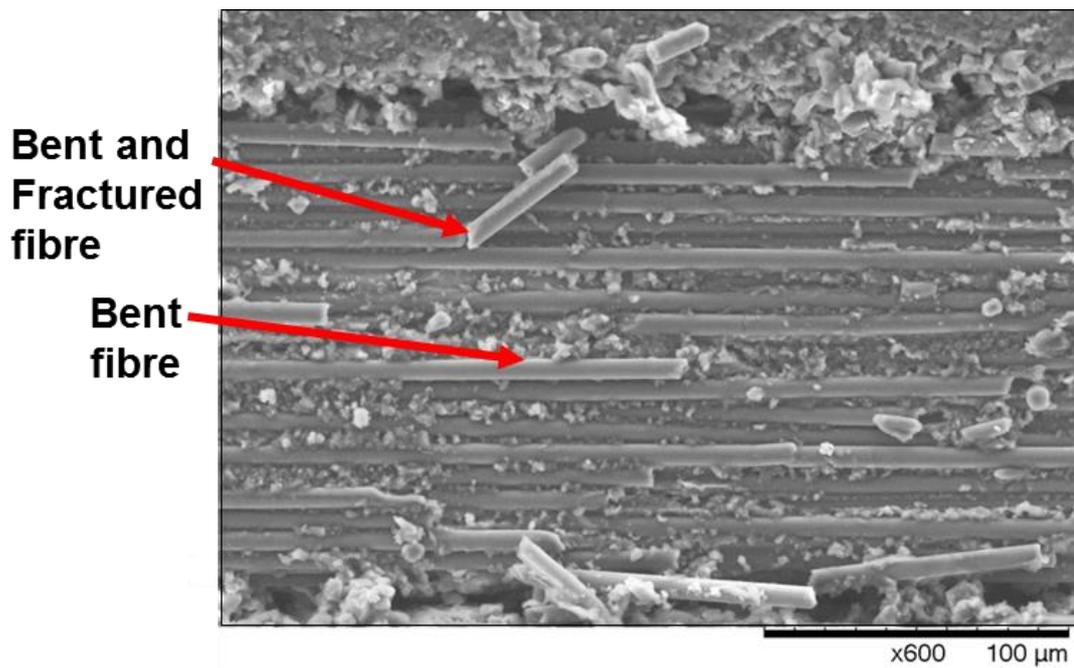
Figure 3-23- A 0 Degree fibre orientation, multidirectional laminate, experimental test 2. (These tests are on multidirectional laminate, SGS tool, Feed 1200 mm/min, 7000RPM)

98

3.3-2 Summary of Surface Characterisation Using SEM

Thorough assessment of surface profile using SEM micrographs have been applied to analyse surface damage and cutting mechanism of the machined multidirectional surfaces. The cutting mechanism on each of the different fibre orientations has been described in detail and also agrees with previous work shown in the literature [20],[21]. The visually described magnitude of damage also correlated with reported roughness measurements in this research. Firstly, the surface profile of the 0 degree fibre orientation appeared reasonably smooth with bent fibres which had been fractured in a bending and crushing mechanism. Secondly, the 45 degree fibre orientation appeared the smoothest, which agreed with calculated roughness measurements, and it was hard to distinguish any individual fibres. There was smeared matrix and cut fibre ends which represented most of the surface profile. Thirdly, on the 90 degree fibre orientation the surface profile was characterised with sheared fibre ends and some un-cut fibres which protruded above the majority of the machined surface. Finally, the 135 degree fibre orientation was characterised by bent and torn fibres and large pits in the surface. Importantly, it was this fibre orientation which was characterised by the greatest magnitude of machining damage and damage depth. The machining process appears to have the most detrimental effect on this surface orientation ply and cause the highest levels of surface damage. This finding was confirmed by roughness measurements and in the literature [3]. These results are useful because they present the extreme variation in surface structure and profile variation on machined which is purely due to the effect of fibre orientation. They show that the most extreme damage and greatest pitts will be located on the 135 degree fibre orientation. Also, that this will have consequence on reliably characterising surface profiles of machined composite surfaces and making accurate and representative surface roughness measurements. Surface roughness measurements must either make an assessment based upon the relative ratio of different fibre orientations

comprising an overall surface profile or take into account the different damages on each layer.

Chapter 4
Main Experiments- Edge Trimming Trials Experimental Procedure

4.1 Experimental Introduction- Carbon Fibre Edge Trimming.

Following from the previous experiments two different edge trimming trials have been performed on CFRP laminates using a three flute PCD milling tool. The PCD tool has been used in these tests because it is closer to the industrial highest standard tooling used for this application. As was stated in the literature review PCD cutting tools have an excellent resistance to wear and can hold a sharp cutting edge, and will therefore cut with superior surface quality for fibrous composite machining. These tests will be further used to compare and validate FE numerical models and create a roughness prediction method which will include the effects of tool wear. The experimental test results will be used to generate regression equations for the effects of machining parameters on surface roughness.

The first test was performed on a unidirectional laminate at two different levels of tool wear, in a worn and un-worn tool condition. The second test is conducted on a multidirectional CFRP laminate with increasingly progressive levels of tool wear. Firstly, the unidirectional tests are performed with two different tool wear conditions, and additionally the machining parameters feed rate and cutting speed have been varied at two levels. Surface roughness measurements have been applied using optical measurement system. The experimental results will be used to create roughness equations using multiple linear regression. Further, measured cutting forced will be used to validate numerical FE models. The FE models will include the effects of tool wear, (cutting edge radius), on the cutting forces using a new 2D and 3D numerical model.

The second multidirectional tests have been performed to assess the surface roughness and machining forces during machining at progressive levels of tool wear. Design of experiments has been employed so that two different feed and cutting speeds have been applied with increasing levels of tool cutting edge radius which will be tracked through the test. Therefore the contribution of feed rate and cutting speed has been assessed independently with sufficient number of repeats, while also not allowing the effects of tool wear to compromise the results. The design of experiments has been applied using statistical software Mini Tab in order to be able to accurately and independently assess the effects of each parameter. P values have been assessed for each parameter used in the test in order to find their statistical contribution to the surface roughness. The R-Sq and histogram of residuals have also been applied in the results section to find the quality of the model fit and suitability of parameters inclusion in the regression model. The multidirectional tests were then used to create regression equations and show the level of statistical contribution for each experimental parameter on the surface roughness, including- S_a, skewness and kurtosis. The optical surface roughness methodology for machined composite surfaces has been applied along with areal surface roughness parameters. Additionally, SEM images have been used to assess surface quality and cutting mechanisms across the different fibre orientations. CT scans have been used to look for sub-surface damage, including delamination which cannot be seen by surface measurement methods.

4.1-1 Edge Trimming Experiments- Unidirectional Test

An edge trimming trial has been undertaken on unidirectional CFRP material at two different fibre orientations- 90 and 45 degrees fibre orientation. The fibre and matrix properties are shown in Table 4-1.

The composite samples were manufactured by lay-up, vacuum bagging and autoclave cured. Machining tests were performed on a 5-axis CNC machine tool manufactured by Cincinnati FTV, as shown in Figure 4-1(a) and Figure 4-1(b). The composite multidirectional samples were 65 mm width by 160 mm in length and 6 mm thick. A SGS 3 flute PCD tool was used shown in Figure 4-2 and with dimensions shown in Table 4-2. A PCD tool was chosen due to its high hardness and resistance to wear and is thus suitable for machining of abrasive carbon fibres. The cutting edge was manufactured by laser cutting and is very sharp, it can therefore shear fibres very cleanly and produce a high surface quality. The average edge radius was measured of the cutting tools using optical focus variation Alicona device. The chosen PCD tool has three flutes which have a zero helix angle. This tool was specially selected because it has a zero-helix angle. This means there will be a constant chip size through-thickness in the material going in the z-direction and simplifies the geometry of the cutting tool mesh. It also means that the experimental comparison with finite element model will be suitable for the unidirectional laminate in both a 3D and 2D machining model using plane stress elements. However, this cutter is still very suitable to composite machining because it has a sharp laser-cut PCD cutting edge and it is able to produce high quality machined surfaces. The aim of these experiments was to capture cutting forces and surface roughness at different levels of tool wear. The cutting forces will then be used to validate FE models. Cutting edge rounding measurements have been applied to quantify tool wear, as identified to be a useful parameter to assess tool wear in machining of FRPs [63]. The cutting edge rounding has then been used an input for FE models and therefore gives a quantitative indication of the current tool condition. This is because it quantifies the initial experimental edge radius at zero tool wear unlike with flank wear measurements. Further predictions of roughness at different magnitudes of tool wear will then be made using FE models.

Table 4-1- Fibre and matrix properties [83].

Reinforcement Fibre Properties		Matrix Properties	
Fibre Type	Carbon	**Matrix Type**	Epoxy
No of Filaments	1200	Glass Transition Temp (^{0}C)	185
Tensile Strength (Mpa)	4900	Density (g/cm3)	1.28
Tensile Modulus (Gpa)	240	Elongation at yield	5 %
Elongation at yield	2.10 %	Flexural Yield Strength (Mpa)	147
Density (g/cm3)	1.8	Flexural Yield Modulus (Mpa)	3.5
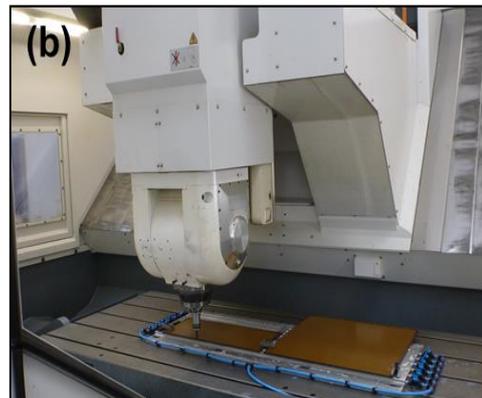
Figure 4-1- (a) Cincinnati 5-axis machine tool body,
(b) Cincinnati 5-axis spindle head.

Table 4-2- Tool properties.

Tool Feature	Value
No. of Flutes	3
Diameter	10 mm
Helix Angle	0°
Average Edge Radius (Unworn)	3.7 µm
Average Edge Radius (Worn)	10 µm
Cutting Edge Material	PCD

Figure 4-2- SGS cutting tool- Poly Crystalline Diamond (PCD).

4.1-2 Cutting Parameters- Unidirectional test

Edge trimming trials were performed using the parameters shown in Table 4-3. Two levels of feed rate and cutting speed were used, a feed of 800 and 1200 mm/min and a cutting speed of 6000 and 8000 RPM. Two material fibre orientations of 45 and 90 degrees were applied. The axial depth of cut (a_p) was kept constant at 6 mm and the radial depth of cut (a_e) at 2 mm. The length of cut was 160 mm for each test, which was the full sample length. A fixture was used to clamp the workpiece and is shown in Figure 4-3. It was bolted to the dynamometer and machine tool bed. Each test was repeated once and the mean F_x and F_y cutting force were recorded using a dynamometer. There were

16 tests separate with each of the experimental parameters applied shown in Table 4-3. Consequently with one repeat of each test, this gave a total of 32 tests.

Table 4-3- Unidirectional test parameters.

Feed Rate (mm/min)	Cutting Speed (RPM)	Axial depth of cut- a_p	Radial depth of cut -a_e	Fibre Orientation
800	6000	6 mm	2 mm	45
1200	8000	-	-	90

The effects of tool wear were assessed by performing tests with worn and un-worn tool conditions. The cutting edge was measured using the optical system and the un-worn (new) tool had an average cutting edge radius measured at 3.7 μm, and the worn tool had an average edge radius measured at 10 μm. A Kistler Dynamometer was used in order to measure the cutting forces. The Kistler dynamometer works by using piezoelectric material which generates an electrical charge when it is deformed. A voltage signal is generated using a charge amplifier which can be used to accurately measure a change in forces. A DAQ box and charge amplifier are shown in Figure 4-4(b) which are connected to a laptop to digitally record cutting forces from an analogue signal. The X,Y and Z machining forces were recorded and the directions are shown in Figure 4-5. The Fx cutting force is in the direction parallel to the tool feed or travel. The Fy force is into the workpiece and is perpendicular to feed direction. A sample time of 20 Seconds was taken and using a sampling frequency of 20,000 Hz. This gives a sampling rate of 133 data points per rotation of the cutting tool, at the maximum cutting speed of 9000 RPM and was considered suitable for high speed machining. Cutting forces were recorded using Dynoware software and the software was used to find the

minimum, maximum and mean cutting forces in the x, y and z directions over the sampling time.
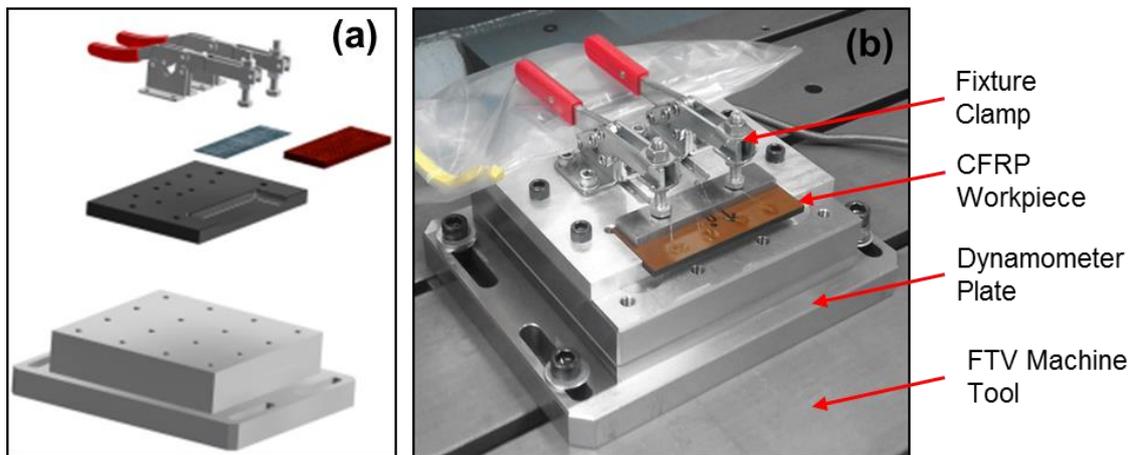
Figure 4-3- Experimental set up
(a) CAD model of fixture, workpiece and dynamometer,
(b) Clamp, fixture, dyno and machine tool.
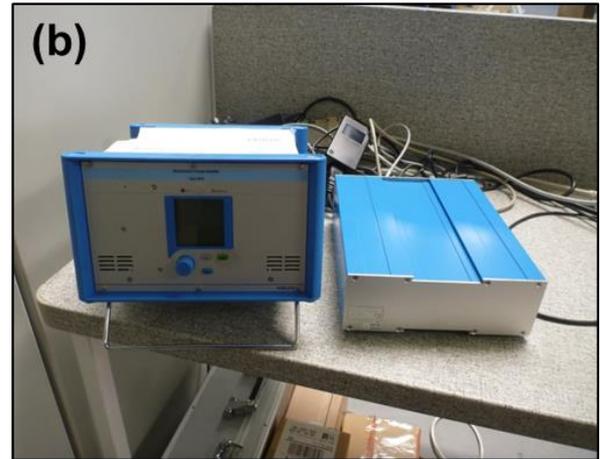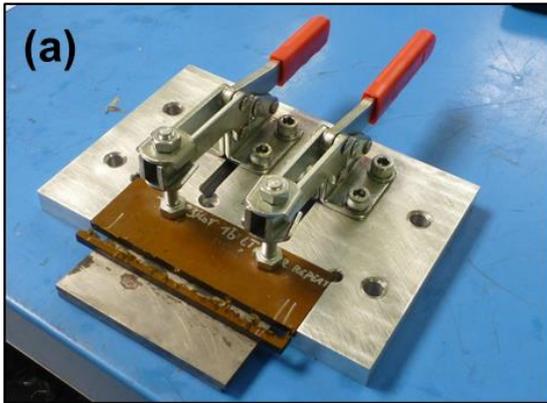
Figure 4-4- Experimental set up,

(a) Composite sample and clamp fixture,

(b) Kistler charge amplifier and A/D converter for dyno.
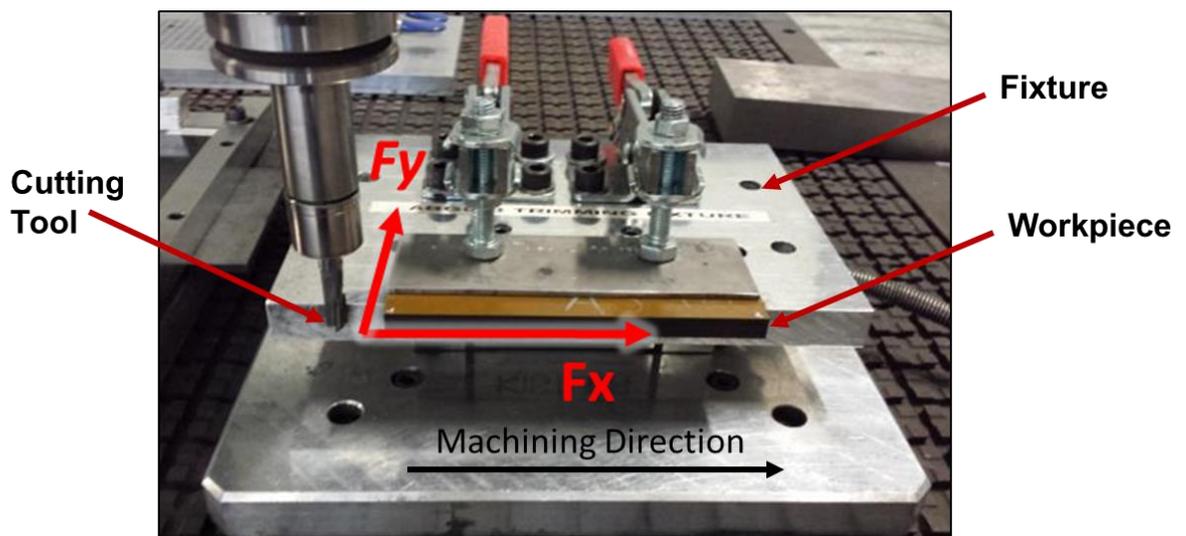
Figure 4-5- Machining forces orientation: Fx and Fy.

4.2 Edge Trimming Experiments- Multidirectional Test

The second edge trimming test has been undertaken on a multidirectional CFRP laminate which will then be compared with numerical models. Regression models will be calculated to find the statistical effect of the different machining parameters and tool condition, and how they will affect the machining forces and surface roughness. The composite is a typically commercially available CFRP material with epoxy resin matrix. It is a high performance aerospace grade composite with high toughness epoxy resin matrix system. The composite fibre and matrix properties are shown in Table 4-4 and Table 4-5. The stacking sequence of the 10 mm thick multidirectional laminate is shown in Table 4-6. The composite was manufactured by pre-preg layup, vacuum bagging and then auto clave cured.

Table 4-4- Multidirectional laminate properties.

Reinforcement Fibre Properties	
No of Filaments	1200
Tensile Strength (Mpa)	4900
Tensile Modulus (Gpa)	240
Elongation at yield	2.10 %
Density (g/cm^3)	1.8

Table 4-5- Epoxy resin properties.

Matrix Properties	
Glass Transition Temp (^{0}C)	185-190
Density (g/cm^3)	1.28

Table 4-6- Multidirectional laminate stacking sequence.

Material Type	Lay-up stacking sequence	Ply Thickness
Unidirectional	(0/+45/0/-45/0/-45/90/+45/0/-45/90/+45/0/0/+45/0/-45/0/-45/90/+45/0/-45/90/+45/0//0/+45/90/-45/0/+45/90/-45/0/-45/0/+45/0/0/+45/90/-45/0/+45/90/-45/0/-45/0/+45/0)	0.185 mm

The cutting parameters used in the multidirectional test are shown in Table 4-7. A varying feed rate was applied at 2 levels of 1000 mm/min and 1200 mm/min and a cutting speed of 7000 and 9000 RPM. A full workpiece thickness axial depth of cut (a_p), of 10 mm was applied, and a constant width of cut (a_e), of 2 mm. The length of cut was 80mm for the multidirectional laminate test. In this test the cutting began with two new tools which were then progressively worn. Then, in order to analyse the effects of increasing cutting edge radius on the machining process the tests were repeated with increasing levels of tool wear. Two new tools were used so that the effects of cutting speed and feed rate could be independently analysed without introducing the effects of tool wear for each of the set of cutting parameters. A total of 40 tests were performed with the two tools, and this gave a total of 10 repeats of each of the 4 independent test conditions but included the effect of increasing tool wear which was measured throughout the test. A test matrix was created as shown in Table 4-8 and the same test matrix was repeated again for a second set of 20 tests, using the same two tools but with increased levels of tool wear. The tests were performed in this order so that effects of the tool wear would not bias the results, and so that the effects of cutting speed and feed rate would be fairly and independently compared between the two tools. Statistical software Minitab was used to create the test matrix, and then the test results will be

used for the basis to create regression equations, realising the effects of cutting parameters on the S_a surface roughness. The tool wear was tracked throughout the test by quantifying cutting edge radius using the Alicona optical system. The same fixture and dynamometer setup was used as applied in the previous test as shown in Figure 4-3-Figure 4-5.

Table 4-7- Cutting parameters used in tests.

Feed (mm/min)	Cutting Speed (RPM)	Tool Number	Length of Cut	Axial Depth of cut (a_p)	Width of cut (a_e)
1000	7000	New Tool 1	80 mm	10 mm	2 mm
1000	9000				
1200	7000	New Tool 2			
1200	9000				

Table 4-8- Test matrix (repeated for tests 21-40)

Test	Feed (mm/min)	Cutting Speed (RPM)	Milling Tool Number	Milling Tool Number
1	1000	7000	1	
2	1000	9000	1	
3	1200	7000		2
4	1200	9000		2
5	1000	7000		2
6	1000	9000		2
7	1200	7000	1	
8	1200	9000	1	
9	1000	7000	1	
10	1000	9000	1	
11	1200	7000		2
12	1200	9000		2
13	1000	7000	1	
14	1000	9000	1	
15	1200	7000		2
16	1200	9000		2
17	1000	7000		2
18	1000	9000		2
19	1200	7000	1	
20	1200	9000	1	

Cutting fluid, which was an oil-water based emulsion, was used in these experiments. In machining it is typical to use a coolant with lubricant properties, because this will decrease friction, remove heat and reduce the chip thickness. Flood coolant was introduced into the cutting area from the spindle head during machining. During composite machining the coolant will also have the role of removing the abrasive chips from the cutting region, and this is desirable because otherwise repeated cutting of chips or fibre fragments could accelerate tool wear, and reduce surface quality. Another advantage of using the coolant is that there will be more heat dissipation and therefore less temperature build-up in the cutting area. This means that matrix burning or softening will be prevented or reduced. Cutting fluid was also used because of

the health concerns due to the inhalation of dust and particles from the machining of fibre composites. The use of coolant will prevent these particles from becoming airborne.

4.2-1 Cutting Tool Edge Radius Measurements

Cutting edge scans were taken of the cutting tool using the edge master software of the Alicona optical system. An optical scan of the cutting edge is used to create a 3D image and then the built-in software takes a number of cross sections over the scan length in order to calculate a mean result. The system can be used to calculate different cutting edge parameters. Figure 4-7 shows how the scan is taken perpendicular to the cutting edge and edge parameters are calculated through the edge cross-section. Figure 4-7(a) and Figure 4-7(b) show an optical focus variation scan for a new tool condition. A scan length of 2 mm is used across the cutting edge, over which, the mean edge radius is calculated over 150 cross sections. Each of the three cutting edges was measured and the mean cutting edge radius (CER) was calculated for each edge. To locate the cutting tool edge under the optical scanning system, a tool holder fixture was used shown in Figure 4-6. The tool holder sits inside the fixture and the tool can be rotated about its axis within the tool holder. A reference mark was used to locate the tool holder on the tool fixture so that each measurement can be repeated in same position for each cutting edge.
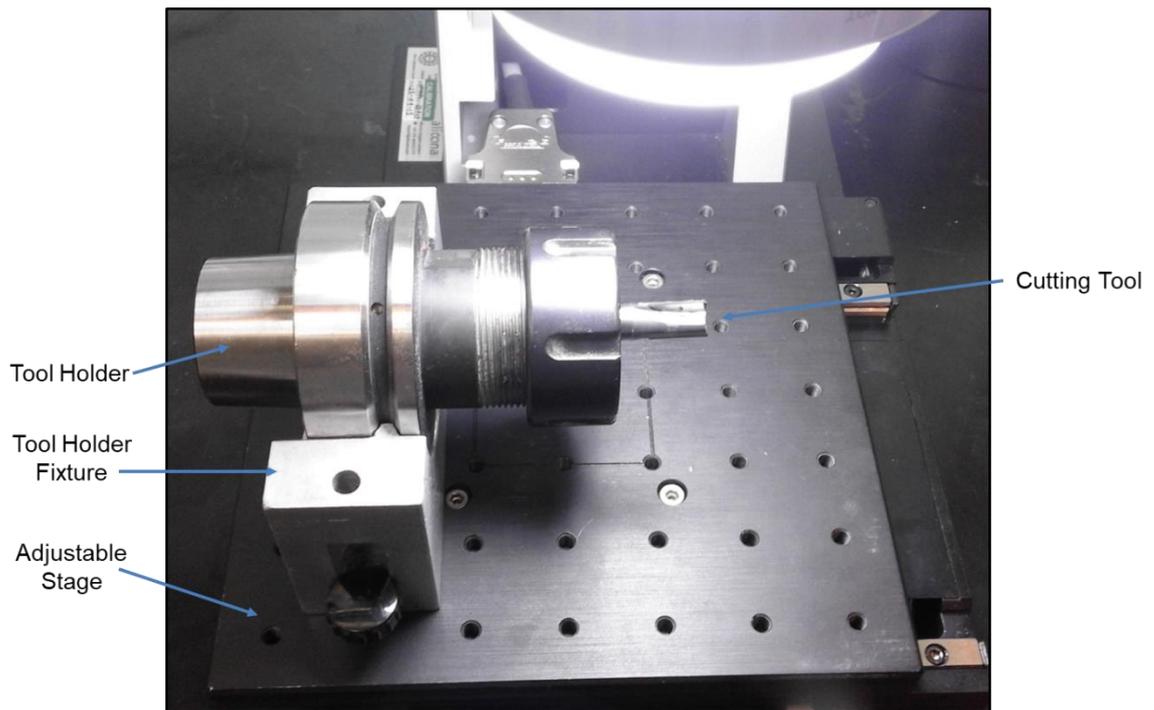
Figure 4-6- Tool holder fixture for CER measurements.

The optical scans were taken throughout the test to track the tool wear and to quantify the cutting edge radius. Some optical microscope images were also used as a qualitative assessment of the tool wear. This was to ensure that the cutting edge was not damaged or has any extreme tool wear, and to look for any edge damage or chips on the cutting edge.
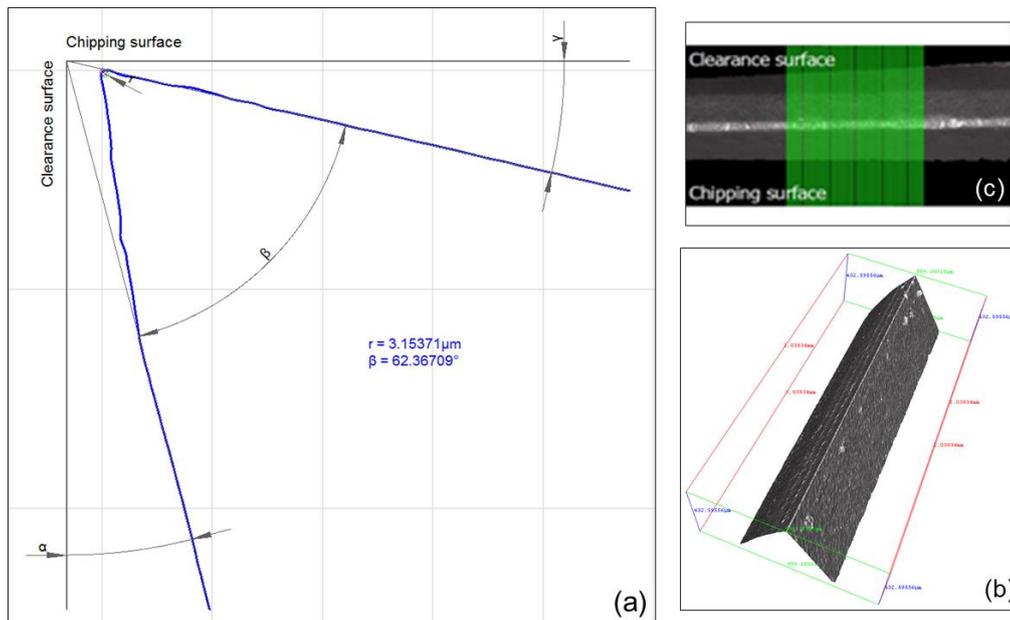
Figure 4-7- Cross section tool cutting edge mean parameters calculation-
optical device (new tool).

4.2-2 Surface Roughness Measurement Method

The length of cut was 180mm in the unidirectional test. To take the measurements scans were taken in three different positions through thickness of the sample- Figure 4-8 and Figure 4-9. Scans were taken in three positions at the beginning, middle and end of the cut. Roughness parameters were calculated and mean roughness and standard deviation can be calculated for each sample. Areal roughness parameters (S_a) were calculated and applied over the whole scan area. Areal roughness parameters (S_a) was applied due to the previously shown variation in surface profile on different fibre orientations and necessary requirement to characterise the whole surface profile in a representative manner. The S_a parameter will include surface profile information including all of the fibre orientations across the full laminate stack thickness and this will minimise any effects of sampling position. The scans were taken in different positions towards the beginning and end of cut to minimise any effects of machining on the sampling position, which may include

116

dynamic effects at the beginning and end of the tool entering and leaving the workpiece respectively. Also the size of the scan of 2mm wide along the sample length in the machining direction, and full workpiece thickness, corresponds to capturing a very large data point cloud of profile information. A 2 mm wide scan corresponds to around 200 individual profilometer path profiles with a stylus head diameter of 10 µm. Therefore a large sampling area is included in each scan of which an average is then taken from the total number of scans.

To take the optical scans a vertical resolution of 100 nm was used along with a lateral resolution of 2 µm. The cut off wavelength to calculate roughness parameters was L_c =800 µm and was used across all samples in accordance with ISO 4288. The cut off wavelength determines the amount of filtering of the profile waviness which is removed.
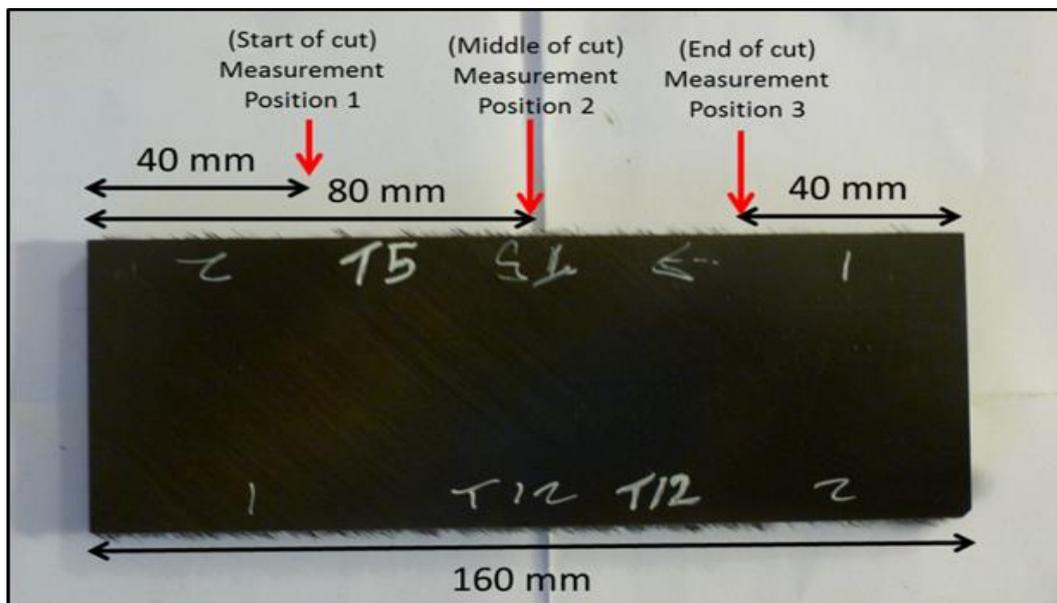
Figure 4-8 – Optical scan positions, (unidirectional sample).
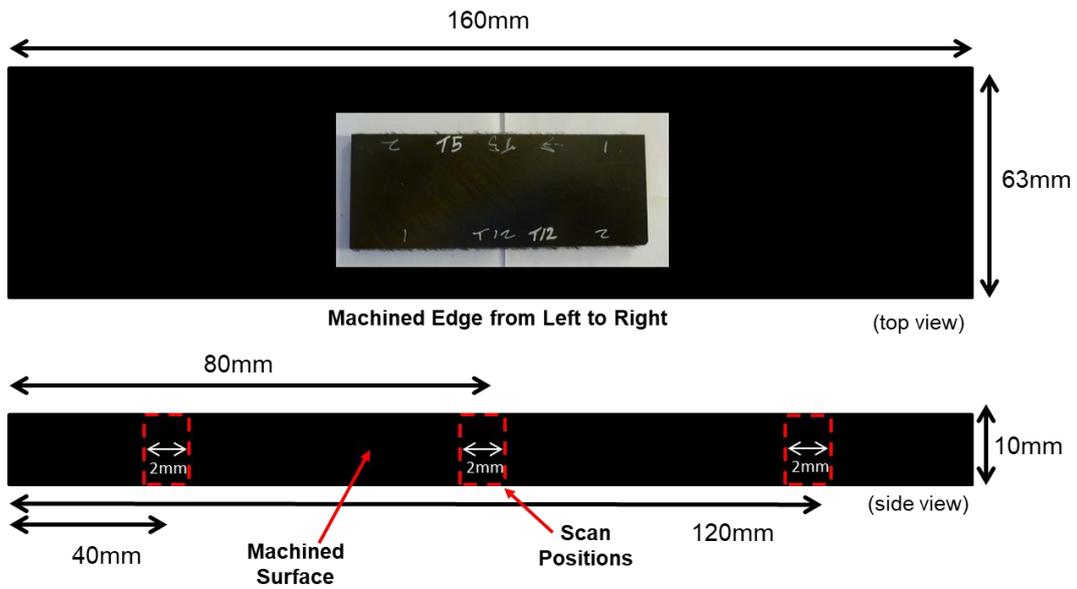
Figure 4-9- Three optical scan positions on sample for roughness calculation,
(unidirectional sample).

In the multidirectional laminate the length of cut was 80 mm and the sample length is 160 mm. Optical scans were applied in two positions shown in Figure 4-10. Each 160 mm long sample was used for two tests. There were scans at 20 mm and 60 mm from the edge which was also repeated on the second sample as shown in Figure 4-10. S_a, skewness and kurtosis parameters were calculated for each of the scan positions and a mean roughness is calculated for each sample from the two scan positions.
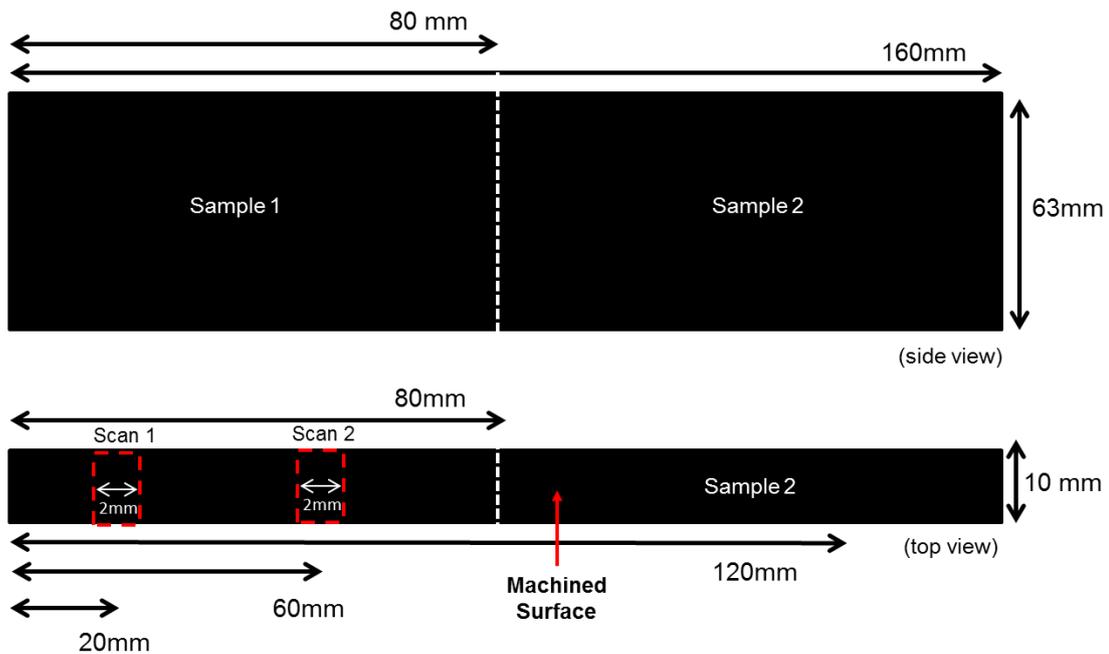
Figure 4-10- Roughness measurement positions, (multidirectional laminate).

Figure 4-11(a) and Figure 4-11(b) show an example of an Alicona optical focus variation scan which is taken of two machined surfaces of a multidirectional carbon fibre laminate with PCD cutting tool. The scans represent the machined surface, where the CFRP multidirectional laminate is cut going from left to right across the page. These samples show the machined surface profile through the whole thickness of the laminate from top to bottom and each of the laminate layers are shown progressing down through the laminate. These scans will then be used to calculate S_a roughness parameters which are characterised over the whole scan area. The variation in surface structure and damage can be seen on the different fibre orientations. It can also be seen that the surface structure in Figure 4-11(b) appears rougher in comparison to Figure 4-11(a) due to use of a worn cutting tool. The suitability of the Alicona optical system will later be assessed for roughness measurements of a machined composite surface.
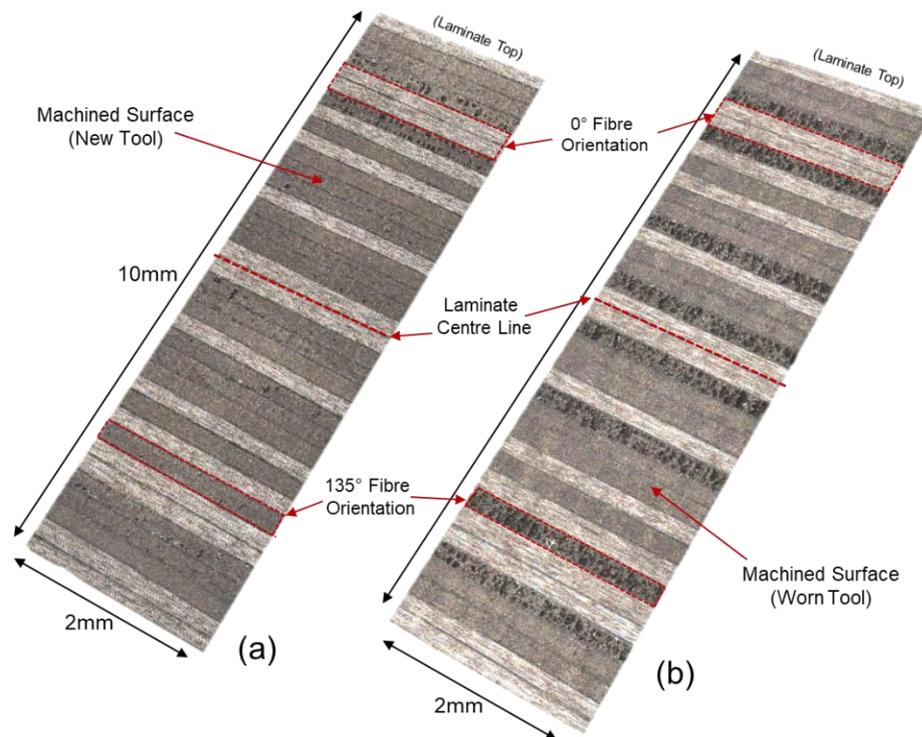
Figure 4-11- Example Alicona optical scans from a CFRP multidirectional
laminate:
(a) Multidirectional CFRP laminate- new tool condition,
(b) Multidirectional CFRP laminate- worn tool condition.

4.2-3 CT Scanning Method

As was highlighted in the literature review, CT scans can be used successfully to look for subsurface damage in fibrous composite materials. CT scans have been performed using Nikon Metrology XTH machine, shown in Figure 4-12. This machine uses a micro-focus X-Ray source which allows accurate inspection at high resolution and 225 or 320 kV source. Machined samples were prepared by cutting into 10 mm wide strips using a band saw, where one edge was already previously machined by edge trimming. Ten millimetre wide samples were required so that a 3 dimensional resolution of 8 μm could be achieved. If the samples are too thick then the resolution which can be achieved is reduced because the section which the x-rays must pass through is wider. A high

resolution is required in order to be able to see down to the fibre level and look for subsurface micro-cracking, voids, de-cohesion or delamination from machining damage. Unidirectional and multidirectional samples from both tests were assessed using the CT scanner. CT scans were performed on machined samples and also on samples which had not been machined. The non-machined samples were taken from the centre of test the material specimens away from the cutting edge. Un-machined samples were used to compare if damage in the material was actually present due to machining, or if there was already defects present in the material from the manufacturing process.

Figure 4-12- Nikon Metrology XTH Micro-CT scanner.

Chapter 5
Edge Trimming Experimental Results

5.1 Experimental Results- Unidirectional Laminate

5.1-1 Machining Force Results

The first set of results from the unidirectional edge trimming test are presented. Cutting forces were recorded from the unidirectional edge trimming test. The mean cutting forces in the Fx and Fy directions are shown in Table 5-1 and Table 5-2 for the 90 degree fibre orientation laminate in unworn and worn tool condition respectively. Table Table 5-3 and Table 5-4 show the mean cutting forces from unidirectional test in the 45 degree fibre orientation laminate. The mean cutting force is calculated from the raw data extracted by the dynamometer as shown in Figure 5-1. The three colours in Figure 5-1 show the Fx, Fy and Fz machining forces in blue, red and green respectively. The mean cutting force is calculated between the two dotted line sections, as shown, and is selected where the cutting reaches steady state conditions.

Figure 5-2 shows the cutting force variation for the Fx and Fy cutting forces over a 0.5 second time period. There is a cyclic pattern to the cutting forces as each tooth of the cutting tool engages the workpiece. Each tool will engage the workpiece and cause a removal of small and dust-like CFRP chips in a fracture type cutting mechanism. Then the rotating cutting edge will pass the workpiece before the next tooth becomes engaged. Thus, there is a cyclic fluctuation of cutting forces, due to intermittent cutting tool engagement, and the fracture of CFRP chips. Shown in Figure 5-2, over a 0.5 second time period, the Fx and Fy cutting forces fluctuate between an upper and lower bound. As a steady state fluctuation of the cutting forces is reached, and it was therefore deemed acceptable to take the mean cutting forces.

Cutting forces were recorded for the tool in worn and new tool conditions and will be later compared with 2D and 3D finite element models. The full test data and calculated average cutting forces from the experimental tests, are shown in the Appendix Part A, and the standard deviation is also calculated for each test repeat.
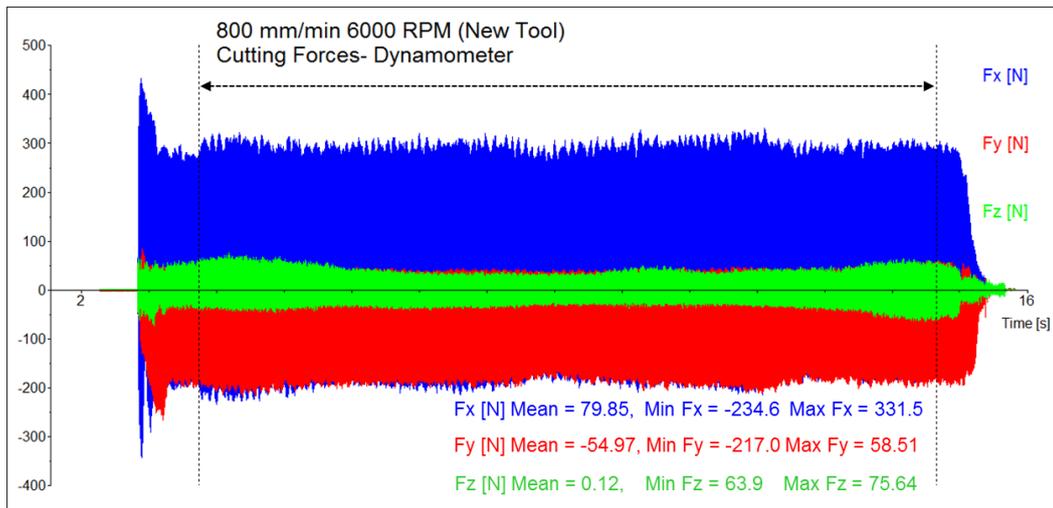
Figure 5-1- Dynamometer output for machining forces at 800 mm/min, 6000 RPM with new tool. Calculation of mean cutting forces.
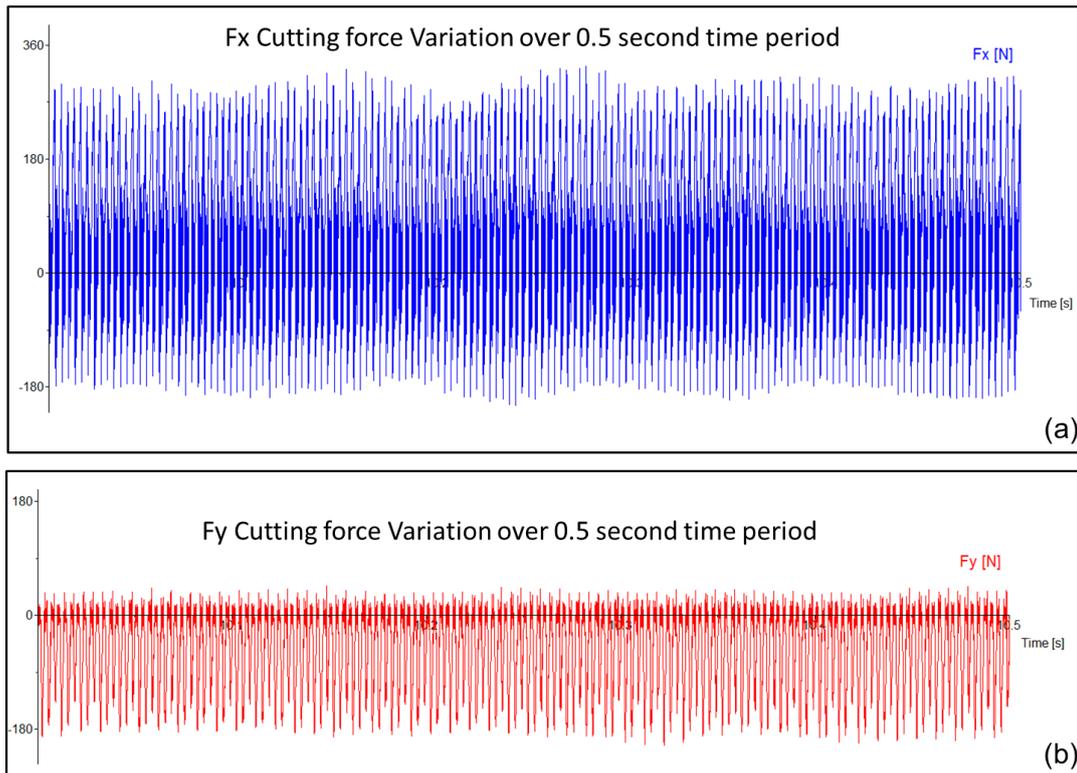
Figure 5-2- Machining force fluctuation over 0.5 seconds of cutting.

(a) Fx cutting force,

(b) Fy thrust force.

Table 5-1- Fx and Fy cutting forces- 90 degree fibre orientation (new tool).

Fibre Orientation	Feed Rate (mm/min)	RPM	Mean Fx (N)	Mean Fy (N)
90	800	6000	80.0	54.9
90	1200	6000	99.5	63.4
90	800	8000	82.1	58.7
90	1200	8000	82.3	60.3

Table 5-2- Fx and Fy cutting forces- 90 degree fibre orientation (worn tool).

Fibre Orientation	Feed Rate (mm/min)	RPM	Mean Fx (N)	Mean Fy (N)
90	800	6000	107.1	131.2
90	1200	6000	120.2	151.5
90	800	8000	92.75	109.9
90	1200	8000	109.1	154.4

Table 5-3- Fx and Fy cutting forces- 45 degree fibre orientation (new tool).

Fibre Orientation	Feed Rate (mm/min)	RPM	Mean Fx (N)	Mean Fy (N)
45	800	6000	74.0	58.3
45	1200	6000	79.4	76.2
45	800	8000	75.0	66.6
45	1200	8000	82.3	85.4

Table 5-4- Fx and Fy cutting forces- 45 degree fibre orientation (worn tool).

Fibre Orientation	Feed Rate (mm/min)	RPM	Mean Fx (N)	Mean Fy (N)
45	800	6000	112.9	112.1
45	1200	6000	128.2	129.2
45	800	8000	101.3	104
45	1200	8000	124.7	129

Shown in Figure 5-3 to Figure 5-6 are graphs of the machining forces against increasing feed- from experiment on the unidirectional laminate. The columns are grouped by the two applied cutting speeds (6000 and 8000RPM), and by tool wear- in new and worn condition. The graphs are shown for the 45 degree fibre orientation laminate in Figure 5-3 and Figure 5-4 for Fx and Fy respectively. Whereas in Figure 5-5 and Figure 5-6 graphs are shown for the 90 degree fibre orientation laminate. The green and red columns show the machining forces in the un-worn tool condition at 6000 and 8000 RPM respectively. The blue and purple show the same cutting speeds for the worn tool conditions. The error bars show the standard deviation between the experiment repeats. One repeat of each test was taken in order to assess the repeatability of the experiment which was a total of 32 tests. It was found that a maximum standard deviation of 12 N between a set of repeats which was equal to a force difference of 17.7 N or a maximum percentage difference of 12.2 %. The repeatability of the tests was therefore found to be reasonable and the main discrepancy between two sets of tests results could be attributed to a slight increase in tool wear in the repeat test.

The experimental cutting forces were found to be significantly higher with the worn than the unworn tool, and the tool wear was found to have a more significant effect on cutting forces than either fibre orientation or cutting parameters. Shown in Figure 5-3-Figure 5-6 there is a significant increase in machining forces with worn tool in comparison to unworn tool. The Fx cutting forces were on average 32 % higher with the worn than unworn tool, while Fy forces were 64 % higher. Cutting forces will increase with tool wear due to blunting of the sharp cutting edge, leading to higher friction and more tool contact area with the workpiece during machining. There will be change in the cutting mechanism to ploughing and tearing rather than fibre cutting, and this

will also negatively affect the surface quality generated. The effects of increased tool wear on the surface quality generated will be further analysed.

 It can also be seen across the majority of the graphs in Figure 5-3-Figure 5-6 that there is an increase in both Fx and Fy machining forces with feed. Increasing feed means there will be a larger chip thickness and therefore more material removed for each pass of the cutting tool. The statistical contribution of each of the parameters; tool wear, feed rate, cutting speed and fibre orientations, and their effects on the measured cutting forces, and surface roughness,- will be evaluated using main effects plots and regression equations in the following sections.
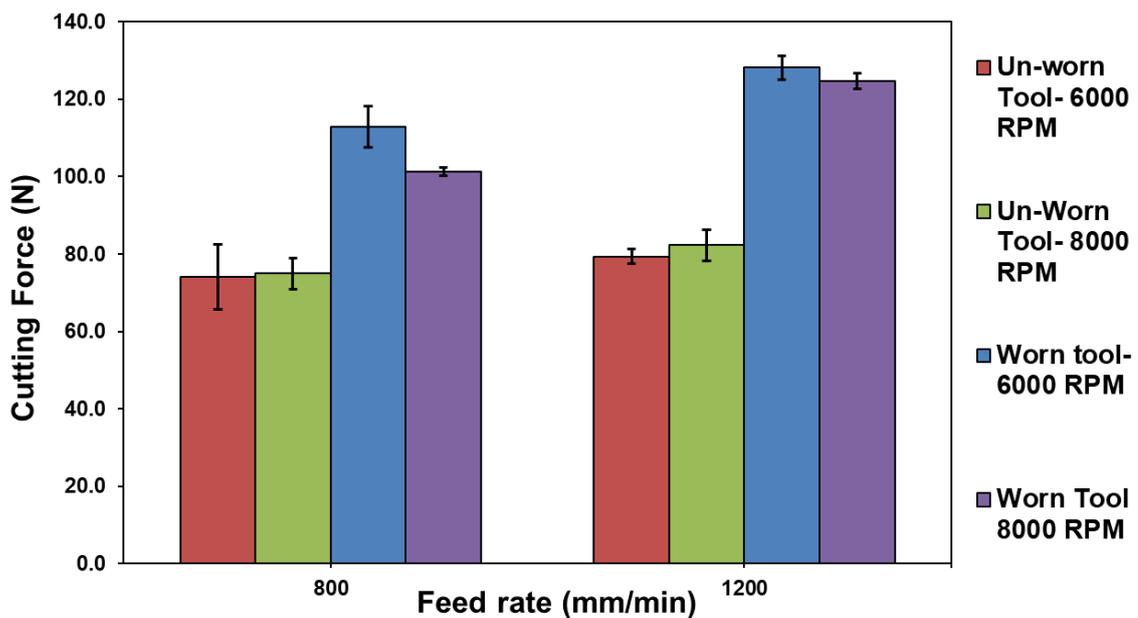
Figure 5-3- Fx cutting force vs feed rate, with worn and un-worn tool. (45 degree fibre orientation).
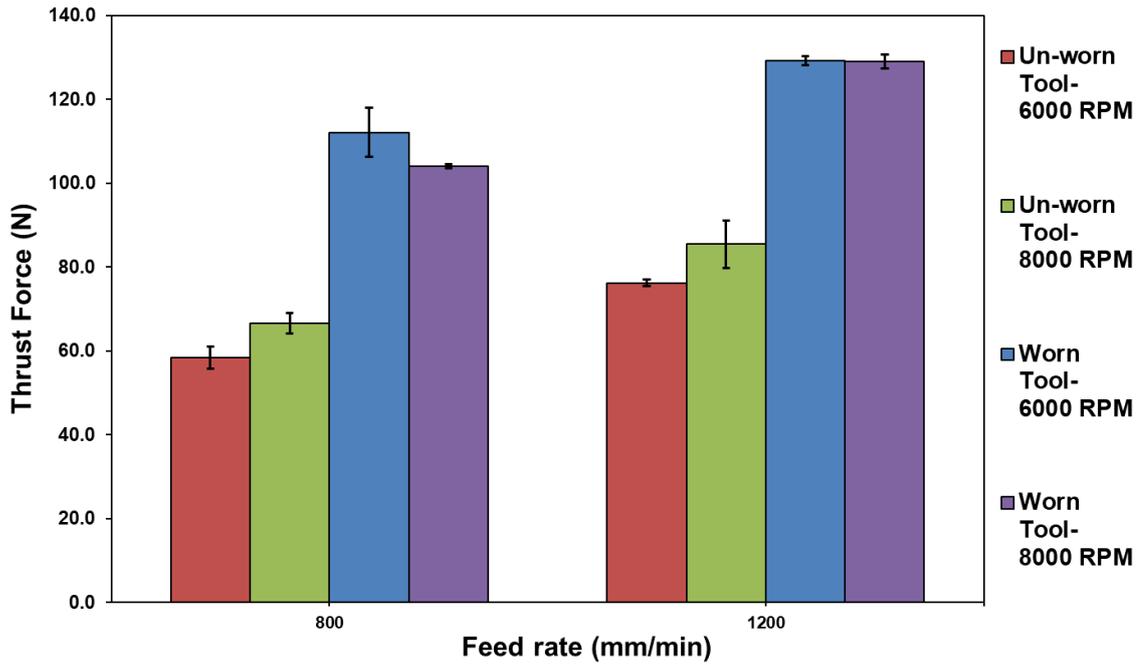
Figure 5-4- Fy thrust force vs feed rate, with worn and un-worn tool. (45 degree fibre orientation).

Figure 5-5- Fx cutting force vs feed rate, with worn and un-worn tool. (90 degree fibre orientation).

129

5.1-2 Cutting Tool Images

Optical microscope images were taken of the tool cutting edge before machining in worn and un-worn conditions. Optical microscope images were taken to qualitatively assess tool condition and wear. The microscope scans were taken of all three cutting edges in the same position for each scan. A fixture was used in order to hold and locate the tool under the microscope. Figure 5-7 shows the SGS PCD tool in new condition, while shows the same tool in worn conditions after experimental wear. It can be seen that there is wear on the cutting edge, which is shown by higher reflectivity and worn spots in Figure 5-8 compared to Figure 5-7. In Figure 5-8 the tool edge appears to show some small chipping and abrasive wear causing cutting edge rounding. Whereas, in Figure 5-7 the cutting edge still appears sharp and there isn't any noticeable worn patches or chips. In composite machining the chips are removed by "compression shearing and fracture" and small dust-like chips are removed, the predominant tool wear mechanism is by edge chipping and abrasion of the cutting edge [3]. In standard metal machining where there is a

130

continuous chip formation, and the predominant removal of material is by plastic deformation, there is commonly flank wear on the cutting tool, which is caused by adhesion and abrasion. In metal machining, the friction on the cutting tool and heat generation can cause a built up edge at the tool-chip interface. These conditions lead to adhesion and crater wear. However, in composite machining crater wear is not as prevalent due to the discontinuous chips and brittle fracture during chip formation which causes less adhesion. As seen in Figure 5-7 the predominant wear of the tool is by chipping and abrasion of the sharp cutting edge causing the edge to become blunted.

Figure 5-7 shows the tool in an unworn state, whereas in Figure 5-8 it can be seen that there has been chipping and edge rounding of the worn cutting tool due to abrasive carbon fibres. It can be seen that the cutting edge is more reflective than the unworn tool in Figure 5-7 because the cutting edge has been chipped to give a larger radius. The pre-worn tool was used in the experiment to see the effects of the degree of wear on the cutting forces compared to the unworn tool.
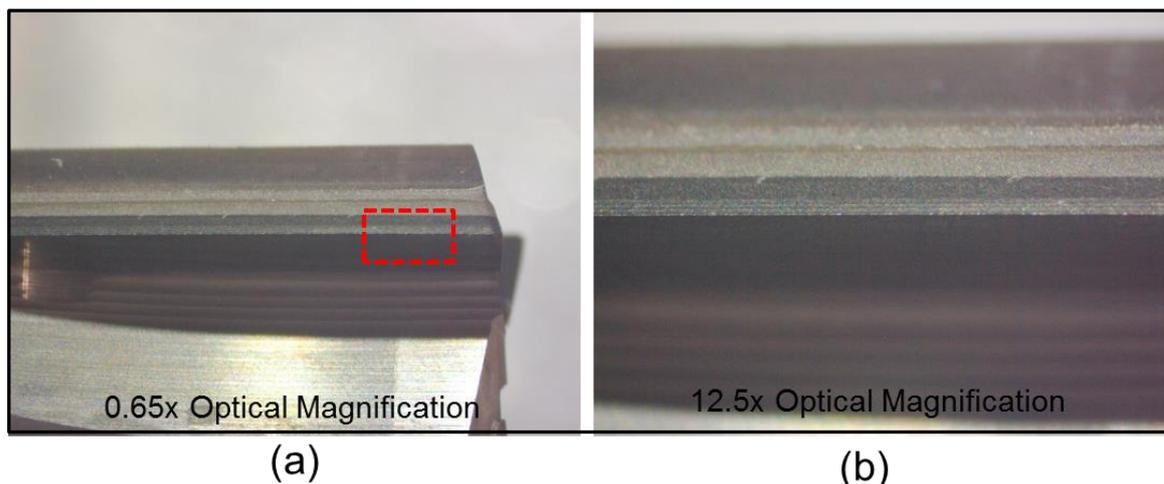
Figure 5-7- Optical microscope images of new unworn PCD tool.
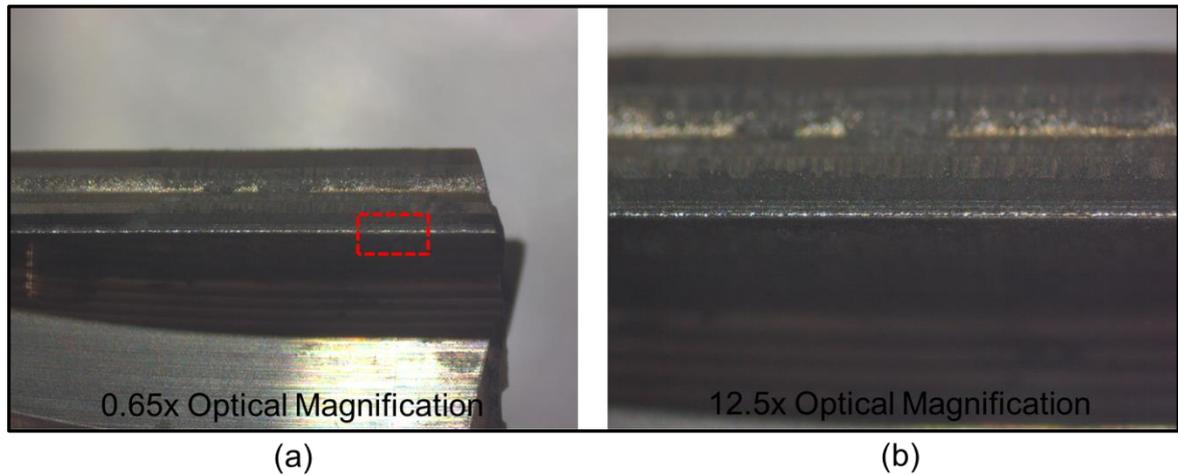
Figure 5-8- Optical microscope images of worn PCD tool.

5.1-3 Cutting Edge Radius- Focus Variation Measurements

The optical system was used to take scans of the tool in worn and un-worn conditions- Figure 5-9(a) and Figure 5-9(b). The cutting edge radius was analysed to track the increase in wear. The PCD tool has a sharp cutting edge which is gradually chipped due to abrasive wear by the fibres. Figure 5-9 shows the unworn tool with a sharp 3.7 μm average cutting edge radius and Figure 5-9b shows the worn tool with 10 μm cutting edge used in the experiments. This PCD tool was manufactured by laser cutting and therefore the new tool has a very sharp edge. The change in geometry can be seen due to wear by chipping and abrasion of the cutting edge. It was therefore found that the cutting edge radius will increase quite significantly with tool wear, and this will therefore have an effect on the cutting forces and surface quality.
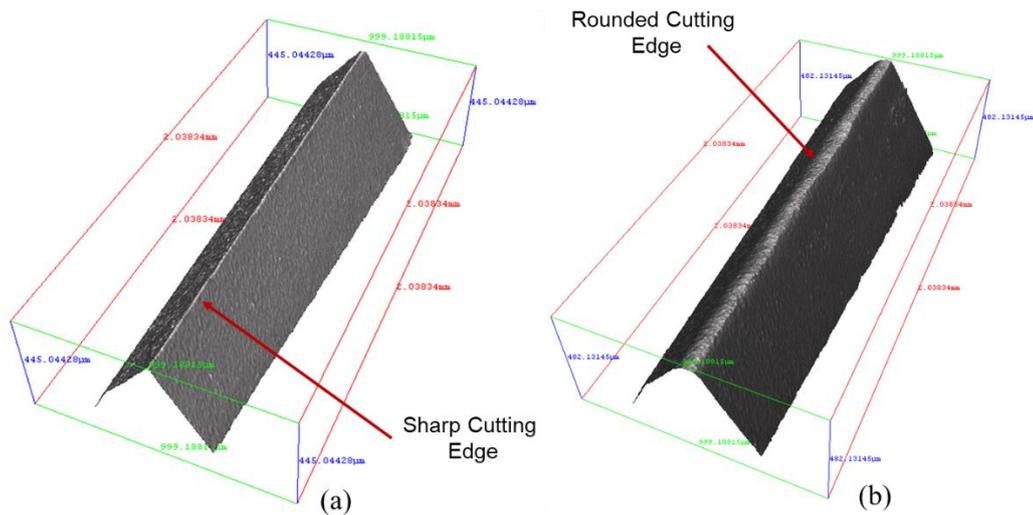
Figure 5-9- Tool cutting edge rounding Alicona scans,
(a) Unworn PCD tool,
(b) Worn PCD tool.

Table 5-5 shows the Alicona edge radius measurements of the worn and un-worn tool from each of the three flutes to find the average edge radius. The standard deviation of the three measurements is also shown, which represents the error in the difference between the three cutting edges. The cutting edge radius (CER) was then used as an input for finite element models.

Table 5-5- Cutting edge radius (CER) from Alicona scans.

Tool Condition	CER Edge 1 (µm)	CER Edge 2 (µm)	CER Edge 3 (µm)	Average (µm)	Standard Deviation
Unworn Tool	4.45	3.56	3.15	**3.7**	0.66
Worn Tool	10.34	10.41	9.30	**10.0**	0.62

5.1-4 Surface Roughness Scans by Optical System

Optical scans were taken of the machined surface using the Alicona focus variation system. Images can be used to qualitatively assess surface damage and then roughness parameters were calculated over the scan area in order to quantify the profile deviations due to machining.

133

Figure 5-10 shows an example of the surface scans taken with the optical system of the unidirectional composite machined surface. Figure 5-10 shows a 2 mm by 2 mm image taken from the centre of the sample, with feed rate of 800 mm/min and 6000 RPM at a 90 degree orientation. The surface is relatively smooth without any large pitts or voids, and the direction of feed can be seen as feed marks moving from left to right- Figure 5-10. To take roughness measurements a full workpiece thickness scan area of 6 mm by 2 mm was taken for the S_a surface roughness measurements- Figure 5-11.
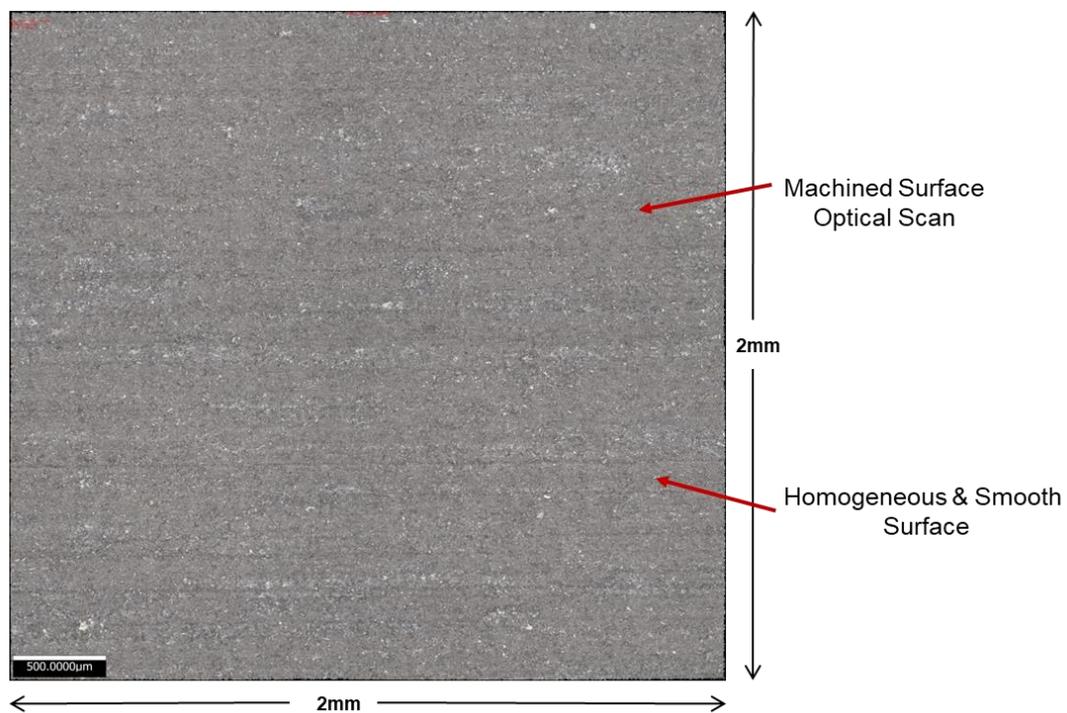
Figure 5-10- 2 x 2mm optical focus variation scan taken from middle of sample. (90 degree fibre orientation, 800 mm/min, 6000 RPM, Worn-tool).
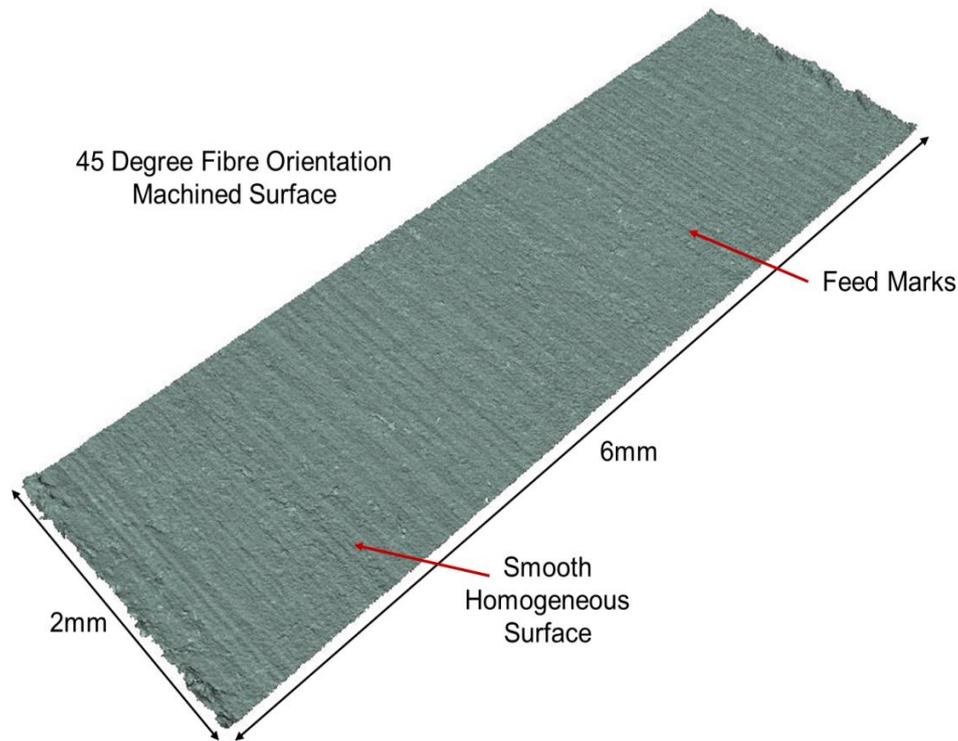
Figure 5-11- Optical surface scan unidirectional laminate. (45 degree fibre orientation, worn tool, 800 mm/min, 6000 RPM).

The average S_a surface roughness measured by the optical system is shown in Table 5-6 and Table 5-7 for each of the cutting speeds, feed rate and fibre orientations. The results for 90 degree fibre orientation and 45 degree fibre orientation are shown in Table 5-6 and Table 5-7 respectively. Un-cut fibres were also recorded and measured on the top and bottom edges of the laminate. It was found that it was more likely to find uncut fibres, (Type II delamination) when machining on the 45 degree orientation- Table 5-7. A machined sample is shown in Figure 5-12, where Type II delamination is shown on the top and bottom of the laminate. The maximum delamination length of 2 mm, shown in Table 5-9, correlated with the worn tool and 45 degree fibre orientation. Whereas, a maximum delamination length of 0.4 mm was found in the 90 degree fibre orientation machined samples, as shown in Table 5-8. The maximum delamination also correlated with the samples with the highest surface roughness. The results showed that the un-cut fibres increased

135

significantly when using the worn tool and for the 45 degree fibre orientation. This result is confirmed by Voss et al. [84], who found that that top-layer delamination and un-cut fibres was most prevalent on fibre orientations between 0 and 90 degrees. It has also been confirmed by Hintz et al. [85], that increasing tool wear and the fibre orientation are significant factors in delamination frequency on top layers of the laminate.

In contrast, during this study a sharp cutting edge of the new tool was able to cleanly shear the fibres of the 45 and 90 degree fibre orientation and leave a smooth surface quality. The presence of top-layer delamination was significantly reduced. In contrast, the worn tool left fibres un-cut, which then spring back elastically and protrude over the machined edge as fibre delamination. This may be because it is harder to shear the fibres on the top and bottom plies where there is less support from surrounding material. In the 45 degree fibre orientation the fibres are facing away from the cutting tool, and have not been cut cleanly as shown in Figure 5-12.

Machined Edge   Un-cut Fibres   Fibre Fuzzing
(Type II Delamination)   (Outer Edges)
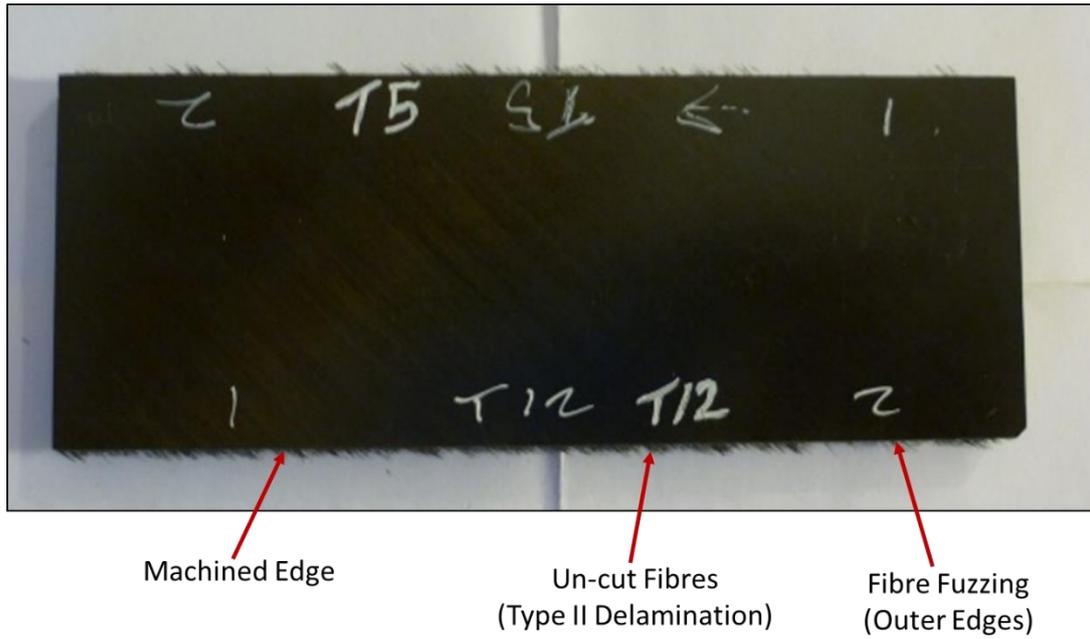
Figure 5-12- Machined unidirectional sample 45 degree orientation showing some un-cut fibres on top and bottom of laminate (worn cutting tool).

Table 5-6- Surface roughness measurements- 90 degree fibre orientation.

Test	Fibre Orientation	Feed Rate (mm/min)	Cutting Speed (RPM)	S_a Scan 1	S_a Scan 2	S_a Scan 3	Average S_a (µm)	Standard Deviation
Unworn	90	800	6000	1.53	1.59	1.41	1.51	0.09
Unworn	90	1200	6000	1.53	1.65	1.63	1.6	0.06
Unworn	90	800	8000	1.59	1.51	1.54	1.55	0.04
Unworn	90	1200	8000	1.51	1.53	1.47	1.5	0.03
Worn	90	800	6000	1.63	1.7	1.72	1.68	0.05
Worn	90	1200	6000	1.98	1.7	1.78	1.82	0.14
Worn	90	800	8000	1.73	1.63	1.72	1.69	0.06
Worn	90	1200	8000	1.66	1.54	1.67	1.62	0.07

Table 5-7-Surface roughness measurements- 45 degree fibre orientation.

Test	Fibre Orientation	Feed Rate (mm/min)	Cutting Speed (RPM)	S_a Scan 1	S_a Scan 2	S_a Scan 3	Average S_a (μm)	Standard Deviation
Unworn	45	800	6000	1.62	1.68	1.62	1.64	0.033
Unworn	45	1200	6000	1.94	2.08	2	2.01	0.071
Unworn	45	800	8000	2.48	2.3	2.23	2.33	0.128
Unworn	45	1200	8000	1.98	2.53	2.32	2.28	0.277
Worn	45	800	6000	1.78	1.85	1.84	1.82	0.038
Worn	45	1200	6000	2.09	2.23	2.17	2.16	0.07
Worn	45	800	8000	2.6	2.52	2.4	2.51	0.101
Worn	45	1200	8000	2.11	2.73	2.43	2.42	0.31

Table 5-8- Delamination Measurements (Type II).

Test	Fibre Orientation	Feed Rate (mm/min)	Cutting Speed (RPM)	Maximum Delamination Length (mm)
Unworn	90	800	6000	0
Unworn	90	1200	6000	0
Unworn	90	800	8000	0
Unworn	90	1200	8000	0
Worn	90	800	6000	0
Worn	90	1200	6000	0
Worn	90	800	8000	0.4
Worn	90	1200	8000	0

Table 5-9- Delamination Measurements (Type II).

Test	Fibre Orientation	Feed Rate (mm/min)	Cutting Speed (RPM)	Maximum Delamination Length (mm)
Unworn	45	800	6000	0
Unworn	45	1200	6000	0
Unworn	45	800	8000	0
Unworn	45	1200	8000	0
Worn	45	800	6000	1.6
Worn	45	1200	6000	1.5
Worn	45	800	8000	2
Worn	45	1200	8000	2

5.1-5 Main Effects Plot- Unidirectional Laminate

Statistical software mini-tab was used in order to look at the mean trends in the data for the surface roughness [80]. Main effects plots show the mean response in the dataset for a particular input and output parameter change. They have been used to show the mean response in the surface roughness and machining forces due the experimental variables from the previous data in

Table 5-6 and Table 5-7. The mean effects on the S_a surface roughness are shown in Figure 5-13. The factors were fibre orientation, CER, feed rate and cutting speed and their corresponding output effect on the surface roughness. The P values for each of the parameters effects on the surface roughness are shown in Table 5-10. The effect of fibre orientation on surface roughness showed the lowest P value in Table 5-10, followed by CER. An increase in surface roughness on the 45 degree fibre orientation was shown in Figure 5-13. The lower surface roughness was found on the 90 degree fibre orientation which is due to a different cutting mechanism with fibre orientation. This also correlates with the maximum delamination shown previously in Table 5-8 and Table 5-9, because there was less un-cut fibres on the top and bottom plies measured on the 90 degree compared to the 45 degree fibre orientation. The

larger surface roughness in the 45 degree orientation can mainly be attributed to the top and bottom edge delamination due to un-cut fibres. Shown in Figure 5-13, the S_a surface roughness also increases with CER due to an increased tool workpiece contact area and higher friction. There were more delaminated fibres and the PCD milling tool is unable to cleanly shear the fibres due the blunt cutting edge. The P value of 0.122 also showed that the statistical contribution of the CER on S_a can be assumed to be significant.

Table 5-10- Parameter effects on Surface Roughness (S_a)- P Values

Parameter	P Value
Fibre Orientation	0
Feed Rate	0.4
Cutting Speed	0.056
CER	0.122
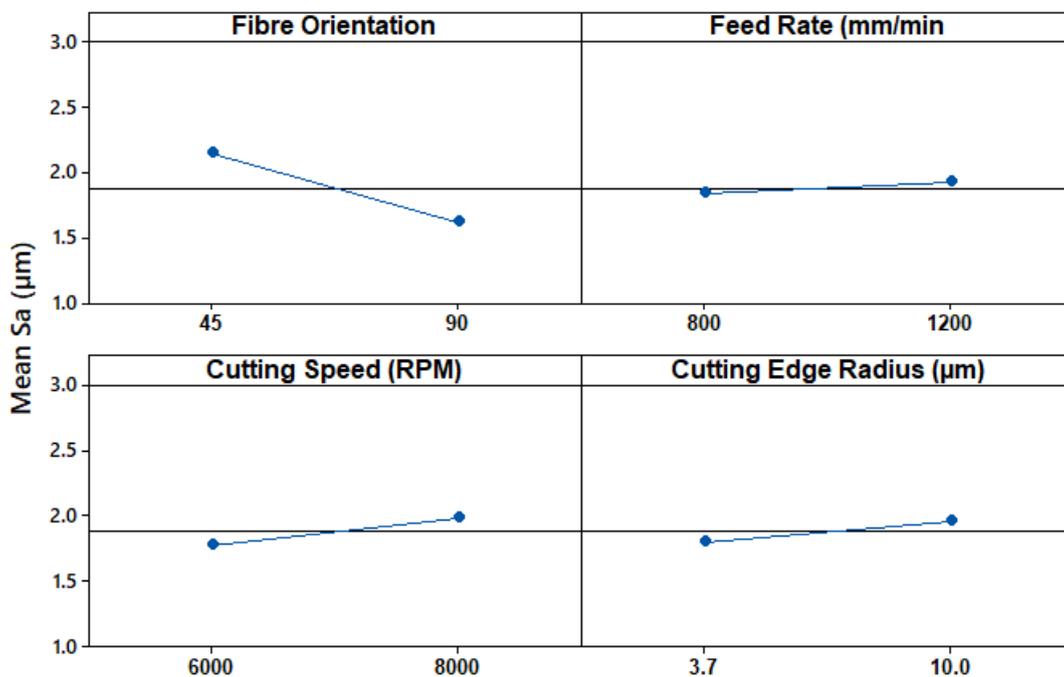
Figure 5-13 – S_a Main effects plot.

140

In Figure 5-14 and Figure 5-15 the main effects plot for the Fx and Fy cutting forces are shown for the Fx and Fy cutting forces. The P values are shown in Table 5-11 and Table 5-12. The feed rate and CER were found to have the lowest P values for the effects on both the Fx and Fy machining forces. In Figure 5-14 the Fx cutting forces increase with an increase in feed rate and decrease with increasing cutting speed. Increasing the feed rate and decreasing the cutting speed will correspond with an increasing chip thickness and larger area of chip removed. This causes the cutting mechanism to change to a mechanical wrenching as opposed to a fibre shearing mechanism [81]. Increase in the cutting edge radius had a corresponding increase in both the cutting and thrust forces. A negligible effect was seen in the two main effects plost for the effect of the material fibre orientation on the Fx and Fy machining forces, which was also represented by the high P values for the effect of fibre orientation in Table 5-11 and Table 5-12.

Table 5-11- Parameter effects on Mean Cutting Force (F_x)- P Values

Parameter	P Value
Fibre Orientation	0.879
Feed Rate	0.007
Cutting Speed	0.118
CER	0
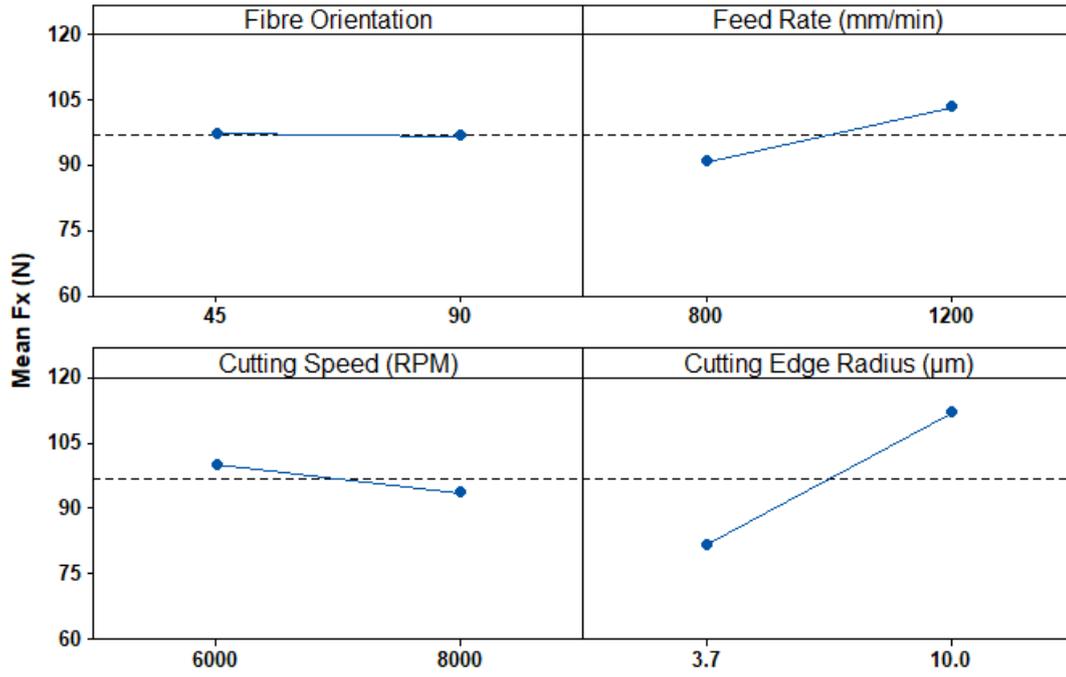
Figure 5-14- Main effects plot for mean Fx cutting force unidirectional test.

Table 5-12- Parameter effects on Mean Thrust Force (F_y)- P Values

Parameter	P Value
Fibre Orientation	0.641
Feed Rate	0.010
Cutting Speed	0.866
CER	0
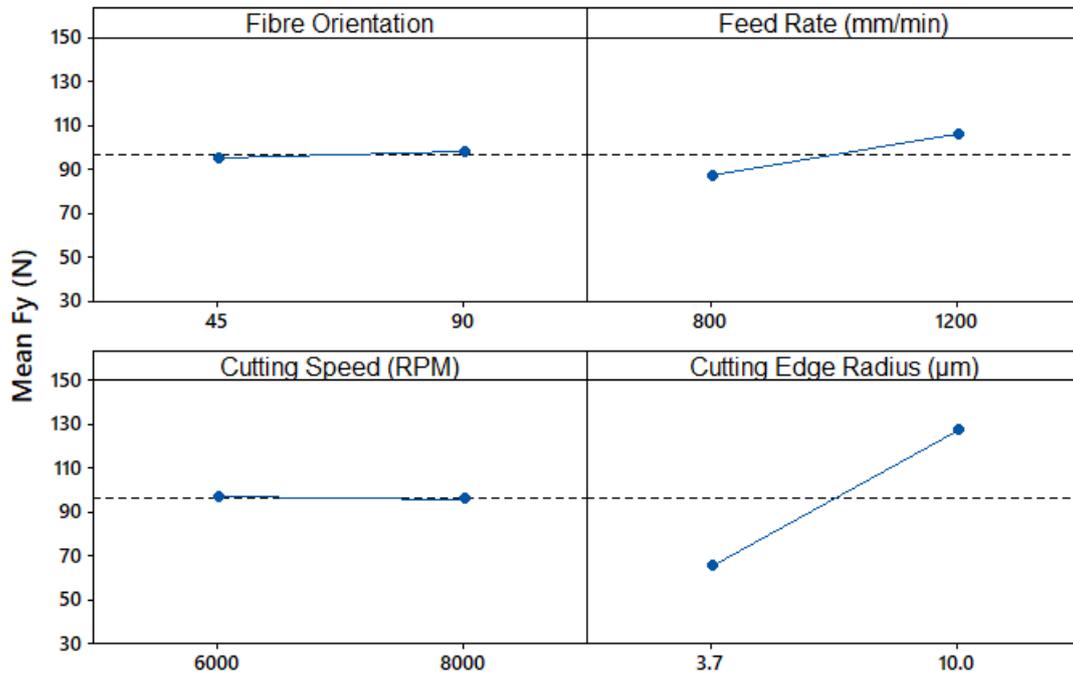
Figure 5-15- Main effects plot for mean Fy thrust force unidirectional test.

5.2 Experimental Results- Multidirectional Laminate

The results from the second multidirectional test are presented. The test was performed successfully with incremental levels of wear on the tool which was tracked by optical system in the cutting edge radius measurements over the test progression. The top and bottom laminate layers of the machined surface were free of un-cut fibres and delamination. Cutting forces have been presented along with measured surface roughness against increasing tool wear and machining parameters. Multiple linear regression models will be applied in next section to analyse the contribution of each parameter and create a regression equation.

Firstly, as the experiment was performed, the tool wear was tracked throughout the test. The cutting edge radius was measured from each of the three cutting edges of the tool to find an average. The average cutting edge radius is shown in Table 5-13 for *Tool 1* and in Table 10-9 for *Tool 2* in the Appendix.

143

Table 5-13- Cutting edge radius from Alicona scans (*Tool 1*).

Test	Feed	Cutting Speed	Edge Radius μm	Distance Machined (mm)
			3.36	0
1	1000	7000	**3.36**	80
2	1000	9000	**3.36**	160
7	1200	7000	**4.94**	240
8	1200	9000	**4.94**	320
9	1000	7000	**5.2**	400
10	1000	9000	**5.2**	480
13	1000	7000	**5.84**	560
14	1000	9000	**5.84**	640
19	1200	7000	**6.11**	720
20	1200	9000	**6.11**	800
21	1000	7000	**6.34**	880
22	1000	9000	**6.34**	960
27	1200	7000	**6.48**	1040
28	1200	9000	**6.48**	1120
29	1000	7000	**6.6**	1200
30	1000	9000	**6.6**	1280
33	1000	7000	**6.6**	1360
34	1000	9000	**6.6**	1440
39	1200	7000	**6.69**	1520
40	1200	9000	**6.69**	1600

5.2-1 Surface Roughness Measurements

Optical scans were taken of the surface using the focus variation system in the two positions on the machined surface described previously. The scan size was 10 mm by 2 mm. An image of the scans taken using optical device is shown in Figure 5-16. This represents the machined surface at different levels of tool wear. These images are 2D images, of a 3D surface profile, which are shown looking directly onto the machined surface- perpendicular to the machined face of the sample. The machined surface goes from left to right across the page where the tool length axis will pass across the surface in the same direction, which is in the direction of feed. In Figure 5-16 is shown the surface quality at increasing levels of tool wear from four different tests at a feed rate

144

of 1000 mm/min and a cutting speed of 7000 RPM. The cutting tool edge radiuses, due to edge wear, and are 3.36 µm, 5.35 µm and 6.38 µm for test 1, test 17 and test 37, respectively. It is shown in the image that there is increased surface damage with an increasing tool edge radius. Also, it can be seen that there is a variation in surface structure and magnitude of visual damage on different fibre orientations. Figure 5-17 shows the surface quality from optical focus variation scans taken at an angle to the plane of the surface, against increasing tool wear from (a) to (c). These are 3D images which detail the optical focus variation system as used to capture surface profile height and colour information. The images show the range of damage on each of the ply layers, where the darker regions represent the more pitted and torn surface of the 135 degree orientation. The lighter regions highlighted in Figure 5-16 and Figure 5-17 represent ply orientations at 0 degrees where the fibres are lying parallel to the machined surface. The laminates each have the same stacking sequence, so that the fibre orientations on each laminate correspond to the following image but with a greater level of cutting tool wear, and consequently have shown a more rough and pitted surface.
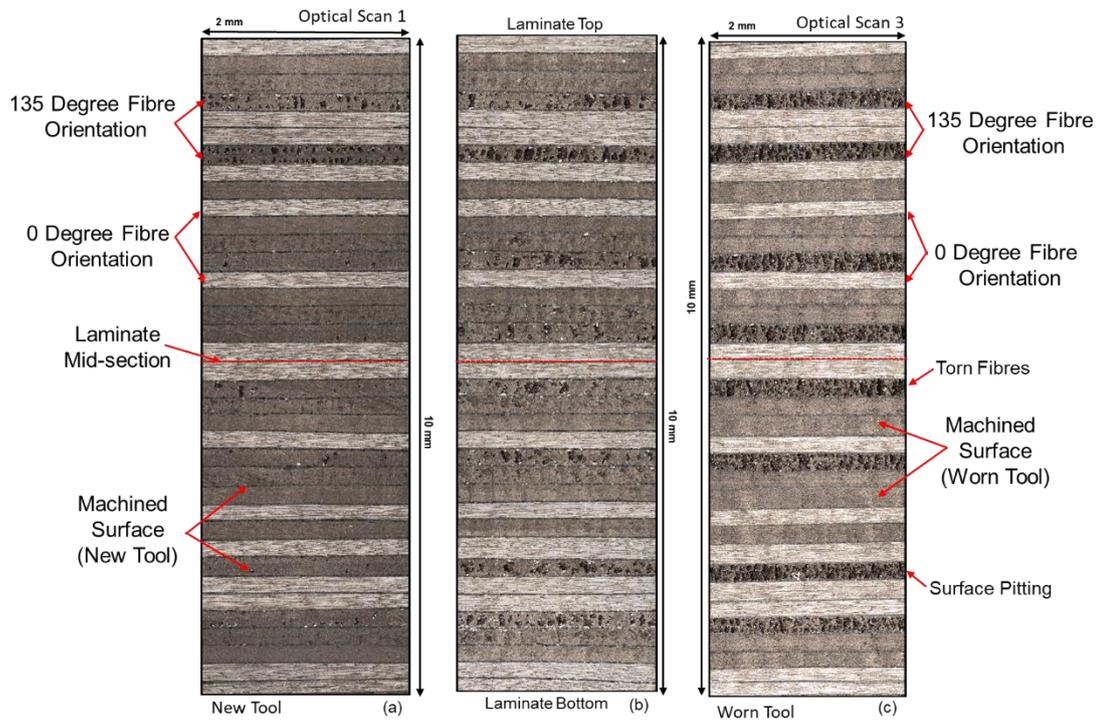
Figure 5-16- Multidirectional optical focus variation scans. Images show a 2D plane image of the machined surface profile texture at increasing tool weal. The full laminate thickness of 10mm is shown.
(a) Test 1, (c) Test 17 (d) Test 37.
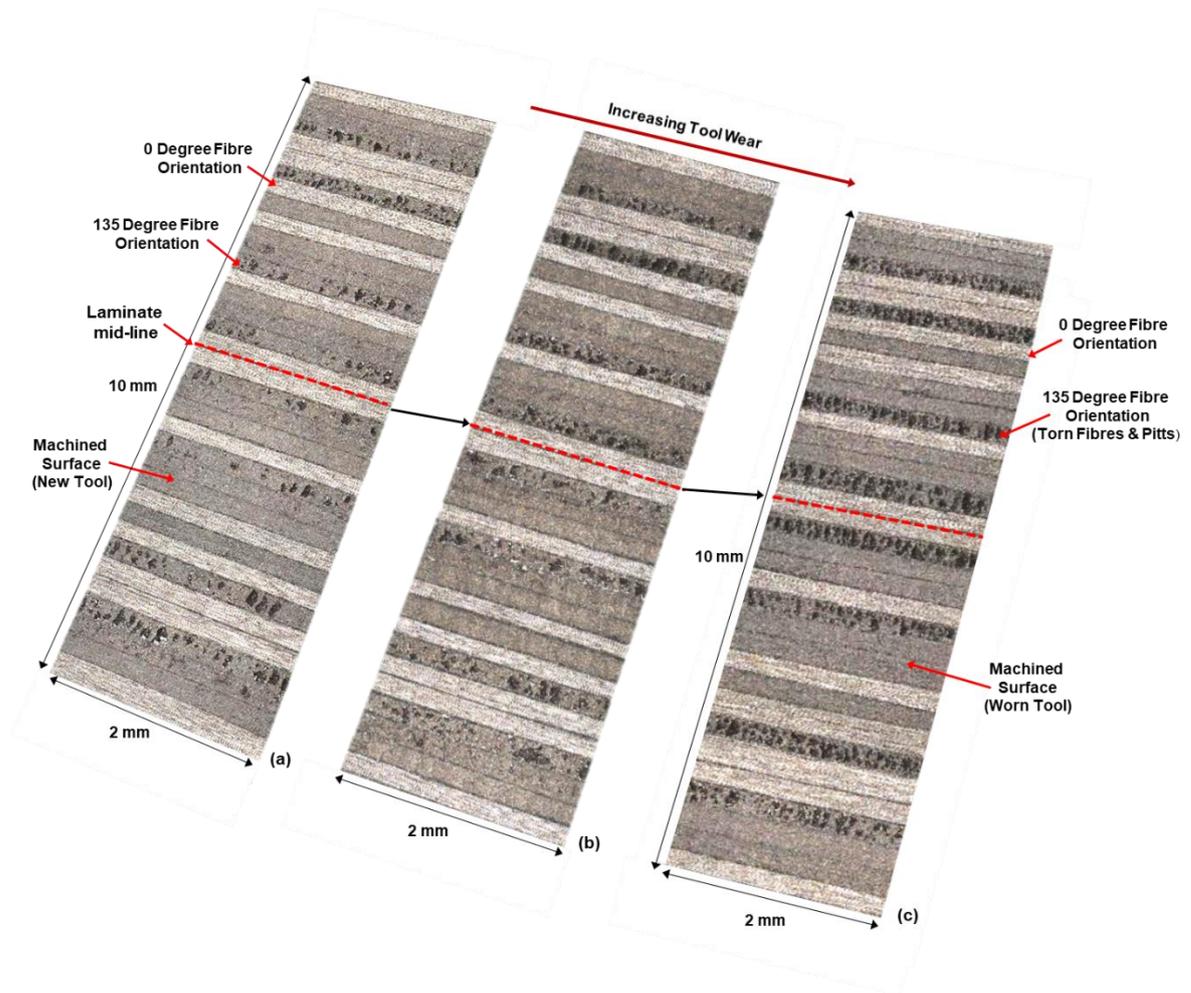
Figure 5-17- Machined Surface Optical scans from focus variation system of multidirectional laminate. . Images show a 3D surface image of the machined surface profile texture at increasing tool weal. The full laminate thickness of 10mm is shown.
(a) Test 7, (b) Test 19 and (c) Test 27.

Surface roughness parameters (S_a, skewness and kurtosis), were calculated for each of the 40 tests. The average of each parameter was calculated from the two positions and is shown in Table 5-14 for tests 1-20 and in Table 10-10 in the Appendix Part A for tests 21-40. The standard deviation from the two measurement positions is shown.

Shown in Figure 5-18 is the increase in roughness with feed grouped by the two different cutting speeds applied, 7000 and 9000 RPM. The error bars

147

represent the standard deviation in the surface roughness measurement in the vertical direction. This is found from the repeat measurement of roughness on one sample in two different positions. The graphs show a higher rate of increase in surface roughness at the larger feed rate of 1200 mm/min compared to 1000 mm/min. An increased roughness with feed correlates with other results from the literature [26]. The highest roughness was seen at the higher feed rate and lower cutting speed, and this will correlate with the greatest chip thickness, as also reported by Azmi et al, [34]. Therefore in order to reduce surface roughness the tool wear should be minimised while using a smaller chip thickness.

Table 5-14- Average S_a calculated from the test samples in Test 1-Test 20.

Test Number	Feed (mm/min)	Cutting Speed (RPM)	Scan 1 S_a (µm)	Scan 2 S_a (µm)	Average S_a (µm)	Standard Deviation
Test 1	1000	7000	1.77	1.71	**1.74**	**0.04**
Test 2	1000	9000	1.89	1.78	**1.83**	**0.08**
Test 3	1200	7000	1.72	1.69	**1.71**	**0.02**
Test 4	1200	9000	1.43	1.29	**1.36**	**0.10**
Test 5	1000	7000	1.84	1.7	**1.77**	**0.10**
Test 6	1000	9000	1.47	1.47	**1.47**	**0.00**
Test 7	1200	7000	1.79	1.93	**1.86**	**0.10**
Test 8	1200	9000	1.82	1.74	**1.78**	**0.06**
Test 9	1000	7000	1.76	1.72	**1.74**	**0.03**
Test 10	1000	9000	1.67	1.63	**1.65**	**0.03**
Test 11	1200	7000	1.93	1.9	**1.92**	**0.02**
Test 12	1200	9000	1.61	1.56	**1.58**	**0.04**
Test 13	1000	7000	1.67	1.77	**1.72**	**0.07**
Test 14	1000	9000	1.65	1.56	**1.6**	**0.06**
Test 15	1200	7000	1.74	1.65	**1.69**	**0.06**
Test 16	1200	9000	1.39	1.48	**1.44**	**0.06**
Test 17	1000	7000	1.45	1.45	**1.45**	**0.00**
Test 18	1000	9000	1.41	1.31	**1.36**	**0.07**
Test 19	1200	7000	2.15	2.13	**2.14**	**0.01**
Test 20	1200	9000	1.66	1.73	**1.7**	**0.05**
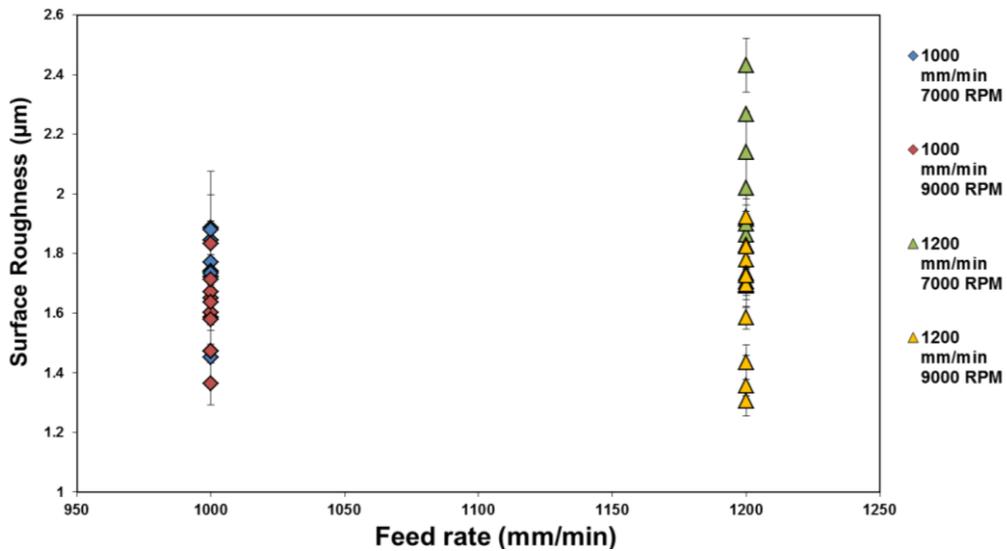
Figure 5-18- Surface roughness (S$_a$) vs feed rate (grouped by applied cutting speed). (Error bars show standard deviation in roughness measurement.)

Shown in Figure 5-19 and Figure 5-20 is the S$_a$ surface roughness scatter plot against increasing cutting edge radius, the lines are fitted and grouped on dependant parameters cutting speed and feed rate. Figure 5-19 shows the increase in surface roughness with cutting edge radius for a cutting speed of 7000 RPM and a feed rate of 1000 and 1200 mm/min. While Figure 5-20 is shown for a cutting speed of 9000 RPM. The horizontal error bars represent the standard deviation in the cutting edge radius measurement for each of the three cutting edge radii. Figure 5-19 and Figure 5-20 both shown an increasing trend in the S$_a$ surface roughness with increased cutting edge radius. There is also shown to be a greater increase in roughness with cutting edge radius at the higher feed rate of 1200 mm/min, and therefore feed rate and cutting edge radius together both have a contributing effect on the roughness. A higher feed rate and higher edge radius will increase the surface roughness significantly.

It was found that there is a relatively large standard deviation in the cutting edge radius measurements, and this can be most likely explained due to the manufacture of the cutting edges, whereby they do not start with exactly the

same initial edge radius. Also each edge will not wear at exactly the same rate due to random variation in the composition of the PCD material in each edge, and the dynamic nature of the tool wear. The wear process is due to brittle fracture of the cutting edge and chipping and is not a constant process. The wear rate will not be constantly consistent across each edge. For each edge scan there is a number of cross sections along the length of each cutting edge to take a mean value. The standard deviation is calculated from the deviation from each of the three different cutting edges. Therefore a relatively large standard deviation between the different edge radii of the three cutting edges is not wholly unexpected.
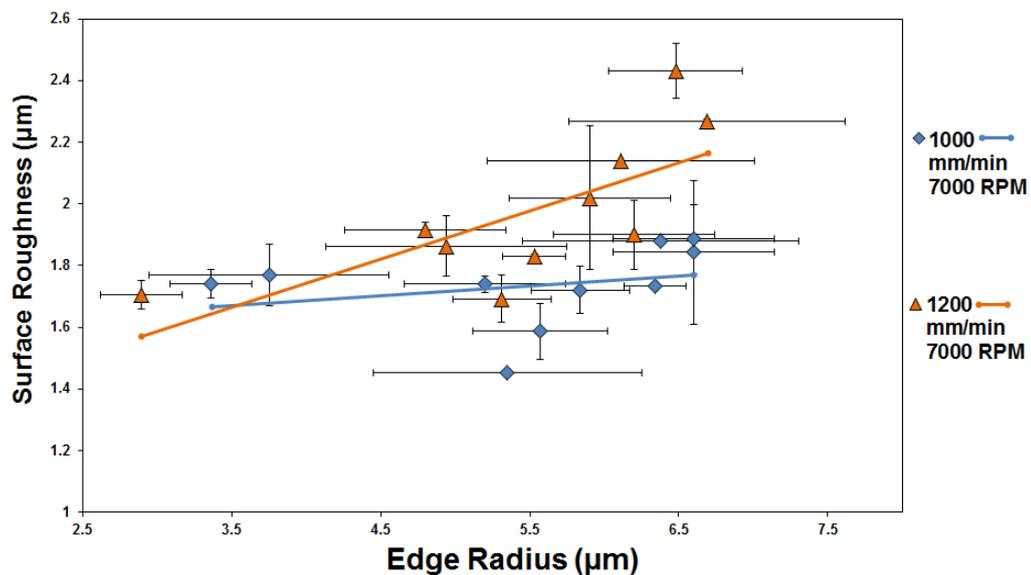
Figure 5-19- Mean S_a against increasing edge radius, grouped by dependant parameters feed rate and cutting speed at 7000 RPM. The error bars show standard deviation in roughness and edge radius measurement.

150
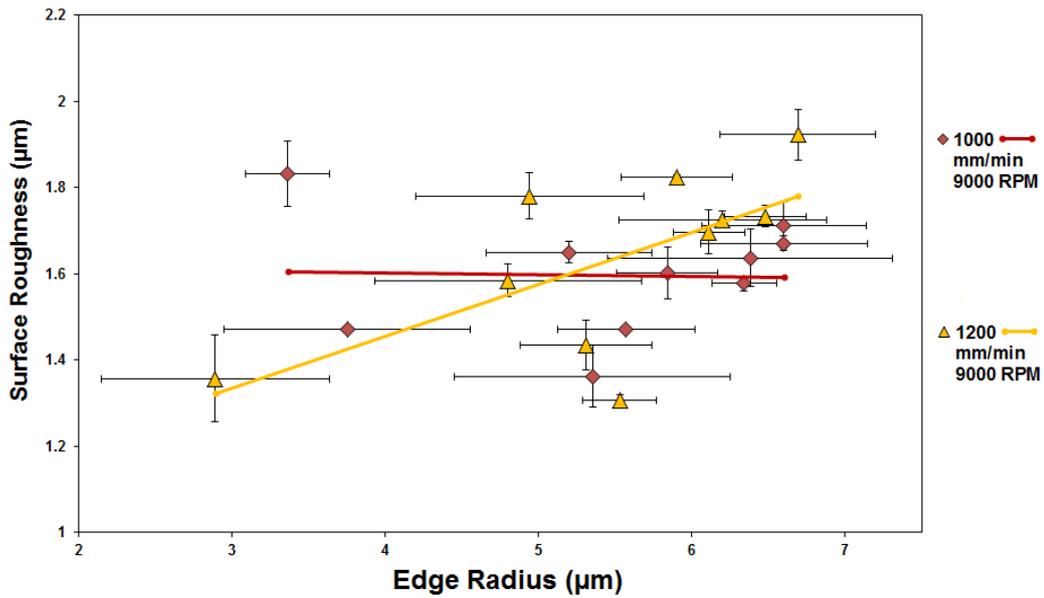
Figure 5-20- Mean S_a against increasing edge radius, grouped by dependant parameters feed rate and cutting speed at 9000 RPM. The error bars show standard deviation in roughness and edge radius measurement.

5.2-2 Machining Forces from Experiment

The mean cutting forces recorded from the experiment using the dynamometer are shown in Table 5-15 for tests 1-4 and 17-20 as an example. The inclusive data is presented for Tests 1-20 and Tests 20-40 in Appendix Part A, Table 10-12 and Table 10-13, including the minimum, maximum and mean cutting forces from experiment. The mean cutting force is calculated from the average cutting force over the length of the cut. A portion is removed at the beginning and end, as shown in Figure 5-21, so that the beginning and end of cut is not included.

Table 5-15- Cutting forces- test number 1-4, 17-20.

Test	Feed Rate (mm/min)	Cutting Speed (RPM)	Mean Fx (N)	Mean Fy (N)
1	1000	7000	32.0	1.6
2	1000	9000	33.2	9.3
3	1200	7000	36.1	1.8
4	1200	9000	38.4	10.6
17	1000	7000	57.5	33.5
18	1000	9000	53.8	39.4
19	1200	7000	60.6	28.2
20	1200	9000	59.7	34.6
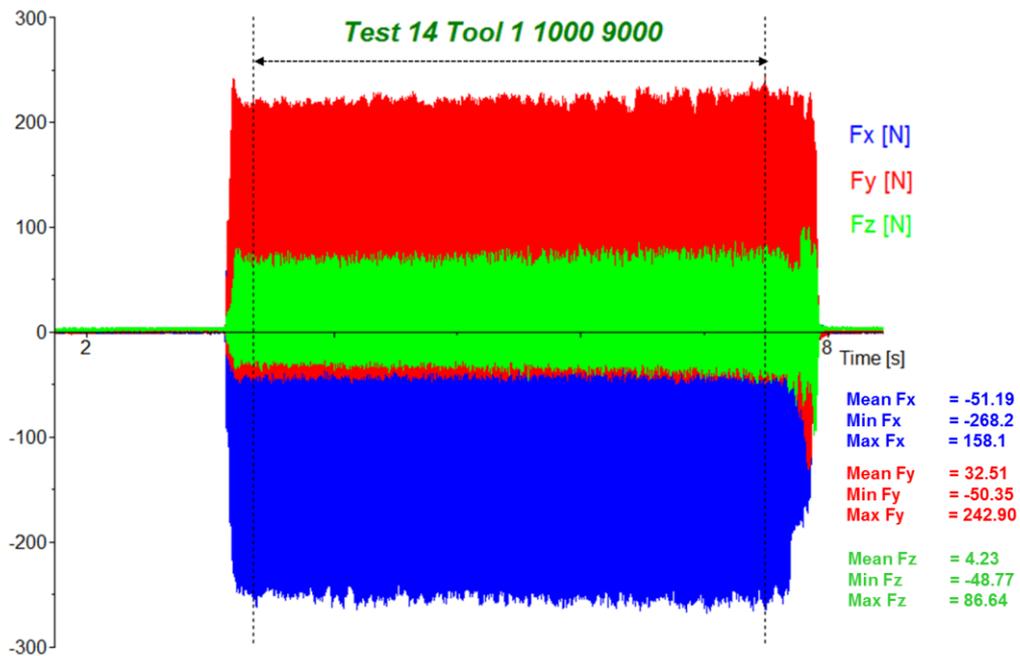
Figure 5-21- Machining forces from multidirectional test dynamometer.

Figure 5-22 shows the increase in Fx machining force with an increased cutting edge radius at a constant cutting speed of 7000 RPM and two different feed rates. Figure 5-23 shows the same output at higher cutting speed of 9000 RPM. There is shown to be a strong increasing trend in the Fx machining forces across both feed rates as the tool edge radius increases. This is caused due to

the increased friction and contact area between the tool and workpiece which will lead to higher machining forces in the cutting direction. Figure 5-24 and Figure 5-25 show the change in Fy thrust force with increasing cutting edge radius at 7000 and 9000 RPM respectively. In both Figure 5-24 and Figure 5-25 there is also an increasing trend in the thrust direction machining forces with edge radius. This may be due to the rounded cutting edge's inability to cleanly shear the fibres causing a change in the cutting mechanism and a higher friction between the tool and workpiece. It can be concluded that higher tool wear due to an increased cutting edge radius caused an increasing trend in both components of the machining forces in the edge trimming test. There are no error bars for the cutting forces because each point represents a single value in the test, where the tests have been repeated, but with an increasing cutting edge radius.
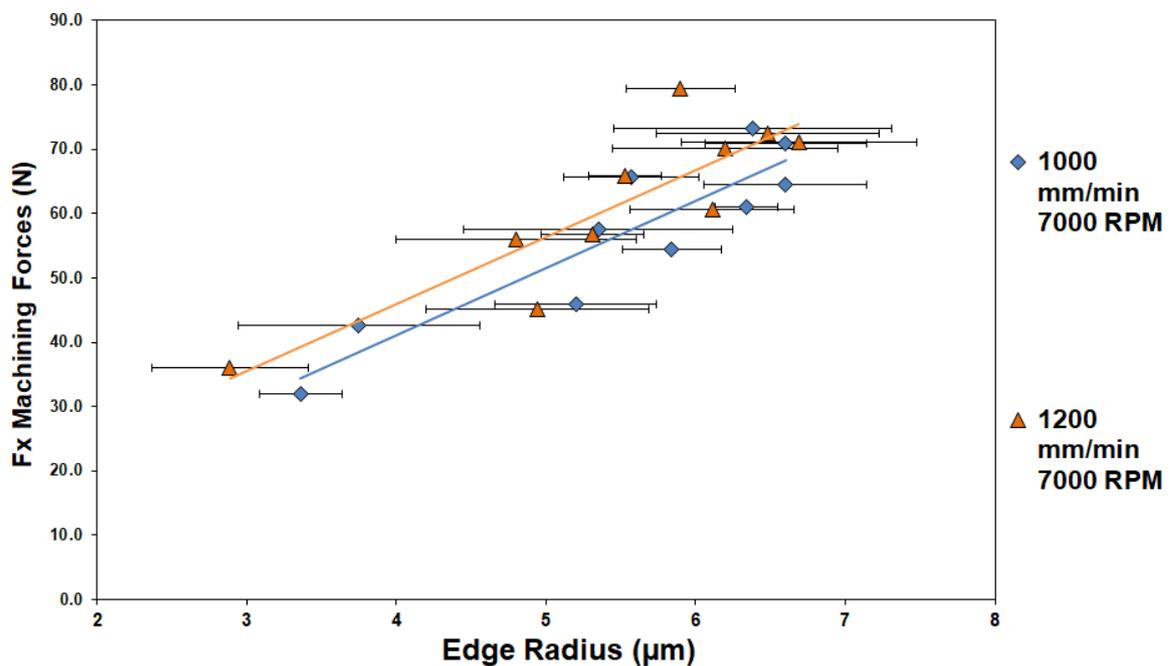
Figure 5-22- Fx Cutting forces against increasing edge radius at 7000 RPM. The error bars represent standard deviation in the edge radius measurement from 3 cutting edges.
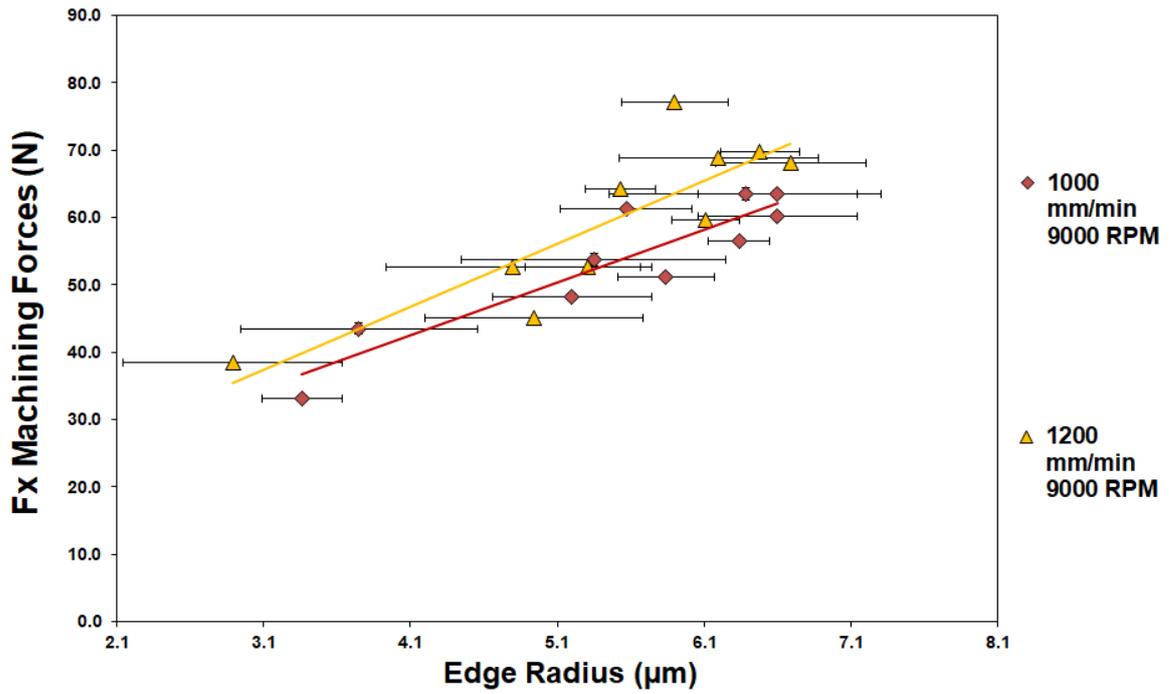
Figure 5-23- Fx Cutting forces against increasing edge radius at 9000 RPM. The error bars represent standard deviation in the edge radius measurement from 3 cutting edges.
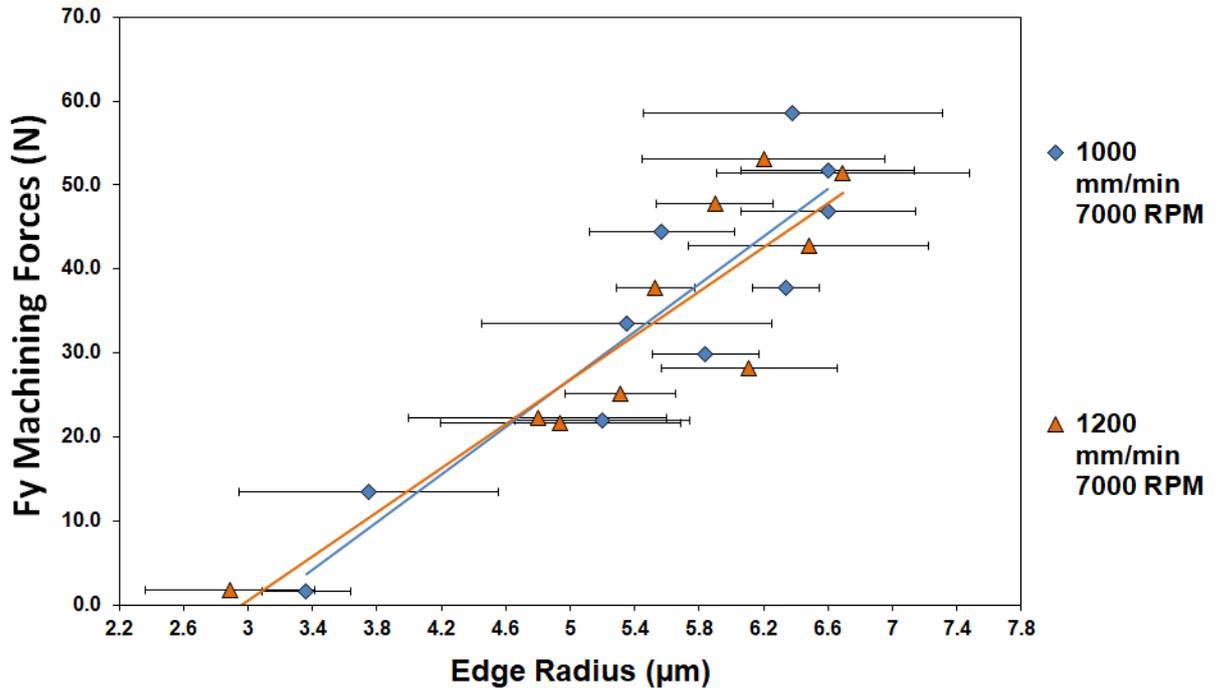
Figure 5-24- Fy Cutting forces against increasing edge radius at 7000 RPM. The error bars (x-axis) represent standard deviation in the edge radius measurement from 3 cutting edges.
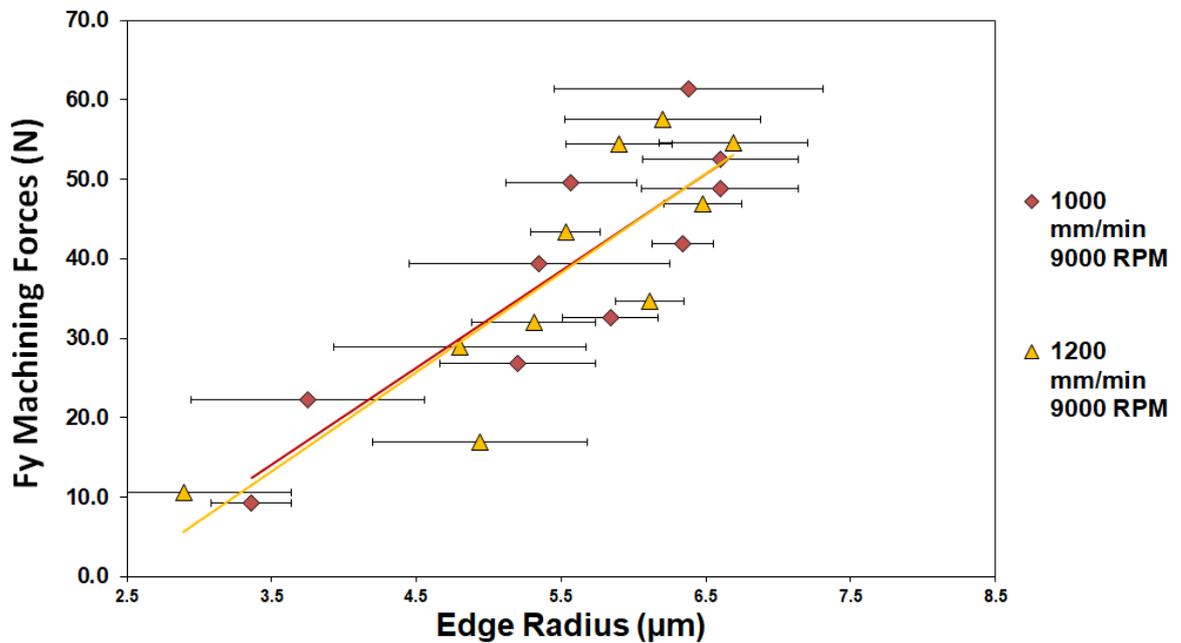
Figure 5-25- Fy Cutting forces against increasing edge radius at 9000 RPM. The error bars represent standard deviation in the edge radius measurement from 3 cutting edges (x-axis).

5.2-3 Main Effects Plots- Multidirectional Laminate

Statistical software mini-tab was used to look at the mean trends in the data [80]. The factors are feed rate and cutting speed which are compared with the average F_x and F_y cutting forces as shown in Figure 5-26 and Figure 5-27 respectively. In Table 5-16 the P values for the feed rate and cutting speed on the F_x machining force are shown. The feed rate has a P value of 0.167 which is more significant than that of the cutting speed at 0.518. The effect of increasing the feed rate was a mean increase in the Fx cutting forces. This correlates with results from the literature [86]. It has been shown that increasing the feed rate in composite machining will generally change the cutting mechanism more from a fibre shearing into a ploughing mechanism, where the fibres will be torn and plucked from the workpiece. Increasing the cutting speed caused a slight decrease in the Fx machining forces, which is due to a decreased chip thickness for each pass of the cutting edge. Yet the effect of cutting speed is found to be fairly insignificant. The P values in Table 5-17 show that the feed rate and cutting speed do not have a very strong statistical effect on the Fy thrust force in machining. This may be due to the relatively small mean change in thrust force with change in machining parameters. Finally, the effect of the experimental variables on the S_a roughness parameter is shown in Figure 5-28. It was found that the feed rate had an increasing trend in the surface roughness which corresponds with previous work and the literature [34],[79]. The P values in Table 5-18 show that the feed rate and cutting speed have a significant effect on the surface roughness. Decreasing the chip thickness has therefore been shown to minimise the areal surface roughness in this instance. N. Nguyen-Dinh et al. [87] have shown that surface quality will decrease with an increase in feed speed, which they attributed to mechanical degradation of the matrix on the machined surface.

Table 5-16- Predictor P values effect on F_x machining force.

Predictor	P Value
Feed Rate	0.167
Cutting Speed	0.518
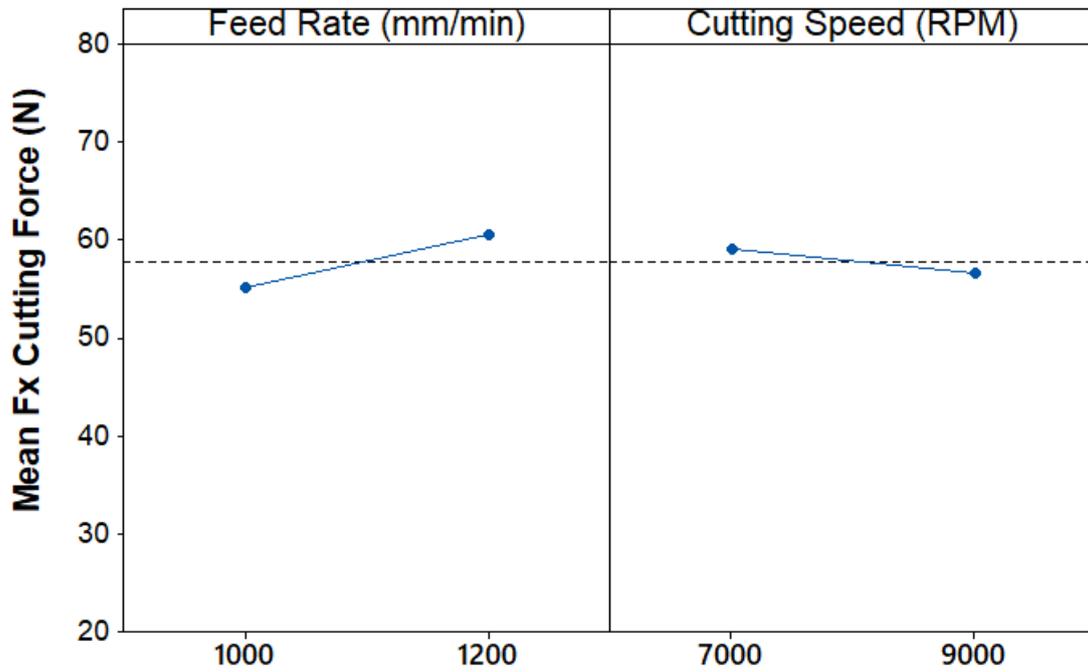
Figure 5-26- Main effects plot for average Fx.

Table 5-17- Predictor P values effect on F_y Thrust Force.

Predictor	P Value
Feed Rate	0.903
Cutting Speed	0.377
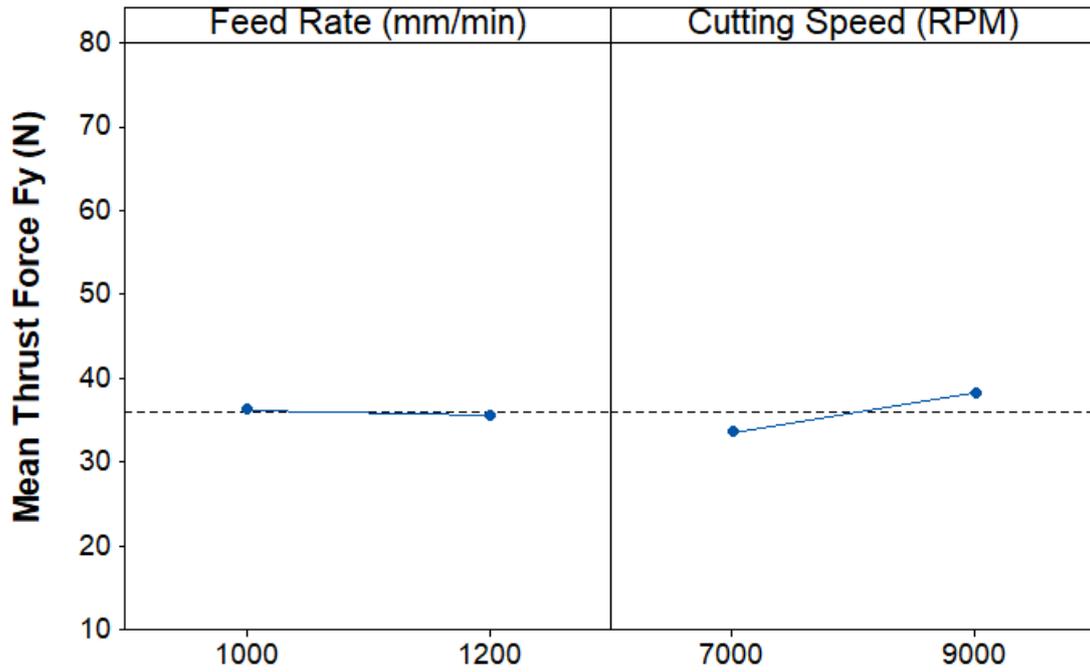
Figure 5-27- Main effects plot for average Fy.

Table 5-18- Predictor P values effect on S_a Surface roughness.

Predictor	P Value
Feed Rate	0.03
Cutting Speed	0
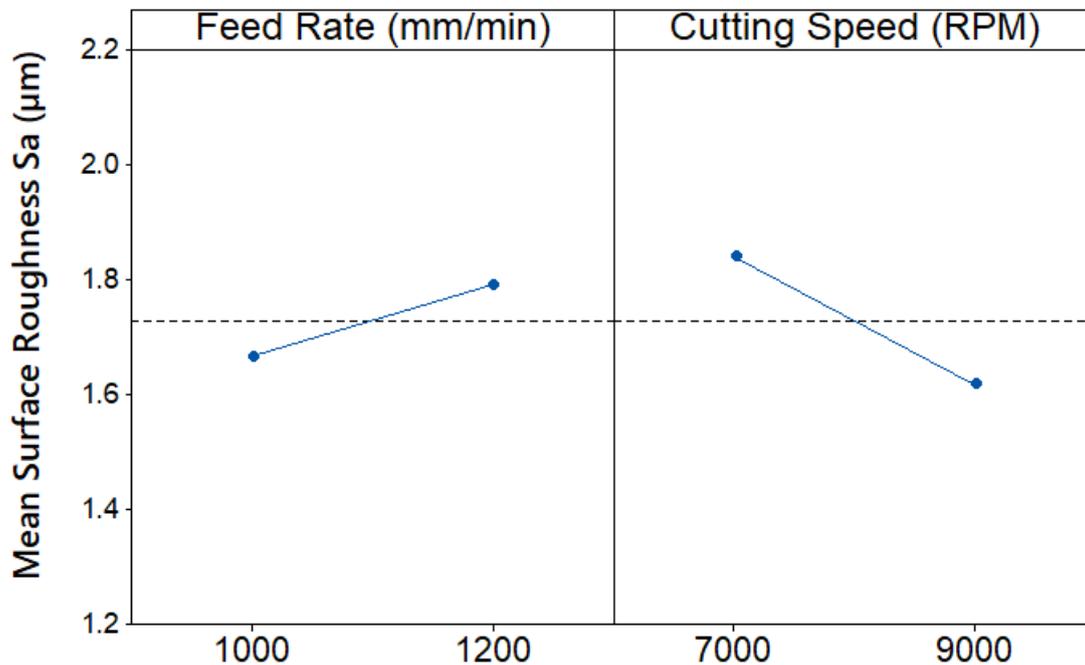
Figure 5-28- Main effects plot for average surface areal roughness parameter S_a.

5.2-4 Effects of Machining Forces on Surface Roughness

The effects of the measured machining forces on the surface roughness, plotted as a scatter diagram grouped by feed rate and cutting speed, are shown in Figure 5-29 and Figure 5-30. In general there appears to be a slightly increasing trend in the surface roughness with both Fx and Fy machining forces. The increasing trend in roughness with an increasing Fx feed force has a steeper slope at the higher feed rate of 1200 mm/min. It is expected that this effect is due to the larger chip thickness. At the lower cutting speed of 7000 RPM there is generally a slightly higher roughness. It can be concluded that the effect of the cutting forces on the surface roughness has an interacting effect with the cutting speed and the feed rate applied.
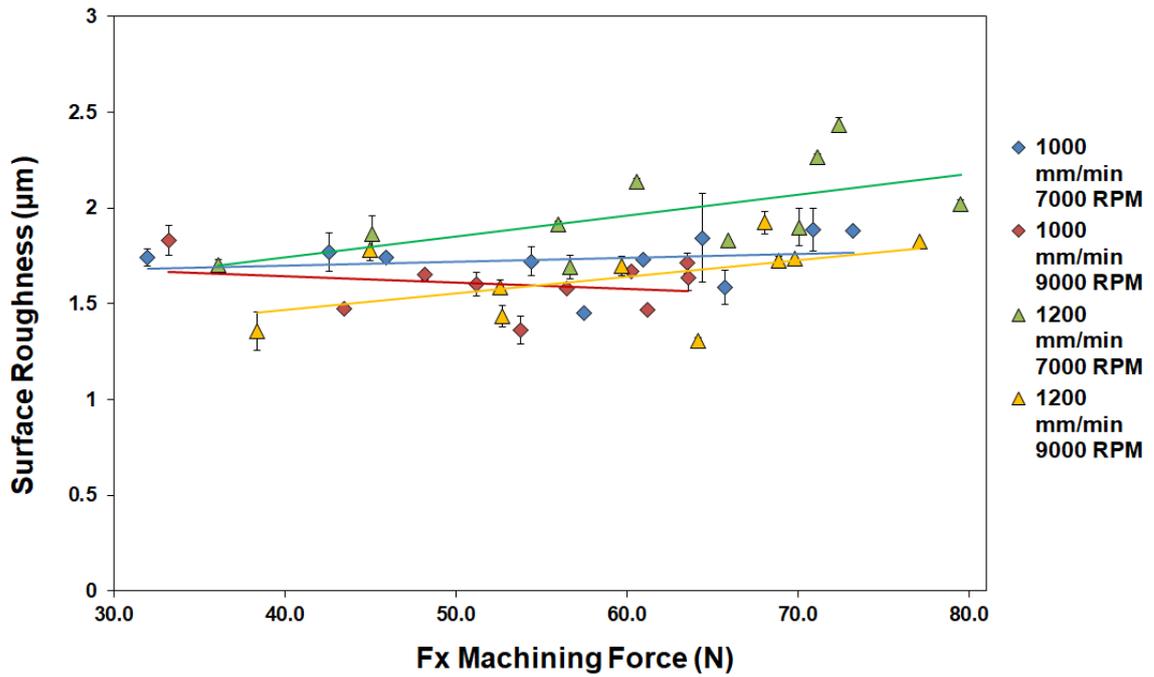
Figure 5-29- Surface roughness (S$_a$) vs Fx machining force from experiment. Grouped by applied cutting speed and feed rate.
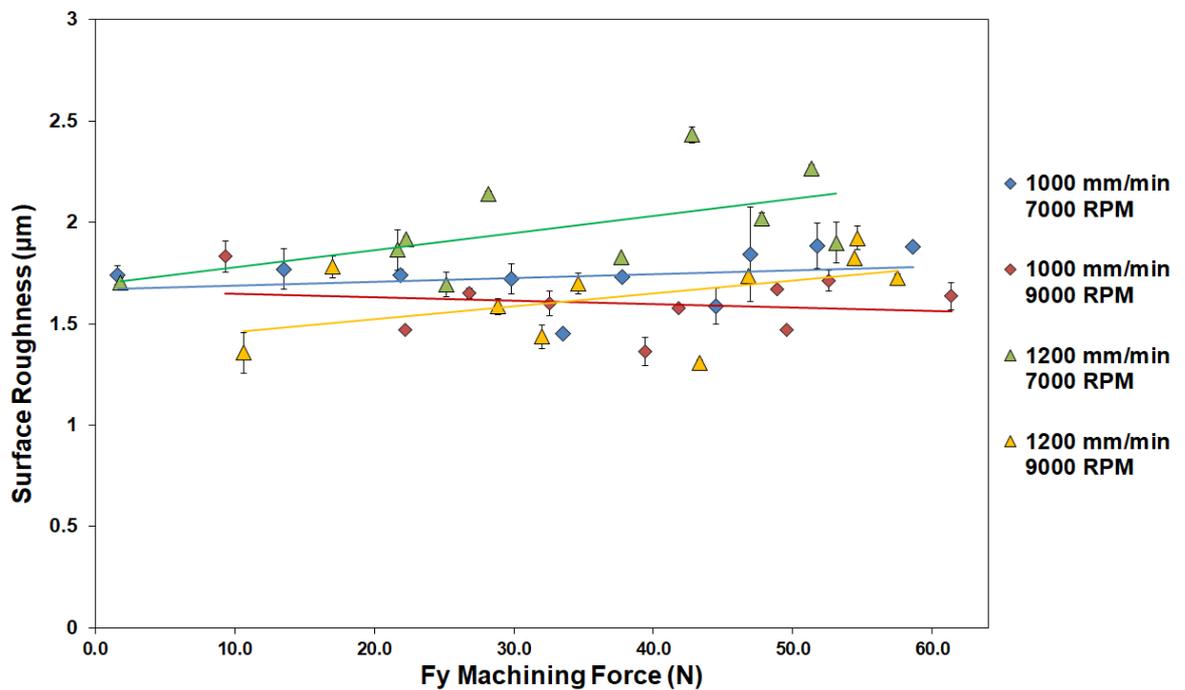
Figure 5-30- Surface roughness (S$_a$) vs Fy machining force from experiment. Grouped by applied cutting speed and feed rate.

5.3 Discussion- Surface Roughness Measurements

It is important to be able to accurately quantify the surface roughness of a fibrous composite material and this should be made possible using a repeatable method. The benefits of the optical system were found to be most apparent when measuring surface roughness of a multidirectional laminate machined surface. This is because the unidirectional laminate has a lower variation in surface texture and it can be concluded that the roughness measurement is less sensitive to stylus path than on a multidirectional laminate. This finding was also reported by Ramulu et Al. [5]. In addition, Ahmad et al. [88], made an assessment of machined surface morphology and showed that fibre orientation will have an effect on measured surface parameters. It was found in this work that the variation or scatter in roughness measurements on the multidirectional laminate, which was calculated using the optical system, was significant, and was considerably higher than that found on the unidirectional laminate. Therefore, the use of the optical device is highly advised on a multidirectional composite surface, (including GFRP), as it provides the ability to account for the different damage types, surface profile and directional measurement properties due to fibre orientation effects. The majority of industrial composite parts are made up of multidirectional laminates to optimise the strength of components by incorporating the directional properties of fibres, and therefore adoption of more accurate methods to quantify surface roughness from machining is necessary. Inability to take into account the different damages on each layer of the laminate will lead to uncertain measurements, and the findings suggest that use of stylus methods to measure surface roughness of a multidirectional laminate will lead to unreliable results.

Usefully, the optical device and areal parameters have been found to be less sensitive to measurement position, or path, than the stylus and therefore

provide a more accurate metric with which to assess machined composite surfaces.

In consequence it would be advisable to use the optical device for surface roughness measurements in this application with the adoption of additional roughness parameters to increase the surface profile information which is quantified. However, if due to the unavailability of this method, some recommendations can be applied if continuing to use stylus measurement for calculating surface roughness of machined surfaces of composites. On a multidirectional laminate it would be appropriate to do transverse measurements, (across the laminate thickness), and therefore passing over multiple fibre orientations. If making measurements parallel to the laminate the layer being measured is uncertain. It would also be advisable to use a greater number of repeat roughness measurements, in multiple positions, than would be applied on a standard metallic or more homogeneous surface. Using the stylus, the roughness measurement will have a larger standard deviation across measurement points due to the variation in surface structure. Additionally, care must also be introduced to use a repeatable method for positioning the stylus on different samples and there should be checks that there are no adhered fibres to the stylus tip.

5.4 Results- CT Scanning of Machined Samples

Micro-CT scans were performed using a CT scanner on machined samples with the method previously described. Firstly the unidirectional CT scanned samples will be shown, followed by the multidirectional samples. The sample views are detailed in Figure 5-31, where the top view is looking from above on the sample, and the left hand edge is being machined. The side view is looking directly onto the plane of the machined face and the front view is looking through thickness in the material travelling into the page in the tool feed direction. The sample views will follow this image orientation across the rest of

the figures. Shown in Figure 5-31 there are un-cut fibres which can be seen as type II delamination on the top and bottom layers of the laminate. This is caused by un-cut fibres during edge trimming which have been bent but not fully cut. They are then are allowed to spring back to their original orientation once the cutting tool has passed and are not cut. These fibres can be removed post-machining.
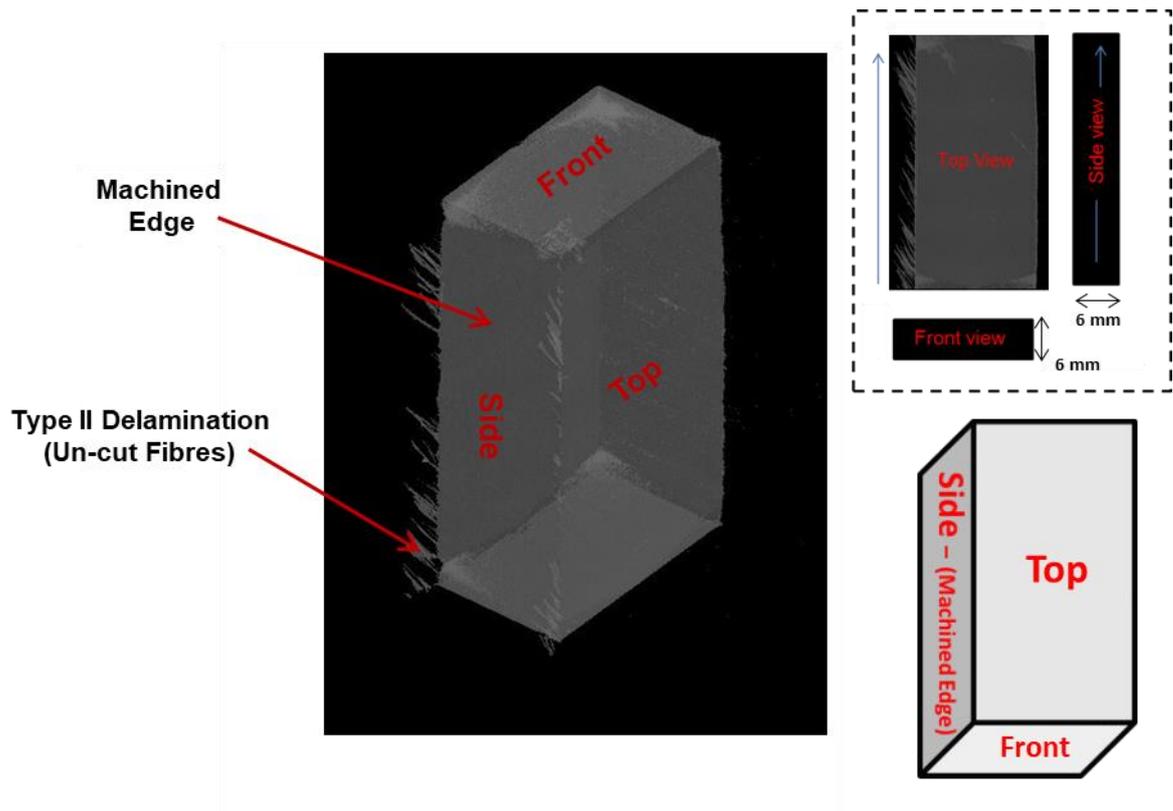
Figure 5-31- CT scan of machined unidirectional 45 degree fibre orientation, showing planar views.

Figure 5-32 show CT scans from the 45 degree fibre orientation unidirectional carbon fibre composite sample, which was edge trimmed with the worn PCD cutting tool- and an average edge radius of 10μm. The sample was machined at a feed rate of 800 mm/min and cutting speed of 8000 RPM. Shown in Figure 5-32 are the three different views for the 45 degree fibre orientation. The images in Figure 5-32(b) and Figure 5-32(c) show cross sections cut through the machined sample in the positions shown. The internal cracks which are

shown in Figure 5-32(a) are then imaged from alternate views through the sample to see the size of internal defects. It is shown that there is some internal cracks and inter-laminar delamination which propagate through the sample.
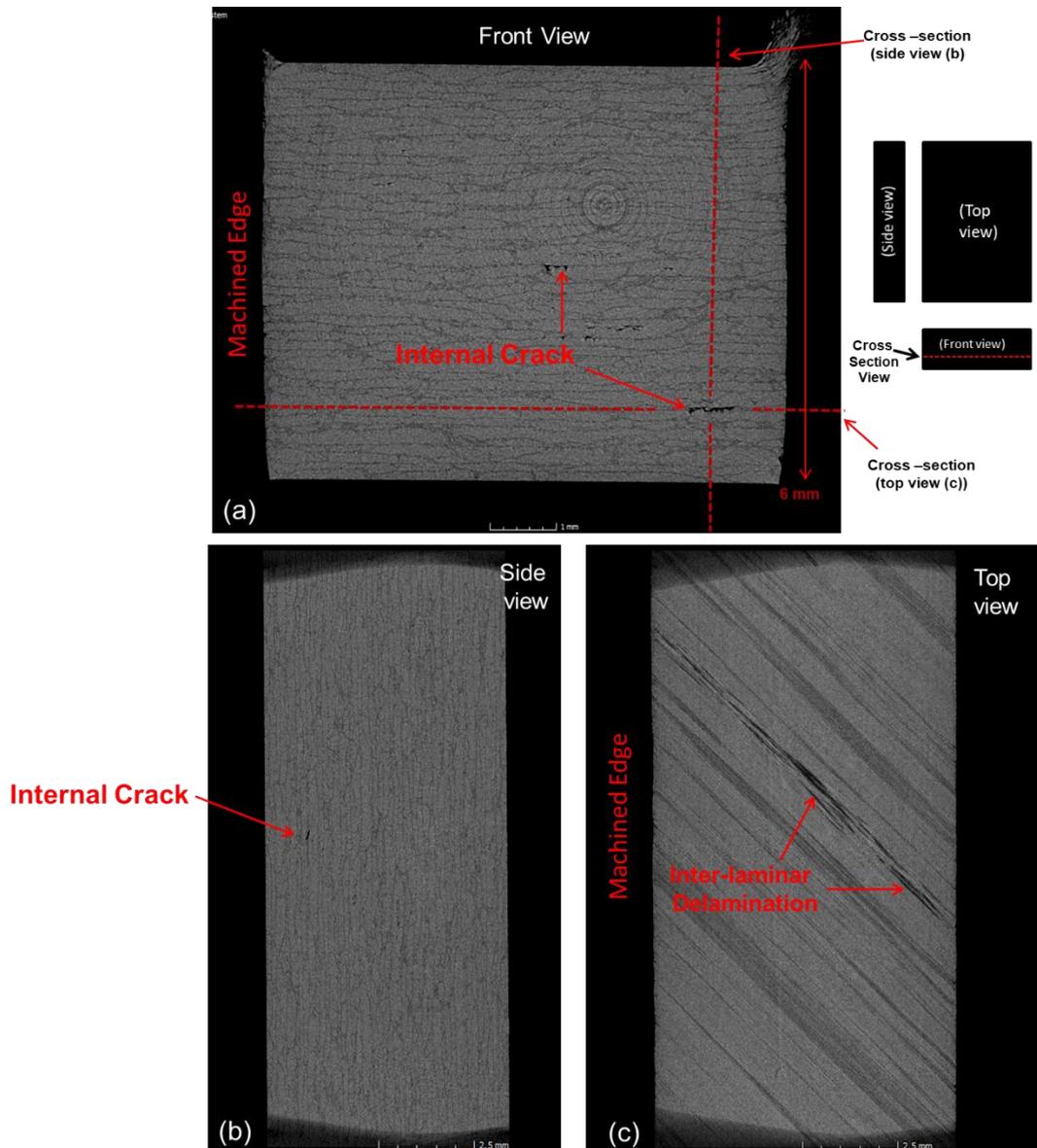
Figure 5-32- 45 degree fibre orientation with internal crack.

Shown in Figure 5-33 are cross-cross section images of the 45 degree fibre orientation machined sample, which was machined with the same parameters as Figure 5-32. The images are shown progressing through thickness in the plane of the top view, in which the planar view is shown by the green rectangle in Figure 5-33(e). Each images show progressive cross-sections from the top

moving through the material thickness from Figure 5-33(a)- Figure 5-33(d). It was found that there was inter-laminar delamination and material voids present, and these defects appear to propagate from the machined edge.
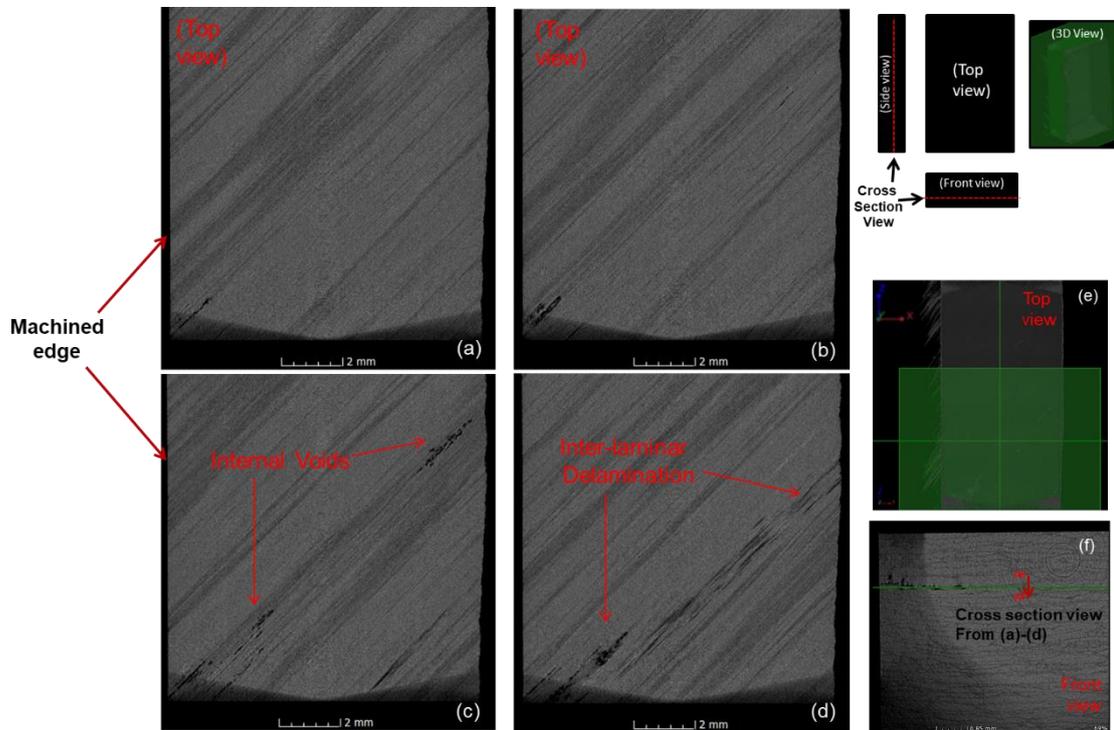
Figure 5-33- Inter-laminar Delamination propagating through thickness shown from the top view of the unidirectional laminate, machined at 45 degree fibre orientation.

Shown in Figure 5-34 is the CT scan images showing the unidirectional edge trimmed 45 degree fibre orientation, which show sample cross-sections of the front view. These images show progressing views through the sample thickness in the front plane from image (a)-(d). Shown in Figure 5-34 the propagation of the same crack along the inter-laminar boundary can be seen. This is a crack between two plies, and the crack appears to grow smaller as it goes deeper into the material and further away from the machined edge. The inter-laminar delamination, shown in Figure 5-34, lies between two plies in the material and this weak layer will allow propagation of cracks, because of the poor strength between adjacent plies.

165
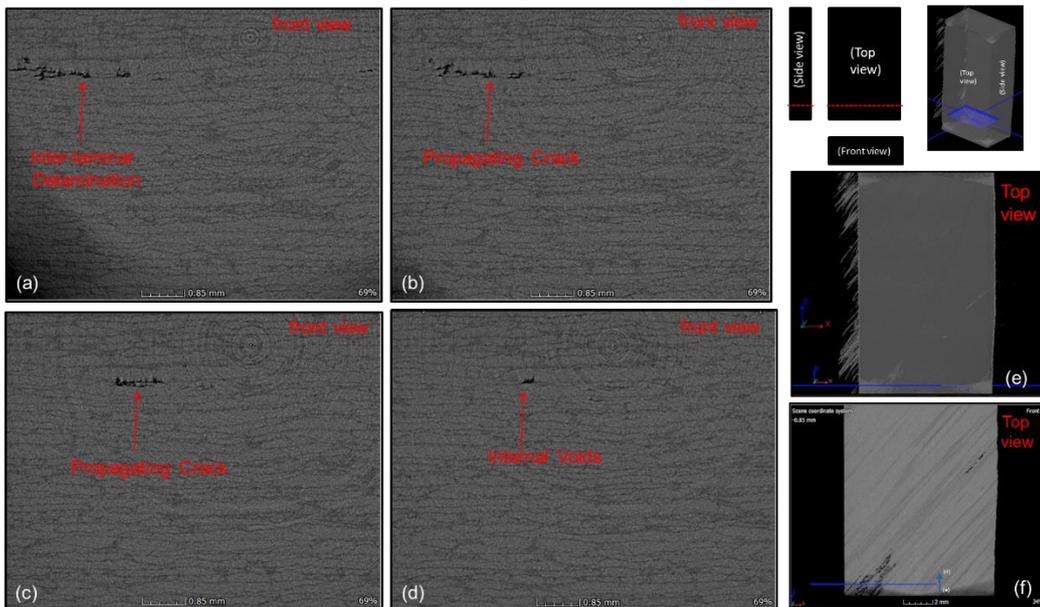
Figure 5-34- CT scans of delamination propagation from machined edge of unidirectional 45 degree fibre orientation laminate.

A 90 degree fibre orientation sample machined with feed rate of 800 mm/min, cutting speed of 8000 RPM and 10 μm mean edge radius is shown in Figure 5-35. CT scan for 90 degree fibre orientation machined sample is shown in Figure 5-35, and the planes in Figure 5-35(b) show the position of the cross-sections. The cross sections are shown in green for the top view, blue for the front view and red for the side view. It was found that there were internal voids between inter-ply layers, and Figure 5-35 again shows that the machining process has propagated some internal machining damage in the unidirectional laminate.
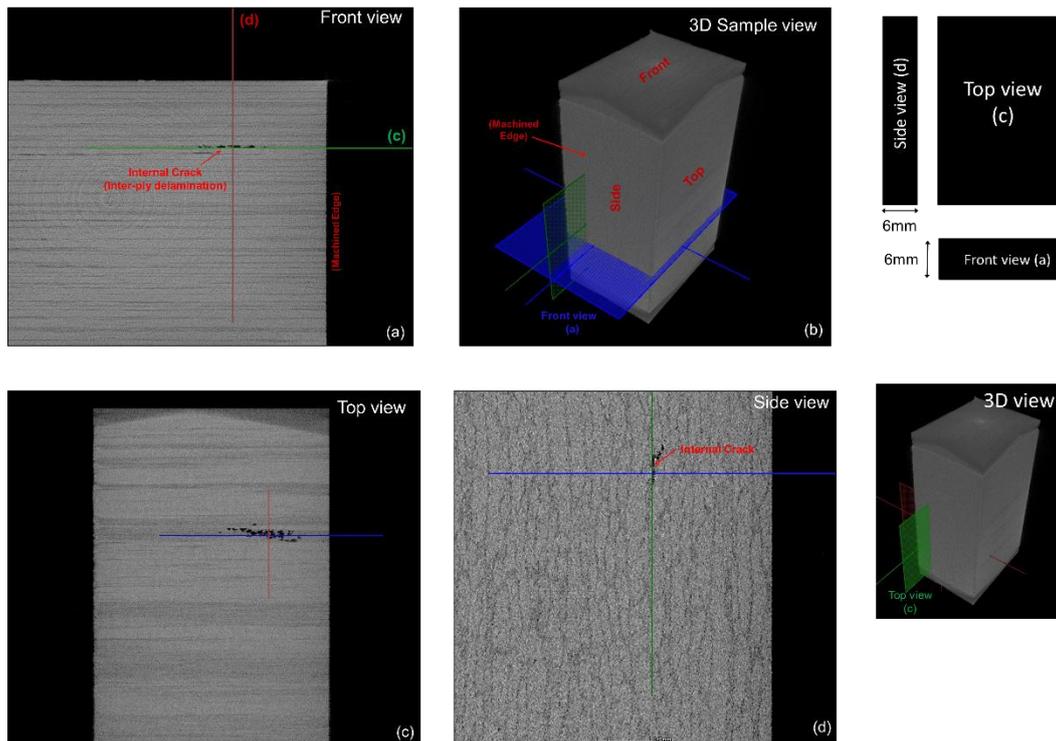
Figure 5-35- 90 degree fibre orientation with internal crack.

In order to make a comparison of machined samples versus non-machined, there was samples which were CT scanned but had not been edge trimmed. These are shown in Figure 5-36 and Figure 5-37 for the 45 and 90 degree fibre orientation respectively. This was to compare the un-machined state versus the machined samples and see if damage has been caused due to machining or if it was already present as voids in the material from manufacturing defects. It can be seen in Figure 5-36 that there is less internal voids or inter-laminar delamination compared to the edge trimmed samples. There is one very small void which can be seen in the centre of the material. It can therefore be concluded, that in the machined samples, machining may have increased the size of internal voids- by propagation of inter-laminar delamination and cracks- in the machined sub-surface of the unidirectional laminates. It is possible that this mechanism may have been caused during machining which has allowed pre-existing voids to propagate into large delaminations, which are formed between ply boundaries in the sub-surface. It is hypothesised, that forces

167

generated during machining may have caused cracks to propagate further as the weaker bond between fibre-matrix and ply boundaries begins to separate. Also, in the unidirectional samples the material strength is predominantly in one direction due to the orthotropic material properties; unlike the multidirectional laminate in which the material will have support in many directions. A multidirectional laminate will give support against flexion and crack propagation in all directions through the material. Hence, in a unidirectional laminate it would be more likely to find crack propagation and sub-surface inter-laminar delamination, produced by machining, than in a multidirectional laminate.
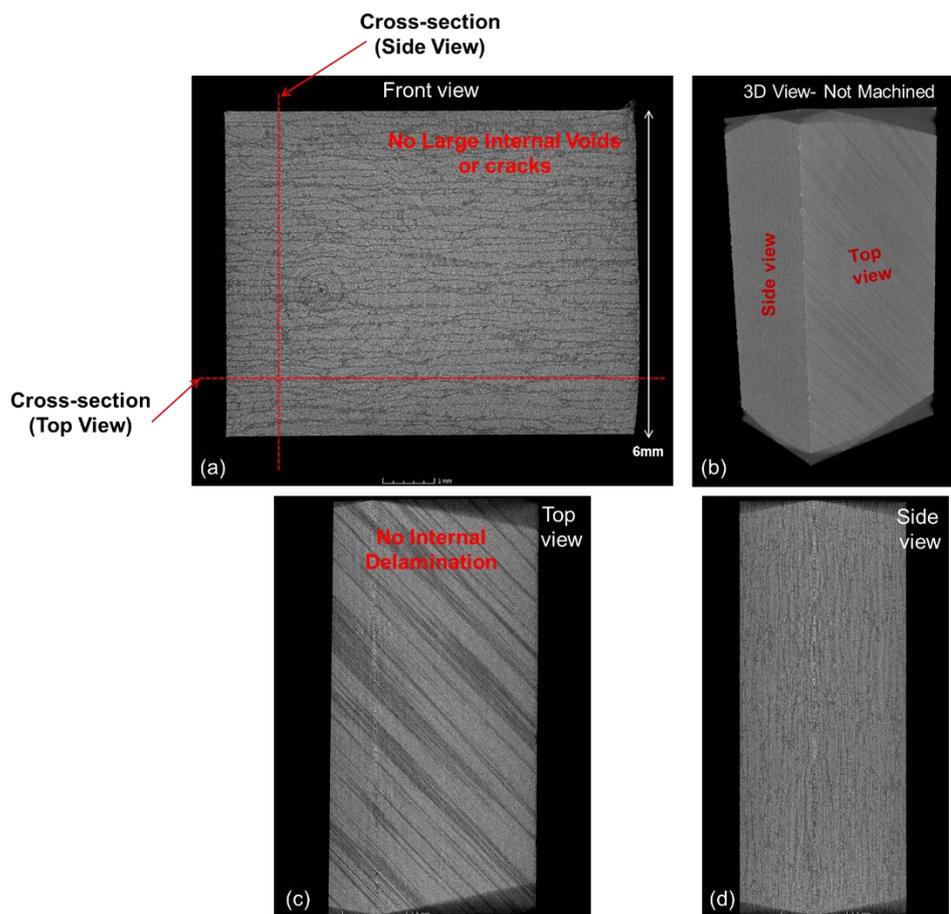
Figure 5-36- CT scans 45 degree orientation, un-machined sample.

Shown in Figure 5-37 is a 90 degree sample, which was not cut by edge trimming, where it can be seen there is still some voids present and some inter-

laminar delamination. The images show cross-sections in the positions shown in Figure 5-37(a). However, the defects were found to be smaller in magnitude than in the edge trimmed samples. It can therefore be assumed that these internal voids could have been propagated due to external forces during the machining process from smaller existing voids. It is also worth noting, that in order to prepare the samples they had to be cut down to a smaller size using a band saw so that an 8 µm resolution could be obtained. It is possible that cutting the samples using this saw could have added some internal damage to the un-machined samples. However, again as in the previous samples on the 45 degree fibre orientation there appears to be larger internal inter-laminar delamination in the edge trimmed samples, than the ones which have not been machined. The machining process has shown that it may have added some internal damage in the unidirectional laminate, in this case. Therefore from CT scanning images, it can be concluded that this technique was capable of finding internal voids and damage in the form of inter-laminar delamination in the samples. Also that the edge trimming process has increased some internal damage in the unidirectional samples due to crack propagation. However some initial voids already present in the material may have allowed these delamination and cracks to propagate. Next an analysis was made on the multidirectional edge trimmed samples using CT images to see if there was any damage present and to compare with the unidirectional samples.
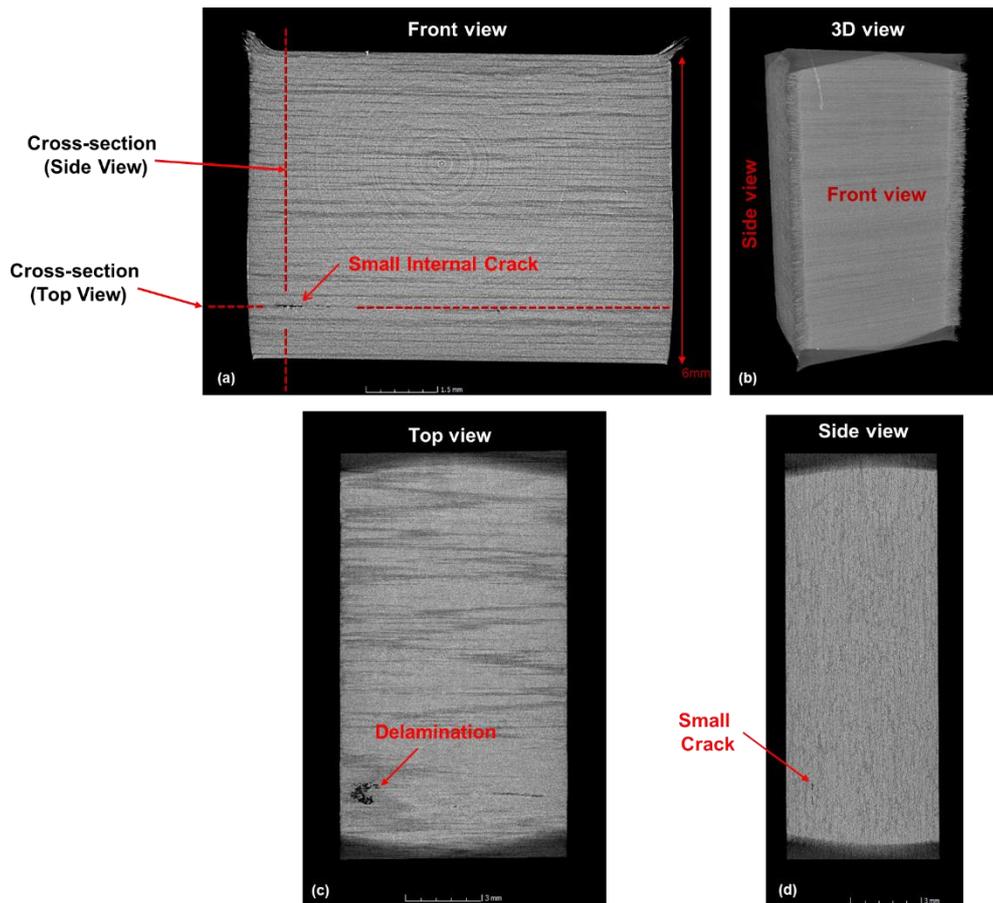
Figure 5-37- CT scans 90 degree fibre orientation, un-machined sample.

5.4-1 Multidirectional Laminate CT Scanning Results

Figure 5-38 and Figure 5-39 show CT scan from multidirectional laminate edge trimming test of the carbon fibre laminate. The sample is from test number 40, which was machined with a cutting speed of 9000 RPM, feed rate of 1200 mm/min and cutting edge radius of 6.7 μm. This was towards the end of the machining test where the cutting edge had become worn so any damage due to worn cutting edge would be more likely. Figure 5-38 shows a cross-section cut through the top view which was used to assess for any inter-laminar delamination across the sample thickness. The machined edge is seen on the left hand side of Figure 5-38. It was found that that there was no significant inter-laminar delamination found in any of the CT scans for the multidirectional laminate samples, as shown in Figure 5-38.
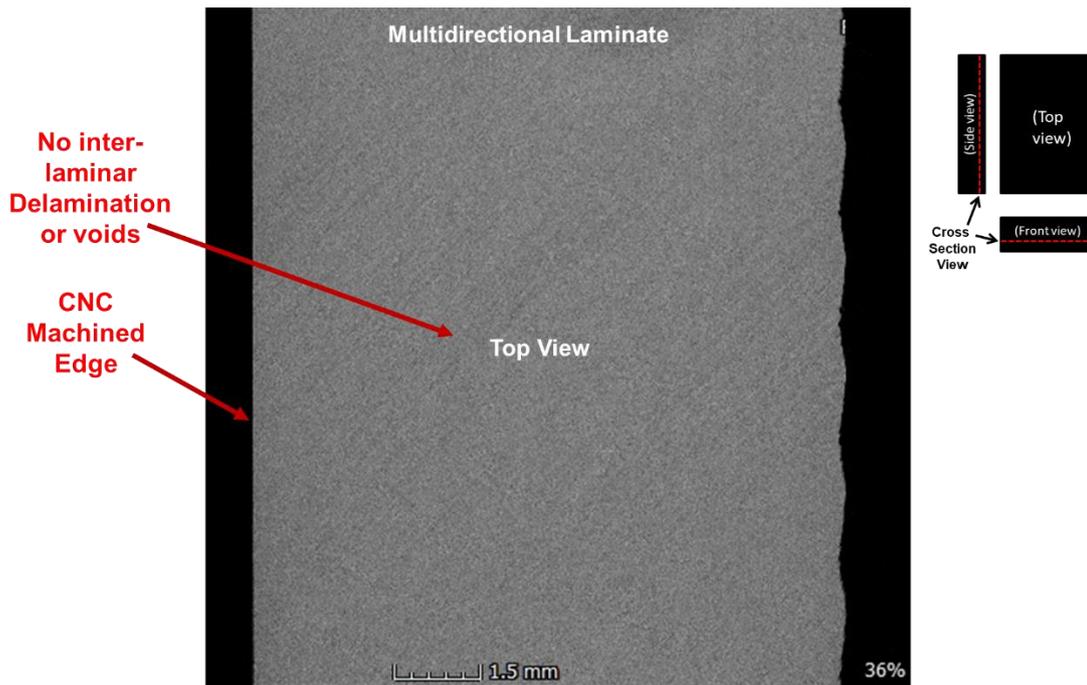
Figure 5-38- Multidirectional laminate- top view showing no internal interlaminar-delamination.

In Figure 5-39 the CT images show the machined surface damage progressing further from the machined edge, shown through the side plane. These images show a cross section through the machined surface, starting very close to the machined surface, at 0.01, 0.02, 0.03 and 0.04 mm away from the edge. Any damage found by the CT images in the multidirectional laminate was therefore localised damage on the surface, which was also captured as shown previously using SEM images. The maximum damage depth was found to be around 0.04 mm from the machined edge, as shown in Figure 5-39(d). This damage is characterised by machining induced surface defects, including surface roughness, fibre pull-out and torn fibres, as shown in Figure 5-39. The maximum damage depth was found on the 135 degree fibre orientations. The variation in surface damage, due to fibre orientation effects, is similar to that shown by the SEM images.
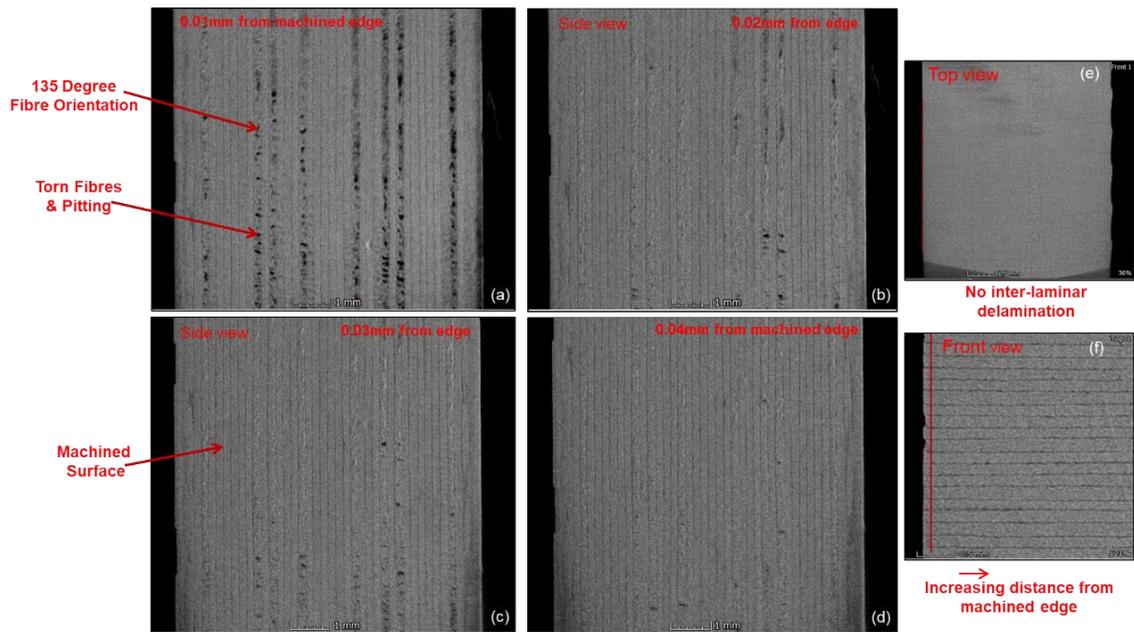
Figure 5-39- Machined surface- CT scans showing damage at progressing distance from the machined edge.

5.4-2 Discussion- CT Scanning Results

CT scanning has been used to assess internal defects in the unidirectional and multidirectional machined samples. The unidirectional machined samples have been compared against un-machined samples to compare the difference in magnitude of internal defects. The CT scans of the unidirectional laminate have shown that sub-surface inter-laminar delamination and cracks, (which cannot be seen by surface measurements), may be generated during CFRP machining. Inter-laminar delamination in the unidirectional laminate may have propagated from small existing voids which were already created during manufacture.

Shown previously in Figure 5-39, for the multidirectional laminate, the variation in surface structure and machining damage type is shown to be dependent upon the material fibre orientation, and the maximum damage depth was on the 135 degree fibre orientation. This maximum damage also correlated with roughness measurements on the multidirectional sample. It was shown that sub-surface defects were not present in the multidirectional laminate with the machining parameters and tool conditions applied in this study. The lack of

172

inter-laminar delamination or significant propagation of sub-surface cracks, as compared to the unidirectional laminate, may be because the different fibre orientations play a supporting role to increase stiffness and reduce inter-laminar delamination. The superior properties of the multidirectional resin compared to the epoxy in the unidirectional laminate may also have played a part in the lack of internal damage. The multidirectional laminate was also 10 mm thick as opposed to 6 mm in the unidirectional and would therefore have more rigidity and stiffness to support bending or flexion. In the future, the machining tests could be repeated with a highly worn tool and harsher machining parameters to find if any internal defects would be generated in these conditions.

These findings have shown that for the multidirectional laminate damage measurement of the machined surface is appropriate, by roughness measurements and SEM images, to capture the extent of machining generated defects. Under the applied machining conditions, in this study, the CT scans did not show any significant sub-surface damage or voids. Therefore it can be concluded, that roughness measurements are the critical measurements to be used for assessing surface damage generated during machining in this circumstance. The implementation of CT scanning has been shown to be a useful technique to check for inter-laminar delamination, which may have been propagated by machining. However in well-chosen machining conditions with a suitable material, which is free of internal voids, then sub-surface damage should not be present and was not shown on the multidirectional laminate. The CT scanning technique was also able to show the depth of defects generated on the 135 degree plies, which were approximately 0.04 mm maximum depth from the machined edge.

Chapter 6
Multiple Linear Regression Modelling

Multiple linear regression modelling is a tool which is used to show the relationship between a set of variables and an output response. In multiple linear regression modelling a number of predictor variables are applied, and the equation aims to fit the variable response as well possible using input model data. Multiple linear regression equations have been calculated, and the aim of these regression equations is to correlate changes in the input parameters, feed rate, cutting speed, Fx and Fy, and cutting edge radius, and their contributing effect on output S_a Surface roughness. The regression equations are calculated from the experimental test data and measured surface roughness. Data is applied from multidirectional and unidirectional test results using the PCD tool. The regression equations will then be used as part of a prediction method for calculating surface roughness and to show the statistical contribution of each of the parameters on surface quality.

6.1 Multiple Linear Regression Modelling- Predictor Effects on Surface Roughness

The surface roughness of a machined profile has a non-deterministic functional relationship with input machining parameters; this is due to the complexity and dynamics of the machining process, complex material surface structure and material inhomogeneity. This means the calculated effects of parameters on roughness cannot be pre-determined, and therefore the use of statistical methods has been applied, because it is a useful way to assess and predict parameter effects on the surface structure from experimental data. In order to find the effect of model parameters on the output surface roughness (S_a), design of experiments has been combined with multiple linear regression methods. This will show the influence of machining parameters on

experimentally measured surface roughness. In the regression models, statistical methods have been applied to check for linear regression model suitability and parameter significance. The regression model has been applied with the areal surface roughness S_a as output response variable and regression equations have also been calculated for skewness and kurtosis parameters.

Software Minitab has been used to analyse the data and find the statistical contribution of each of the input parameters. Linear regression assumptions have been assessed by checking for data normality and equal variance of residuals. The R-Sq, Histogram and residual response have been used to check model assumptions and the effectiveness of the fit from the predictor line to the data response. The design of experiments has been applied as previously shown. A stepwise method has been used in combination with parameter P values and model R-Sq values to assess the statistical significance of each parameter and the need of their inclusion for the regression equations.

6.2 Regression Analysis- Multidirectional-laminate

A multiple linear regression analysis was performed from the test data in Chapter 5.2 using statistical software Minitab. Design of experiments was performed using 2 levels of feed rate and cutting speed and progressively increasing levels of tool wear. A stepwise method was used to assess the inclusion or removal of different model terms. Experimentally measured parameters were the cutting forces and the surface roughness. The predictor parameters for the model are feed rate, cutting speed, tool edge radius and cutting forces in the Fx and Fy direction. The inclusion of interaction terms between the predictor parameters has also been assessed which can improve model prediction capabilities. From graphs shown in the results sections of the multidirectional test, it looked probable that there is some interaction between cutting forces, feed rate and edge radius. Interaction terms in the model allow for the possibility that a predictors effect on the response may vary at different

176

levels of one of the other predictor variables. For example, the effect of the feed rate on the surface roughness may also depend upon the current level of tool wear or cutting speed, and therefore the need for inclusion of interaction terms will be considered, and included where required.

Firstly a fitted line plot was used to assess the effects of each individual predictor on the surface roughness. The fitted line plot is shown for each of the 5 predictors in Figure 6-1 and the response which is the measured S_a roughness by optical system. A fitted line plot is also shown for the interaction terms in Figure 6-2. The fitted line plot gives an indication of the trend of the predictor effect on the surface roughness and the suitability of inclusion of the different predictor variables in regression equation. It shows the general trend in that the predictor effect will have on the surface roughness, and also the strength of the significance of that parameter on the roughness.

Shown in Figure 6-1 are fitted line plots with the R-Sq and S values. The coefficient of determination (R-Sq) represents the strength of the predictor effect on the surface roughness, and the R squared value is used in order to find how well the regression equation fits the experimental data. The R-Sq value gives an indication of how well the model explains the variability of the data response around the mean and is calculated as the ratio of the explained variation to the total variation. A high R squared value tells us that the regression equation fits the experimental data well and that the majority of the data lies close to the regression line. Also, a high R-Sq means that the predictor has a strong effect on the surface roughness. The S value is known as the residual standard error and is used to find the sample variance of each of the populations of data from the fitted regression line. The closer the data lies to the regression line the lower the S value will be. Thus it gives an indication of the mean variance of the sample points from the fitted line.

The prediction interval (PI) with a 95 % confidence is shown for the fitted line plots in Figure 6-1 and Figure 6-2 by the dotted red line. This means that if a new predicted point is made within this parameter range using the equation then there is a 95 % confidence that it will lie within the upper and lower bounds of the shown lines.

In Figure 6-1 the parameters with the highest R-Sq value are the cutting speed followed by Fx cutting force, edge radius and feed rate. It was found that reducing the cutting speed seems to have a positive effect on surface roughness, while increasing the other three parameters has an increasing effect on the roughness. The Fy thrust force has a low R-Sq value which suggests that changes in this predictor do not have a strong effect on the surface roughness. The cutting speed and Fx cutting force have a low S value due to having a low sample variance around the fit predictor line. The feed rate has a higher S value due to having some sample variance around the 1200 mm/min data point, which may indicate some interaction effects from other parameters.

The need for interaction effects between predictors has firstly been assessed by using fitted line plots. Looking at the interactions fit line plots in Figure 6-2, the predictors with the highest R-Sq are the interaction of the feed rate and cutting edge radius, feed rate and cutting force (Fx). The interactions tell us at higher levels of cutting edge radius the effect of increasing feed appears to have a stronger effect than at lower levels of tool wear. Interactions between cutting speed and other variables including, cutting edge radius, Fy and Fx, appears to have very little significant effect on the surface roughness, as shown by the zero R-Sq value and low gradient of the fit lines in Figure 6-2 and Figure 6-3. This interaction effect tells us that a change in cutting edge radius does not seem to impact the effect of cutting speed on surface roughness or alternatively the cutting speed effect on surface roughness appears to be independent of tool wear.

178

It has been found that the feed rate and cutting edge radius interaction effect on the surface roughness are linked. Therefore without inclusion of this interaction effect in the multiple linear regression model, the joint effect of changing both feed rate and cutting edge radius would not be captured effectively.
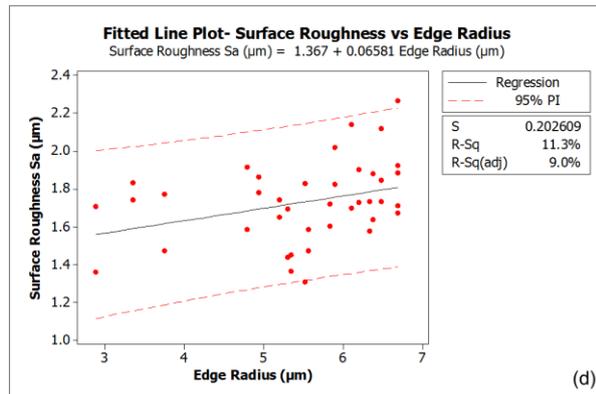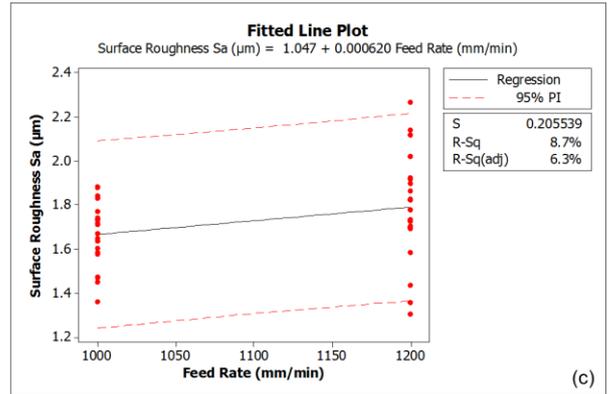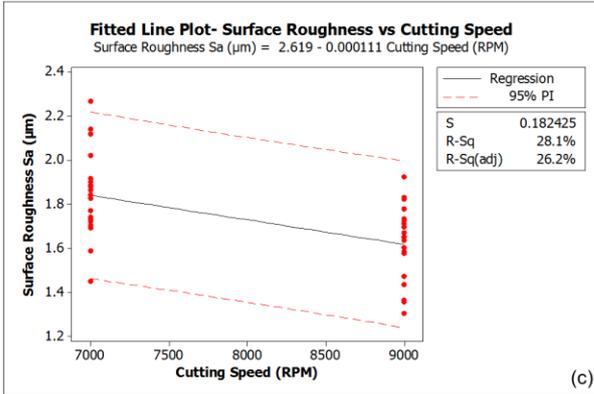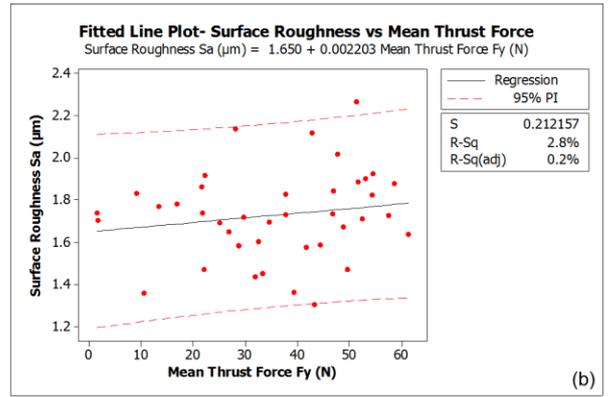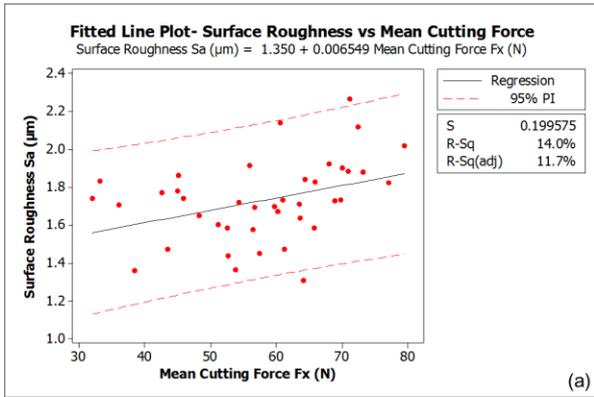
Figure 6-1- Fitted line plot for predictor variables effect on surface roughness, shown with 95 % confidence interval, (a) Mean Fx, (b) Mean Fy, (c) Feed rate, (d) Edge radius.
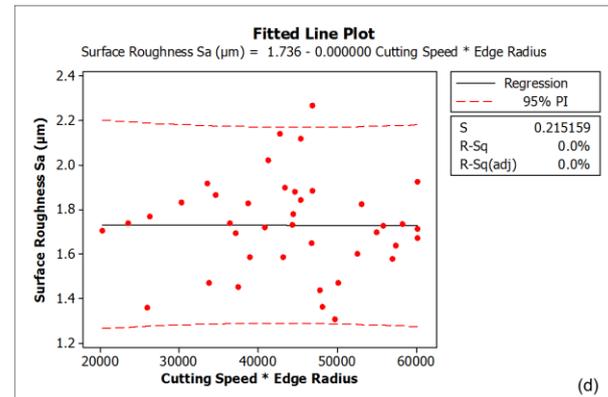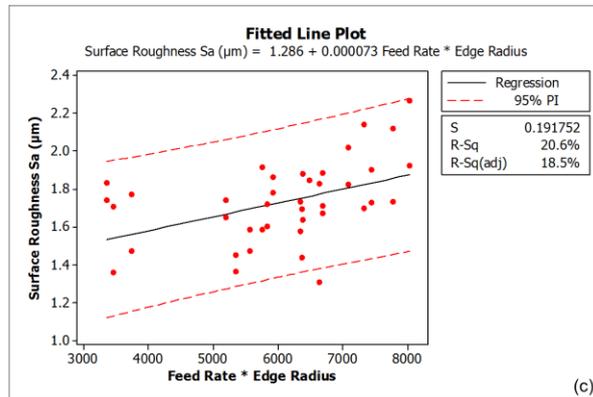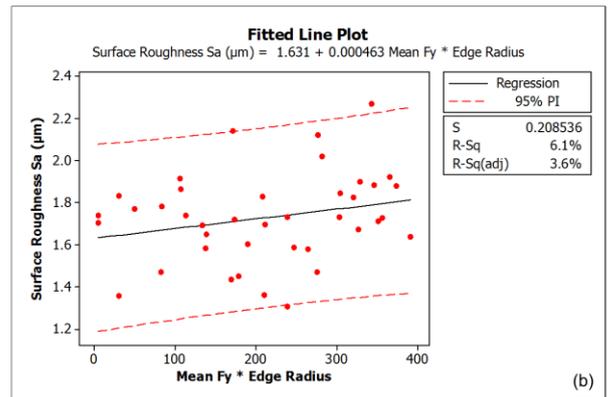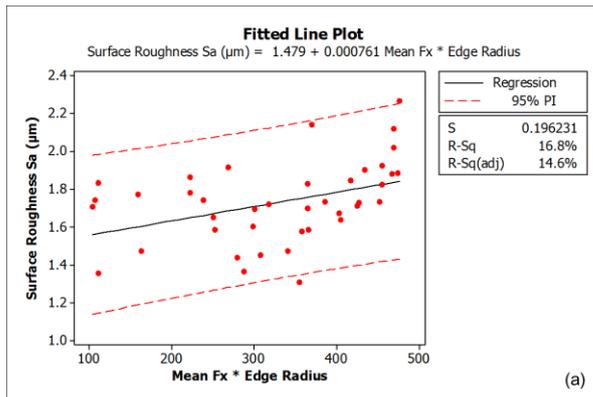
Figure 6-2- Fitted line plot for interaction variables effect on surface roughness, shown with 95 % confidence interval: (a) Mean Fx * Edge Radius, (b) Mean Fy * Edge Radius, (c) Feed rate * Edge Radius, (d) Cutting Speed * Edge Radius.

181
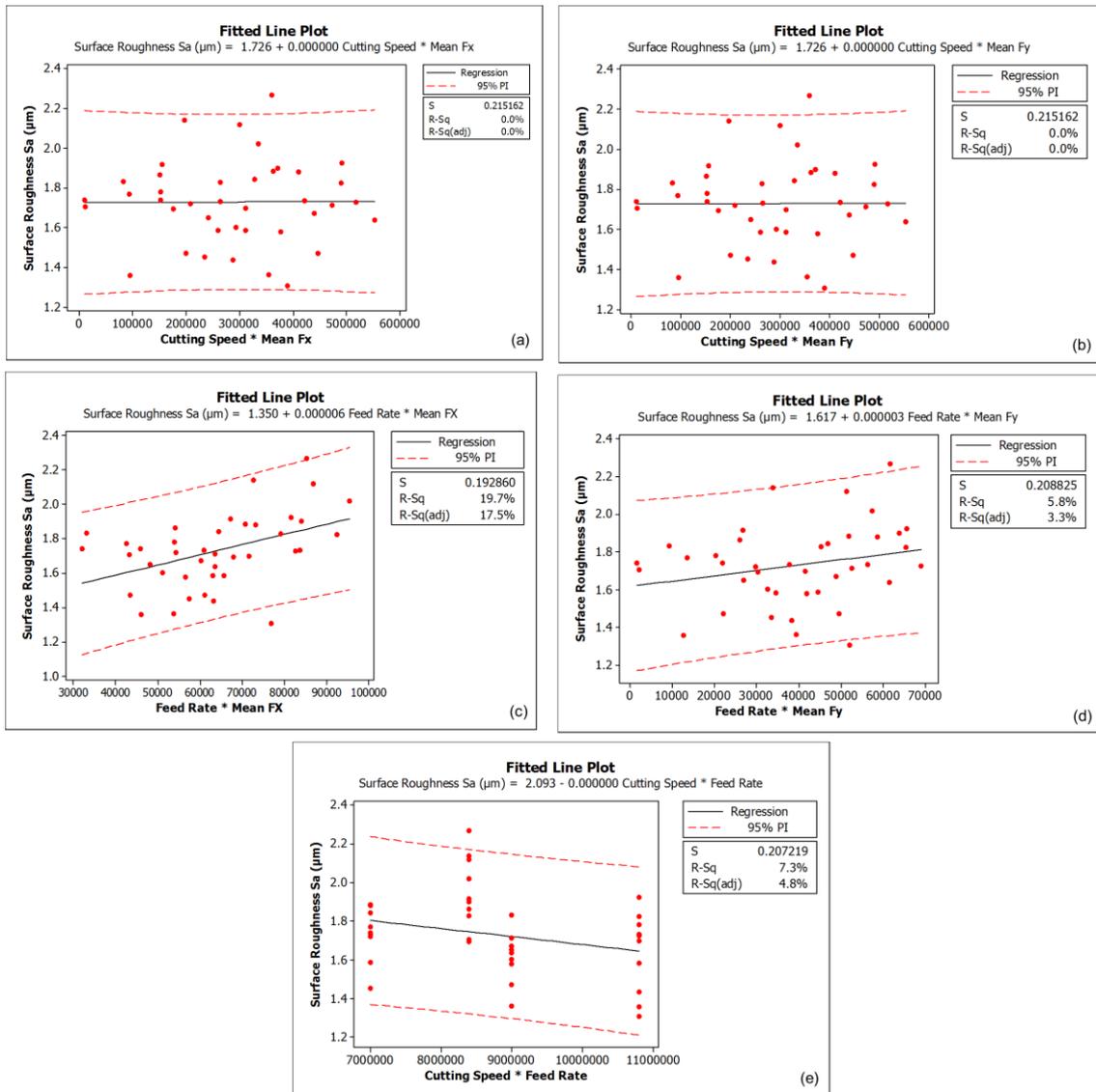
Figure 6-3- Fitted line plot for interaction variables effect on surface roughness, shown with 95 % confidence interval: (a) Cutting speed * Mean Fx, (b) Cutting Speed * Mean Fy, (c) Feed Rate * Mean Fx, (d) Feed Rate * Mean Fy, (e) Cutting Speed * Feed Rate.

6.2-1 Selection of Predictor Variables

In order to assess the suitability of the regression equation fit and the need for inclusion of each different predictor variables a stepwise method has been applied. This method assesses the importance of different predictor variables, with and without their inclusion in the model. This method has been applied while using the R-Sq and the adjusted R-Sq (adj) to look at the ability of model

182

to fit observed data. The R-Sq is similar to the R-Sq, except that it is adjusted for the number of predictor terms in the model. This means if a new predictor is added to the model which does not improve the model accuracy (greater than would be improved by chance), then the R-Sq (adj) will reduce, whereas the R-Sq would always increase due to the addition of another predictor. For that reason the R-Sq (adj) is useful to find whether the addition of another predictor term is beneficial to the model or if it should be removed because it is not improving model accuracy.

Figure 6-4 shows the regression model output with the 5 predictor terms included but without any inclusion of the interaction variables. The predictors with the highest contribution to the roughness are cutting speed and edge radius, as they have the lowest P values. R-Sq values and residual plots have been checked for different variations of the model to find if there is an improvement in the model fit. The R-Sq value is 49.8 % and the R-Sq (adj) is 42.4 % for this model- Figure 6-4. As shown in Figure 6-5 there are the four residual plots of this model output. The residual plots are used to look for data normality and fit of the regression line to the observed variables. In order to use the assumption of a linear regression model then there should be a normal distribution of the data. As the relationship between the response and the predictors is a statistical one in this case then a checks must be made for the suitability of the use of a linear regression model.

The histogram of residuals is shown in Figure 6-5 which shows the error in the response of the observed data points from the regression equation. The histogram of residuals is used to see whether the residual response has a normal distribution or is skewed away from the mean regression line. It is a useful check to see whether any skewness exists in the data or there are extreme outliers. As shown in Figure 6-5, the data shows fairly normal

distribution, but is not fully symmetric about the centre line, and some skewness is shown in the upper portion of the data.

The residual response of the data vs run order is shown in Figure 6-5, where each point represents the deviation of the data point from the fit regression line. This is used to see if there is any noticeable trend in the data as the test progresses. The test looks for a random distribution of error terms as the test increases. It appears there is a fairly random distribution of the points over the test range, shown in Figure 6-5, which suggests there are no obvious experiment deviations or errors. The residual response vs run order is useful to perform because it can pick up on any experimental errors as the test progresses: for example due to drift in the dyno plate, or an error in the test setup. The R-Sq represents the fit of the data to the regression line but does not reliably suggest if there are any biases or mismatches in the data distribution, which could therefore be missed by relying solely on the R-Sq. Mismatches in data distribution could be due to poor fit of the regression equation at certain limits, or experimental errors. Therefore a random distribution is the ideal for the variation in error terms of each data point, as the test number increases. Shown in Figure 6-5 the test bias due to errors caused by experimental run order can be assumed to be negligible.

The residual response of the data from the calculated regression line is shown in Figure 6-5 in the normal probability plot. This plot is similar to the histogram and is used to show the deviation of the error terms from a normal distribution. It is used to identify skewness and kurtosis of the data and a poor fit of the regression equation. A normal distribution is represented by a straight line and the data points which lie close to this straight line are representative of a normal distribution. An assumption required in order to use a linear regression model is that there is a normal distribution of the error terms. Shown in Figure

there is some trend away from the straight line in the upper portions of the model and there is some skewness present.

It has been shown in histograms and normal probability plots that there may not be a fully ideal fit of the regression equation to observed data for the S_a surface roughness. Therefore histograms and normal probability plots will be compared in further models using stepwise method, and with the inclusion of additional interaction terms. This will see if skewness in regression line fit to data in upper portions can be reduced. Further checks will be included on R-Sq values to find if overall model fit is improved with additional terms.

```
Regression Analysis: Surface Roug versus Mean Cutting, Mean Thrust

The regression equation is
Surface Roughness Sa (µm) = 1.38 + 0.00123 Mean Cutting Force Fx (N)
                            - 0.00387 Mean Thrust Force Fy (N)
                            + 0.000586 Feed Rate (mm/min)
                            - 0.000101 Cutting Speed (RPM)
                            + 0.105 Edge Radius (µm)


Predictor                        Coef      SE Coef       T       P
Constant                       1.3832       0.4406     3.14   0.003
Mean Cutting Force Fx (N)     0.001227     0.008350    0.15   0.884
Mean Thrust Force Fy (N)     -0.003871     0.006409   -0.60   0.550
Feed Rate (mm/min)           0.0005864    0.0003517    1.67   0.105
Cutting Speed (RPM)         -0.00010130  0.00003513   -2.88   0.007
Edge Radius (µm)              0.10539      0.05179     2.04   0.050


S = 0.161225   R-Sq = 49.8%   R-Sq(adj) = 42.4%
```

Figure 6-4-Regression analysis output with initial predictors.
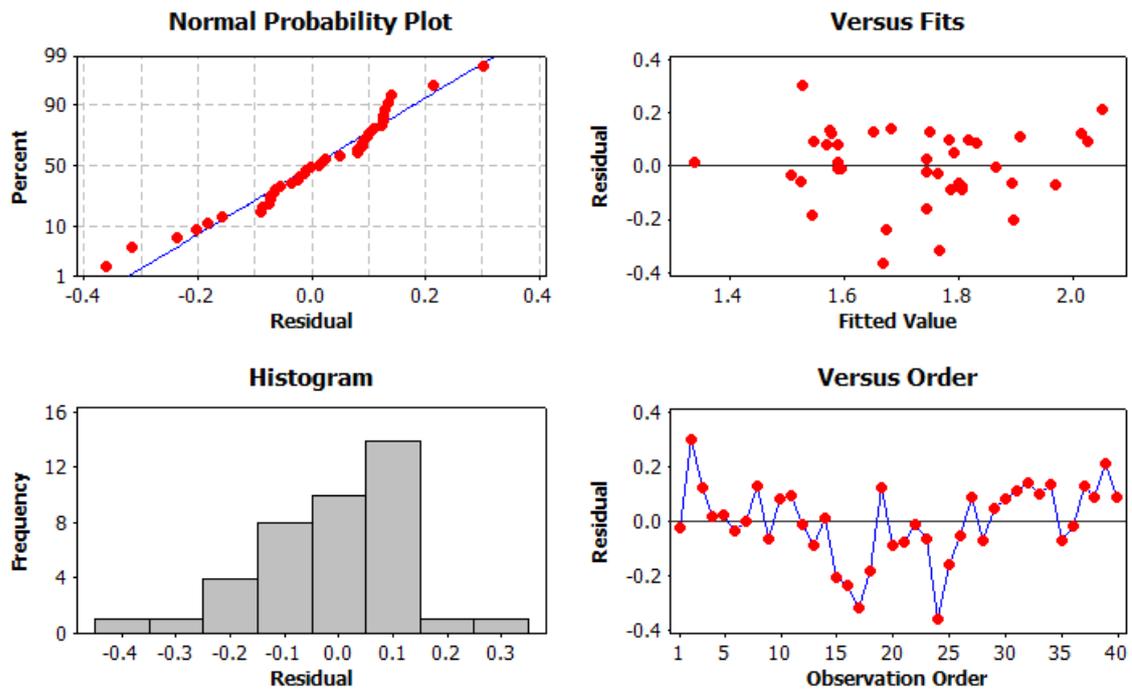
Figure 6-5- Residual plots of S_a surface roughness for first multiple linear regression model attempt.

Using a stepwise method and including the predictor terms and interactions of predictors was then applied to see if this would increase the capability of the model to fit the observed data. Including the interaction effect for the predictor of Feed Rate * Edge Radius gives an improvement to the model prediction with an improvement in the R-Sq and R-Sq (adj) to 57.5 % and 49.8 % respectively, shown in Figure 6-6. As a result there appears to be an improvement in the model capability to be able to fit the observed data with the inclusion of the feed rate and cutting edge radius interaction term. The interaction terms cutting speed with edge radius showed no significant improvements to model predictive capabilities and was therefore not included in the model predictions. This interaction would be expected to have little effect on the model predictive capability as shown previously in Figure 6-2. It has a negligible effect on surface roughness in the fitted line plot and a low R-Sq value.

186

```
Regression Analysis: Surface Roug versus Mean Cutting, Mean Thrust

The regression equation is
Surface Roughness Sa (µm) = 4.78 - 0.00215 Mean Cutting Force Fx (N)
                            - 0.00155 Mean Thrust Force Fy (N)
                            - 0.00236 Feed Rate (mm/min)
                            - 0.000111 Cutting Speed (RPM)
                            - 0.499 Edge Radius (µm)
                            + 0.000553 Feed Rate * Edge Radius


Predictor                        Coef      SE Coef       T      P
Constant                        4.784        1.446    3.31  0.002
Mean Cutting Force Fx (N)     -0.002151     0.007915  -0.27  0.787
Mean Thrust Force Fy (N)      -0.001549     0.006057  -0.26  0.800
Feed Rate (mm/min)            -0.002356     0.001243  -1.90  0.067
Cutting Speed (RPM)          -0.00011059  0.00003301  -3.35  0.002
Edge Radius (µm)                -0.4992       0.2511  -1.99  0.055
Feed Rate * Edge Radius       0.0005533    0.0002255   2.45  0.020


S = 0.150496   R-Sq = 57.5%   R-Sq(adj) = 49.8%
```

Figure 6-6- Regression model output with additional model predictors.

The optimum model fit was found by inclusion of selected predictor terms shown in Figure 6-7. This was found by using stepwise method to remove and include specific terms depending upon their contribution and the overall ability of model to fit observed data. An R-Sq value of 73.5 % was found with an adjusted R-Sq (adj) of 66.7 % which is a significant improvement over the initial model prediction shown in Figure 6-4. The Thrust Force (Fy) has been removed as an individual term to the model due to having a low contribution to model prediction, but it is still included in interactions with edge radius and feed rate because these interaction terms showed an overall improvement in the model prediction.

Shown in Figure 6-8 are the four residual plots for the optimum regression equation. The histogram and normal probability plots show a clearer normal distribution than was seen in the original regression equation in Figure 6-5. Most of the points lie close to straight line in the normal probability plot and show no significant skewness or extreme outliers. The use of stepwise method to include or remove additional parameter terms has led to an improved model prediction and consequently this regression equation has been applied

for model fit. Shown in Figure 6-7 the overall R-Sq value of 73.5 % for the regression equation fit to the data seems reasonable due to random scatter in the S_a measurements. This scatter in roughness could be anticipated as there will always be some variation in surface structure of machined CFRP and the measurements could be expected to have a reasonably high standard deviation.

```
Regression Analysis: Surface Roug versus Mean Cutting, Feed Rate

The regression equation is
Surface Roughness Sa (µm) = 6.54 - 0.0155 Mean Cutting Force Fx (N)
                            - 0.00330 Feed Rate (mm/min)
                            - 0.000080 Cutting Speed (RPM)
                            - 1.04 Edge Radius (µm)
                            + 0.000850 Feed Rate * Edge Radius
                            + 0.00363 Mean Fx * Edge Radius
                            + 0.00320 Mean Fy * Edge Radius
                            - 0.000024 Mean Fy * Feed Rate


Predictor                       Coef     SE Coef       T       P
Constant                       6.544       1.274    5.14   0.000
Mean Cutting Force Fx (N)    -0.01549     0.02813   -0.55   0.586
Feed Rate (mm/min)          -0.003295    0.001561   -2.11   0.043
Cutting Speed (RPM)       -0.00008003  0.00002793   -2.87   0.007
Edge Radius (µm)              -1.0411      0.3157   -3.30   0.002
Feed Rate * Edge Radius     0.0008496    0.0003741    2.27   0.030
Mean Fx * Edge Radius       0.003634     0.004649    0.78   0.440
Mean Fy * Edge Radius       0.003202     0.003364    0.95   0.349
Mean Fy * Feed Rate      -0.00002386  0.00001883   -1.27   0.215


S = 0.122639   R-Sq = 73.5%   R-Sq(adj) = 66.7%
```

Figure 6-7- Final regression equation output with final predictors and interaction terms included.
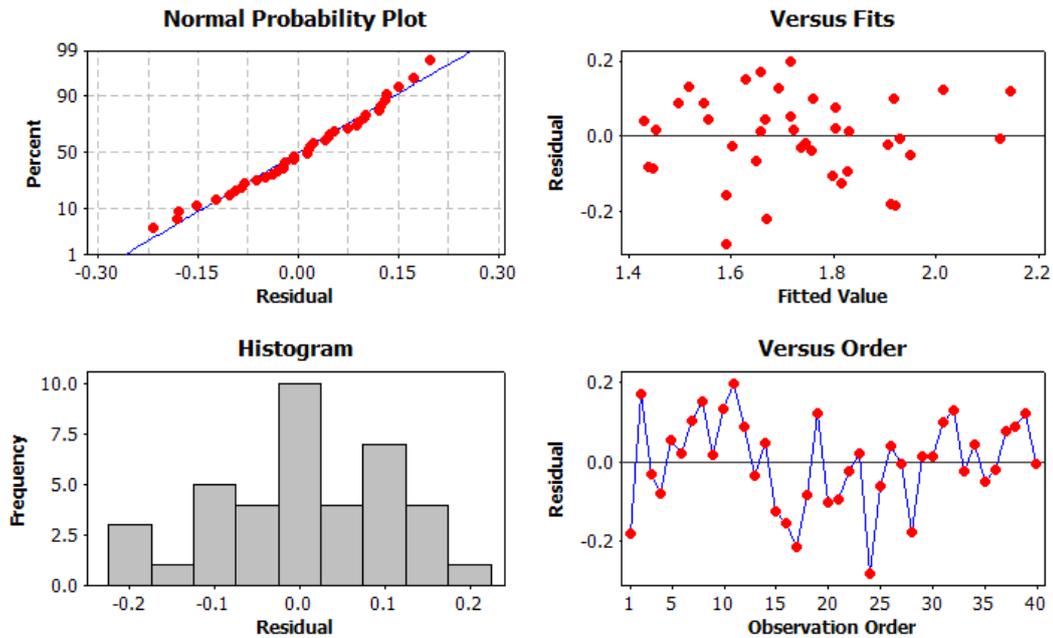
Figure 6-8- Residual plots of S_a surface roughness for best model fit.

The final regression equation for the S_a roughness from experimental data is shown in Equation 2:

Equation 2:

$$S_a = 6.54 - 0.0155\,F_x - 0.0033\,F_r - 0.000080\,RPM - 1.04\,E_r$$
$$+ 0.00085\,F_r\,E_r + 0.00363\,F_x\,E_r + 0.0032\,F_y\,E_r$$
$$- 0.000024\,F_y\,F_r$$

Where F_r is the feed rate in mm/min, RPM is the cutting speed in rotations per minute, and E_r is the edge radius in μm and the other values are interaction terms. The P values for each of the contributing variables is shown previously in Figure 6-7. The P value indicates the statistical contribution of the variable on the regression model. A low P value indicates that the indicator has a strong statistical influence on the predicted output, in this case surface roughness. The lowest P values were found for the edge radius, cutting speed and the interaction between feed rate and edge radius. Also, the interaction between Fy machining forces and feed rate. These parameters have most significant effect on the surface roughness and thus a change in these parameters will

189

have a strong correlating effect on surface roughness. Increasing the cutting edge radius has been found in previous studies to have a significant effect on the surface roughness. This is because a sharp cutting edge is very important in cleanly cutting the fibres in composite machining. A greater cutting edge radius will change the cutting mechanism from fibre shearing and cutting to fibre bending and ploughing. This has been found during this study to cause larger chunks of material to be removed, especially on the 135 degree fibre orientation, leading to torn fibre chunks and pits on the surface. Consequently the regression model tells us that a sharp cutting tool will be important to have high surface quality which is low in surface defects and fibre pull-out. The cutting speed was also found to have a statistical effect on the surface quality of the composite surface. A higher cutting speed causes a decrease in chip thickness and correlates with a lower surface roughness. Minimising the feed rate was found to improve surface quality, which agrees with previous work from this project [79],[89].

6.3 Regression Equations- Skewness and Kurtosis

 Skewness and kurtosis have previously been shown to be useful to give more a more thorough information on surface quality and profile shape of a machined non-homogeneous composite surface. They were shown to characterise machining defects including torn fibre chunks and un-cut protruding fibres. The skewness and kurtosis were found to be useful indicators of machining damage which is not included in the R_a and S_a roughness parameter, Therefore multiple linear regression equations have been assessed for these parameters on the multidirectional laminate to find the effects of changes in process parameters.

The regression equation for the skewness and kurtosis was also calculated and is shown in Equation 3 and Equation 4 for the skewness and kurtosis respectively.

190

Equation 3:

$$Rsk = 17.1 - 0.423\ F_x - 0.359\ F_y - 0.0179\ F_r - 1.75\ E_r$$
$$- 0.000291\ F_y F_r + 0.000344\ F_r F_x + 0.00174\ F_r E_r$$
$$- 0.000017\ RPM\ E_r$$

Equation 4:

$$Rku = -247 + 7.6\ F_x - 5.75\ F_y + 0.138\ F_r + 0.00625\ RPM$$
$$+ 18.5\ E_r - 0.398\ F_x\ E_r + 0.327\ F_y\ E_r - 0.00466\ F_r\ F_x$$
$$+ 0.0035\ F_y\ F_r - 0.00096\ RPM\ E_r$$

Normal probability plots for the skewness and kurtosis are shown in Figure 6-9 and Figure 6-10. A reasonably normal distribution was found for the normal probability plots and histograms for skewness and kurtosis, however the statistical fit of the regression equations was not as strong as in the S_a roughness model. A R-Sq of 53.2 % and a R-Sq-(adj) of 41.1 % was found for the skewness fit to the regression model. While the best model fit was an R-Sq of 23 % and R-Sq-(adj) of 15 % for the kurtosis regression model. The R-Sq values are lower for the regression equations in the skewness and kurtosis equations compared to the S_a mode. Especially the kurtosis which was found to show a poor fit of the regression equation to the data. The reasons of this are that each of the process variables did not show a very strong effect on the skewness and kurtosis. There is a higher standard deviation in the skewness and kurtosis measurements due to profile variation across the surface. Another reason for the difference is due to the fibre orientations of each of the different layers. It has been found that the skewness and kurtosis will behave differently on each fibre orientation. Due to the cutting mechanism and chip removal on the 135 degree fibre orientation there was found to be a decrease in skewness with an increase in cutting edge radius caused by torn fibre chunks and more machining damage. There was a decrease in kurtosis due to the increase in large rounded valleys on the 135 orientation. However on the 90 degree fibre

orientation there is a different effect, the increase in cutting edge radius causes more un-cut fibres protruding from the surface profile and an increase in skewness. There are sharp protruding fibres which cause an increase in kurtosis which is generally increasing with feed rate and cutting tool wear. Therefore there is an opposite effect on the skewness and kurtosis on different fibre orientations due to machining damage. This explains poorer fit of the model which tries to take into account the whole surface structure, compared to the S_a parameter where an increase in machining damage will always cause a mean increase in roughness.
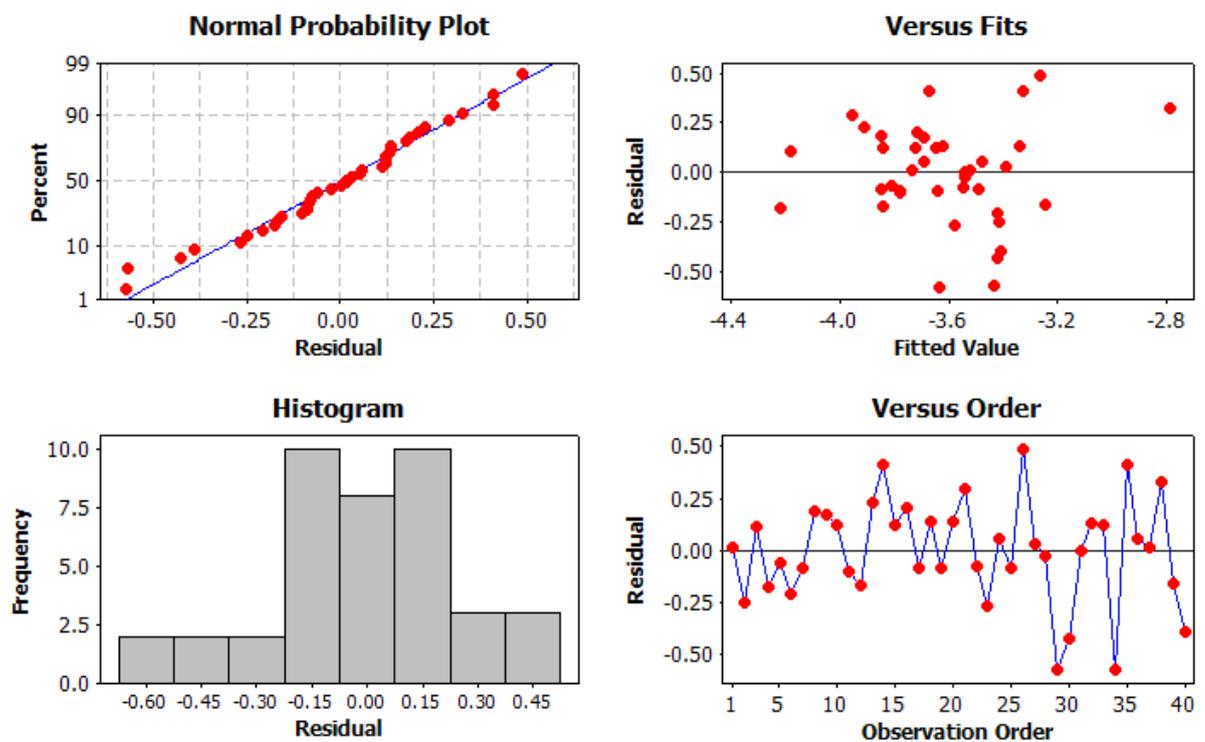
Figure 6-9- Residual plots for skewness, histograms of residuals, normal probability plot and residuals versus run order.
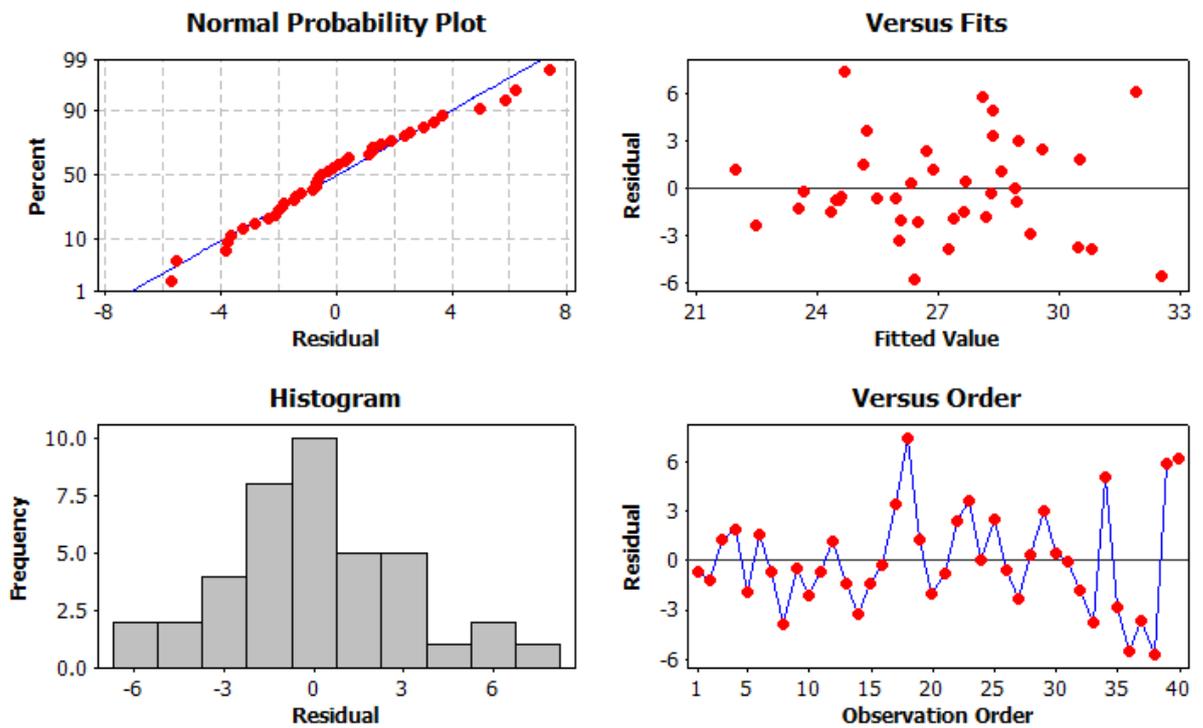
Figure 6-10- Residual plots for kurtosis, histograms of residuals, normal probability plot and residuals versus run order.

The P values of each of the contributing predictor variables for the skewness and kurtosis is shown in Table 6-1. The lower the P value indicates a stronger statistical significance of that parameter and its effects on either the skewness or kurtosis. The parameter with the strongest effect on the skewness was the feed rate followed by the thrust force and cutting force. The interactions of feed rate with the cutting forces were also shown to have a strong effect on the skewness.

Table 6-1- Skewness and kurtosis P values for experimental parameters.

Parameter	Skewness P Value	Kurtosis P Value
Constant	0.001	0.01
Feed Rate	0.0001	0.014
Cutting Speed	-	0.237
Edge Radius	0.093	0.236
Mean F_x	0.006	0.002
Mean F_y	0.001	0.006
Feed Rate * Mean F_y	0.002	-
Feed Rate * Mean F_x	0.008	0.004
Feed Rate * Edge Radius	0.061	-
Cutting Speed * Edge Radius	0.163	0.299
Mean F_x* Edge Radius	-	0.162
Mean F_y* Edge Radius	-	0.124

6.4 Multiple Linear Regression Equation- Unidirectional Model

Again, multiple linear regression method has been used to assess the predictors response on the surface roughness and create equations for the unidirectional test. A regression equation has been made for the 90 and 45 degree fibre orientation surfaces and following this surface roughness predictions will be made from FE model data at increased levels of tool wear. The same method was applied as in the previous regression model, where the effect of each parameter was assessed individually on the surface roughness and a stepwise method was used to remove or include predictor variables based upon the overall fit of the model by R-Sq and R-Sq-(adj). Histogram of residuals and normal probability plots were assessed to look for normal distribution of error terms or if there is any model skewness. Equation 5 shows the multiple linear regression equation for the 90 degree fibre orientation output on S_a surface roughness due to the corresponding parameters. Where

194

F_r is the feed rate in mm/min, RPM is the cutting speed in rotations per minute, and E_r is the edge radius in µm.

Equation 5, (90 degree fibre orientation):

$$S_a = 0.899 + 0.00026 * F_r - 0.00006 * RPM + 0.00821 * F_x - 0.00462 * F_y + 0.0567 * E_r$$

The P values for each of the parameters contributing to the surface roughness is shown in Table 6-2. The P value indicates the statistical contribution of that variable on the regression model, and the lower the P value then the higher the statistical contribution of that parameter to the surface roughness. A low P value indicates that the indicator has a strong statistical influence on the predicted output, in this case surface roughness. Therefore changes in parameters with a lower P value are likely to have a greatest change in the surface roughness. The parameter with the highest contribution to surface roughness was the cutting edge radius followed by the thrust and feed forces. Therefore tool wear and increasing the cutting edge radius, are most probable to cause a lower surface quality due to roughness.

Table 6-2- P Values of parameters from regression equation.

Parameter	P Value
Constant	0.213
Feed Rate (mm/min)	0.464
Cutting Speed (RPM)	0.676
Feed Force (Fx)	0.385
Thrust Force (Fy)	0.317
Edge Radius	0.175

In this model the need for interaction terms was not required as a good model fit was found with the inclusion of standard predictor variables. This was shown by the R-Sq value of the regression equation which was 93.8 %, which indicates a good model fit. A R-Sq value of 100 % would have all of the data points lying on the fitted regression line. This R-Sq value tells us that a high proportion of the data lies close to the regression line and the model therefore has a good fit with the experimental data within the ranges of parameters studied.

The histogram of residuals is shown in Figure 6-11 which shows the response of the regression equation. The histogram of residuals is used to see whether the residual response has a normal distribution or is skewed away from the mean regression line. In Figure 6-11 the data has a quite normal distribution and is fairly symmetric around the centre line. It is a useful check to see whether there is a trend in the data or extreme outliers exist.

The residual response of the data from the calculated regression line is shown in Figure 6-12. This plot is similar to the histogram and is used to show the deviation of the data points from a normal distribution. A normal distribution is shown by the straight line in this plot and points which lie away from this line do not represent a normal distribution. It can then identify skewness and kurtosis of the data and a poor fit of the regression equation. The points from this data all lie close to the straight line and therefore have a normal distribution. An assumption required in order to use a linear regression model is that there is a normal distribution of the data, and it therefore appears in this instance that this is the case. The calculated regression equation will accordingly be used to make further roughness predictions.
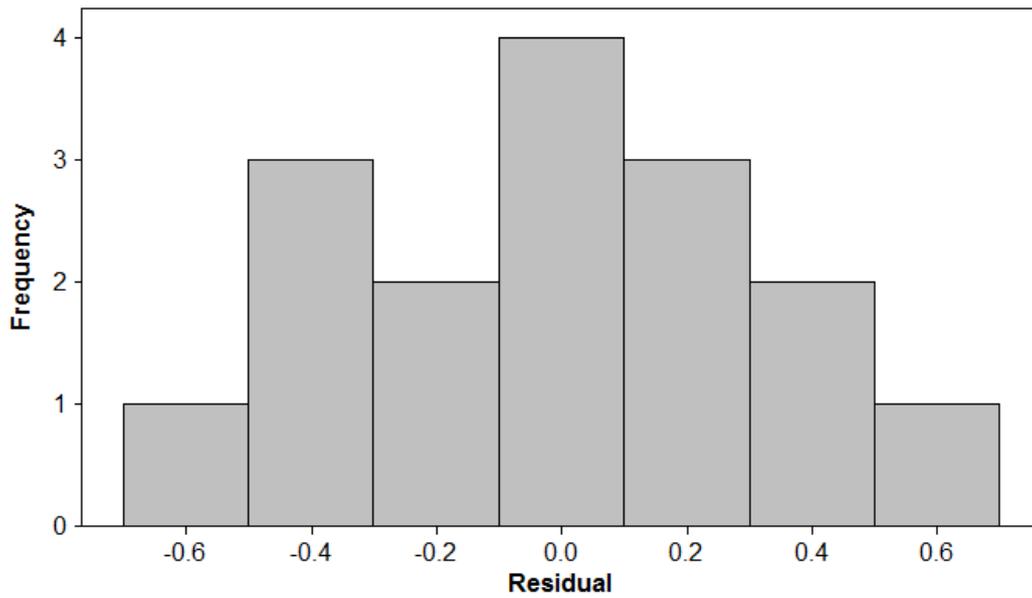
Figure 6-11- Histogram of residual response for Sa regression equation showing fairly normal distribution.
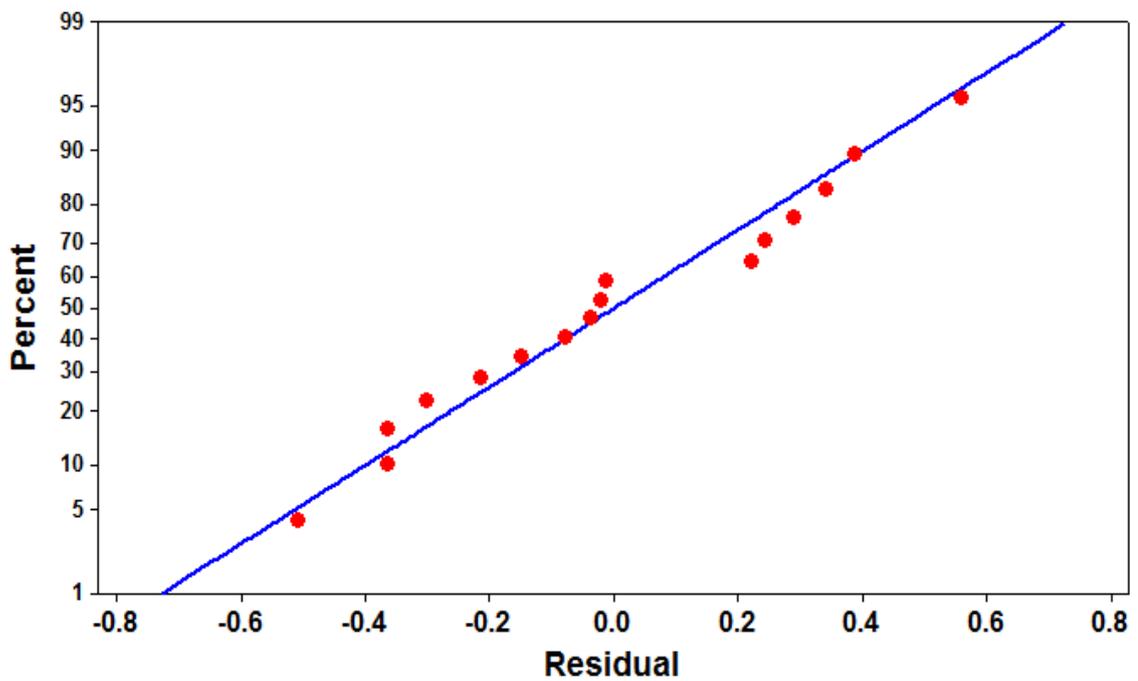
Figure 6-12- Normal probability plot for surface roughness (S_a) response

Chapter 7
Introduction- FE Modelling of Machining

 The modelling of machining of carbon fibre is a complex process and is highly non-linear. This is due to geometric nonlinearities arising from the large deformation of the cutter and workpiece material, material degradation and failure as well as the contact conditions. Material non-linearity arises principally from the failure of the material - in this case, the Hashin failure model. The contact non-linearity originates from the interaction between the cutter and the continuously changing workpiece cutting surface, which introduces friction, touching, sliding and separation contact behaviours. The analysis of composite milling using FE methods is an area which requires research, as there is a limited amount in the literature. Also the prediction of the effects of tool wear and surface damage on the milling process is an area which requires further study. For this reason these areas have been chosen as a focus for development in this research.

7.0-1 FE Edge Trimming of CFRP
 The project aim has therefore been to develop novel 2D and 3D FE models for a CFRP edge trimming process. This has required application of new modelling strategies for an edge trimming process. A user subroutine has been used to control cutter displacement by modifying the time step and advancing local adaptive re-meshing has been applied to the workpiece. 2D models have been developed for assessing the effects of tool wear due to an increased cutting edge radius.

 Experimental machining results have been compared with unidirectional and multidirectional edge trimming tests discussed in the experimental sections. The unidirectional tests are compared with 2D plane stress model and 3D models at different levels of tool wear. Multidirectional CFRP tests have been

compared with 3D models and regression equations to predict roughness values. The 3D model uses a sharp cutting edge which represents a tool in a new cutting condition.

MSC Marc software has been used for this research. A comparison was performed in order to analyse the suitability of different methods in order to characterise the machining process. ABAQUS Explicit and MSC Marc which is primarily an implicit solver have both been compared using 2D equivalent homogeneous models and multiphase models to model both the fibre and matrix as separate phases with a bonding strength modelled by cohesive elements. It was found that there were some advantages to using the implicit solver Marc due to the results from the ABAQUS explicit solver being very sensitive to time step size. The time step size used was found to have a strong influence on the final solution and whether the simulation would successfully complete. It was also found that, in the explicit solver, a very large number of small time steps were required since the complexity of the problem demanded a refined mesh. The very large number of time steps meant that the computational time became very high. The implicit nature of the Marc analysis used in this research is not subject to the stability limit and, therefore, does not require such large time steps. The user can use tools such as adaptive convergence control, which will be discussed, in order to have a suitable and stable load step and which was found to be useful in an intermittent machining problem like milling. Therefore new 3D and 2D milling simulations were developed with finite element software Marc and used to find output cutting forces, for different cutting parameters and tool wear condition.

7.1 Method- FE Modelling of Composite Milling

7.1-1 CFRP Properties- EHM Model

An equivalent homogeneous material (EHM) approach is used to model the composite workpiece material properties. This is used to model the workpiece

200

stiffness and elastic behaviour as a single phase with orthotropic properties and is based on laminate theory. A Hashin progressive damage material model [8], has been used to trigger the initiation of failure at an integration point, along with the subsequent stiffness degradation of the composite elements following until complete failure and element removal. The mechanical properties used in the simulations for the unidirectional laminate are shown in Table 7-1. The composite material is modelled as orthotropic, which means it has a different modulus parallel to the fibre to that in the transverse fibre direction. The stiffness matrix for the material properties is shown based on laminate theory, where E_{11} is the stiffness parallel to the fibres, E_{22} is perpendicular to the fibres, (in the plane of the laminate), G_{12} is the shear modulus and ν_{12} and ν_{21} are the Poisson's ratio in the two orthogonal directions. Equation 6 shows the stiffness relation for the orthotropic material in the fibre and transverse directions [90]. The values are calculated from the modulus, poisons ratio and shear modulus as shown in Equation 7-Equation 10. The properties for the multidirectional laminate are shown in Table 7-2 and the fibre and matrix constituent strengths are shown in Table 7-3.

$$\begin{bmatrix} \sigma_{xx} \\ \sigma_{yy} \\ \tau_{xy} \end{bmatrix} = \begin{bmatrix} Q_{11} & Q_{12} & 0 \\ Q_{21} & Q_{22} & 0 \\ 0 & 0 & Q_{66} \end{bmatrix} \begin{bmatrix} \varepsilon_{xx} \\ \varepsilon_{yy} \\ \gamma_{xy} \end{bmatrix} \qquad \text{Equation 6. [90]}$$

Where:

$$Q_{22} = \frac{E_{22}}{1 - \nu_{12}\nu_{21}} \qquad \text{Equation 7. [90]}$$

201

$$Q_{11} = \frac{E_{11}}{1 - v_{12}v_{21}}$$ Equation 9. [90]

$$Q_{12} = Q_{21} = \frac{v_{12}E_{22}}{1 - v_{12}v_{21}}$$ Equation 8. [90]

$$Q_{22} = G_{12}$$ Equation 10. [90]

Table 7-1- CFRP mechanical properties for Hashin FE model- unidirectional. REF [83]

Mechanical Property-Unidirectional Laminate	
Tensile Modulus- ($E1_t$) (GPa)	148
Tensile Strength- (X_t) (MPa)	2375
Transverse Tensile Modulus ($E2_t$) (GPa)	51
Transverse Tensile Strength (Y_t) (MPa)	68
Compressive Modulus ($E1_c$) (GPa)	119
Compressive Strength (X_c) (MPa)	1465
Transverse Compressive Strength (Y_c)	150
Poisson's Ratio (v)	0.3
Inter-laminar Shear Strength (S_{13}) (MPa)	113
In Plane Shear Strength (S_{12}) (MPa)	112
In Plane Shear Modulus (G_{12}) (GPa)	4.7

Table 7-2- CFRP mechanical properties for Hashin FE model- multidirectional. REF [91]

Mechanical Property-Multidirectional Laminate	
Tensile Modulus- ($E1_t$) (GPa)	165
Tensile Strength- (X_t) (MPa)	2980
Transverse Tensile Modulus ($E2_t$) (GPa)	66
Transverse Tensile Strength (Y_t) (MPa)	72
Compressive Modulus ($E1_c$) (GPa)	150
Compressive Strength (X_c) (MPa)	1860
Poisson's Ratio (υ)	0.3
Inter-laminar Shear Strength (S_{13}) (MPa)	110
In Plane Shear Strength (S_{12}) (MPa)	108
In Plane Shear Modulus (G_{12}) (GPa)	4.4

Table 7-3- Constituent carbon fibre and matrix properties

Carbon Fibre Properties	Matrix Properties
Tensile Strength- 4900 MPa	Tensile Strength- 111 MPa
Compressive Strength- 1860 MPa	Compressive Strength- 214 MPa

7.2 Hashin Progressive Damage Material Model

In composite machining there will be a combination and accumulation of different damage modes, the fibres and matrix will be progressively damaged in both tension and compression. The damage will depend upon material strengths, the tool position and material fibre orientation. It is therefore important that a material model which takes into account all possible damage

modes is used. A Hashin damage model is often used in order to model the progressive failure of composites and can be implemented into finite element code. The Hashin failure damage model is used to delete the elements based on the fibre and matrix strength properties. This failure model has typically been used by other researchers in composite machining [68],[72],[6]. The Hashin model takes into account four different failure modes which are used to relax the stiffness of damaged elements. The failure modes taken into account for fibre composites includes fibre tension, fibre compressive failure, matrix cracks and matrix crushing. Before any damage has taken place, the composite will have a linear elastic response with orthotropic properties. Then once the failure criterion has been reached there will be a degradation of the stiffness. The failure indices from the Hashin failure criterion are computed separately and the post-processing section can be used to see the extent of each damage mode in the material. Damage propagation and failure can therefore be seen due to each failure mode. This can be applied to layers of a laminate with different fibre orientations or stacking sequences which is useful for a composite machining simulation.

 A description of how Marc controls the failure of elements by the Hashin method is described. Firstly in order to control failure a failure index is used for each of the four following different failure modes, fibre tension, fibre compression, matrix tension and matrix compression. The failure index is calculated for each integration point in the element, and where the failure index value is greater than one there is an initiation of failure and degradation of element stiffness. The failure strength properties are used along with the different failure criteria, and once one of the failure criteria has been met then there is a degradation of the element stiffness. The criterion used to calculate the failure index for each of the four different failure modes is shown in Equation 11-Equation 14.

The first failure mode is fibre tension, where $\sigma_1 > 0$:

$$\left(\frac{\sigma_{11}}{X_t}\right)^2 + \frac{1}{S^2}\left(\sigma_{12}{}^2 + \sigma_{13}\right) = 1 \qquad \text{Equation 11}$$

The second failure mode is fibre compression, where $\sigma_1 < 0$:

$$\left(\frac{\sigma_{11}}{X_t}\right) = 1 \qquad \text{Equation 12}$$

The third failure mode is matrix tension, where $\sigma_1 + \sigma_3 > 0$:

$$\frac{1}{Y_t{}^2}(\sigma_2 + \sigma_3)^2 + \frac{1}{S_{23}{}^2}\left(\sigma_{23}{}^2 - \sigma_2\sigma_3\right) + \frac{1}{S_{12}{}^2}\left(\sigma_{12}{}^2 - \sigma_{13}{}^2\right) \qquad \text{Equation 13}$$

The fourth failure mode is matrix compression, where $\sigma_2 + \sigma_3 < 0$:

$$\begin{aligned}\frac{1}{Y_c}\left(\left(\frac{Y_c}{2S_{23}}\right)^2 - 1\right)(\sigma_2 + \sigma_3) &+ \frac{1}{4S_{23}{}^2}(\sigma_2 + \sigma_3)^2 \\ &+ \frac{1}{S_{23}{}^2}(\sigma_{23}{}^2 - \sigma_2\sigma_3) + \frac{1}{S_{12}{}^2}(\sigma_{12}{}^2 + \sigma_{13}{}^2)\end{aligned} \qquad \text{Equation 14}$$

Where:

X_t and X_c - *Maximum allowable stresses in the E_{11} direction in tension (t) or compression (c).*

Y_t and Y_c - *Maximum allowable stresses in the E_{22} direction in tension (t) or compression (c).*

Z_t and Z_c - *Maximum allowable stresses in the E_{33} direction in tension (t) or compression (c).*

  S_{12} - *Maximum allowable in-plane shear stress.*

  S_{13} - *Maximum allowable 23 shear stress.*

  S_{31} - *Maximum allowable 31 shear stress.*

Once the failure criterion has been met then the element stiffness will be reduced. The elements stiffness is reduced using a stiffness reduction factor-r_i. This will begin when one of the failure index are greater than one. The stiffness

of each modulus is reduced using the following reduction factors as shown in Equation 16-Equation 20.

$$E_{11}{}^{new} = r_1 E_{11}{}^{orig} \qquad \text{Equation 16}$$

$$E_{22}{}^{new} = r_2 E_{22}{}^{orig} \qquad \text{Equation 15}$$

$$E_{33}{}^{new} = r_3 E_{33}{}^{orig} \qquad \text{Equation 17}$$

$$G_{12}{}^{new} = r_4 G_{12}{}^{orig} \qquad \text{Equation 18}$$

$$G_{23}{}^{new} = r_5 G_{23}{}^{orig} \qquad \text{Equation 19}$$

$$G_{31}{}^{new} = r_6 G_{31}{}^{orig} \qquad \text{Equation 20}$$

The reduction factors are calculated as shown in Equation 21-Equation 25. Where F_f is fibre tensile failure, F_{fc} is fibre compressive failure, F_m is matrix tensile failure and F_{mc} is matrix compressive failure. The reduction factors r_1 and r_3 are taken from the fibre tensile and compressive failure, r_2, r_4 and r_5 from the matrix tensile and compressive failure modes. The value for r_1 and r_3 when there is a failure in the fibre tension or fibre compressive modes is 0.01 which is the residual stiffness factor and is the maximum reduction in stiffness.

$$r_1 = r_3 = 0.01 \qquad \text{Equation 21}$$

If there is matrix compressive failure but not significant fibre damage then the overall element stiffness can be reduced using Equation 19.

$$r_2 = -(1 - e^{1 - F_{mc}}) \qquad \text{Equation 22}$$

In the case of matrix tensile damage the shear reduction factor will be calculated by Equation 20.

$$r_4 = -(1 - e^{1 - F_m}) \qquad \text{Equation 23}$$

In the case of matrix compressive failure the shear reduction factor will be calculated using Equation 21.

$$r_4 = -(1 - e^{1 - F_m}) \qquad \text{Equation 24}$$

$$r_4 = r_5 = r_6 \qquad \text{Equation 25}$$

The reduction factors allow a coupling between the failure modes and a gradual degradation of element stiffness due to combinations of each failure type. The new stiffness matrix will be updated for the element with the new properties taking into account the four different failure modes. In this way it is possible to combine the effect of the different failure modes without instantly removing the element stiffness or strength. So the different damage types will be combined into an overall damage and reduction in stiffness which will tend towards zero. There is a progressive failure and there will generally be a reduction in element stiffness due to matrix tensile or compressive damage, followed by fibre failure. Also, the damage does not heal after unloading and therefore damage is retained if elements do not completely fail.

7.3 Contact Body Elements and Boundary Conditions

The main body of the cutter was modelled as a rigid body with meshed solid elements to define the tool surfaces while the workpiece is modelled with solid deformable elements. However, a smaller section at the tip of the cutter is given elastic properties of the PCD in order to better simulate the contact

conditions at the tool workpiece interface shown in Figure 7-1. An elastic modulus of 925 Gpa was used for the PCD tool tip, in accordance with data from the literature [92],[93].

The main cutter body is assigned infinite stiffness material properties so that the structural pass can be skipped, (thus saving computational time). The rigid cutting contact body is given X-translational and Z-axis rotational velocity boundary conditions, to simulate cutter feed and rotation. For the 2D model quadrilateral elements with 4 mid side nodes, plane strain and full integration were used for material and cutter. While hex elements with 8 nodes and full integration were used in the 3D model for the workpiece, but reduced integration elements with hourglass control were used for the tool. Due to the time taken to run the simulation the use of reduced integration elements was advantageous. This will reduce the time taken for the stiffness assembly matrix and stress recovery for each iteration, by reducing the number of integration points for the stiffness matrix from 8 to 1 in the hex elements or 4 to 1 in quad elements. The plane strain elements were applied with a thickness of 6mm in

the 2D model to simulate the workpiece material thickness. While in the 3D model the full thickness of the workpiece was modelled. A Lagrangian spatial framework is used, in which the material is fixed to the mesh and moves with any deformation of elements. The assumed strain option was switched on in both the 2D and 3D simulations to improve the bending performance and the displacement accuracy of four node or brick elements, but with a minor increase in computational cost.

The cutting tool geometry was measured using an optical microscope, and the cutting edge radius was measured using the Alicona optical system. To create the cutting tool geometry in the model, the first cutting tool edge geometry was produced using lines in the 2D model, or surfaces in the 3D, and then meshed. Then the other cutting edges were created by duplicating around the Z-axis. In milling there is a continuous change in chip thickness as the tool rotates and the thickness is determined by the depth of cut, machining parameters, cutting tool geometry and wear. Therefore the size of the chip was not pre-calculated and was determined by the input parameters in the model.

Touching contact is used between the workpiece and tool with a coefficient of friction of 0.08 and a Coulomb bilinear friction model. The coefficient of friction used was taken from the literature based on the friction coefficient between PCD material and CFRP [94]. Research by Chardon et al. [94] found that the coefficient of friction between PCD and Carbon fibre was very low: around 0.06-0.08 for PCD tools. A lower adhesion is found for PCD tools compared to carbide coated tools and this can explain why PCD tools have a low wear and a high surface quality during composite machining. A. Mondelin et al. [95] also found that there was a coefficient of friction of 0.1 for diamond coated tools and CFRP in dry conditions- and 0.06 in wet.

The contact between the cutter and workpiece is based on a direct constraint method. In Marc this is called a node to segment method which was used in this analysis. The two bodies are defined as touching contact bodies otherwise two unconnected nodes from different bodies will pass through one another. The user selects the contact body based upon all of the elements in that body and then Marc will evaluate the element surfaces or edges to be used in contact detection. Here the cutter is the primary or touching contact body, and the workpiece the second contact body, which is similar to the master and slave contact definition in ABAQUS. The cutter has the finer mesh to ensure that no workpiece contact is missed. Contact constraints are only initiated when the node of the cutter comes within the outside distance tolerance of the workpiece elements, which is shown in Figure 7-2. When this happens, the node of the cutter is projected onto contact with the segment contacted body of the workpiece. Internal equilibrium between the two contact bodies is preserved through subsequent Newton-Raphson iterations and the node remains in contact unless the contact force becomes less than the relatively low separation force, and they will separate. Equally if the node passes through the element (but remains within the inside distance tolerance), it will be projected onto the segment of the element surface and contact is initiated, as shown in Figure 7-2(b). If the penetrating node passes through the element and inside the distance tolerance of the element, then the increment must be split and recycled, in order to prevent penetrating nodes.

(a)　　　　　　　　(b)
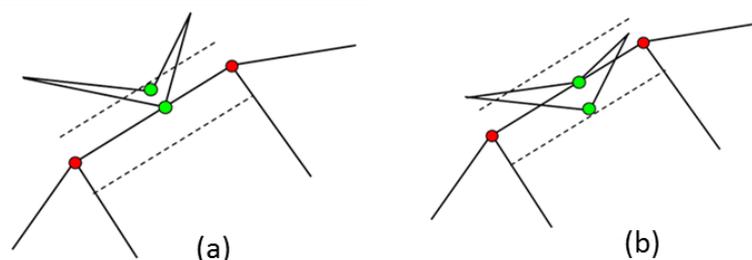
Figure 7-2- (a) Outside distance tolerance,
(b) Inside distance tolerance.

The separation force can be set by the user, as well as the distance tolerance. Although the default distance tolerance is recommended, which was used in this case, and is calculated from $1/20^{th}$ of the smallest element edge. The contact surfaces are updated after each increment, whereupon the elements may have been previously deleted or displaced. In each increment, firstly the material and geometric non-linearity are subject for targeting of convergence. Subsequently, then if the contact conditions in the analysis change, for example a new node comes into contact, or a node separates from contact, then the increment will be split. This will initialise a new iteration and the new contact conditions will be introduced into the equilibrium equations. The Newton-Rhapson iterative procedure will then continue until the convergence criteria is suitably met.

A contact table is used in MSC Marc which controls the contact interaction properties between each of the different bodies and which contact interaction is used. Two different contact interactions were used, a touching contact was used between the workpiece and cutter, as previously described, and the other contact interaction is a glued interaction between the workpiece and a geometric body. These geometric bodies act as a stationary surface or line which act as a fixed boundary condition and hold the workpiece in place preventing rotations or displacements. This is shown in the Figure 7-1 as the "Fixed_Side" and "Fixed_Base" geometric bodies.

In order to simulate the motion of the cutter the rigid tool contact body is assigned velocity boundary conditions. A rotational velocity about the Z axis and a translational velocity boundary condition in the X is used to give rotation and feed movement respectively. Large rotations option was switched on during the analysis. This was used in order to ensure strain objectivity of the tool elements to prevent any distortion of the tool as it rotates. Without this, the tool elements would distort with the rotational velocity applied. The

geometry of one cutting edge was created using points and lines before being meshed to form elements. The other cutting edges were then duplicated around the Z axis so that they would have the same mesh size and element distribution as the original.

The cutting forces were calculated after a steady state depth of cut was reached. During conventional milling the size of the chip being cut will change with rotational position, and the chip size will be determined by the feed and speed. The size of cut will change for each combination of feeds and speeds. However, a consistent size of chip will be still removed, per tool rotation, once a steady depth of cut is reached. Therefore the machining simulations were started when the workpiece was in an un-machined state which is shown previously in Figure 7-1 and in Figure 7-3. Then the cutter is allowed to progress until a steady state size depth of cut is removed which is depicted in Figure 7-4. The size of chip is therefore dependent upon the input machining parameters, and material properties, as there is no pre-calculation of the chip separation zone being used.
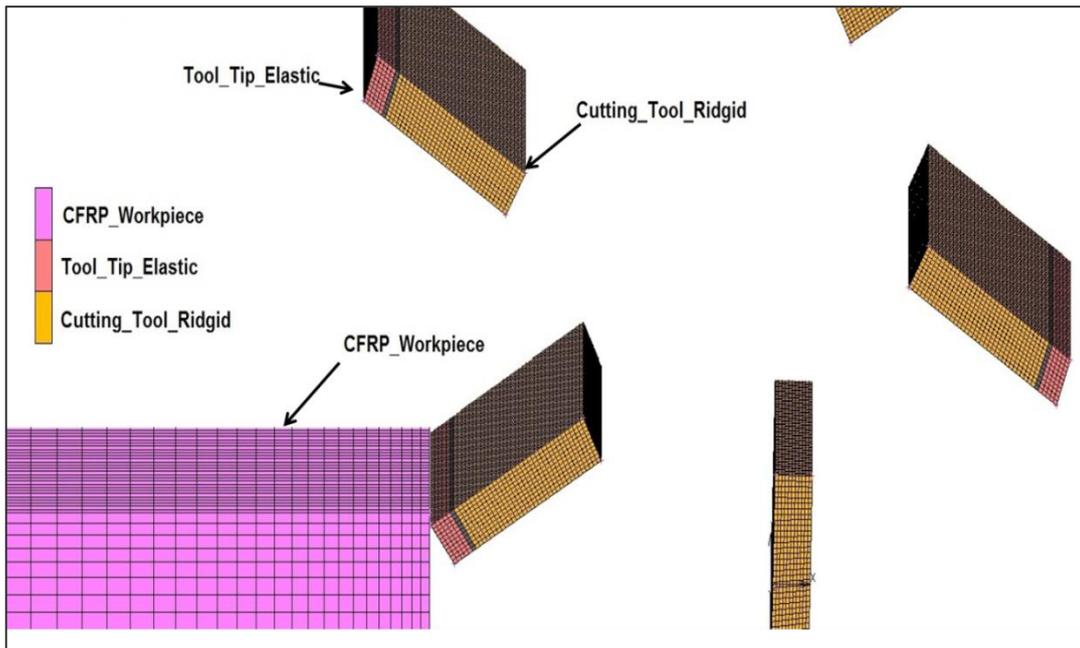
Figure 7-3- 3D Milling simulation with contact bodies.
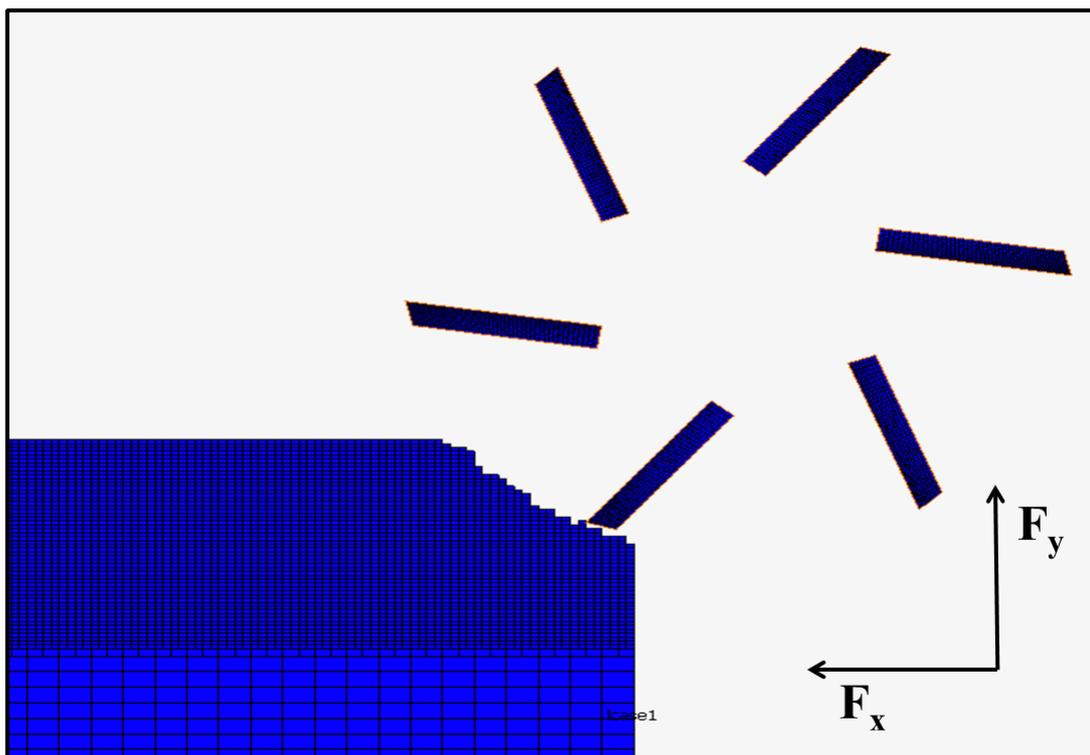
Figure 7-4- 2D steady state depth of cut reached.

The forces were taken from the geometric body which is used to constrain the workpiece. It was found that due to the rotation of the cutter there were some points where the tool is not in contact with the workpiece, and the cutting

forces were close to zero. These points were filtered out to take the average force across the increments where the cutter is in contact with the workpiece.

7.4 Adaptive Convergence and Local Mesh Adaptation

In order to solve the non-linear equations Marc uses an incremental-iterative Newton Raphson solution method to solve the equilibrium equations for internal and external forces. Each increment may require a certain number of iterations in order to converge on an equilibrium state. The Newton Raphson method is used solve the equilibrium equations containing the nodal displacement and tangent stiffness matrix, against the internal and external load vectors. An advanced adaptive convergence control was used in the simulations, which allows the load step to reduce or increase within specified limits, and at different rates according to the level of nonlinearity currently being experienced. This means that the load step will automatically reduce or increase as required to optimise the number of iterations required in the analysis. This is instead of using a constant load step. Therefore, the load step can be cut back when an increment fails to converge possibly due to sudden material failure or new contact conditions. The load step will automatically reduce by Marc if the previous increment has taken more than the user-specified "target" number of increments. Using adaptive load control the load step can also be increased if the solver easily converges and then the subsequent increment load step size is increased, decreasing the simulation time. This is useful in a milling simulation because there are points at which there is no contact between the tool and workpiece and the time step increments will be automatically increased. The use of a load step factor can be applied, in this case 1.4 was used, which is the maximum ratio at which the load step reduction, or increase, of the subsequent increment. The change in the subsequent increment is applied as a function, including the load step factor, number of previous increments and target number of increments.

The convergence is based on the residuals and the user has the option of choosing to converge on a combination of residual force and iterative displacements. Default values for the convergence tolerance are provided, but they may also be controlled by the user. It was chosen to converge on both residual forces and iterative displacements as this will give the higher accuracy by ensuring there is equilibrium on not only forces but also displacements. It is useful to ensure displacement equilibrium in the presence of contact and also to ensure movement of the cutter is accurate. In order to try and reduce the simulation time multiple threads from the central processing unit were used across all the stages of the simulation for the assembly and recovery of the stiffness matrix and of the matrix solver.

Adaptive re-meshing has been used in the cutting zone using 3 levels which allows the elements to decrease to 1/8th of the initial element size by successive element divisions. Local adaptive re-meshing of the workpiece was applied using the node in region cylinder method shown in Figure 7-5. This worked by allowing a subdivision of the elements which were within a user specified radius. This method worked well because a re-meshing diameter could be given which was slightly larger than the tool edge radius. Elements will therefore subdivide slightly ahead of the cutting tool tip.

Tool Tip. Local Mesh Refinement

Local Adaptive Meshing of workpiece elements within region cylinder.
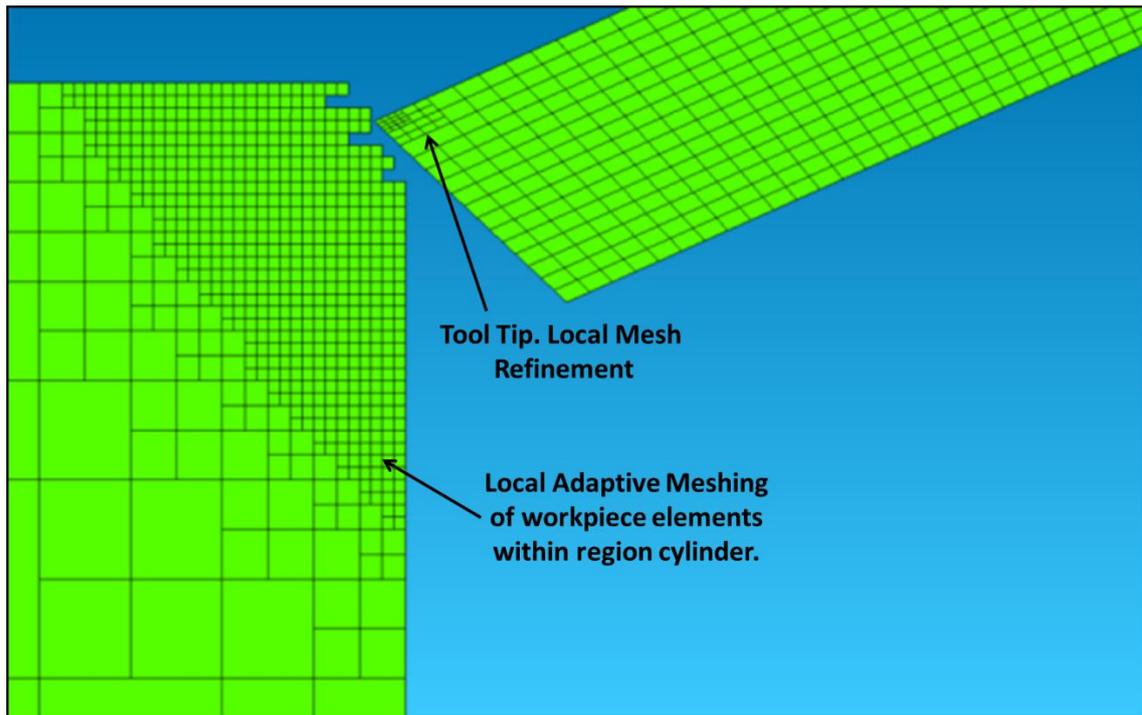
Figure 7-5- Local adaptive re-meshing of workpiece and tool tip.

The re-meshing zone is contained within a cylinder which moves at the same feed rate as the tool. The movement of the radius of the re-meshing zone is applied to a separate created node which is not connected to the cutter or workpiece. The node is created at the centre point of the tool diameter and is given the same feed velocity as the tool. The cylinder movement is tied to this created node and therefore the elements will re-mesh before the tool starts to cut them. This means only a portion of the workpiece elements which are nearby the cutting zone will have a fine mesh. For the re-meshing an increment frequency of 9 was used, which means that rather than re-meshing elements every increment, division will occur on every 9th increment and not overly waste computational time. Hence, the solver will not constantly be searching for elements to subdivide every increment. Additionally, a small portion of the cutter tip was also assigned local adaptive re-meshing properties so that there are a sufficient number of nodes contacting the workpiece at the tool tip. This will increase the number of contacting nodes through thickness in the Z direction, preventing high levels of stress at contacting nodes.

216

The contact method implemented within Marc takes into account the constantly updated cutting face of the workpiece as a contact surface. So, once the material workpiece elements have been removed the boundary contact surfaces of the workpiece are continuously being updated as the tool cuts further into the workpiece. The use of local mesh refinement also ensures the size of elements being removed will be consistent throughout the analysis, not leading to changes in convergence or cutting forces due to element size effects.

7.5 Tool Wear- Cutting Edge Rounding

In the 2D FE analysis a tool wear model has been implemented to see if the developed model can accurately assess the effects of tool wear due to increase in cutting edge radius. This has been included in the FE model and applied as a small cutting edge radius at the tool tip. A very fine mesh has been used at the tool tip, with a 0.3 meshing bias moving towards the cutting edge. A meshing bias means there will be a progressively finer mesh size when moving in a user chosen direction. This meshing bias was applied in both the X and Y directions. A cutting edge radius of 3.7μm and 10μm has been included in the 2D FE model as measured optically in the experiment. This has been used to show the effects on output machining forces and how increasing tool wear will affect the machining process. The tool tip mesh has been implemented as shown in Figure 7-6(a) and Figure 7-6(b). This is shown for the new tool which has a 3μm edge radius and the worn tool which has a 10μm edge radius.

In addition, to predict the effects of a more extreme increase in tool wear an additional set of FE tests with increasing cutting edge radius up to 30 microns was applied, using progressive 5 micron steps, which will also be correlated with a hypothetical predicted increase in roughness.
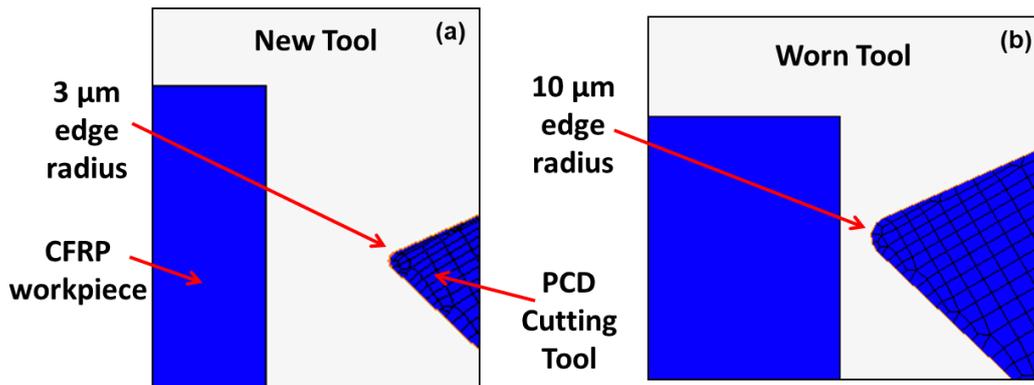
Figure 7-6- Worn and un-worn cutting tool 2D FE mesh:

(a) New tool,

(b) Worn Tool.

It was not possible to include the changing cutting edge radius in the 3D model due to the very large number of elements required at the tool tip. Modelling of the tool edge radius in the 3D FE model using solid elements lead to severe element distortion and an extremely large number of elements in the through thickness Z-direction, therefore the computational time of the analysis was unfeasible.

7.6 User Subroutine Utimestep

A user subroutine (utimestep) has been used with the 3D model in order to control the movement of the cutter body more efficiently. This subroutine is called at the end of each converged increment and allows the load (or time) step for the next increment to be modified if required. The subroutine is written in Fortran. The Fortran code enables the cutter rotational speed to be increased immediately after one tip has finished cutting and until the next tip becomes close to the workpiece, at which point the rotational speed is reduced again by constraining the load step to a small fraction of the local workpiece element size. This reduces the simulation "idle" time, allowing for more elements to be used in the cutting area, more time for contact of the cutters

218

with the workpiece and, therefore, the capture of more consistent cutting forces without additional computational cost.

In an implicit nonlinear finite element programme it is both possible and useful to have a varying load step size. The size of the load step is allowed to vary from increment to increment (also within an increment) depending upon the current convergence difficulties. Although a flexible adaptive loading control has been implemented in Marc, there remains a significant idle time between the actual cutting portions in this specific cutting analysis. This is because it takes the cutting tool a number of increments for the load step to increase sufficiently (using the previously described load factor), to allow large rotational displacements. The load step has to decrease significantly during cutting due to the non-linear contact conditions and failure of elements. Ideally the user wants the cutter load step to increase instantaneously after cutting has finished for each cutter tip and decrease the simulation time. With Marc's adaptive loading control which was initially implemented and used in the 2D model successfully, a load step factor of 1.4 was originally used to allow both an increase and decrease in the previous load step by 40 %. The load step factor applied is based on the number of iterations taken to solve the current increment. If the number of iterations in the increment are less than a user-defined number of desired iterations, then the subsequent increment load step will be increased using a relationship that is a function of this load step factor. To further improve efficiency, this user subroutine has, therefore, been created to decrease the simulation time by immediately increasing the load step when cutting has just ended for each cutter, as well as immediately decreasing the load step when a cutter is in close proximity to the workpiece. The additional control over the rotational speed during cutting is also a benefit. This was of greater use in the 3D model due to the higher required computational resources and significantly reduced load step.

In the subroutine, the cutter rotational velocity is controlled whilst cutting by the edge length of the current smallest element in the workpiece after element re-meshing. To provide information regarding the location of the cutter tips to the user-subroutine a single node on each of the cutter tips is selected. After determining the closest of these nodes to the workpiece, the node is checked for a location greater than the current maximum height in the y coordinate of the workpiece. If this is the case, then the load-step is increased to allow the next cutting tip to come into position quickly. Should an increment fail to converge within the user-defined number of iterations, a cut-back will occur. The increment will be automatically restarted with a smaller load step. The cut-backs are determined by Marc prior to calling the user subroutine and reduce the amount of administrative effort required in the subroutine in handling this.

The subroutine was found to significantly decrease the simulation time for the 3D model by reducing the cutter idle time. This reduction allowed for an increase in the number of elements in the cutting zone, as well as more consistent cutting forces due to smaller and a more mesh granularly defined load increment while cutting. A further benefit arising from the more accurate capture of cutting forces was more stable convergence behaviour during contact and the subsequent element deactivation upon failure.

Chapter 8
Results- FE Modelling of Composite Machining

The FE results from unidirectional and multidirectional edge trimming tests are presented. A comparison of mean cutting forces between experiment and FE will be presented to validate FE models. The change in cutting forces at different levels of tool wear will be predicted using FE models and compared with experiment.

8.1 FE Results Unidirectional Edge Trimming Test

8.1-1 Cutting Force Comparisons

The cutting forces were recorded from a unidirectional edge trimming FE model and a comparison is made using 2D and 3D simulations. To simulate the effects of tool wear in the 2D FE analysis a 3.7 microns and 10 microns cutting edge radius was implemented as measured in experiment. An image of the 2D simulation with deactivated elements is shown in Figure 8-1 and the Fx and Fy machining force definition is explained. The 3D simulation is shown in Figure 8-2 and Figure 8-3 with the direction of cutting tool rotation applied as a velocity boundary condition. Adaptive re-meshing was successful in the cutting zone and workpiece elements were deactivated using the Hashin damage model without causing model instabilities. Computations were performed on Intel Core 2.7 GHZ processor with 16 GB internal RAM.

222
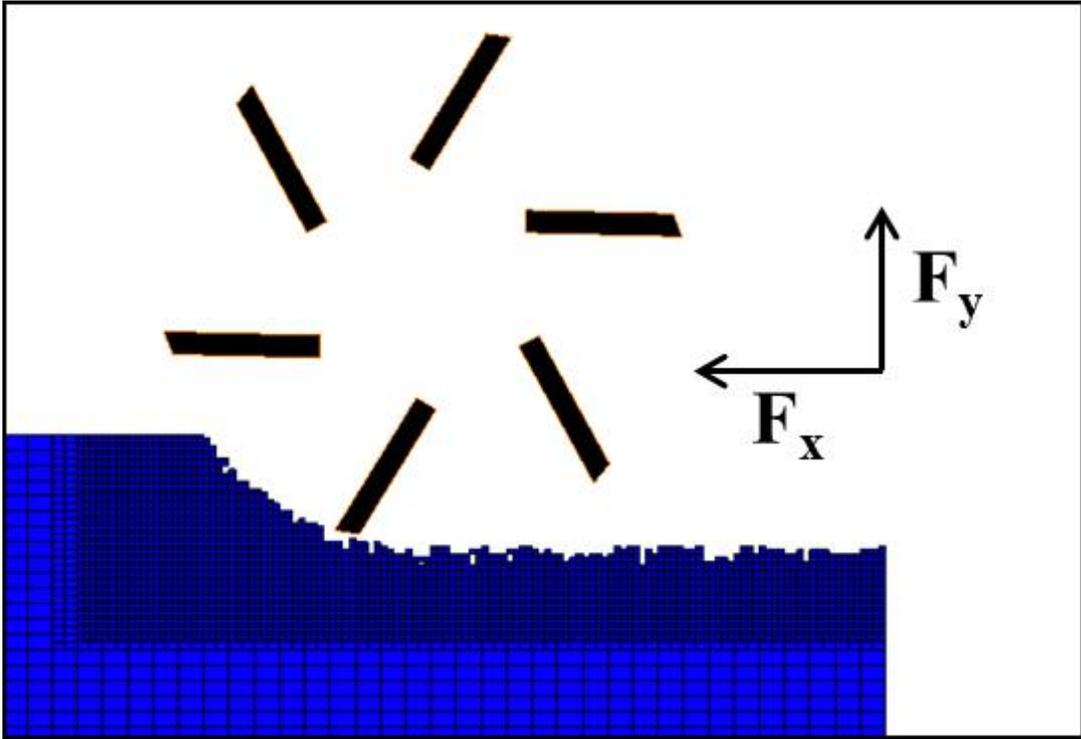
Figure 8-1- 2D edge trimming simulation with composite elements and Fx and Fy machining force orientation.
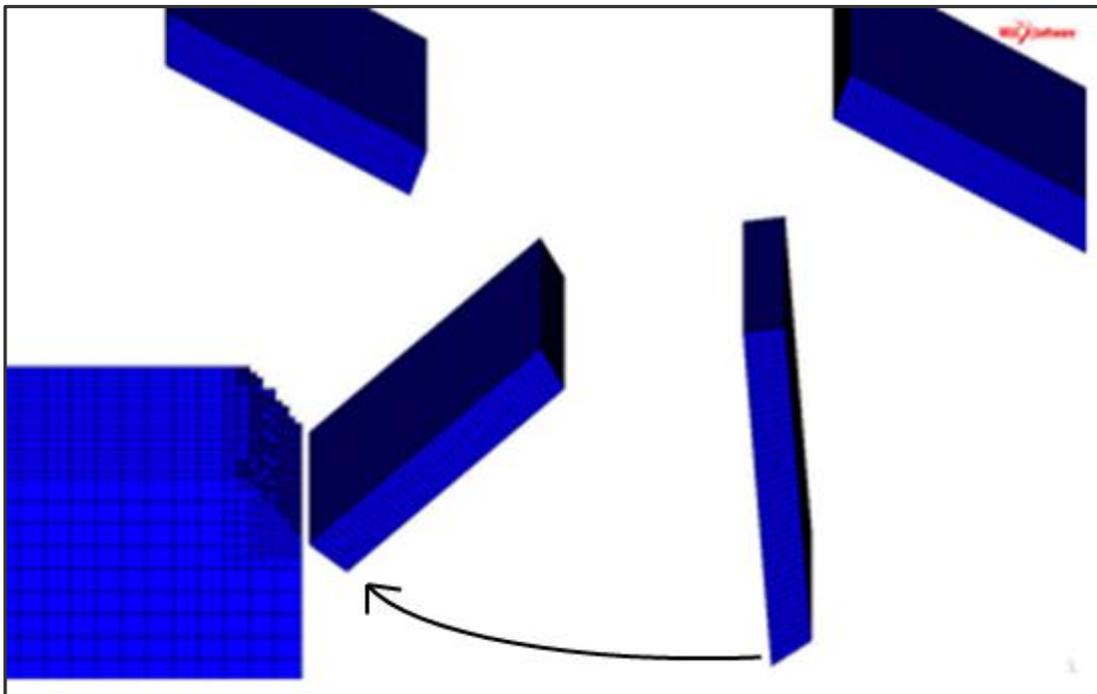
Figure 8-2- 3D Edge trimming simulation with composite elements and advancing adaptive meshing.
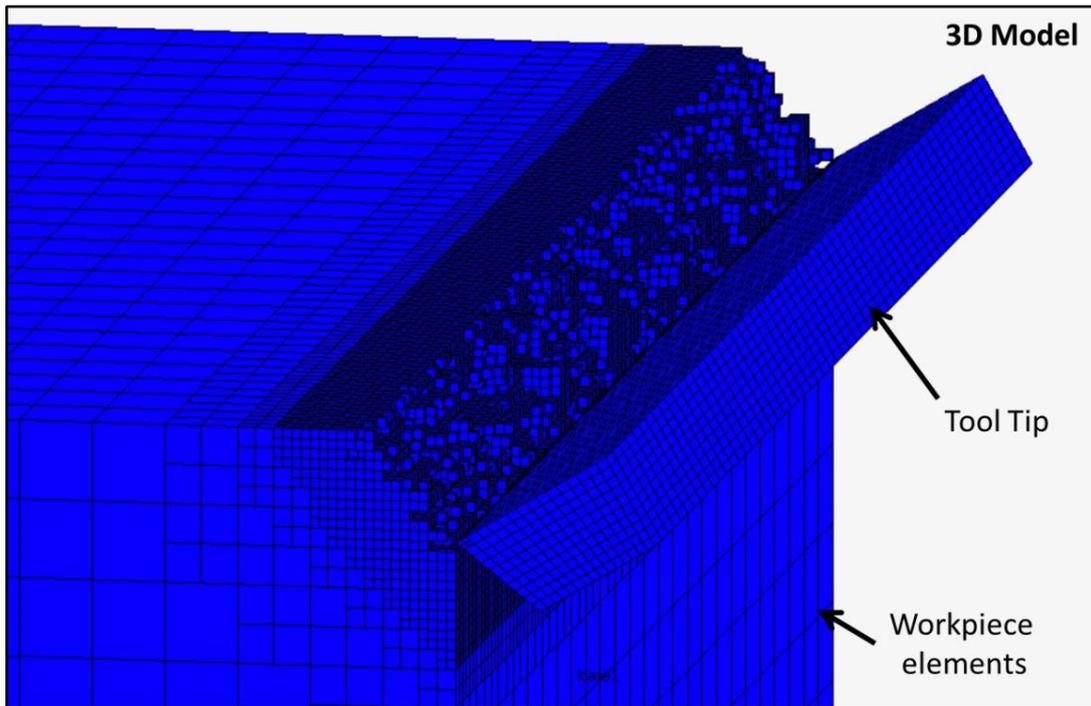
Figure 8-3- 3D Simulation with deactivation of orthotropic composite elements by Hashin damage model.

Mean cutting forces have been calculated from FE simulation once full depth of cut had been reached at steady state cutting conditions. Figure 8-4 and Figure 8-5 show examples of the output forces from 2D simulation in the Fx and Fy direction respectively. Mean cutting forces are calculated from when the cutting tool is cutting the workpiece and therefore zero values were omitted from the mean cutting force calculation. Both Figure 8-4 and Figure 8-5 show a portion of the cutting forces which has been selected to make a calculation of the average cutting forces. The initial section of cutting has been omitted until steady state cutting is reached. In Figure 8-4 it can be seen that the cutting forces fluctuate and that there is intermittent cutting when the cutting tool comes in and out of contact with the workpiece. The cutting forces have a range of values due to fluctuation of contact forces and variation in material damage. Some individual outliers can be seen in the forces due to large contact stresses. The cutting forces in the Fy direction vary between positive and negative values due to the rotation of the cutting tool.

224
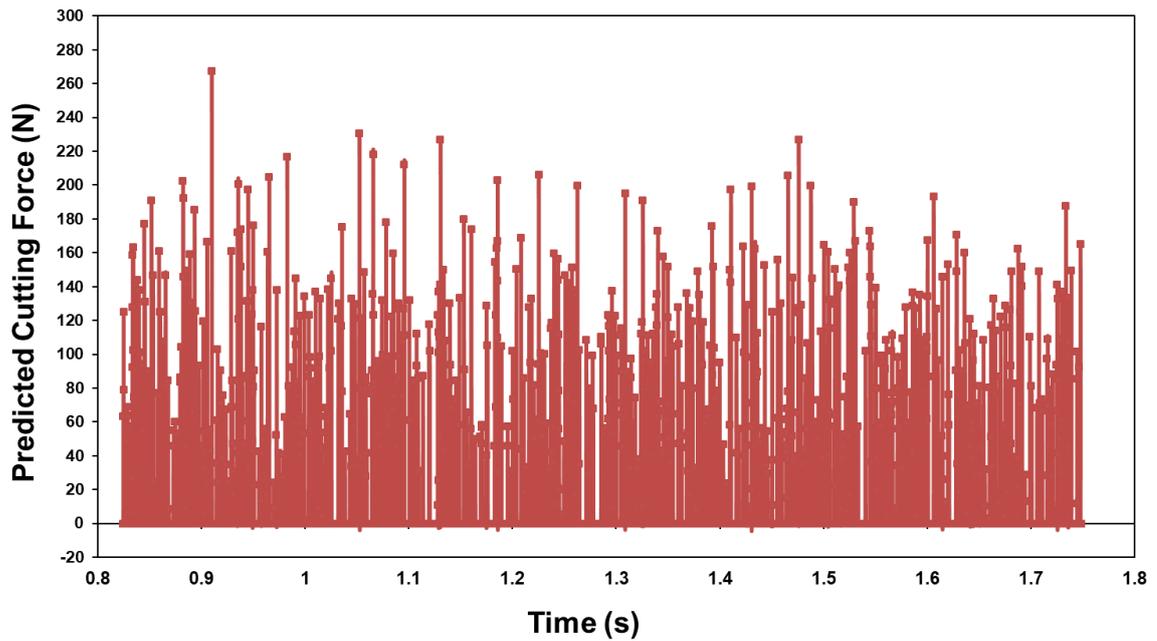
Figure 8-4- Fx cutting force output from FE model.
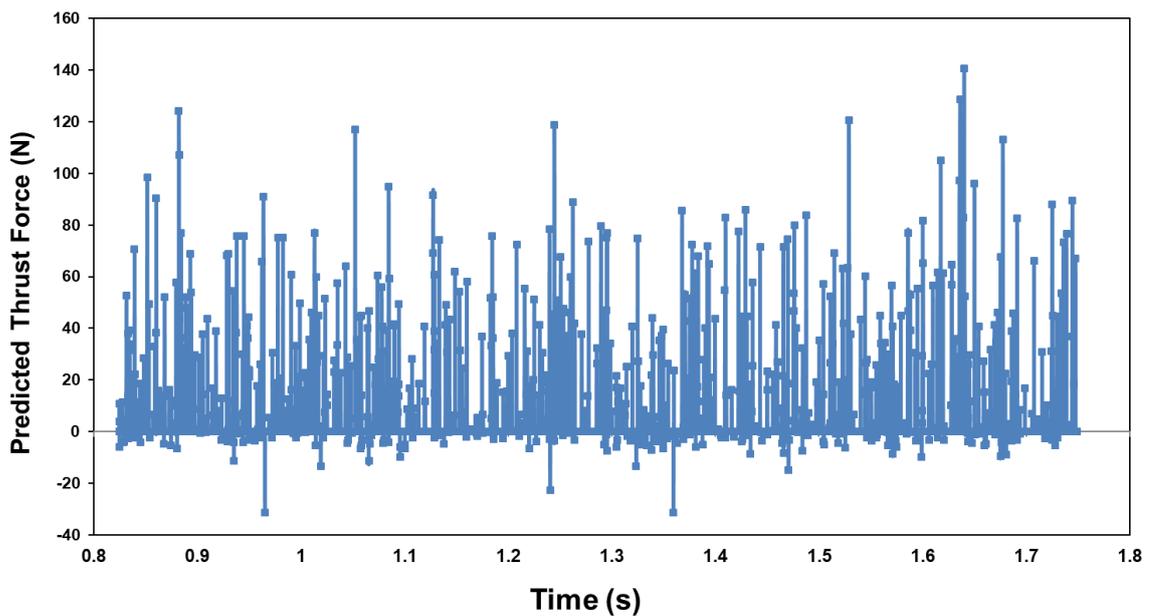
Figure 8-5- Fy thrust force output from FE model.

Mean cutting forces in the Fx and Fy direction were calculated from FE simulations and are shown in Table 8-1 for 2D simulation with the worn and unworn cutting tool edge radius. Table 8-1 also shows cutting forces for the 3D FE simulation.

Table 8-1- Mean cutting forces from FE model.

Fibre Orientation	Feed Rate	RPM	Mean Fx 2D (New/Worn)	Mean Fy 2D (New/Worn)	Mean Fx 3D	Mean Fy 3D
90	800	6000	74.0, 84.1	22.6, 31.4	93.1	52.8
90	1200	6000	76.3, 96.4	13.3, 32.3	108.6	72.7
90	800	8000	69.7, 88.2	17.4, 33.2	148.4	141.1
90	1200	8000	95.0, 88.2	13.3, 41.6	82.3	64.8
45	800	6000	76.1, 89.0	22.9, 31.2	101.7	88.3
45	1200	6000	95.8,100.1	30.4, 41.6	96.4	142.5
45	800	8000	72.4, 90.7	19.1, 32.0	123	94.7
45	1200	8000	71.2, 97.3	16.3, 36.8	113.9	118.8

Charts of the cutting forces for each of the different experiment parameters are shown in Figure 8-6-Figure 8-9. Cutting forces are shown for the experiment in the unworn tool and worn tool conditions and the 2D FE simulation with unworn (3.7μm edge radius), and worn (10 μm edge radius). The cutting forces are shown for the 3D simulation with a fully sharp cutting edge. The 90 degree fibre orientation Fx cutting forces are shown in Figure 8-6 at a 6000 RPM cutting speed, and the same cutting parameters for the Fx in the 45 degree fibre orientations are shown in Figure 8-7.

The Fx cutting forces were found to be reasonably well correlated between the FE model and experiment. The percentage difference calculated between the experiment and 2D model was -12 % in the Fx forces for the unworn tool condition at 90 degree fibre orientation, at 800 mm/min and 6000 RPM. While a difference of +10.1 % was found for the Fx forces between experiment and 3D model for the same conditions. It was found in general that the 3D simulation predicted higher cutting forces than the unworn 2D model.

However the Fy forces were not as well predicted by the 2D model as the Fx forces and were underestimated by the model. They were better predicted by

the 3D model with a +5 % difference between the experimental and FE model for the Fy forces whereas the Fy cutting forces had an average difference as much as -50 % lower in the 2D model. This is because the 2D model is a plane strain model and does therefore not take into account out of plane effects. It has been shown that there can be out of plane fibre displacement in composite machining which may account for the lower machining forces in the 2D model [21]. It is also hypothesised as to why Fx cutting forces were predicted generally higher in the 3D than 2D model. It was also found that there is a small variation in through thickness element damage seen in the 3D model which was previously shown in Figure 8-3.

The effect of increasing the cutting edge radius in the 2D simulation had a corresponding increase in the cutting forces which were on average 17 % and 62 % higher for the Fx and Fy forces respectively. In the experiment the cutting forces were on average 32 % and 64 % higher for Fx and Fy respectively. Therefore the model was able to give reasonably accurate interpretation of the increase in machining forces due to tool wear. This method is therefore useful to calculate how changes in cutting edge radius due to tool wear may affect the overall machining forces and how they may impact the machining process. This can be used as a method to prevent machining forces reaching a maximum cut-off value. Also, the maximum tool wear by cutting edge radius can be predicted which will ensure an effective machining process.
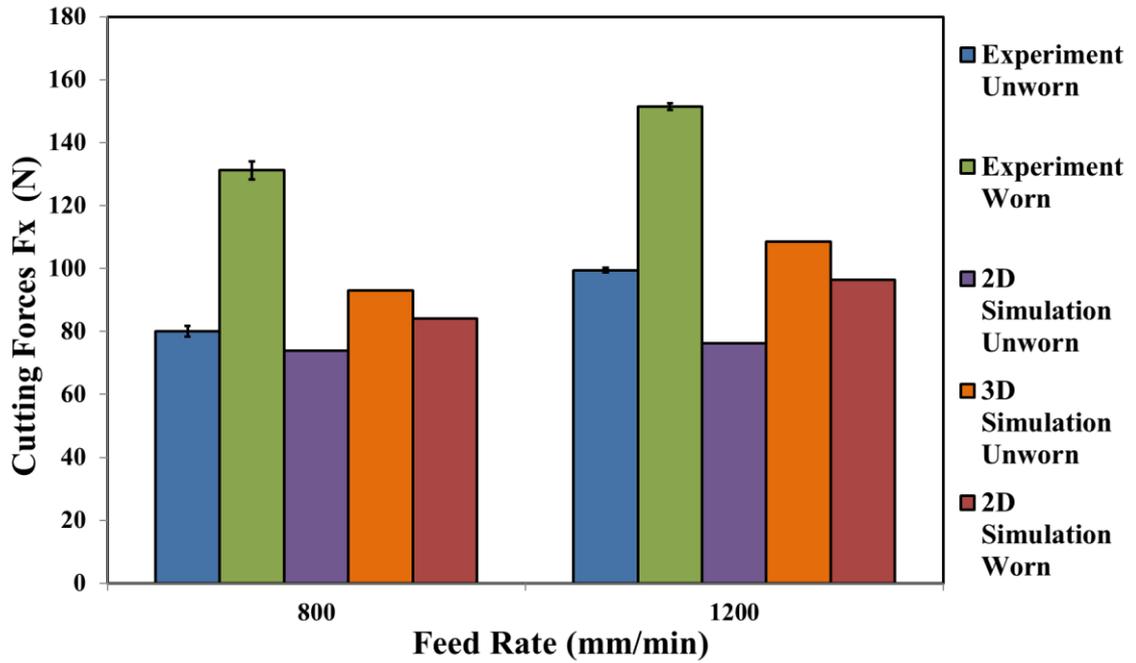
Figure 8-6- Fx cutting forces vs feed rate from experimental and FE for 90 degree fibre orientation at 6000 RPM.
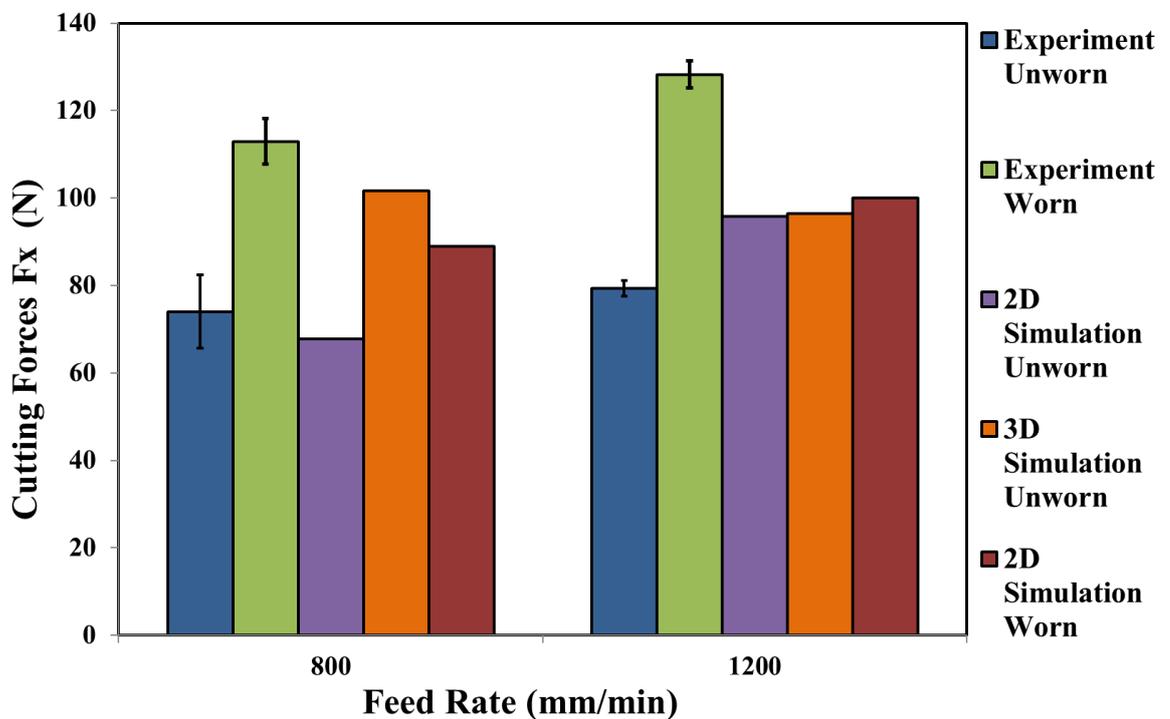
Figure 8-7- Fx cutting forces vs feed rate from experimental and FE for 45 degree fibre orientation at 6000 RPM.

228
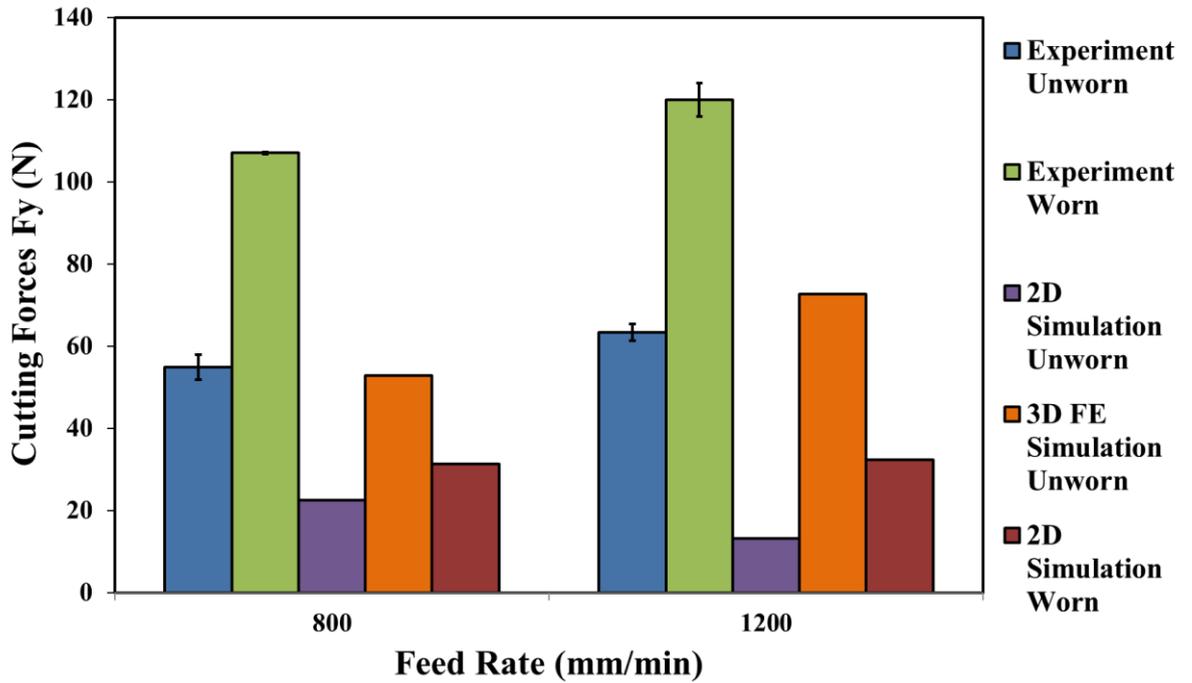
Figure 8-8- Fy cutting forces vs feed rate from experimental and FE for 90 degree fibre orientation at 6000 RPM.
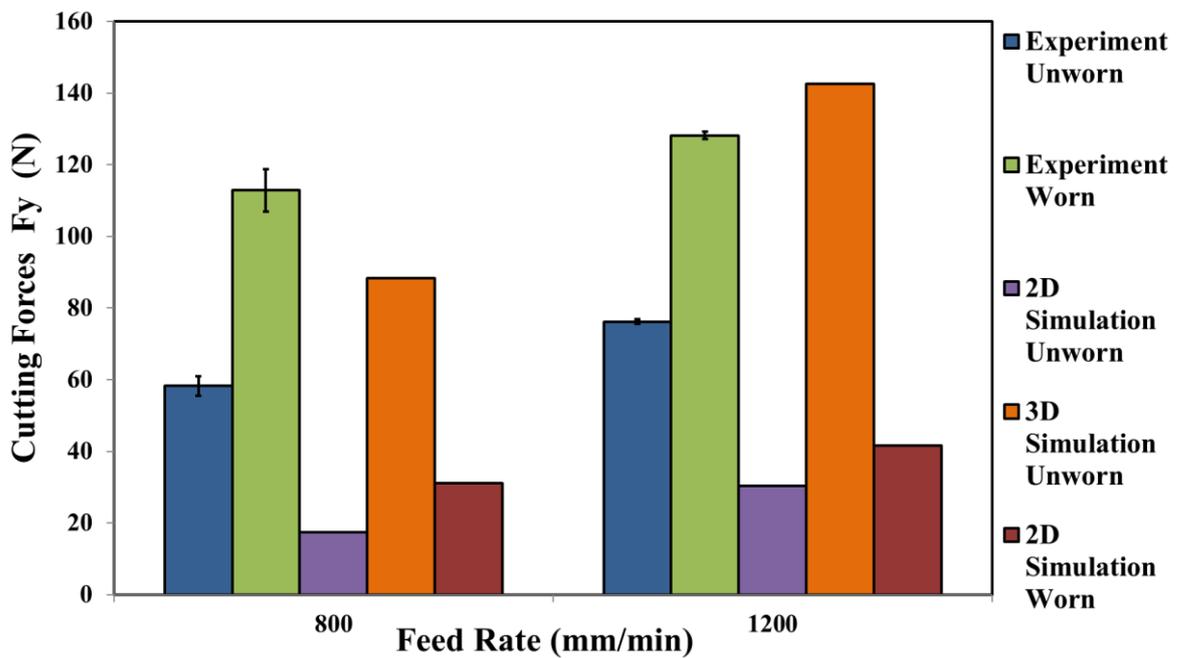
Figure 8-9- Fy cutting forces vs feed rate from experimental and FE for 45 degree fibre orientation at 6000 RPM.

8.1-2 Predicted Tool Wear Effects on Cutting Forces

In order to predict the effects of increasing the cutting edge radius using the FE model an additional virtual set of progressive tool wear was calculated in the FE model. The cutting edge radius was increased progressively in 5µm steps from 0 to 30 µm to calculate the virtual change in cutting forces. This is a useful analysis to make because it can be used to find when the cutting forces may become unreasonably high and cause material damage, thus allowing an informed decision about when tool replacements should be made. In Table 8-2 and Figure 8-10 the effect of increasing cutting edge radius is shown. The FE model showed a steady increase in the Fx cutting forces with tool wear which would be expected for an increased friction because more of the tool tip is in contact with the workpiece. A larger contact area will also cause the cutting mechanism to change to fibre tearing rather than predominantly a fibre shearing cutting mechanism. An increase of 50 % in the Fx cutting forces was found when going from a 5 µm to 30 µm edge radius. This will also correspond with a decrease in surface quality as shown previously in the experimental section. The Fy cutting forces were found to be more constant due to an increase in cutting edge radius and were not as strongly affected as the Fx cutting forces. This is a useful result because it shows that the increase in cutting forces due to an increase in tool wear can be predicted by an FE model. Therefore the increase in cutting forces due to cutting edge radius can be combined with known effects of cutting forces from experiment to make an assessment of surface quality. The next section will look at directly predicting surface quality using a combination of FE and regression equations.

Table 8-2- Cutting forces with increasing levels of tool wear (2D FE model.)

	Edge Radius (microns)	Mean Fx	Mean Fy
<- Increasing wear	0	70.5	6.12
	5	71.0	6.12
	10	81.2	7.14
	15	81.2	5.61
	20	102.2	6.12
	25	107.8	5.10
	30	105.1	5.61
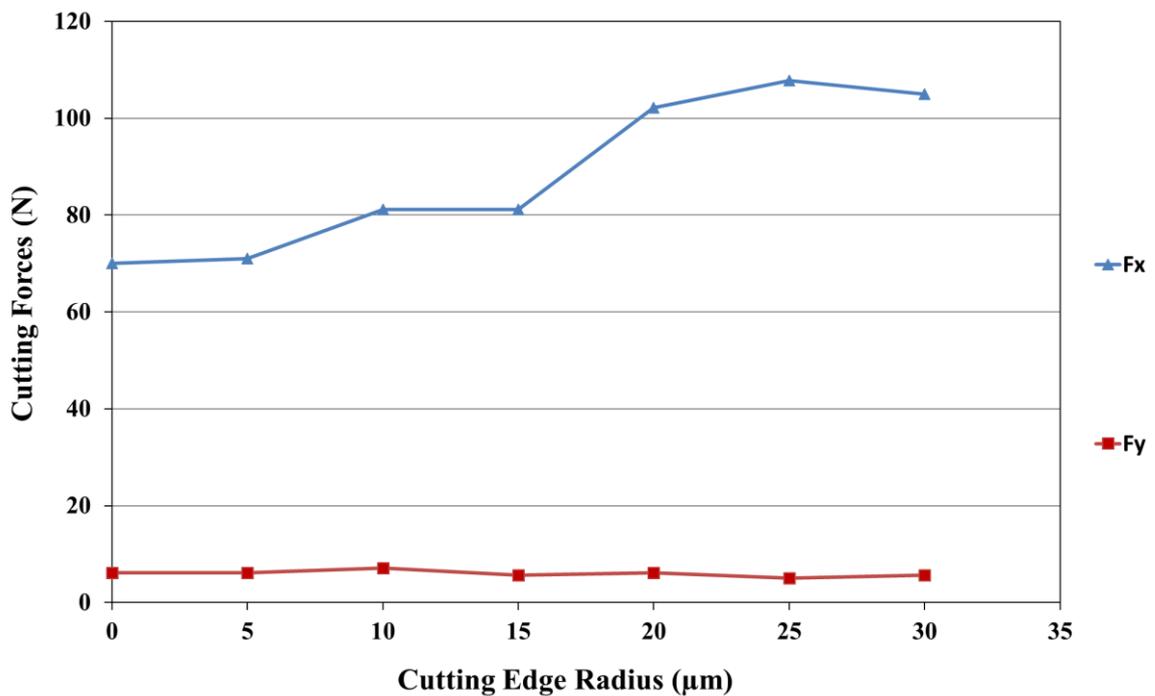
Figure 8-10- Effect of an increasing cutting edge radius on Fx and Fy from FE model. (45 Degree Fibre Orientation, 1200 mm/min & 6000 RPM).

8.2 Surface Roughness Prediction- Unidirectional Model

Predictions have been made for the S_a surface roughness using the forces calculated from FE the model. From the previous results shown in Table 8-2 with a cutting edge radius of 5 µm, and a feed rate of 800 mm/min, cutting

speed of 6000 RPM, there was a predicted cutting force of Fx= 71 N and Fy= 6.12 N. This will give a predicted calculated S_a of 1.72 μm for a fibre orientation of 90 degrees. Shown in Table 8-3 is the value for the predicted S_a against an increasing cutting edge radius. In Figure 8-11 the graph of predicted S_a against cutting forces is shown which has been calculated by a combination of the predicted cutting forces from FE model and the regression equation. The unknown parameter is the machining forces which must be predicted by the FE model. There is a generally steady increasing trend in S_a roughness with an increasing edge radius. The chart shows a slight decrease in the slope of the line as the cutting edge radius increases which is an effect of the change in geometry at the tool tip. The increase in S_a roughness with cutting edge radius is expected because the tool loses its ability to cleanly shear fibres and an increased friction due to a higher contact area between the tool and workpiece.

Table 8-3- Predicted S_a against increasing cutting edge radius.

Edge Radius (microns)	Mean Fx	Mean Fy	Predicted S_a
5	71.0	6.1	1.7
10	81.2	7.1	1.8
15	81.2	5.6	2.4
20	102.2	6.1	2.8
25	107.8	5.1	3.2
30	105.0	5.6	3.4
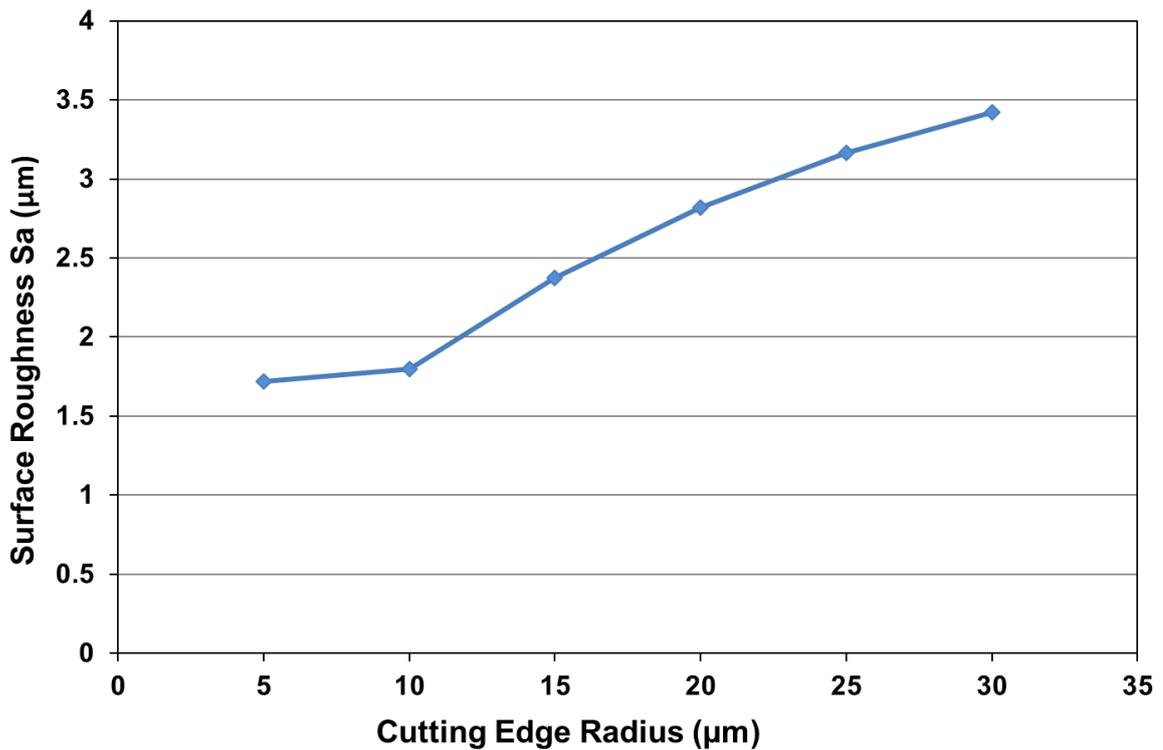
Figure 8-11- The predicted increase in S_a surface roughness with cutting edge radius.

The combination of FE model and regression equation has been found to be a useful method to predict the critical cutting edge radius at which point the predicted S_a will cause large machining damage. This can be used to give machinists an idea of when cutting tools should be replaced and prevent unnecessary damage to components. PCD cutting tools can also be reground to sharpen the cutting edge, so, a critical limit can be applied to the edge radius at which point the tool should be reground.

This method allows predictions of surface roughness at varying machining parameters with increasing levels of tool wear to make a judgement on safe machining conditions without having to do many experimental tests. It was also seen previously that the increased surface roughness was correlated with an increased delamination frequency and magnitude. Therefore minimising the

233

roughness and using roughness as a predictive measurement could be used as a method to reduce delamination issues during machining.

The combination of 2D FE model and regression equation was therefore able to be used as a strategy for predicting roughness. An increasing trend in roughness was predicted with tool wear. Predictions were made using output forces from FE model and it was found that there was a 100 % increase in S_a roughness value when the edge radius increased from 5 to 30 µm edge radius. This represents the change in cutting edge radius from a relatively new to a significantly worn tool [89]. The accuracy of the prediction is determined by the fit of the regression equation to experimental data and by the accuracy of cutting force predictions of the 2D model. Due to the under prediction of thrust forces from the 2D model there will therefore be some error in the roughness prediction capabilities using the 2D model. For this reason the 3D model was also assessed using a roughness prediction strategy from the multidirectional test results which will be presented subsequently. These results will be compared with experiment. This also allowed the assessment of roughness prediction on a multidirectional laminate with multiple fibre orientations.

8.3 Surface Damage Assessment

8.3-1 Hashin Damage Model

This section deals with an assessment of the damage and element removal caused by the Hashin damage model. The failure indices from the Hashin damage model are used to remove damaged elements. An analysis of the surface damage during the removal of material has been assessed to look at surface damage and which damage mechanism has caused removal of material. The surface damage in the 10 micron 2D edge trimming model due to the magnitudes of the different failure indexes in the Hashin damage model has been assessed. This has been done to find which of the different damage

mechanisms is most responsible for failure in a composite edge trimming process and to find if this has any dependency on fibre orientation. In Figure 8-12 the progression of failure from the first failure index is shown over successive increments as the tool rotates. Figure 8-12 shows the first failure index magnitude which is fibre tension over a successive set of increments as an element is removed. It was found that there is generally fairly localised damage due to fibre tension. However in Figure 8-12(b) there is some low level fibre damage propagating into the material which is away from the tool-workpiece contact zone.
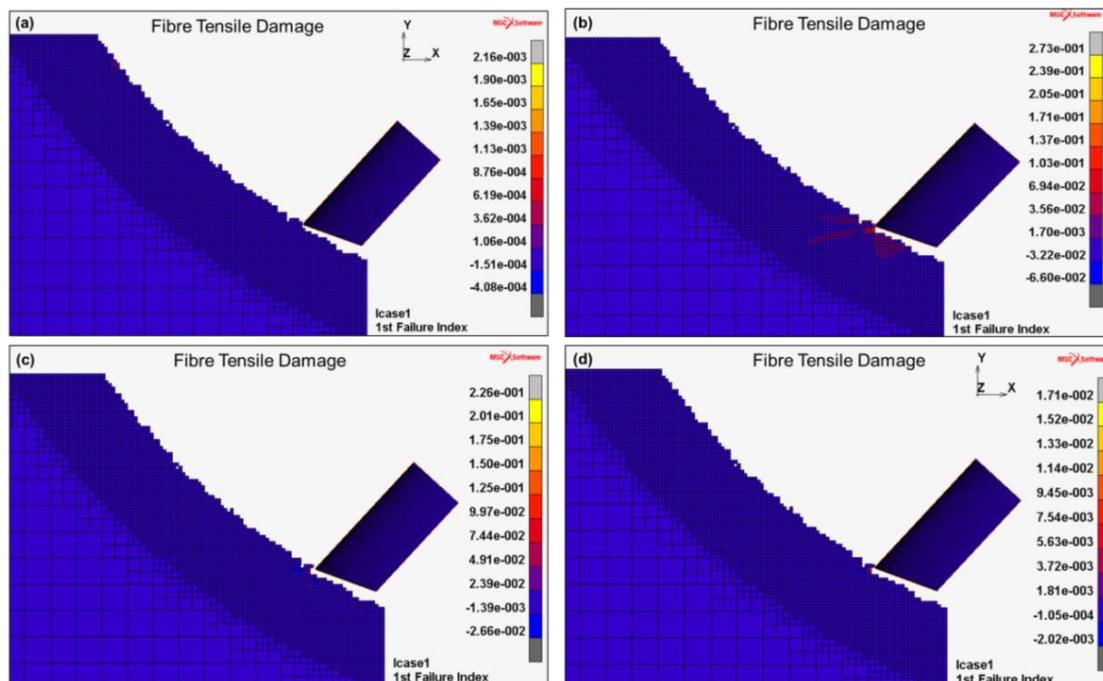
Figure 8-12- Tensile fibre failure magnitude (1st Failure index), over subsequent increments. (90 degree fibre orientation, 10μm edge radius, 800mm/min Feed and 6000RPM)

In Figure 8-13 the 4th failure index is shown for the same point over the same set of increments as in Figure 8-12. The magnitude of damage was found to be higher in the 4th failure index which is a matrix compression mode, than in the other failure modes in this set of machining conditions and 90 degree fibre orientation. The magnitude of the failure indexes is shown in Figure 8-14,

positioned at a single node over successive increments. This node is in the process of being removed as the tool passes causing element failure. The 4th failure index is found to be the highest in magnitude followed by the 3rd and 1st, which are matrix compression, matrix tension and fibre tension respectively. In Figure 8-13 it was found that there was more damage shown in red propagating further into the material further than in Figure 8-12. The matrix compressive damage was therefore found to have a higher magnitude and widespread damage than the other failure modes in the 90 degree fibre orientation. This could be expected due to the weaker strength of matrix compared to the fibres. It therefore represents that widespread matrix compressive and tensile damage and then fibre tensile damage cause element failure in the 90 degree fibre orientation.
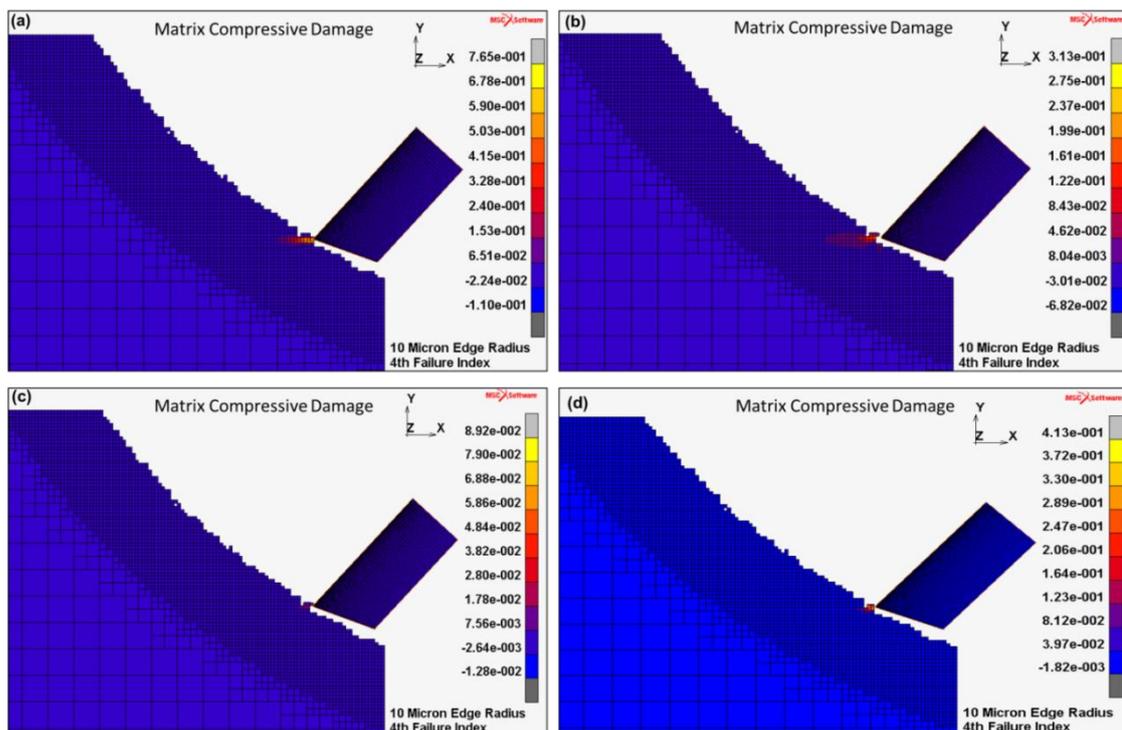
Figure 8-13- Matrix compressive failure magnitude (4th Failure index), over subsequent increments. (90 degree fibre orientation, 10µm edge radius, 800mm/min Feed and 6000RPM)
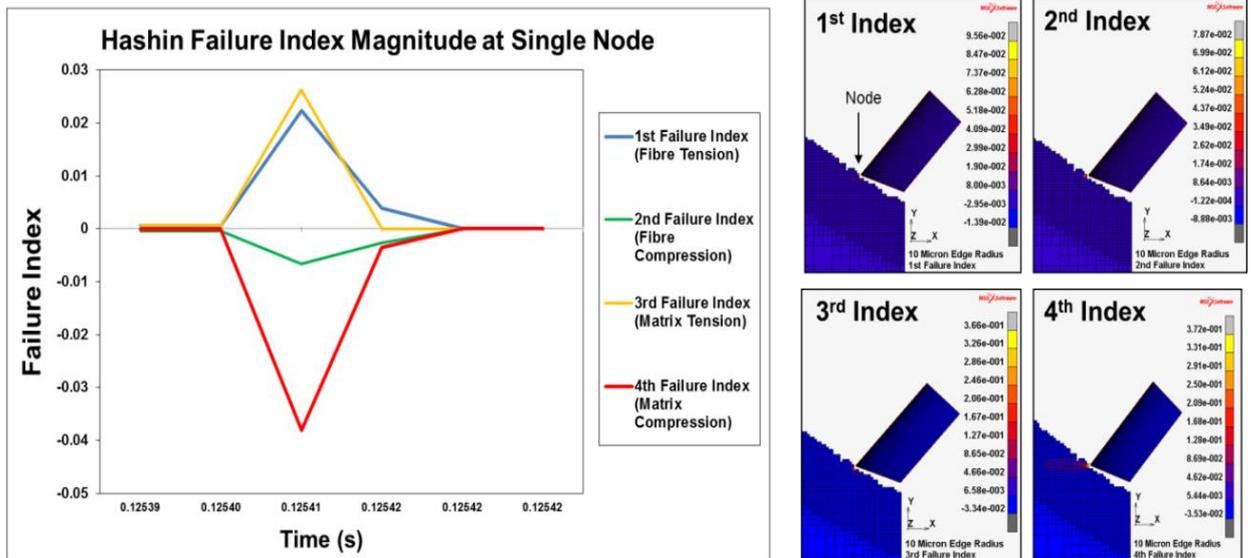
Figure 8-14- Hashin failure index at single node over successive increments leading to element failure. (90 degree fibre orientation, 10 μm edge radius, 800 mm/min Feed and 6000RPM)

In Figure 8-15 and Figure 8-16 the failure index for the Hashin damage model on the 45 degree fibre orientation is shown, machined with worn 10 μm edge radius tool at 800 mm/min feed and 6000 RPM. Figure 8-15 shows the 1st failure index which is fibre tensile failure in successive increments as the tool is rotating. It can be seen that there is a fairly localised damage area at the point of contact between tool and workpiece. Figure 8-16 shows the magnitude of each of the failure indexes at a node leading up to failure of an element. The 3rd failure index which is matrix tension has the highest magnitude before element failure. There is also damage caused due to the 2nd and 4th failure index which are fibre compression and matrix compression respectively. The 3rd failure index therefore appears to be the main mechanism leading to material failure and material removal in the 45 degree fibre orientation, while in the 90 degree fibre orientation the 4th failure index appears to have a higher magnitude leading to failure. This is due to the different cutting mechanism and material strength when loaded in different material fibre orientations.

237
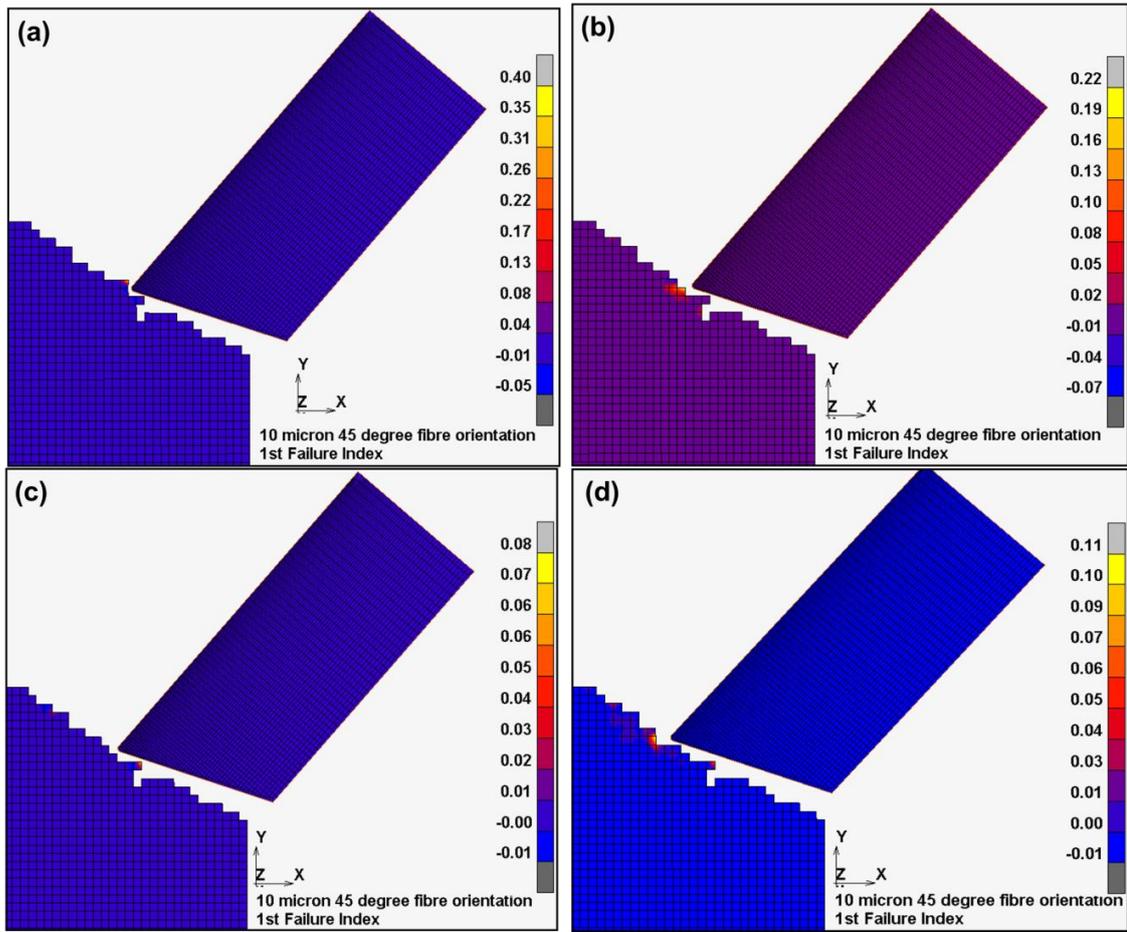
Figure 8-15- Fibre tensile failure magnitude (1st Failure index) in subsequent increments (a)-(d). (45 degree fibre orientation, 10μm edge radius, 800mm/min Feed and 6000RPM)
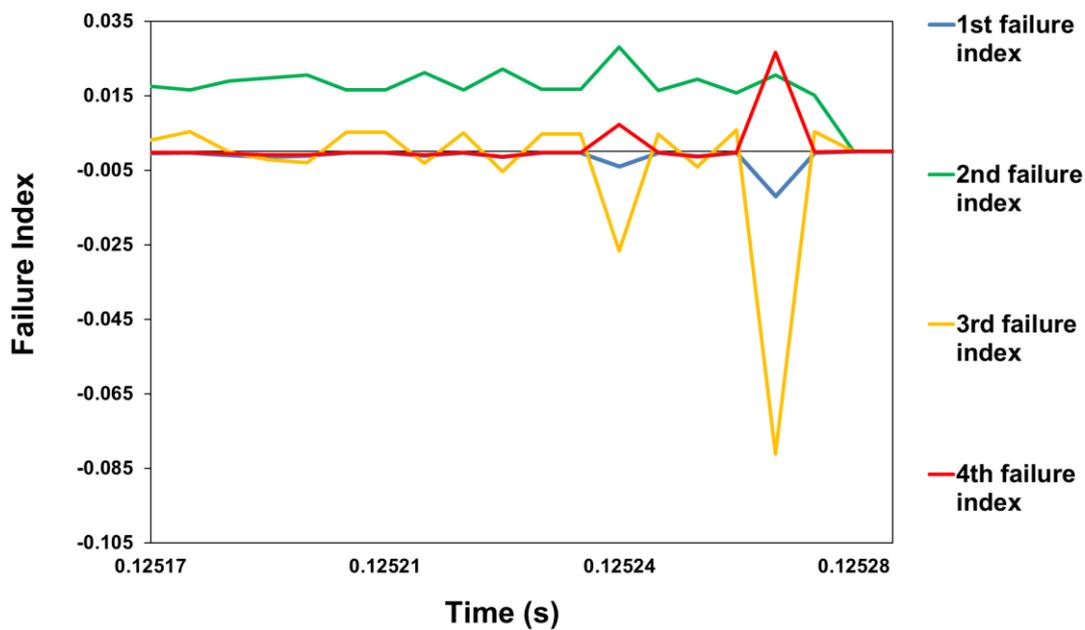
Figure 8-16- FE model- Hashin failure index at single node position over successive increments. (45 degree fibre orientation, 10μm edge radius, 800mm/min Feed and 6000RPM)

The total equivalent Von Mises stress is shown in Figure 8-17(a) and the total equivalent elastic strain is shown in Figure 8-17(b). The total Von Mises stress is localised in the elements around the tool tip and workpiece zone and there is some stress in the tool tip which has elastic properties of PCD. The maximum stress shown in the workpiece is 1208 MPa at element node during removal of an element. This shows that there are high localised stresses at the point of material failure. The maximum tensile strength of the fibres is strength of the CFRP is 4900 Mpa in tension and 1860 Mpa in compression. However the matrix strength in tension is 111 MPa and 214 MPa in compression. In consequence the maximum stress reached in the elements is much higher than required for matrix failure. There can then be failure of the matrix in compression and tension which will then allow localised crushing and fracture of fibres. The maximum total strain is 0.03 and the material is brittle and has a low strain to failure in Figure 8-17(b). The strain to failure of the matrix and fibre

239

is approximately 0.02 and 0.05 respectively. This suggests the results for the total strain at nodal points close to failure from FE model are in line with what would be expected when failure is present. Again the strain appears to be quite localised to the tool tip workpiece contact area where the high areas of localised stress were seen. This would agree with the findings that the majority of damage appears to be localised on the surface in the form of roughness and torn fibre or matrix cracking damage. Stress and strain which was not localised in the tool tip area would suggest high workpiece damage in other areas and possible loss of integrity to workpiece during machining. This work has shown that FE models can be useful to look at machining damage during machining and look for damage which may propagate away from machined area. High localised stresses should be found where small particles or fragments of chip will be removed which are caused with more damage to workpiece in matrix tension and compression which then allows localised crushing and breakage of fibres, as shown by the magnitudes of the different Hashin damage failure indexes.
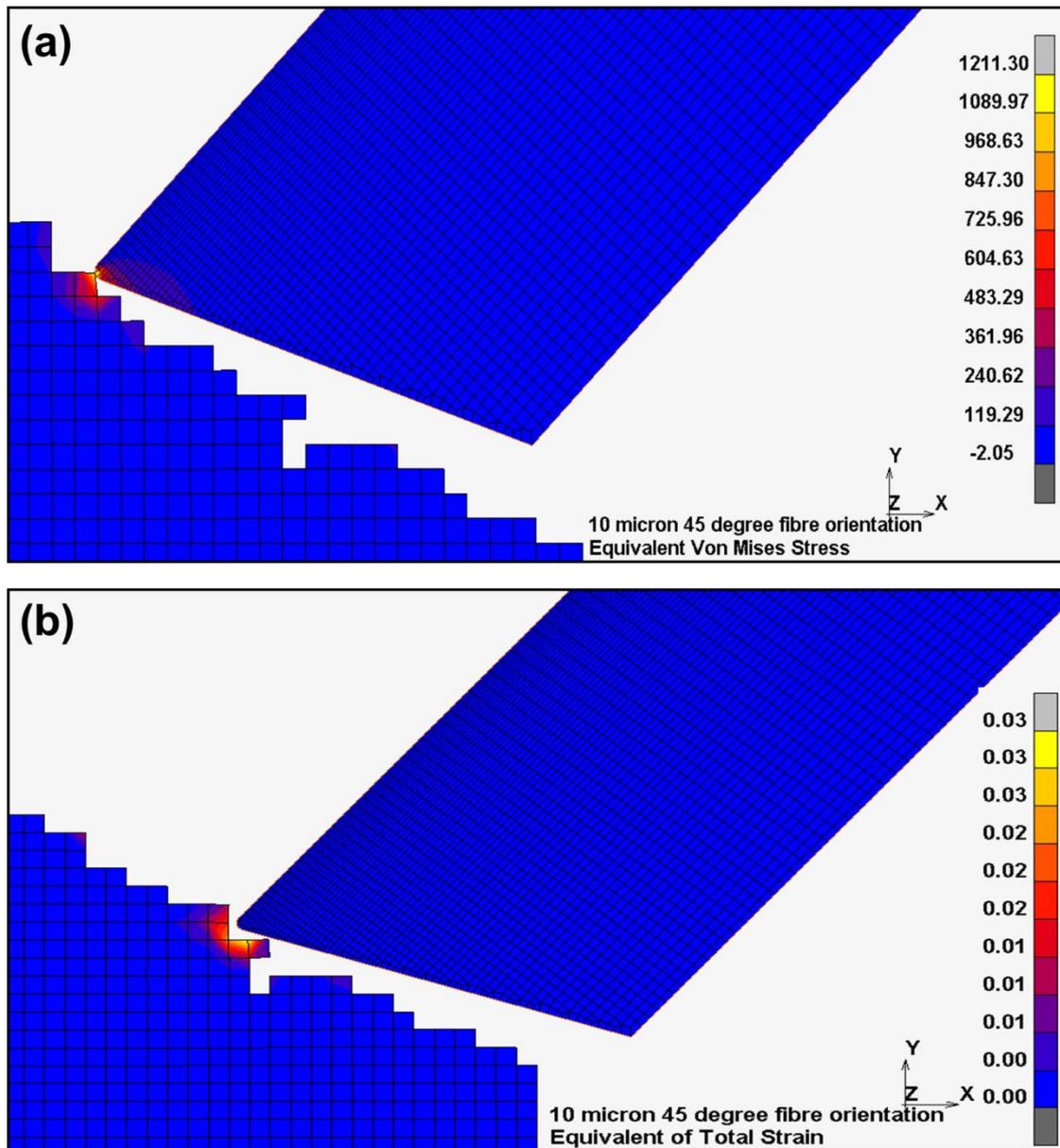
Figure 8-17- (a) Equivalent Von Mises stress,
(b) Equivalent total strain.
(45 degree fibre orientation, 10μm edge radius, 800mm/min Feed and 6000RPM)

8.4 Convergence Study

8.4-1 Mesh Sensitivity

A convergence study and sensitivity study of model parameters has been performed. Firstly, the effect of mesh size and adaptive mesh refinement level on the force results. A sensitivity study was also performed on the force and

displacement residuals used for convergence, and on the friction factor, to see how a change in these parameters will affect the output result. Different element edge lengths were applied with three adaptive mesh levels as compared shown in Table 8-4 and Figure 8-18 using feed of -1200 mm/min and cutting speed of 6000 RPM with a 90 degree fibre orientation. For each refinement level the element which is refined will be split into four new elements. So for a refinement level of one, the element edge length will be one half of the original, and then one quarter of the original element edge length for a refinement level of two. It can be seen that the mesh size has a significant effect on the output force and, it appears that decreasing the mesh size causes a decreasing cutting force due to smaller CFRP elements being removed during each increment. For that reason having a sufficient level of mesh refinement will be required in order that the cutting forces are not over predicted by the model due to larger elements being removed with a high stiffness. The adaptive meshing was applied to move with the cutter body and so the elements are continually refined as the cutter progresses further into the workpiece.

Table 8-4- Mesh Refinement Sensitivity

Mesh Refinement Level	Element Edge Length (mm)	Element Area (mm^2)	F_x (N)	F_y (N)
1	0.15	0.0225	100.2	14.5
1	0.1	0.01	90.1	14.4
2	0.075	0.00563	70.9	12.5
2	0.05	0.0025	68.1	12.6
3	0.0375	0.00141	62.9	12.1
3	0.0025	0.00000625	60.7	12.3
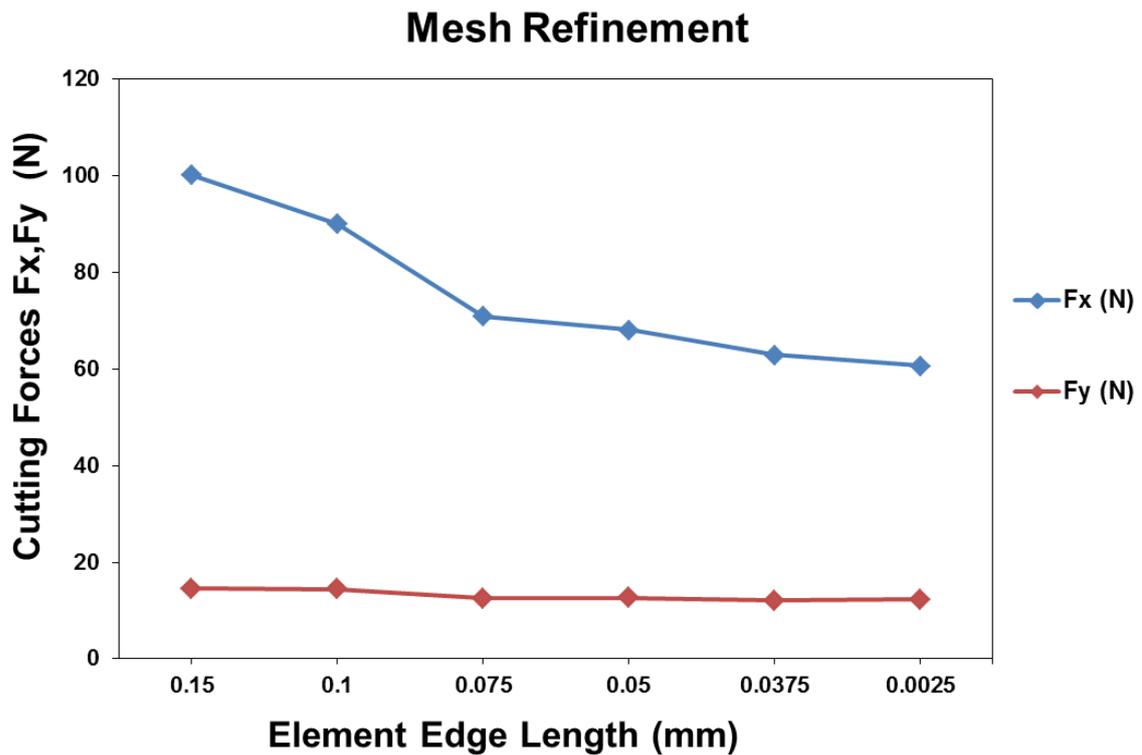
Mesh Refinement

Figure 8-18- Mesh refinement against decreasing element size.

The graph shows a reasonable convergence with decreasing mesh size. It was found that there was a general decreasing trend in the cutting forces with increasing mesh refinement. The average force to remove the larger elements was generally higher. The user subroutine improved the convergence of forces by ensuring the same load step size during cutting. An adaptive refinement level of 3 was applied in the model.

8.4-2 Friction Factor Sensitivity

The sensitivity of the friction factor on the output forces was analysed by changing it in incremental steps and leaving the other parameters constant. Which was analysed in the 2D simulation using a fibre orientation of 90 degrees. It can be seen in Table 8-5 and Figure 8-19 that changing the friction factor from a maximum of 0.3 to 0.05 did not cause an extreme change in magnitude of the cutting forces. A change of 11.9 % was calculated in the Fx cutting forces when the friction factor changed between 0.3 to 0.05, and a 16.3

243

% change in the Fy cutting forces. While changing the friction factor between 0.05 and 0.1 gave a percentage change of 1 % and 2.8 % for Fx and Fy respectively. We know from sources in the literature that the friction factor lies within 0.05 and 0.1 for composite machining- Figure 8-19, and hence the uncertainty in the known friction factor is not predicted to be one of the strongest parameters causing an error in the analysis.

Table 8-5- Friction Factor Sensitivity Study.

Friction Factor	F_x (N)	F_y (N)
0.3	78.6	20.3
0.25	87.6	24.1
0.2	87.7	24.0
0.15	87.7	24.1
0.1	89.5	24.6
0.05	88.6	23.9
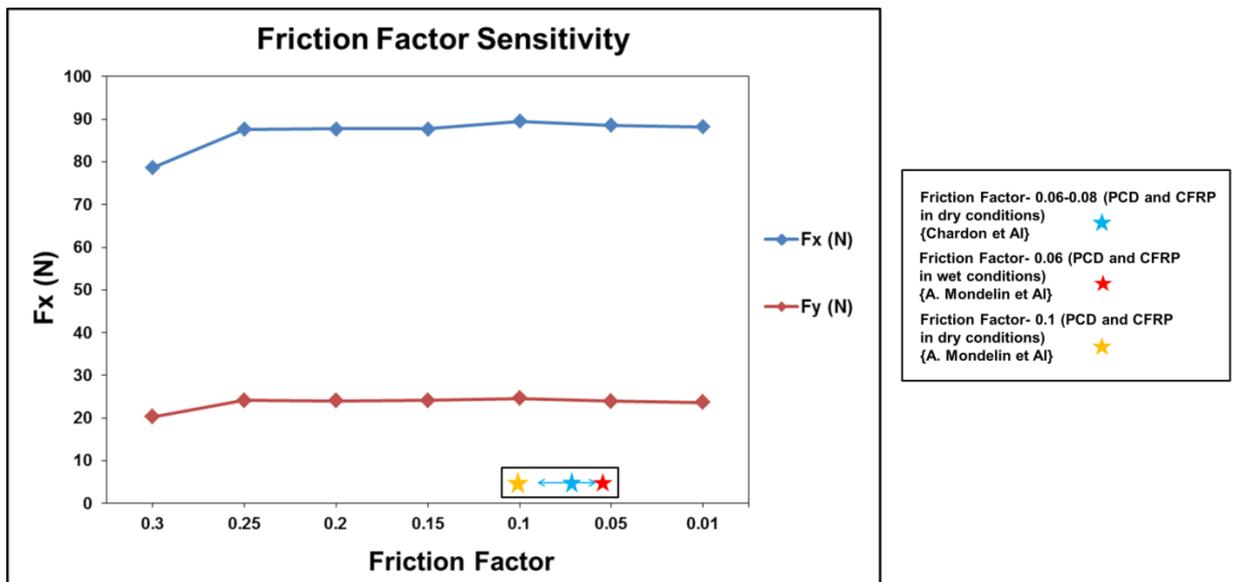
Figure 8-19- Friction factor sensitivity.
Adapted from: Chardon et Al. [94], Mondelin et Al. [95].

8.4-3 Force and Displacement Residuals Convergence Sensitivity

 The tolerance of the nodal displacement and force residuals used for convergence was analysed and its sensitivity on the output forces recorded. The relative convergence method was used to perform the sensitivity study. This convergence works by comparing the maximum residual load with the maximum reaction force ratio, and for successful convergence it must be less than the tolerance chosen by the user. For example a tolerance of 10 % could be chosen by the user, and this means the the ratio of the maximum residual load to the maximum reaction force must be less than 0.1. The relative residual method is useful because the allowable residual load will scale with an increasing maximum residual force. Whereas if an absolute convergence tolerance is used the value will be constant throughout. By decreasing the value of the tolerance the size of the residual which is allowed for convergence will reduce, this will also increase the computation time but should increase the accuracy of the analysis. The effect of the displacement tolerance was also analysed. The displacement tolerance is based upon the ratio of the correction to the incremental displacement vector (for that iteration), to the actual displacement change of that increment.

 In Table 8-6 the force and displacement tolerance were decreased from 0.1 to 0.0005 and the relative criterion was applied. There is a slightly decreasing trend in the cutting forces as the tolerance is decreased from 0.1 to a minimum of 0.0005 of -6 % in the Fx forces shown in Figure 8-20.

Table 8-6- Displacement & force tolerance sensitivity.

Force Tolerance	Displacement Tolerance	F_x (N)	Fy (N)
0.1	0.1	87.6	24.3
0.05	0.05	88.8	22.9
0.01	0.01	85.7	22.5
0.005	0.005	85.6	22.5
0.0025	0.0025	86.1	23.8
0.0001	0.0001	84.7	22.4
0.00005	0.00005	82.3	21.1
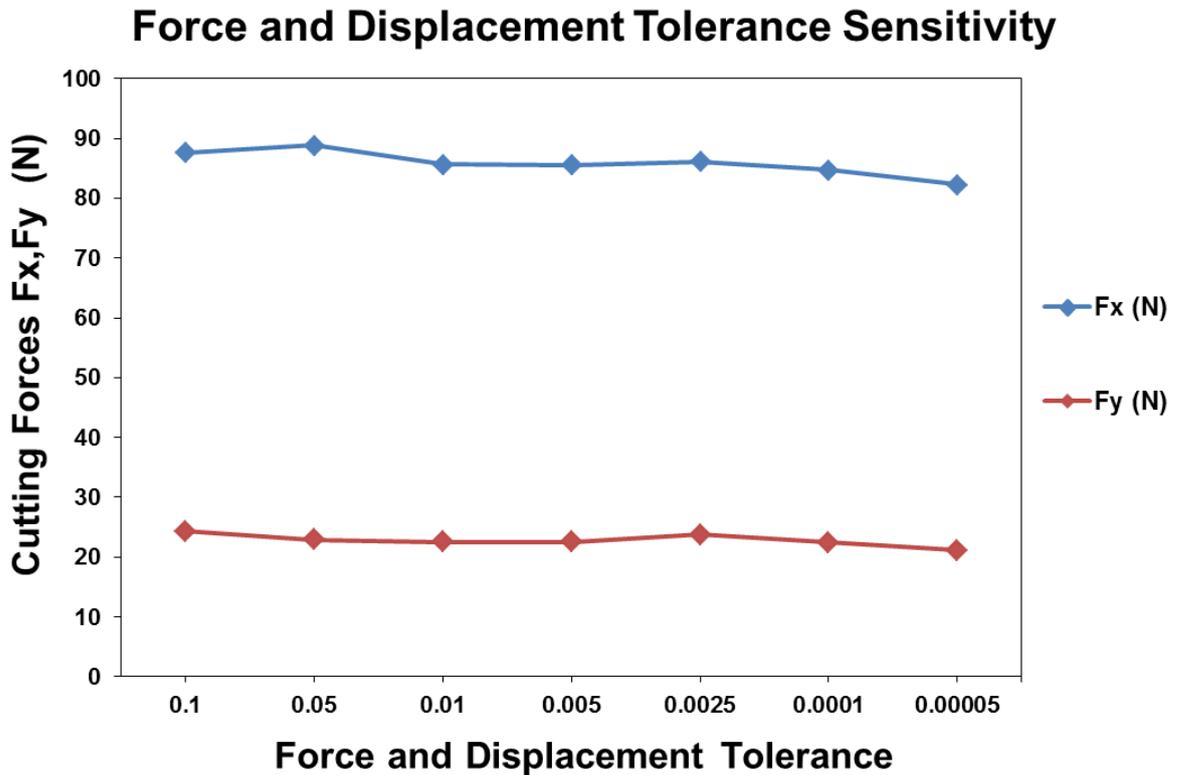
Figure 8-20- A convergence test for force and displacement tolerance sensitivity.

8.5 2D FE Model Discussion

The 2D model was successful in analysing the change in cutting forces due to change in cutting edge radius due to tool wear. With further research this approach could be implemented with different cutting tool geometries and higher levels of wear. The effect of different cutting edge radius on different laminate thickness and fibre orientations could also be studied. The roughness prediction model showed a 100 % increase in roughness when going from a 5μm tool to a 30μm tool which replicates going from a near new tool condition to a high level of wear. Surface damage and element failure was assessed using the Hashin damage model failure indices, total stress and total strain. It was found that element failure was predominantly due to 3rd and 4th failure index, which were matrix tension and compression. This is due to their weaker properties than in fibre tension and compression. There was found to be a slightly different magnitude in each of the Hashin failure indices depending upon the fibre orientation. In the 90 degree orientation matrix compression was found to have the highest magnitude before failure, whereas in the 45 degree matrix tension was found to have the highest magnitude just before element failure.

There were some problems initially with the model, the nodes of the cutter would penetrate into the workpiece causing very high spikes in cutting forces and a failure of the model to converge. This problem could be prevented by reducing the maximum load case time. Reducing the maximum load case factor restricted the growth of the load steps during the adaptive convergence control to a range suited to the cutting tool. The minimum load case time also had to be made sufficiently small, in this case to allow smaller time steps during increments which were proving difficult to converge due to material contact. It was also found that there were big fluctuations in cutting forces when elements were removed, however this was greatly improved by using adaptive mesh

refinement and locally decreasing the element size in the cutting area. Then smaller elements would be removed for each pass of the cutting tool and the removal of material would be more gradual, causing lower fluctuations in cutting forces and so a more representative cutting model. The use of the user subroutine to control the cutter movement depending upon the refined mesh size, and on each cutting speed, helped to control the load factor to further improve the cutting forces and convergence issues which lead to a more consistent cutting force output.

Sensitivity and convergence studies of model parameters found that the mesh refinement and the convergence criterion of residual force and displacement both had a significant impact on the output forces. The friction factor was found to have a less significant impact on the output forces and hence a small error in the known friction factor is therefore not expected to give a large error in the model output. The friction factor was taken from the literature for between PCD and CFRP material with a cutting fluid. The use of cutting fluid was beneficial because it will have lubricating and cooling effect. This will reduce temperature build-up in the cutting area and thermal effects due to matrix softening. As the thermal effects were not taken into account in the FE model the use of flood coolant was consequently important to prevent high cutting temperatures and matrix softening. As stated previously the carbon fibres have stable mechanical properties up to a temperature of 1200 °C, while the matrix has a glass transition temperature of 185 °C, at which point there will be some softening. During the machining test there was no detected burning smell of the matrix.

There is an expected uncertainty in comparing numerical finite element model with real machining experiment. Modelling of machining is a complex process with high material deformation and strain rates, high cutting temperatures and complex contact at tool workpiece interface. Some uncertainty could be

expected in mechanical properties determination, due to the nature of chip removal in machining, where small localised chips are removed in a fracture type cutting mechanism, whereas mechanical testing to determine material properties is determined from larger scale tension and compression testing. Characterization of material behaviour at high strain rates or deformations often requires extrapolation from measured experimental results because obtaining this data experimentally is very difficult [96]. However, composites fail typically in a brittle fracture cutting mechanism, and generally have a low strain to failure. The material model and mesh is based upon a macroscopic scale (mm) and equivalent homogeneous material, whereas the carbon fibre diameter is around 5μm on microscale. The EHM model does not thus analyse the damage on the scale of individual fibre bundles or tows. The Hashin damage model does, however, take into account the different possible failures of fibres and matrix in tension and compression based on the measured material strengths for a specific fibre volume fraction of material. It is also a progressive model which takes into account the combination of different damage modes and as a result allows for a combination of matrix and fibre tensile or compressive damage. In a machining process there is a combination of different damage mechanisms and the matrix and fibre are both being damaged in compression and tension. The cutting mechanism and damage will also be different depending upon the material fibre orientation and tool position. So the model does analyse the combination of the different possible failure modes. However this model is generally based on larger scale material properties testing (using tensile and inter-laminar shear properties) and therefore there will be some uncertainty when applied to a machining problem. The inertial effects of the milling process were ignored since there is a consistent size of chip removed once a steady state depth of cut is reached.

8.6 FE Surface Roughness Prediction- Multidirectional Laminate

The aim of this section is to predict surface roughness of a multidirectional machined CFRP composite. Novel roughness predictions have been made by combining FE models and regression equations from experiments.

3D FE models were used to simulate the edge trimming process of a multidirectional CFRP laminate. The machining forces from the FE model are calculated and recorded as an output. Following this, roughness predictions have been made, and the effects of changing different machining parameters on the surface quality will be discussed.

Firstly machining force outputs from FE model are presented and compared with recorded machining forces from experiment. The 3D model has applied the user subroutine to control the time step size and cutter displacement. Consequently, surface roughness predictions will be made under different cutting speeds, feed rate and tool condition and compared with experimental parameters.

In order to validate the quality of predictions, an additional set of comparisons have been made between experimental and predicted roughness values. These additional predictions were made with two new feed rates and cutting speeds which lie out width the model training data range. An additional feed rate of 1400 mm/min and cutting speed of 11000 RPM was compared between experimentally measured roughness and predicted Sa. The object of these additional parameters was both to validate the model and to see how accurately roughness predictions could be made outside of the model data training range.

8.6-1 FE Cutting Forces from 3D Multidirectional Model

The 3D FE Models were run and the mean cutting forces have been calculated and compared with experiment. The mean cutting forces have been calculated from the output data shown in Figure 8-21 and Figure 8-22 respectively for the Fx and Fy machining forces. Figure 8-21 and Figure 8-22 show cutting force outputs from 3D model at a feed rate of 1200 mm/min and cutting speed of 11000 RPM.
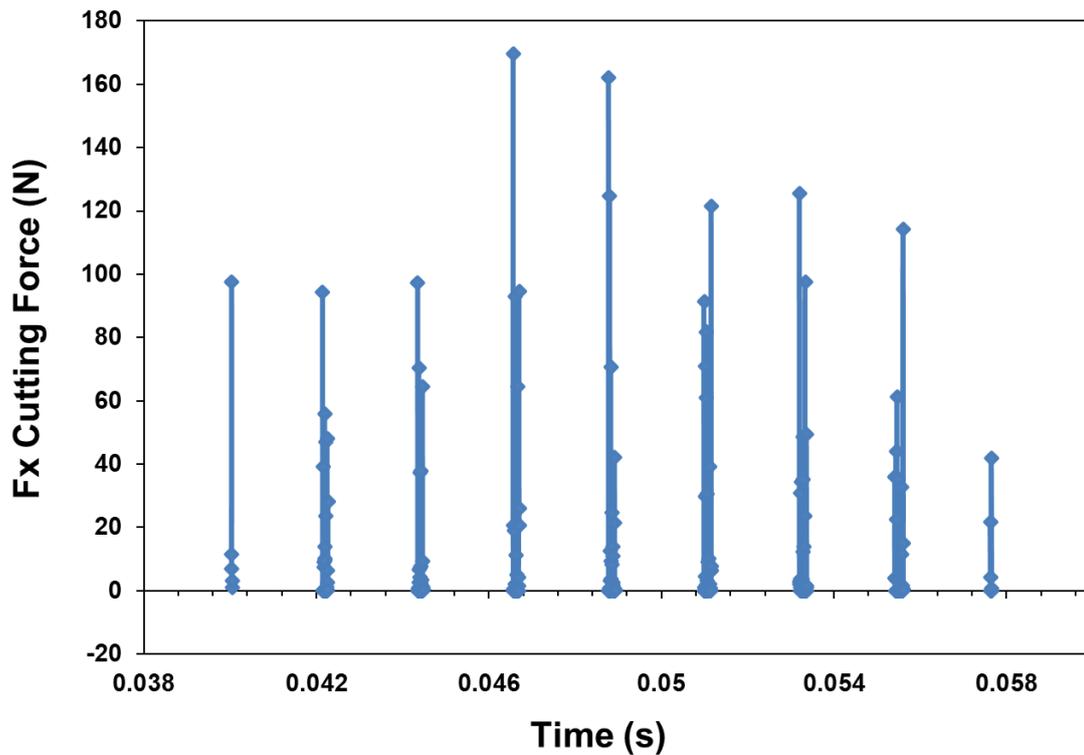
Figure 8-21- 3D FE model cutting forces (Fx). vs Time
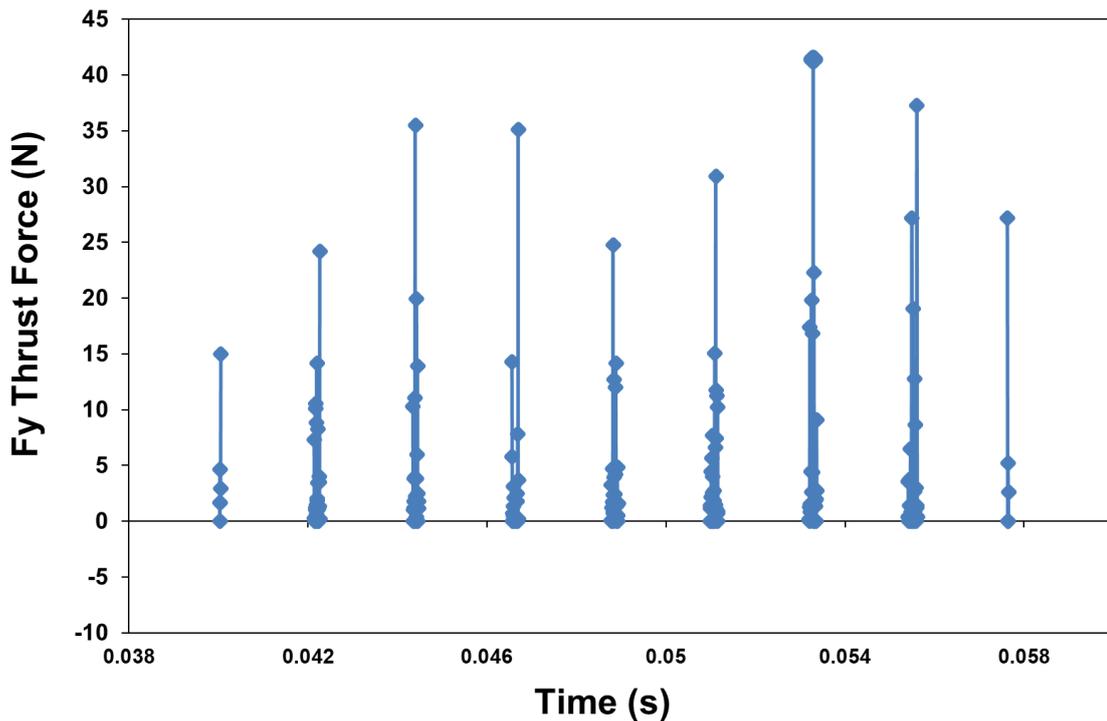
Figure 8-22- 3D FE model thrust forces (Fy) vs time.

The mean cutting forces from the experiment are taken from an average of tests 1-8 where the tool was started in new condition. Where Table 8-7 and Table 8-8 show the comparison between FE model and experiment for the Fx and Fy forces respectively. A difference varying between ±15 % is seen for the Fx forces and experiment, while a maximum difference of -75 % was found for the Fy forces. The predictions are quite reasonable with the majority being within ±15 % from the experimental value. There is an expected error or variability in the prediction due to the complexity of the carbon fibre machining process and FE model and therefore this was deemed a reasonable accuracy. In general it was found that the Fy cutting force were slightly under predicted and this issue is commonly also seen in metal cutting and other orthogonal cutting simulations [9],[97]. The relatively large error of -75 % in the Fy cutting forces predicted at 1000 mm/min and 7000 RPM may be due to the difficulty in predicting thrust forces, due to the average forces being calculated from both positive and negative values. Also, 3D model only used a sharp cutting edge to

252

represent a fully new tool and the prediction could be expected to improve if a worn cutting edge radius was included.

Table 8-7- Comparison between FE model and experimental Fx forces. (Experimental forces are an average from tests 1-8 with close to new tool condition.)

Feed Rate (mm/min)	Cutting Speed (RPM)	FE Model Feed Force (Fx)	Experimental Feed Force (Average from Tests 1-8) (Fx)	% Difference
1000	7000	44.3	37.3	+15.8
1000	9000	42.1	38.4	+8.9
1200	7000	37.7	40.6	-7.4
1200	9000	35.8	41.7	-15.2

Table 8-8- Comparison between FE model and experiment Fy forces. (Experimental forces are an average from tests 1-8 with close to new tool condition.)

Feed Rate (mm/min)	Cutting Speed (RPM)	FE Model Feed Force (Fy)	Experimental Feed Force (Fy) (Average from Tests 1-8)	% Difference
1000	7000	10.2	17.7	-75
1000	9000	11.9	15.75	-27.8
1200	7000	14	11.75	17.5
1200	9000	15.4	13.8	11

A comparison between FE and experimental predictions is shown for the F_x cutting forces in Figure 8-23 and Figure 8-24. In Figure 8-25 and Figure 8-26 is shown the same comparison of experimental and FE predicted forces for the F_y cutting force. The experimental values are calculated as a mean value for the edge radii as shown in the Figure 8-23 to Figure 8-26.
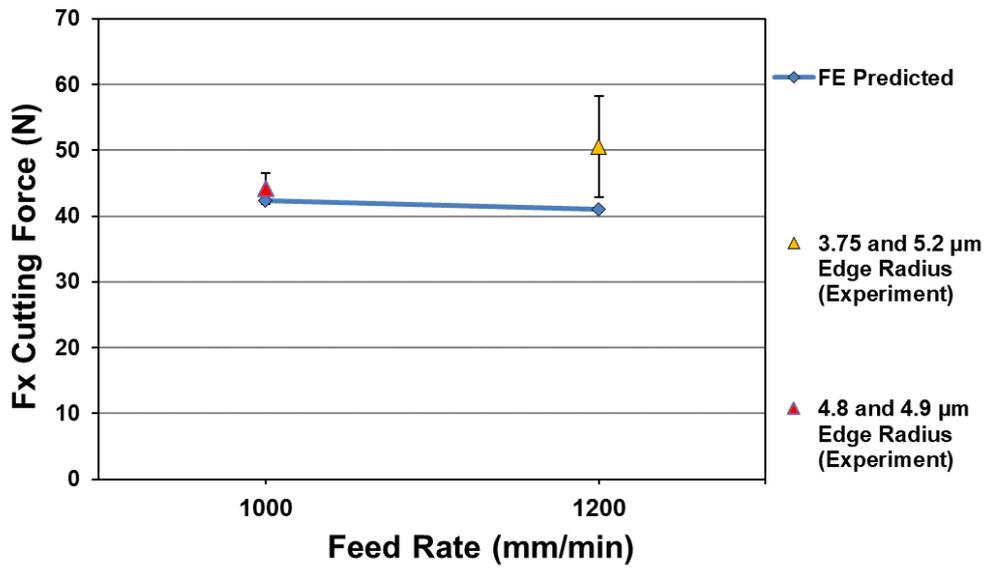
Figure 8-23- Experimental and FE model Fx cutting forces vs increasing feed at 7000 RPM.
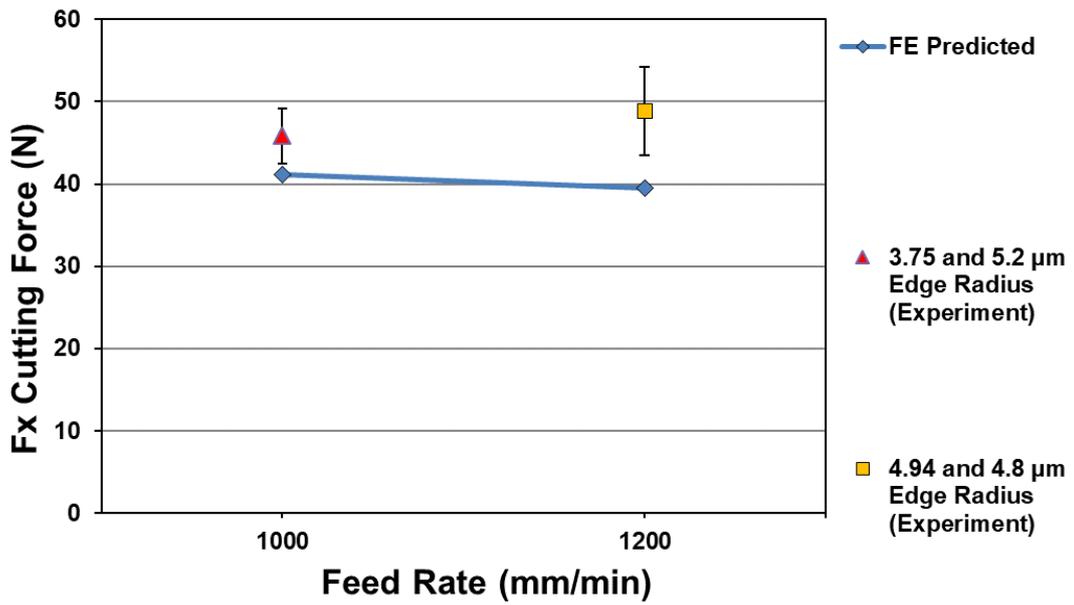
Figure 8-24- Experimental and FE model Fx cutting forces vs increasing feed at 9000 RPM.

254
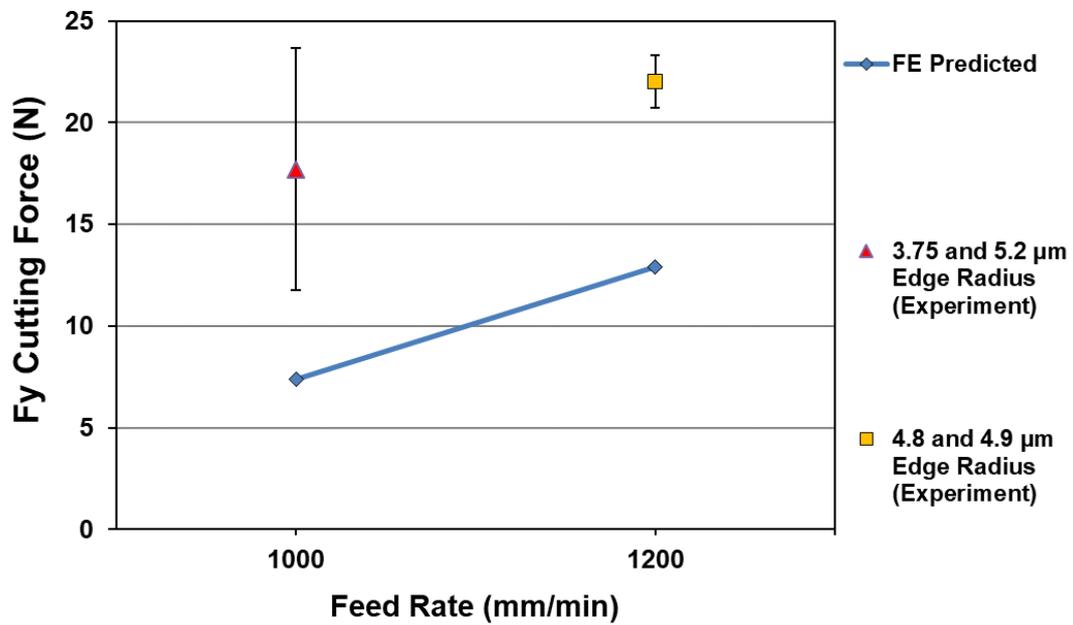
Figure 8-25- Experimental and FE model Fy cutting forces vs increasing feed at 7000 RPM.
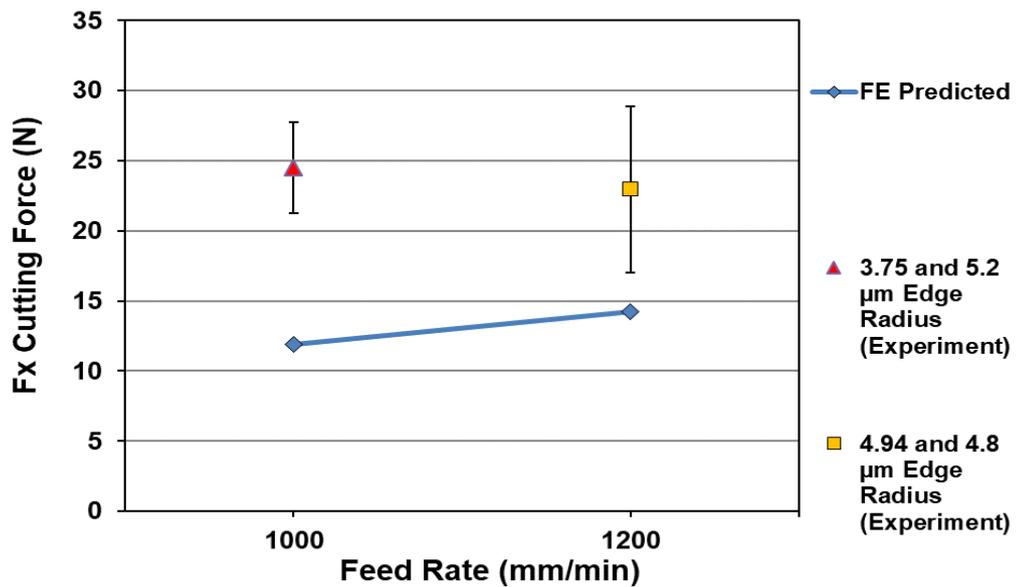
Figure 8-26 - Experimental and FE model Fy cutting forces vs increasing feed at 9000 RPM.

8.6-2 Effect of Parameter Change on Roughness

The calculated regression equation for the surface roughness was shown previously in Equation 2. This was used in combination with force outputs from FE to see the effects of parameter changes on the roughness. Due to each of the different process variables having a different contribution or statistical effect on the surface roughness, it was useful to see how a change in each of the process variables will change the surface roughness graphically. A bar chart is shown in Figure 8-27, where each of the process parameters has been increased by 20 % while the other parameters will remain constant. The corresponding effect on surface roughness is thus shown due to an increase in each one of the parameters individually. For example when machining at a feed rate of 1200 mm/min and a cutting speed of 7000 RPM with tool edge radius of 6 μm and cutting forces of 42.6 N and 14.1 N for Fx and Fy respectively. This would equate to a predicted S_a surface roughness of 2.03 μm. Then to find the expected effect of the feed rate increasing by 20 % to 1440 mm/min then the surface roughness will increase to 2.38 μm which is a 0.35 μm increase in roughness. Additionally if the cutting speed was to increase by 20 % to 8400 RPM then there would be a -0.11 μm decrease in surface roughness according to the regression equation. The effect of an increasing feed and thrust force has a less strong effect on the surface roughness with a slight increase and decrease respectively. Looking at Figure 8-27, increasing the feed rate has the strongest corresponding increase in the surface roughness, followed by the edge radius. Increasing the cutting edge radius by 20 % shows an increase in the surface roughness of 0.22 μm. However, it was found earlier that the combined effect of increasing the tool wear and feed rate together will have a strong contributing effect on the roughness. A useful result was therefore found, that if the feed rate and tool wear are both increased by 20 % then there would be a 0.8 μm increase in the roughness which is over double of that

of increasing the feed rate alone by 20 %. From this result it can be concluded that one important way of minimising surface roughness is to decrease the feed rate at higher levels of tool wear. Therefore as tool wear increases the feed rate can be reduced to stay within roughness limits.
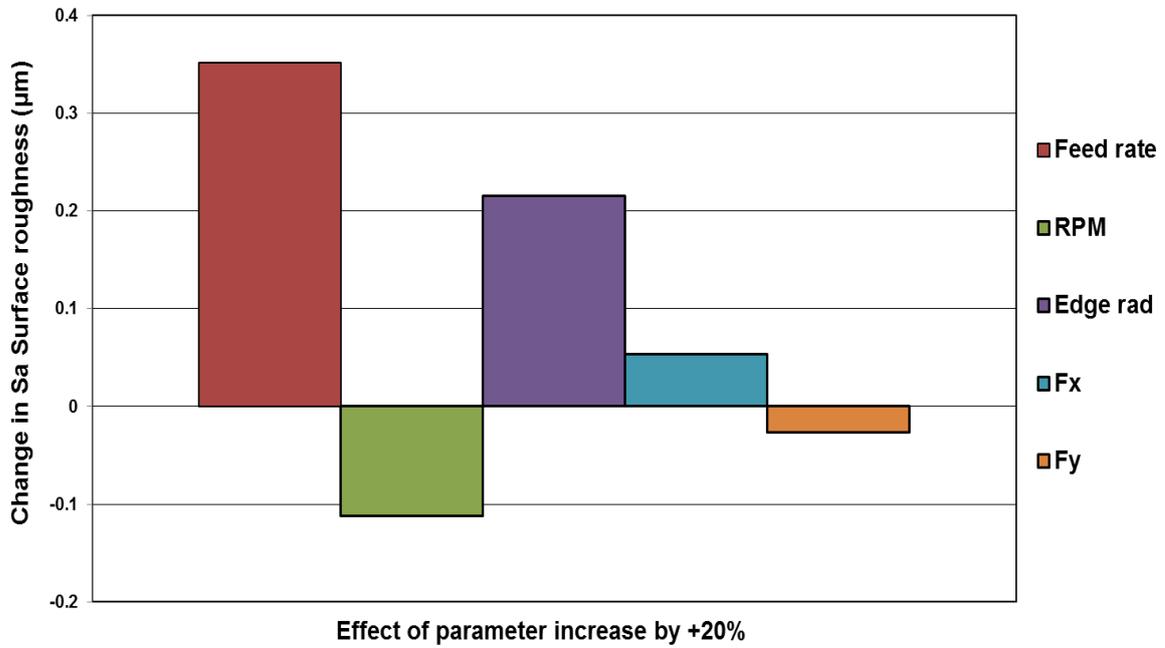
Figure 8-27- Effect of a 20 % increase in process parameters on the S_a surface roughness.

8.6-3 Roughness Predictions from FE Comparison with Experimental Results

Next the predicted cutting forces from the FE model were combined with developed experimental regression equation to calculate the new predicted surface roughness. The predicted surface roughness has been compared with additional experimental results. The experimentally measured roughness at various cutting edge radius is used to validate predictions made using FE model and regression equations. The S_a predictions have been calculated from the FE obtained force outputs shown in Table 8-9 and then compared with experiment.

Table 8-10-Table 8-13 and Figure 8-28-Figure 8-31 show the comparison between predicted S_a roughness and experimentally measured roughness. The

values which have been highlighted are additional parameters at 1400 mm/min and 11,000 RPM which lie outside the range of the experimental data set used to train the regression model. These additional parameters (shown in red) are stepped up values for the cutting speed and feed rate. They were used as additional model validation points to see how well the model will predict roughness at extreme ranges of the model training limits, compared with experiment. They were also used as additional validation points to find how an increased feed rate and cutting speed outside the regression model limits might affect the surface roughness, and how accurately a prediction at these ranges could be made. The standard deviation of the experimentally measured roughness is shown in the graphs of Figure 8-28-Figure 8-31 by the error bars shown.

Table 8-9- Predicted machining FE forces from 3D model. (Values to be used as additional validation points are shown in red.)

	Feed Rate (mm/min)	Cutting Speed (RPM)	Feed Force (Fx)	Thrust Force (Fy)
(FE)	1000	7000	44.3	10.2
(FE)	1000	9000	42.1	11.9
(FE)	1000	11000	41.8	12.7
(FE)	1200	7000	41.1	14.2
(FE)	1200	9000	39.5	15.4
(FE)	1200	11000	41.2	16.3
(FE)	1400	7000	57.8	12.2
(FE)	1400	9000	45	13.1
(FE)	1400	11000	37.2	11.2

258

Looking at the graphs for the predicted roughness shown in Figure 8-28 in the first column, there is a feed rate of 1000 mm/min and a cutting speed of 7000 RPM (for an edge radius of 5.95 µm). An experimental surface roughness of 1.66 µm was measured and is shown in dark red, and with a standard deviation of 0.10. The predicted roughness was 1.78, which has a difference of +7 % between experimental and predicted values, as is also shown in Table 8-10. In the third column of Figure 8-28 there was an experimentally measured roughness of 2.6 µm with a standard deviation of 0.09 µm. The predicted Sa roughness was 3.68 µm, and there is a percentage difference of +34.4 % between experimental and predicted roughness. The third column is highlighted in red because it lies outside of the parameter limits used in the model training data. Therefore the model was able to more accurately predict roughness values within the range of parameters used to train the regression equation. It was found that the predicted roughness was slightly over projected at the higher feed rate of 1400 mm/min.

In general the predictions of roughness made using the FE and regression model method were found to lie within ±10 % of the experimentally measured value, although not always lying within the experimentally measured standard deviation. The additional predicted values for roughness which were made at parameters of feed and cutting speed out-with the model training data were less accurate and an over prediction by as much as +34 % was found. However, less accurate predictions were expected at the additional ranges of feed rate and cutting speed, and this is because the regression equation was not trained using experimental data at these limits. It is expected that with a larger training data set extended to more parameters then this error would be reduced. In the future, further experimental tests could therefore be performed to extend the limits of the model and further increase the accuracy of

roughness predictions across a wider range of cutting speeds, feed rates and tool wear.
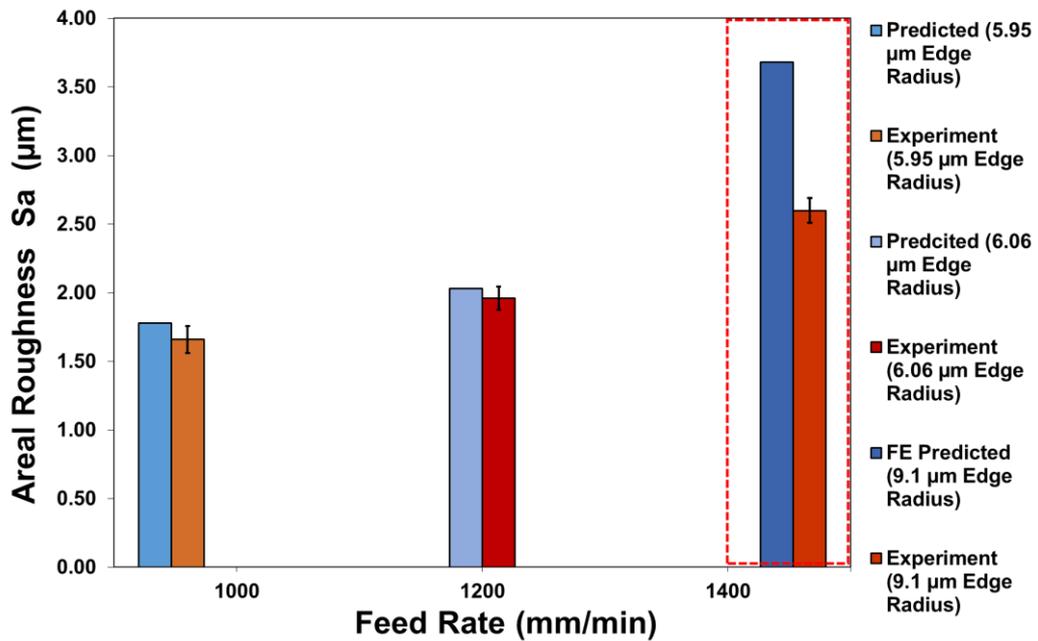
Figure 8-28- Experimental vs FE predicted S_a surface roughness at increasing feed rate at constant 7000 RPM. Error bar represents standard deviation between averaged set of test results with a different edge radius.

Table 8-10- Predicted vs Experimentally Measured Sa, 7000RPM, at various edge radius. (Additional validation points shown in red)

Feed Rate	Cutting Speed (RPM)	Edge Radius (μm)	Experimental Sa (μm)	Predicted Sa (μm)	Percentage difference (%)
1000	7000	5.95	1.66	1.78	+6.98
1200	7000	6.06	1.96	2.03	+3.51
1400	7000	9.1	2.6	3.68	+34.39
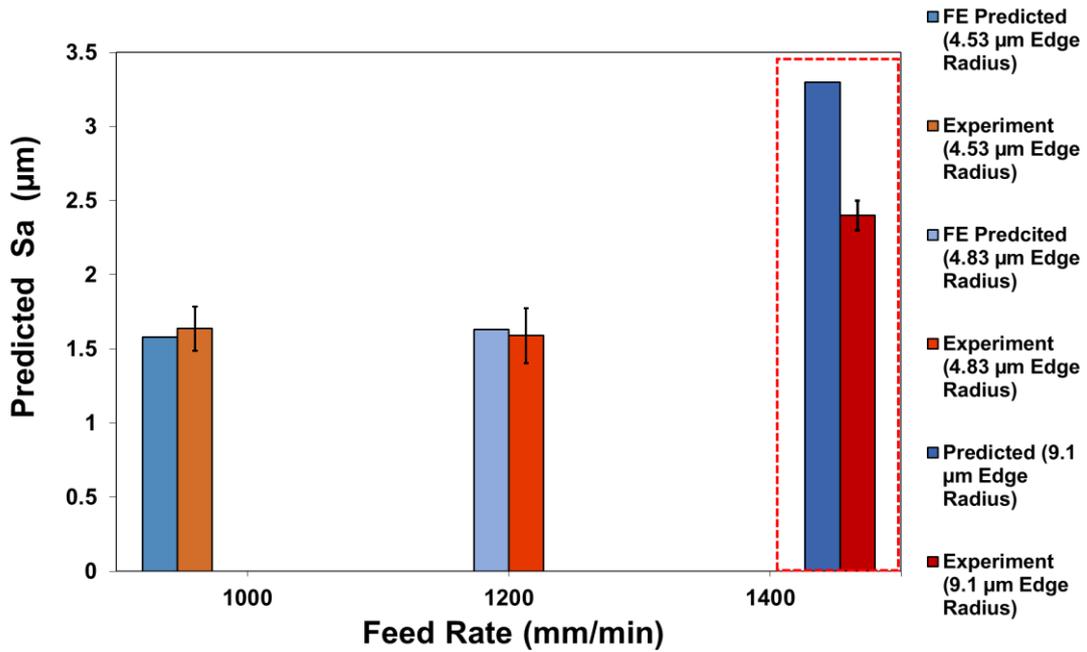
Figure 8-29- Experimental vs predicted S_a surface roughness at increasing feed rate at constant 9000 RPM. Error bar represents standard deviation between averaged set of test results with a different edge radius.

Table 8-11- Predicted vs Experimentally Measured Sa, 9000RPM, at various edge radius. (Additional validation points shown in red)

Feed Rate	Cutting Speed (RPM)	Edge Radius (µm)	Experimental Sa (µm)	Predicted Sa (µm)	Percentage difference (%)
1000	9000	4.53	1.64	1.58	-3.73
1200	9000	4.83	1.59	1.63	+2
1400	9000	9.1	2.4	3.3	+32
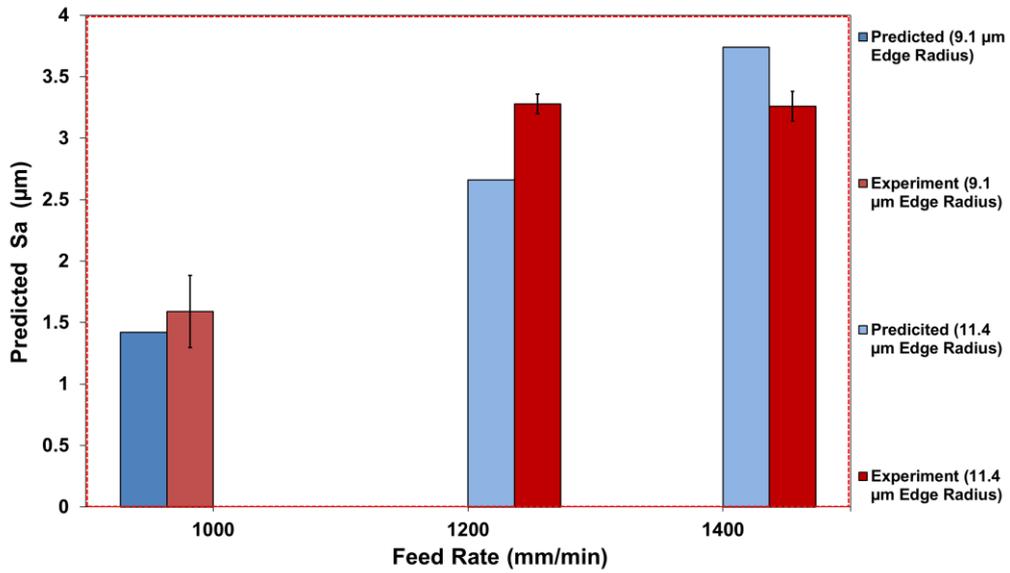
Figure 8-30- Experimental vs predicted S_a surface roughness at increasing feed rate at constant 11000 RPM. Error bar represents standard deviation between set of test results.

Table 8-12- Predicted vs experimentally measured Sa, 11000RPM, at various edge radius. (Additional validation points shown in red)

Feed Rate	Cutting Speed (RPM)	Edge Radius (µm)	Experimental Sa (µm)	Predicted Sa (µm)	Percentage difference (%)
1000	11000	9.1	1.59	1.42	-11.30
1200	11000	11.4	3.28	2.66	-20.88
1400	11000	11.4	3.26	3.74	+13.71
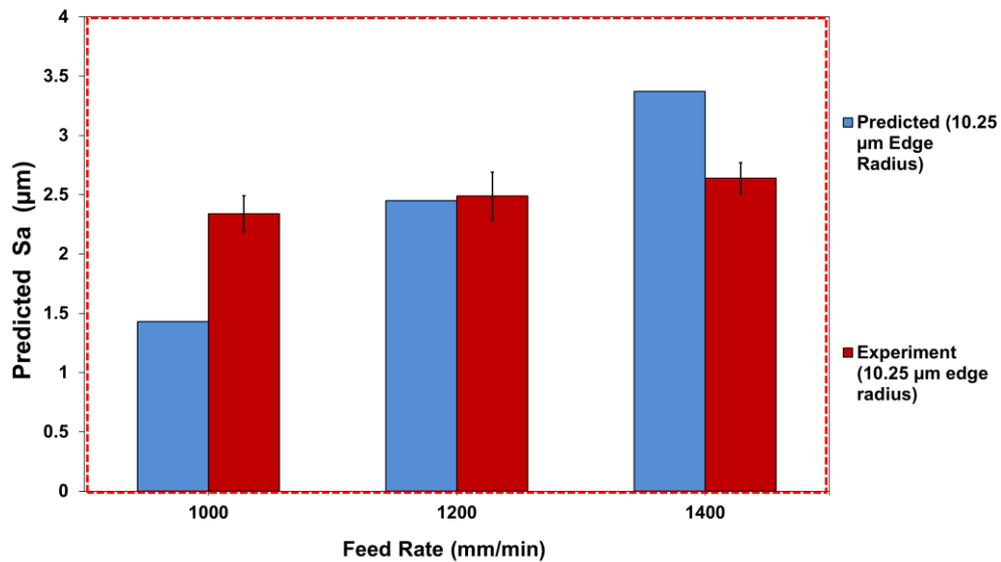
Figure 8-31- Experimental vs predicted S_a surface roughness at increasing feed rate at constant 11000 RPM, (10.25 μm edge radius). Error bar represents standard deviation between averaged set of test results with a different edge radius.

Table 8-13- Predicted vs experimentally measured Sa, 7000RPM, at various edge radius.

Feed Rate	Cutting Speed (RPM)	Edge Radius (μm)	Experimental Sa (μm)	Predicted Sa (μm)	Percentage difference (%)
1000	11000	10.25	2.34	1.43	-48.28
1200	11000	10.25	2.49	2.45	-1.62
1400	11000	10.25	2.64	3.37	+24.29

In conclusion, the predictive method for calculating roughness using a combination of regression modelling and FE methods proved successful at making new projections for roughness within the range of the limits of the parameters used in the model training data. In the author's opinion, the method proved more successful than trying to use FE methods alone for the prediction of roughness. There are extreme difficulties in trying to directly

263

quantify roughness from an FE model and the size of the FE mesh would directly affect the roughness measurement which would be made, making accurate predictions questionable. This has been confirmed by Xu and Mansori, [73],[74].

  It is worth emphasising that these predictive models will only be appropriate for the material type and cutting tool geometry which has been used in this test. It would also be advisable that the same surface roughness measurement strategy is used to obtain the same accuracy of measurements and comparable results. However the model training data could be extended to a wider limit of parameters using the same test conditions and combined with existing data in order to increase the range at which accurate roughness predictions could be made. It can be concluded that the model is a useful tool for calculating critical limits for input parameters such as cutting edge radius, cutting speed and feed rate whereupon machining parameters can be optimised to ensure that the roughness will remain within certain limits. Once the model has been developed it reduces the requirement for as many experimental tests in order to assess and predict the surface roughness.

8.6-5 Multidirectional Laminate 3D Model- Through Thickness Damage

 The through thickness damage in the 3D model has been assessed to see how the damage would vary across the laminate, and to find the influence of different fibre orientations. An image is shown in Figure 8-32 of the equivalent Von Mises Stress through thickness in the 3D multidirectional model. There is a variation in through thickness stress and it appears there are more widespread stresses propagating further into the material on some fibre orientations more than others. This is due to the orthotropic strength of the material and as a result certain fibre directions will be weaker depending upon their orientation in relation to the tool cutting path. There are also localised regions of stress depending upon the tool workpiece contact areas which are determined by the

continuous process of different material deformation points. The material deformation is a non-constant process which does not reach uniformity through thickness in the material of a multidirectional laminate.

In order to see how the different failure index of the Hashin damage model varied through thickness it was plotted along a point. This was plotted using a nodal path going from one edge to the other. The path length is 10mm which is the workpiece thickness and the axial depth of cut. There is strong variation in the magnitude of damage due to the different failure index, especially the 2nd, 3rd and the 4th. The variation of the entire four failure index is plotted in Figure 8-33. Some of the variations in magnitude of the failure indexes can be explained by the change in fibre orientation through thickness and by isolated contact points causing a high stress gradient. In Figure 8-33 it can be seen that there is a spike in the magnitude of the 2nd, 3rd and the 4th failure index at around 3.1 mm through the workpiece thickness. This is due to an isolated point of tool-workpiece material contact causing material deformation and damage. Isolated contact points are initiated between the tool tip and workpiece due to the material non-homogeneity, material deformation, and the different chip removal mechanism on each of the different layers. Different layers of the laminate thickness will have small fragmented chip removal and will each fracture at different model increments and stresses. When there is a small areal point of contact there will be an isolated high stress gradient. Then, in this case there appears to be high magnitude of damage in the 3rd and 4th matrix damage failure modes, and in the 2nd fibre compression failure index, which then leads to an element failure. In experiment this will cause a small fragmented chips released by material fracture.

Therefore, the 3D model is required when simulating a multidirectional laminate to accurately represent through thickness damage variation. There will

be a variation in through thickness damage due to material non-homogeneity, isotropic properties and continuous damage progression.
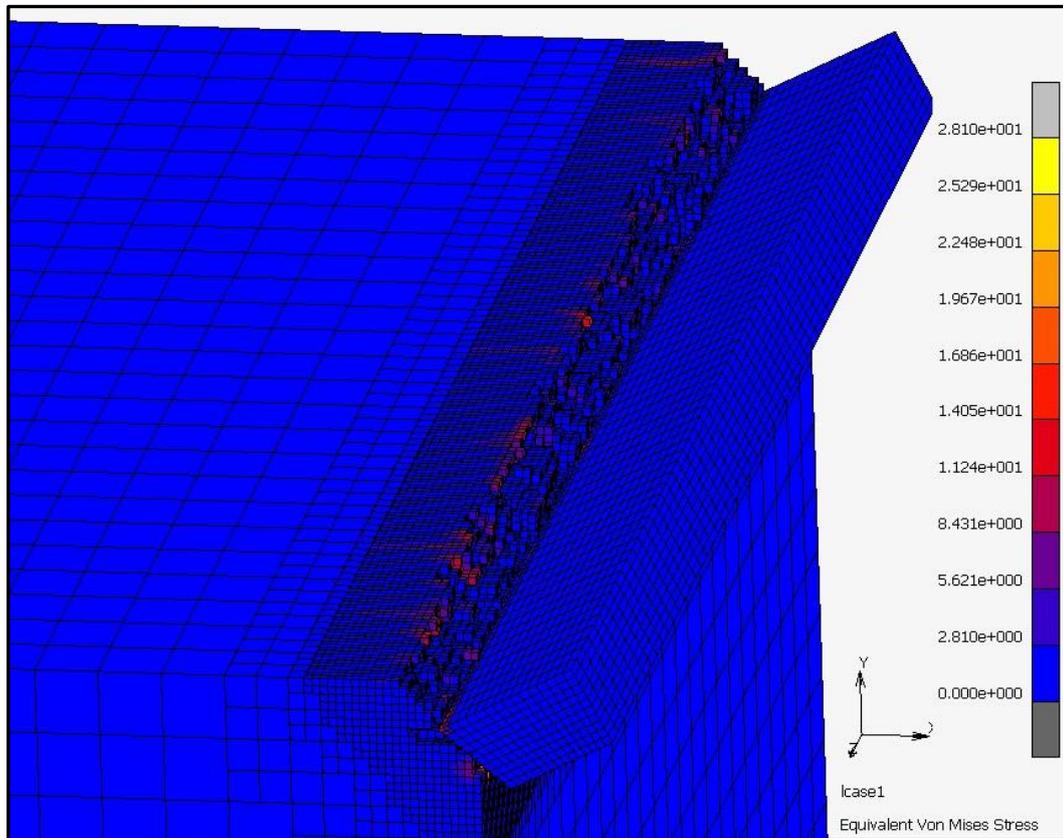
Figure 8-32- Von Mises stress through thickness, 3D FE edge trimming model.
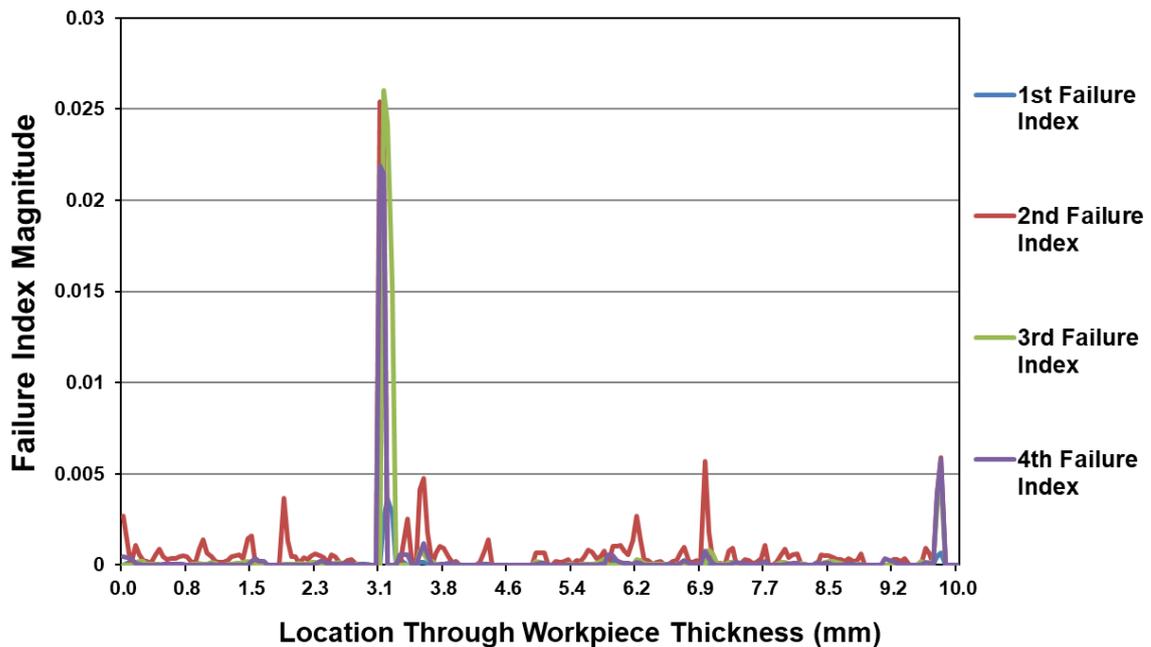
Figure 8-33-Through thickness of 3D model Hashin failure index damage.

8.6-4 Predicted Increase in Roughness Due to Tool Wear

Previously in the 2D model it was found that there would be a 50 % increase in Fx cutting forces and a 100 % increase in S_a roughness when tool wear increased from a 5 micron to 30 micron edge radius. In this case, in the 3D model, using the regression equation calculated for the multidirectional test the increase in roughness has been calculated when the edge radius increases from 5 microns to 30 microns. It is found that the predicted Sa surface roughness will increase from 1.87 µm to 6.15 µm (at a feed rate of 1200 mm/min and 7000 RPM). This is shown in Table 8-14 and is a 3 times increase in roughness. The higher percentage increase in roughness in the multidirectional laminate, (compared to the unidirectional), is predominantly due to the additional different fibre orientations- noticeably the 135 fibre orientation- which shows the greatest increase in magnitude of machining damage with tool wear. Therefore the lay-up of the laminate and the different fibre orientations will also have an effect on the amount of increase in roughness due to tool wear.

267

In Table 8-14 it is shown that the theoretically predicted roughness will increase at a higher rate when the feed rate is increased to 1400 mm/min. There will be roughly a 5 times increase in roughness going from 1.98 µm to 10.68 µm. This is caused by the interaction effect between cutting edge radius and feed rate, which means at the higher feed there will be a greater increase in roughness. This is a useful result because it tells us that at low levels of tool wear it is acceptable to use a high feed rate and consequently machining productivity could be increased.

From previous studies, a roughness variation between 2-8 µm was seen using a PCD tool in wet conditions at varying conditions of tool wear increasing up to a 45 µm edge radius [89]. Therefore the predicted roughness in Table 8-14 lies within a reasonable range that could be expected from an edge trimming experiment.

Table 8-14- Predicted change in roughness with an increasing cutting edge radius. (Multidirectional test.)

Cutting Edge Radius (µm)	Surface Roughness (Sa) (Feed 1200 mm/min)	Surface Roughness (Sa) (Feed 1400 mm/min)
5	1.87	1.98
10	2.73	3.72
15	3.58	5.46
20	4.44	7.2
25	5.29	8.94
30	6.15	10.68

8.6-6 Predicted Skewness and Kurtosis

Skewness parameters have been predicted using the regression model and compared with measured values in experiment which is shown in Figure 8-34. Skewness has been found to be a useful parameter which explains surface characteristics not fully represented in the mean average roughness R_a or S_a. Interestingly, it was found that an overall predictive model for the whole mutli-directional surface using skewness and kurtosis was not an ideal description of the surface damage. This was emphasised by the lower R-Sq and R-Sq(Adj) for the regression equations compared to the S_a roughness parameter regression model. The prediction of the skewness was found to be less accurate than the S_a roughness parameter. It has been found, that because the different fibre orientations of the laminate have a different surface structure, they will have a different machining damage and then behave differently due to changes in edge radius. For example in the 135 degree fibre orientation the surface skewness was generally found to decrease with an increase in tool wear, shown in Figure 8-35. This was because of an increase in torn pits and fibre chunks, and caused more valleys in the surface, (and a negative skewness). However in the 0 degree fibre orientation there was generally a slight increase in skewness with tool wear. This was caused by bent fibres protruding above the machined surface and a positive or more hill shaped profile -Figure 8-36.
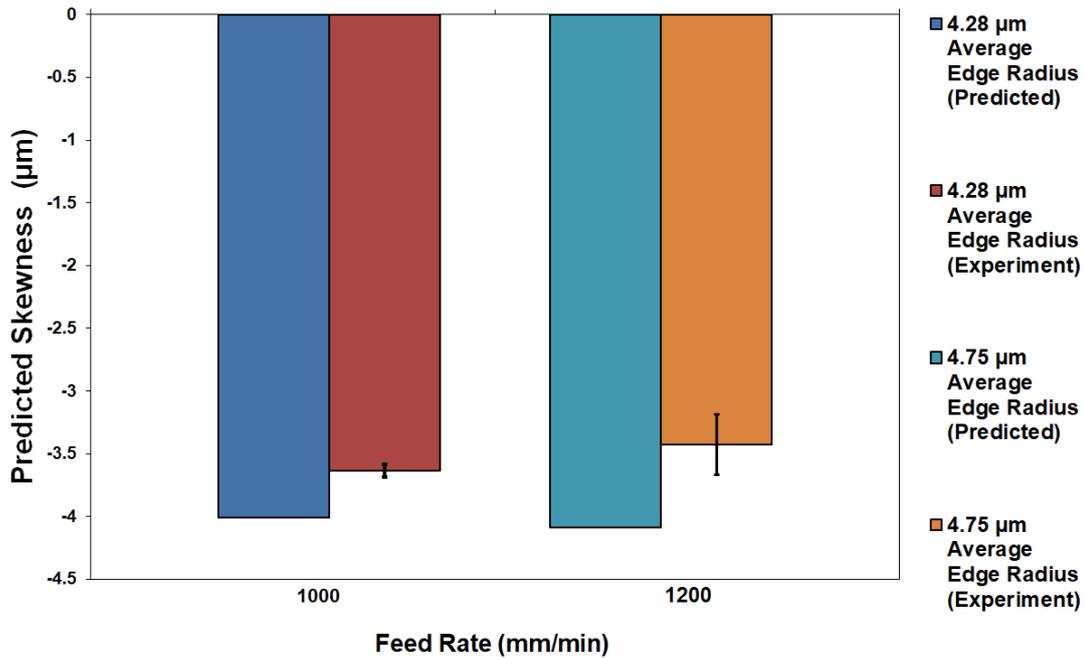
Figure 8-34-Predicted skewness values vs experiment.

The trend in the skewness with an increasing cutting edge radius is shown for the 0 degree fibre orientation and 135 degree in Figure 8-35 and Figure 8-36 respectively. A slight increase in skewness is shown with increasing edge radius in Figure 8-35 for a 0 degree fibre orientation which may be due to the effect previously described. In the 135 degree fibre orientation there was a slight decrease in skewness seen with increasing tool wear- Figure 8-36. This is due to increasing damage depth and larger voids and chunks of removed material. An interesting result has been shown that the effect of skewness and kurtosis will be individual to each fibre orientation and therefore surface characterisation for skewness must be assessed across individual fibre orientations to fully represent the surface structure.

Figure 8-35- The 0 degree fibre orientation, change in skewness vs increasing cutting edge radius.

Figure 8-36- The 135 degree fibre orientation, change in skewness vs increasing cutting edge radius.

8.7 Discussion- Findings, Surface Roughness Prediction

Surface roughness has been shown to be a useful indicator of machining damage. It indicates whether there may be a problem in the machining process such as worn tool or poorly selected machining parameters. It has been shown by the use of CT scanning that there was no noticeable sub-surface

271

delamination or cracking in the multidirectional laminate. Most of the damage was visible surface damage close to the machined surface and a maximum machining damage depth of 0.04 mm was shown. Consequently for this laminate it was deemed acceptable to focus on roughness measurements as an indicator of machining damage. The work has developed roughness measurement strategies and use of additional roughness parameters, including skewness and kurtosis. It has also helped to add further information about the machined surface damage mechanism and profile structure. Use of S_a areal roughness parameters and optical system has led to a more accurate and reliable measurement of roughness and therefore more confidence in being able to predict the effects of changing machining parameters and tool wear. Importantly, without being able to accurately measure roughness and understand the effects of machining on different fibre orientations it will be more difficult to make improvements to the integrity of machined components or increase the efficiency of machining fibrous composite components. Accordingly the outcomes of this work are considered to be useful for industry and to further academic study into machining of composites (especially in milling of CFRP). Improvements in numerical FE methods for edge trimming of CFRP have been applied, and a novel roughness prediction tool has been demonstrated.

The 3D FE and roughness prediction method from multidirectional laminate showed a 300 % increase in roughness when increasing from a 5 microns to 30 microns edge radius. Whereas the unidirectional laminate saw a 100 % increase in roughness when the same increase in cutting edge radius was applied. A larger rise in roughness was seen at a higher feed rate when tool wear increased due the interacting effect between feed and edge radius.

The change in skewness and kurtosis was also predicted and these parameters have been previously found to be a useful predictor of torn fibre chunks and

protruding fibres. However it was found that the change in skewness and kurtosis will be specific to each different fibre orientation. For example the change in skewness on one fibre orientation due to a process parameter change may not apply equally to different fibre orientations. A decrease in skewness was seen with an increasing edge radius on the 135 degree fibre orientation, while the opposite was found on the 0 degree fibre orientation.

A good correlation was seen between experimentally and predicted values for S_a surface roughness using the regression equation and FE models. A prediction within 10 % of experimental and predicted roughness was found in the multidirectional model. This prediction was less accurate when extended to an increased feed rate which did not lie within model training data range. The use of interaction terms in the regression equation was found to increase the accuracy of model fit. Fx cutting forces were generally well predicted by the 2D and 3D models. The Fy thrust forces were in general under predicted by FE models which will cause some error in the prediction of the surface roughness. However, the Fy forces had a smaller overall contribution to the surface roughness than the other variables, namely feed rate or cutting edge radius, and therefore the contribution to the overall error in the prediction of the surface roughness is less significant. Ahmad et al. [88], has researched the effects of machining parameters on heat generated during machining and the effects on surface morphology. It was shown that increased feed rate can lower the heat transferred into the material and may improve surface quality, and this could be a mechanism for error in the simulated predictions.

It should be highlighted that the 3D roughness predictive method will only give accurate roughness predictions when applied with the same material and stacking sequence. If the material stacking sequence was changed or the percentage of different fibre orientations which make up the laminate, then there would be some change in overall surface roughness due to the different

cutting mechanisms on each ply as explained previously. If a change in cutting tool geometry or material make up was applied then a set of machining trials should be performed to give a new regression equation. If a change to the laminate fibre orientation stacking sequence is applied then it would be possible to make a representative model for each different fibre orientation of the laminate and have an overall average surface roughness based on the percentage of constituent laminate fibre orientations making up the overall laminate stack. This would be useful if many changes were to be made to the laminate stacking sequence, but without the need for extra machining trials. The surface roughness of each fibre orientation on the machined laminate surface could be measured individually to have a regression model for each layer.

Chapter 9
Discussion & Outputs

From the experiment and FE modelling results it can be concluded that the fibre orientation will play a significant role in the cutting mechanism, as confirmed in the literature [3],[20]. Also, in respect to the direction of cut, the 135 degree fibre orientation was found to be the critical fibre orientation for highest machining damage. The surface structure of this fibre orientation was characterised by torn fibres and pitted surface, which was verified by CT and SEM images. It was found that there is a great variation in surface structure on different layers of the laminate and this has implied consequences for applying accurate surface roughness measurement.

A conclusion of this work, is that surface roughness measurements may over or under represent the overall surface damage if all plies of the laminate and different fibre orientations are not contributed proportionally in a measurement. The 135 orientation degree fibre orientations plies have shown the surface structure with the highest roughness and machining damage, but it is also the fibre orientation which is most affected by changes in process parameters. This means that increases in feed rate and tool wear will have a corresponding negative effect on surface quality, and this effect will be most pronounced on the 135 positive fibre orientations. It has been shown that an increase in torn fibre chunks and fibre pull-out will be characterised in the skewness parameter by a negative value, again, this result was most prominent on the 135 degree fibre orientation.

The use of Alicona focus variation optical device was found to increase the reliability of surface roughness measurements applied with the use of S_a areal roughness parameters. Consequently, the use of the areal roughness parameters is recommended to accurately quantify the overall damage of

276

multidirectional machined laminates. Skewness and kurtosis were found to be useful additional roughness parameters because they give more thorough information about surface profile and machining defect types. These parameters can quantify surface structure and machining damage: indicating the whether the surface is dominated by uncut fibres, torn fibres or pitting‐ and these effects are not fully represented by using the commonly used R_a or S_a parameters. The 135 degree fibre orientation resulted in a negative skewness, which was shown by the presence of machining defects‐ including torn fibre chunks and pitting. The 90 degree fibre orientation showed the highest kurtosis due to the presence of protruding un-cut fibre tips. It has been found that skewness and kurtosis should be best assessed on an individual ply level, or separate fibre orientations, to most expansively and reliably characterise machining damage.

Experimental results have shown that tool condition and machining parameters will play a critical role in the machined surface quality and chip removal mechanism. Cutting tool wear was found to have a significant effect on surface quality and edge delamination. Edge delamination, in the form of un-cut fibres (Type II), was found to increase with tool wear; and delamination was most frequent on top and bottom laminate layers of the 45 degree fibre orientation. Edge trimming trials were performed using a PCD cutting tool, and then regression models were created to show the statistical influence of different machining parameters on surface roughness and cutting forces. Cutting edge radius measurements were taken using an optical system and then used as an input for regression equations and FE models. Tool wear was found to be predominantly due to cutting edge rounding by abrasive wear and chipping of the cutting edge, which was confirmed by optical microscope images and optical focus variation device. The cutting edge radius parameter was applied to measure tool wear and has been used effectively to indicate

current tool condition. The presence of substantial crater wear was not seen on worn cutting tools when machining of CFRP, due to the brittle and discontinuous chip formation- unlike in metal machining where there is chip adhesion and continuous chip formation. The tool wear and feed rate were both shown to have a strong statistical influence on the surface roughness, skewness, and kurtosis. Additionally, the tool wear and feed rate were found to have a strong interaction effect on the surface roughness, this meant that machining at a high feed with a worn tool will lead to a significantly higher roughness, compared to machining at a high feed rate without a worn tool. As a consequence of this result, to improve surface quality, the feed rate should be reduced when the cutting tool becomes highly worn. It has been found that the feed rate and cutting speed will predominantly change the surface roughness due to changes in chip thickness, and that increasing chip thickness will lead to higher roughness and machining damage, as confirmed in the literature [26]. Increasing the cutting speed caused a decrease in chip thickness and generally a lower surface roughness, which was again confirmed by the literature [35],[40]–[42].

 Modelling tools have been developed for the analysis of milling of CFRP using an edge trimming process and zero helix PCD tool. These developments included new 2D and 3D edge trimming models using finite element MSC Marc software, and a Hashin damage model, for simulation of edge trimming of unidirectional and multidirectional laminates. The new modelling methods were used to develop a surface roughness prediction tool that used a combination of FE methods and regression equations, calculated by experimental analysis. A user subroutine was applied to control simulation load step; additionally the use of moving adaptive local re-meshing was applied to the workpiece and moved with the tool path. The modelling tools have been shown to be capable of predicting machining forces at different machining parameters, material

fibre orientations and cutting tool edge-condition. The 2D FE model implemented a changing cutting tool tip mesh, representative of the experimentally measured cutting edge radius, to assess the effects on the cutting forces. In the FE model adaptive re-meshing and adaptive convergence control were used to increase accuracy of the milling model- where there is intermittent cutting and a continuous change in the chip thickness during the rotation of the cutting tool. The user subroutine was applied to control the size of the time step and cutter motion in the 3D model, which improved convergence and reduced the simulation time. The effect of tool wear was assessed in 2D models using different cutting edge radii and implemented in the cutting tool FE mesh. This model was able to predict the effect of tool wear on increasing cutting forces with reasonable accuracy. Cutting forces were predicted with greater accuracy than thrust forces by the 2D model. 2D FE predictions for the increase in cutting forces were made from a 5 micron to 30 micron cutting edge radius and showed a 100 % increase in surface roughness on the 90 degree fibre orientation unidirectional laminate. The 3D model made predictions of the Fx feed force within ± 15 % of the experimental values, while a maximum difference of -70 % was seen in the Fy thrust forces. The poorer prediction in the Fy forces has previously been found in the literature. However, a better prediction may be possible with the inclusion of the cutting edge radius in the 3D model. This would however require significantly higher computational resources, making it unfeasible.

Being able to predict the effects of tool wear is important because the wear rate can be very high in composite machining, particularly for CFRP materials, and tool wear has been shown to lead to a significant decrease in surface quality. Tool wear has been shown to cause an increase in machining defects, including un-cut fibres and delamination. Consequently, being able to predict the effects on surface quality of an increase in tool cutting edge radius will

allow machinists to make more informed decisions about when a milling tool has become critically worn. It has been shown that diamond cutting tools such as PCD will optimise machined surface quality, however these tools are expensive. It is of interest to industry to use these tools right up to end of life before replacement or re-grinding, because of their expense. Being able to quantify when cutting tools have reached their end of life using FE prediction is useful, because it can be used to determine when prohibited damage may be introduced into the component. This will safeguard a cost effective machining process and prevent scrapping of material due to failure to conform to surface quality limits.

A sensitivity study has been performed on the effects of friction factor, force and displacement tolerance residuals on the FE output forces. It was found that small changes in the friction factor did not cause a highly sensitive change in the output results and therefore a small error in the applied friction factor is not anticipated to be a significant contributor to output errors in the FE analysis. The output forces were found to be sensitive to the mesh size, as a decreasing mesh caused a decreasing trend in the cutting forces. The user subroutine allowed the size of the load step to be controlled and it was used to reduce large fluctuations in cutting force output.

The machining forces and surface quality were measured from experiment and predictive tools have been created to assess the effects of tool wear and predict roughness. A novel approach has used regression models in combination with FE models to predict the effects of machining parameters and machining forces on the surface roughness. Interaction effects between parameters were assessed using linear regression modelling and a step wise method was applied to generate regression equations. In general it was found that reducing tool wear and chip thickness will improve surface quality. Surface roughness was predicted in combination with novel 3D FE milling models and

regression models. These models show the capability of FE methods to be applied to complex composite machining problems in order to make predictive assessment of outputs including surface quality. It has been shown that there is a predicted 300 % increase in S_a roughness of the multidirectional laminate when tool wear increases from 5μm to 30μm. Surface roughness predictions were found to lie close to or within the error shown by standard deviation in the experimental results. It must be emphasised that there will always be a reasonable amount of scatter in measurements of surface roughness due to the inherent variation of surfaces, material properties and material non-homogeneity. Therefore there will be some uncertainty in the generated regression equations, and also a greater uncertainty in predictions which lie outside of the model limits or lie at the extreme range of model predictions. This was shown, in this case, because the model made poorer predictions for feed rates and cutting speeds which were extrapolated outside of the model range. Therefore to increase model predictive capabilities over a larger range then more parameters levels must be included in experiments. Additionally to this, there will always be some uncertainty in data based models and as a result further work could make an effort to include a multi-scale approach or include direct predictions from FE. This will become possible as computational resources become more extensive.

SEM images were used in order to study the surface structure across different fibre orientations of a multidirectional laminate and verified the findings from experimental surface roughness measurements. It was shown that the 135 degree fibre orientation was dominated by pits or torn fibre chunks and the fibres had been bent out of plane. Whereas the 90 and 45 degree fibre orientations were dominated by sheared fibres and had a lower surface roughness than the 135 degree fibre orientation. The 0 degree orientation was found to have fibres which had been de-bonded, bent and then fractured. It

was also found that machining with a worn tool on the unidirectional laminate, Type II delamination was found to be prevalent on the 45 degree plys which were located on the top and bottom outer edges of the laminate. These defects were in the form of un-cut fibres protruding from the top and bottom layers of the laminate. This finding advocates the adoption of new machining strategies to avoid certain fibre orientations, or to include a design for manufacture approach which will apply different lay-up directions on the top and bottom of laminate to prevent delamination and un-cut fibres. In this case it has been shown that 45 degree fibre orientation plys should be avoided on the outer layers because they show an increased frequency of type II delamination, which is enhanced with tool ageing.

CT scanning has been found to be capable of showing the presence of internal voids in the unidirectional laminate caused by machining. It was found that some sub-surface damage was present due to the manufacturing process which was increased in magnitude by machining. CT scanning process showed that the multidirectional laminate was found to be free of internal voids or any inter-laminar delamination caused by the machining process. This lack of internal damage can be predominantly explained by the overall constituent degree of directional stiffness and high level of consolidation during manufacture of the multidirectional laminate. A scanning resolution of 8 μm was applied using 3D micro CT scanner. CT scanning has thus been shown to be a useful additional tool to look for machining damage and can show the presence of internal cracks, voids and inter-laminar delamination. However due to the need to prepare small samples, (which must be destructively cut), and the cost and time of the CT scanning it is unsuitable for everyday checking of all components presently. For this reason roughness measurements are a more practical technique to test at reasonable cost and time for damage due to machining of CFRP components in industry.

Chapter 10
Conclusions

The main aims of this research were to assess the surface damage generated and the surface roughness measurement methods for a composite edge trimming process. New surface analysis techniques and roughness parameters have been applied to quantify surface damage of a machined multidirectional laminate. The second aim was to develop new FE methods and surface roughness prediction tools for an edge trimming process during CFRP machining. The research has used surface analysis techniques to assess surface damage and has developed methods to predict the effects of different machining process parameters on the surface roughness using regression equations and FE modelling.

A summary of the conclusions is presented:

1. New roughness measurement strategies have been developed using an optical focus variation device and additional roughness parameters. This has increased reliability of roughness measurements and understanding of damage caused during machining. Areal roughness parameters have been found to increase roughness measurement accuracy of post-machined surfaces from the uncertainty due to material inhomogeneity and variation in damage on different fibre orientations. It is suggested that roughness measurements should systematically include a relative ratio of all fibre orientations in a composite lay-up.

2. Skewness and kurtosis roughness parameters have been used to characterise surface quality of a machined CFRP composite edge. When included in surface quality it is found that they can each individually give a more thorough information on surface structure and defects than using R_a or S_a

284

parameters alone. They can indicate the presence of torn chunks and un-cut fibres. Firstly, the skewness can indicate the presence of torn fibre chunks and deep valleys from machining damage. Alternatively, the kurtosis was able to describe the presence of sharp protruding fibres on the 90 degree fibre orientation, while on the 135 degree fibre orientation it indicated wide valleys caused by torn chunks. Machining damage and torn fibre chunks were found to be most prevalent on the 135 degree fibre orientation compared to the 0, 45 and 90 degree fibre orientations. The 135 degree fibre orientation was also found to have a greater increase in roughness than the other fibre orientations when there was a change in feed rate or tool wear. A detailed description of defects and cutting mechanism on each of the different fibre orientations was presented. Histograms were used to present the different surface structure due to profile distribution on each of the fibre orientations, which was found to vary significantly due to different machining damage, machining defects and cutting mechanism.

3. Machining tests were performed on a multidirectional laminate using a PCD tool at progressive levels of wear. Regression models were created which show the contribution of different machining parameters and tool wear on machined surface roughness and machining forces during edge trimming. Statistical methods and design of experiments were applied in order to show the significance of parameters on surface roughness. The cutting edge radius was found to be the most significant parameter and showed an increasing trend in the surface roughness and machining damage. Feed rate and cutting speed were also found to be significant parameters, and an increasing chip thickness was shown to increase R_a and S_a surface roughness. It was shown using statistical methods that feed rate and tool wear had a strongly interacting effect on the surface roughness and this is due to an increased ploughing and tearing cutting mechanism when the cutting edge becomes more rounded.

285

Also, at higher feeds the fibres are torn and pulled from the material, rather than being abrasively cut, and this effect is accelerated at higher levels of wear.

4. Novel 2D and 3D composite milling finite element models have been developed and compared with experimentally obtained machining forces at different levels of tool wear. New methods have been applied, including the use of a user subroutine and adaptive re-meshing. The effect of tool wear has been analysed on machining forces in a 2D FE model and compared with experimental results. The FE models have been combined with experimental regression models to make a prediction tool for surface roughness at different machining parameters on a multidirectional laminate. New modelling methods have been developed using MSC Marc implicit modelling software and a subroutine used to adapt the time step size. Two dimensional models have been used to assess and predict the change in cutting forces due to increasing levels of tool wear. A predictive assessment of the increase in cutting forces due to increasing cutting edge radius with wear was made in unidirectional laminate. It was found that there was a 50 % increase in the Fx cutting forces when tool wear increased from a 5 micron edge radius to a 30 micron edge radius in the unidirectional test. This was shown to correspond with a 100 % calculated increase in the predicted S_a surface roughness.

Three dimensional predictive models have shown that the surface roughness would increase from 1.87 μm to 6.15 μm, by a factor of three, when cutting edge radius changed from 5 μm to 30 μm. The predictive model also showed that increasing the feed rate from 1000 mm/min to 1400 mm/min while maintaining a constant cutting speed of 7000 RPM would have a corresponding 65 % increase in S_a surface roughness, on the multidirectional laminate. The experimentally predicted roughness was found to be accurate within ±10 % when lying within the range of the regression model training data. However, when the feed rate was increased outside of the model training limits

to 1400 mm/min, there was an over prediction of 30 % by the FE model, compared to experimentally measured S_a. Therefore the best predictions for surface roughness will lie closer to the regression model data training limits. This means that predictions can likely be improved by extending the range of the experimental training data set with further trials. Also, by including the change in cutting edge radius due to tool wear in the 3D simulations. The results and project findings have shown increase in cutting edge radius will be a critical factor in the accuracy of comparison between numerical and experimental results. It was also shown that the Fy machining forces may be under predicted, in accordance with the literature, and this was found especially in the 2D FE models.

5. SEM and CT scans have been applied to look at surface and sub-surface machining damage. SEM images showed that a different surface structure, machining damage type and chip removal mechanisms are present on different fibre orientations. A detailed analysis of the cutting mechanism and damage type was made of the 0, 45, 90 and 135 degree fibre orientations by use of SEM images. The fibre orientation was found to be a critical factor in the machined surface quality and damage type and therefore on the surface roughness measured. This has confirmed that the use of the optical surface roughness measurement system and areal roughness parameters will be beneficial for a composite surface. It is therefore advised that areal parameters be used to quantify surface damage of a multidirectional composite due to the inhomogeneous structure and variation in damage on different fibre orientations. Internal CT scans were performed on an edge trimmed CFRP sample and showed the presence of voids, and of propagating cracks in the form of inter-laminar delamination. There was no internal subsurface damage found on the multidirectional laminate using CT scanning, including the tests comprising of the most worn tool condition. Inter-laminar voids were found on

the unidirectional laminate and the voids were found to have a higher magnitude in the machined samples. Consequently, it is probable that the machining process increased sub-surface damage in the unidirectional laminate. However some voids may have been present from manufacture and preparation of the samples. CT scanning was found to be capable of showing inter-laminar delamination and voids, and is therefore a useful technique to check for either manufacturing defects pre- or post-machining and for internal machining defects which cannot be seen on the surface. However it has the disadvantage of being a destructive technique because the samples must be cut into small specimens in order to achieve a high image resolution so as to be able to see small fibre scale diameter defects.

6. The use of different CVD and PCD cutting tools have been compared in wet and dry cutting conditions - with different feed rates and cutting speeds, and increasing levels of tool wear, to investigate their effects on surface roughness and machining forces. It was found that the CVD abrasive style router performed well in wet conditions and produced a high surface quality at a high production rate, and performed significantly better in wet than dry cutting conditions. This work has been summarised in REF [89].

11.1 Future Work

Some potential developments in composite machining have been outlined and there are a number of areas where this work can be continued in the future. Firstly, improving modelling predictive capabilities in the field of composite machining of CFRP can continue. Modelling of the end milling process would be a challenging but useful further continuation of this work. Additionally, modelling the effects of using different complex tool geometry in combination with the roughness prediction tool will allow the quantitative development of new cutting tool geometries. New tool geometries can be optimised with machining parameters in order to see the effects on the cutting forces and surface damage caused.

The effects of tool wear incorporating different cutting tool geometry and coatings at different machining parameters can be further optimised to improve CFRP machining productivity and cost/meter of machining. Direct improvements of the current work will include the effects of edge radius change in the 3D FE model. This should be implemented with use of supercomputer to increase computational power due to large number of elements required. It is therefore recommended that future work should combine developments in modelling of new and more complex cutting tool geometries with additional experimental tests. These tests and FE models can be used to make assessments of how to reduce machining forces and tool wear rate. The testing should be optimised to obtain a high material removal rate and still maintain a reasonable surface quality.

A diagram has been created which is shown in Figure 10-1 and shows a large range of possible input and output factors which could be included in a composite machining study. It was created to show the possible data and parameters which should be considered as variables in future composite machining testing. The diagram shows a multitude of possible development

areas in machining of CFRP and how the combination of different data sets should be used to fully extend the understanding of the machining process. New tests can be compared with benchmarked results and used to develop further regression modelling tools to encompass larger data sets. These developments can be incorporated with industrial applications and therefore drive further research opportunities. Increased testing to develop regression models will include a further range of parameters and can be correlated with mechanical performance of machined material.

A useful addition would be the application of thermocouples to experimental test to quantify cutting temperatures and find the correlation between machining temperatures and surface damage. Previous researchers have developed thermocouple sensor for in process temperature measurement in a milling process [98]. Applying experimental measurement of generated machining temperatures and introduction of thermal analysis to modelling strategy could increase accuracy of FE simulations by including the effects of matrix glass transition temperature and material thermal softening. The validation of the effects of temperature in a structural thermal model can be applied to show how softening of the matrix will affect both the machining forces and surface quality. As the surface quality could be affected by both matrix burning and matrix smearing, this could be a by-product of machining at elevated temperatures or with excessive cutting tool wear. Experimental tests using thermocouple can also be used to create a regression model which includes the effects of different tool geometries and tool wear on the generated machining temperature and the resulting induced surface quality. This would be a further improvement on the current work, and combining experimental tests with the continued use of the new recommended optical technique for measuring surface roughness will allow more thorough surface damage detection.

290

Some research into cryogenic machining has shown some benefits in composite machining, using either liquid nitrogen or compressed CO_2. Researchers have shown that tool wear is reduced and that there may be some improvements in surface quality and a reduction in damage depth [99]–[102].The reduction in temperature causes an increase in hardness and modulus of the matrix which will cause a change in cutting mechanism. Some additional work into milling using cryogenics would thus be useful to further understand the cutting mechanism and focussing on machined surface quality at reduced temperatures. The application of cryogenics could be applied with different geometry tools.

New FE modelling strategies can be applied, incorporating the use of additional damage models like Puck or new damage models from the literature. This may allow better estimation of cutting forces, especially the Fy cutting forces in 2D model which were shown to be under predicted. They may be able to better represent the matrix damage during machining. Another method which can be applied would be the use of a 2 phase cohesive model for the 2D simulation of milling and may allow better estimation of cutting forces and show the damage in the matrix and fibre phases separately. This method could then also be applied to roughness measurement prediction with a similar method to that applied in this research. A two phase model could be compared with an EHM model and experimental tests on a unidirectional laminate. In the future it may be possible to attempt a 3D two phase model with cohesive elements but it is expected this would use very high computational resources. Also the individual material properties of the two constituent material fibres and matrix may not correctly represent the overall material strength in a machining process when applied to the composite material two-phase model. It is recommended that additional strain rate testing of material should be applied and then be implemented into finite element code. This will show how machining is effected

by strain rate and time dependant loading at increased cutting speeds during machining.

In FE modelling, further analysis can apply 2D models with an extremely fine mesh to see if it is possible to make a direct comparison between machined surface quality and surface roughness from experiment with FE models. Although the current method does look at how the different failure index of the Hashin damage model will vary through thickness of the workpiece, it does not directly quantify surface roughness from damage of surface elements.

Another potential area for future work is the use of CT scanning techniques, which should be further applied to a large scale machining test with different cutting tool geometries and increased levels of tool wear. Machining parameters and tool wear should be pushed above normal standard operating conditions to promote sub-surface damage. This will show at what point there is a material breakdown and increase in inter-laminar delamination. It was seen from the unidirectional CFRP samples that there is inter-laminar delamination to the material caused during an edge trimming operation. Therefore CT-scanning should be combined with fatigue and load testing to find a correlation between harsh machining conditions and material strength. This would be a useful study for industry to understand under which point safe machining conditions will still be obtained, and when will there be a critical damage to components due to machining. CT scanning will allow this to be correlated with internal damage to components from machining. The use of image analysis methods could also be applied in combination with CT scanned images to look at volume fraction of damage or delamination, a grey scale of pixels could be used to quantify damage size. In summary, this study has focussed on surface damage and roughness measurements, yet a number of different possible future research opportunities are available for composite machining researchers.
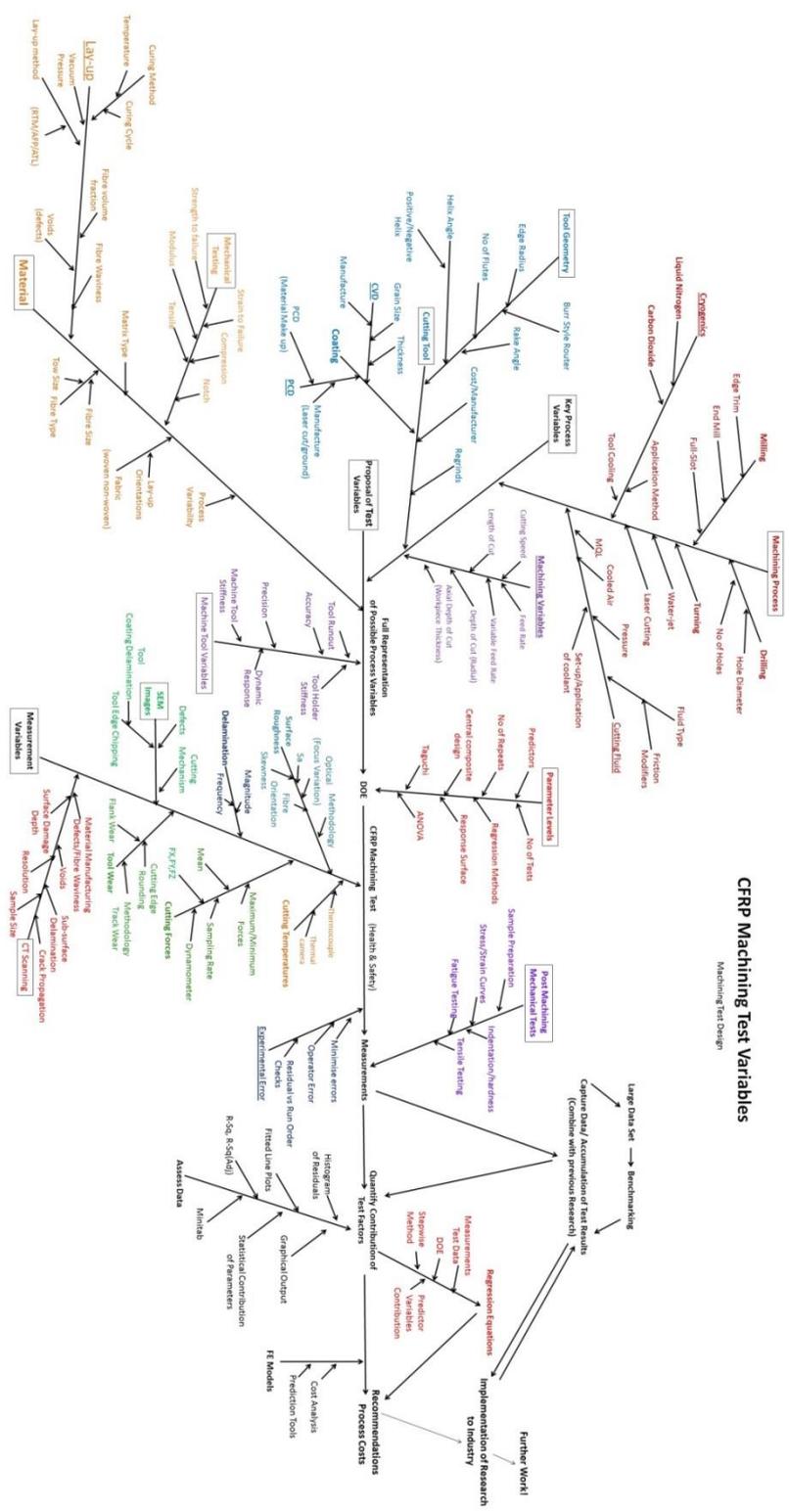
Figure 10-1- Future work- test variables.

Publications

1. "An optical method for measuring surface roughness of machined carbon fibre-reinforced plastic composites," *J. Compos. Mater.*, vol. 51, no. 3, pp. 289–302, 2017, N. Duboust, H. Ghadbeigi, C. Pinna, S. Ayvar-Soberanis, A. Collis, R. Scaife, and K. Kerrigan.
2. "Machining of Carbon Fibre: Optical Surface Damage Characterisation and Tool Wear Study," *Procedia CIRP*, vol. 45, pp. 71–74, 2016, N. Duboust, D. Melis, C. Pinna, H. Ghadbeigi, A. Collis, S. Ayvar-Soberanis, and K. Kerrigan.
3. "2D and 3D Finite Element Models for the Edge Trimming of CFRP," *Procedia CIRP*, vol. 58, pp. 233–238, 2017, N. Duboust, C. Pinna, H. Ghadbeigi, S. Ayvar-Soberanis, V. A. Phadnis, A. Collis, and K. Kerrigan.

References

[1]   H. Hocheng and C. Tsao, "Comprehensive analysis of delamination in drilling of composite materials with various drill bits," *J. Mater. Process. Technol.*, vol. 140, no. 1–3, pp. 335–339, Sep. 2003.

[2]   R. Teti, "Machining of Composite Materials," *CIRP Ann. - Manuf. Technol.*, vol. 51, no. 2, pp. 611–634, Jan. 2002.

[3]   J. Sheikh-Ahmad, *Machining of Polymer Composites*. Boston, MA: Springer US, 2009.

[4]   M. Haddad, R. Zitoune, H. Bougherara, F. Eyma, and B. Castanié, "Study of trimming damages of CFRP structures in function of the machining processes and their impact on the mechanical behavior," *Compos. Part B Eng.*, vol. 57, pp. 136–143, Feb. 2014.

[5]   M. Ramulu, C. W. Wern, and J. L. Garbini, "Effect of fibre direction on surface roughness measurements of machined graphite/epoxy composite," *Compos. Manuf.*, vol. 4, no. 1, pp. 39–51, Jan. 1993.

[6]   V. A. Phadnis, F. Makhdum, A. Roy, and V. V. Silberschmidt, "Drilling in carbon/epoxy composites: Experimental investigations and finite element implementation," *Compos. Part A Appl. Sci. Manuf.*, vol. 47, pp. 41–51, Apr. 2013.

[7]   K. Giasin, S. Ayvar-Soberanis, T. French, and V. Phadnis, "3D Finite Element Modelling of Cutting Forces in Drilling Fibre Metal Laminates and Experimental Hole Quality Analysis," *Appl. Compos. Mater.*, vol. 24, no. 1, pp. 113–137, 2017.

[8]   C. Santiuste, X. Soldani, and M. H. Miguélez, "Machining FEM model of long fiber composites for aeronautical components," *Compos. Struct.*, vol. 92, no. 3, pp. 691–698, Feb. 2010.

[9]   M. Arola, D. Ramulu, "Orthogonal cutting of fiber-reinforced composites a finite element analysis," *Int. J. Mech. Sci.*, vol. 39, no. 5, pp. 597–613, 1995.

[10]   T. L. Anderson, *Fracture Mechanics: Fundementals and Applications*, 3rd Editio. Boca Raton: CRC Press, 2005.

[11]   R. D. Adams and P. Cawley, "Defect types and non-destructive testing techniques for composites and bonded joints," *Constr. Build. Mater.*, vol. 3, no. 4, 1989.

[12]   D. Hull, *An introduction to composite materials*. Cambridge: Cambridge University Press, 1981.

[13]   P. Maimí, P. P. Camanho, J. A. Mayugo, and C. G. Dávila, "A continuum damage model for composite laminates: Part I – Constitutive model," *Mech. Mater.*, vol. 39, no. 10, pp. 897–908, Oct. 2007.

[14]   C. Sauder, J. Lamon, and R. Pailler, "The tensile behavior of carbon fibers at high temperatures up to 2400 °C," *Carbon N. Y.*, vol. 42, no. 4, pp. 715–725, Jan. 2004.

[15]   C. Sauder, J. Lamon, and R. Pailler, "Thermomechanical properties of carbon fibres at high temperatures (up to 2000 °C)," *Compos. Sci. Technol.*, vol. 62, no. 4, pp. 499–504, Mar. 2002.

[16]   A. Koplev, A. Lystrup, and T. Vorm, "The cutting process, chips, and cutting forces in machining CFRP," *Composites*, vol. 14, no. 4, pp. 371–376, Oct. 1983.

[17]   G. I. Santhanakrishnam, R. K. Murthy, and S. K. Malhotra, "Machinibility characteristics of fibre reinforced plastics composites," *J. Mech. Work. Technol.*, vol. 17, pp. 195–204, 1988.

[18]   Y. Karpat, O. Bahtiyar, and B. Değer, "Mechanistic force modeling for milling of unidirectional carbon fiber reinforced polymer laminates," *Int. J. Mach. Tools Manuf.*, vol. 56, pp. 79–93, May 2012.

[19]   J. Sheikh-Ahmad, N. Urban, and H. Cheraghi, "Machining Damage in Edge Trimming of CFRP," *Mater. Manuf. Process.*, vol. 27, no. 7, pp. 802–808, Jul. 2012.

[20]   X. M. Wang and L. C. Zhang, "An experimental investigation into the orthogonal cutting of unidirectional fibre reinforced plastics," *Int. J. Mach. Tools Manuf.*, vol. 43, no. 10, pp. 1015–1022, Aug. 2003.

[21]   D. Wang, M. Ramulu, and D. Arola, "Orthogonal cutting mechanisms of graphite/epoxy composite. Part I: Unidirectional laminate," *Int. J. Mach. Tools Manuf.*, vol. 35, no. 12, pp. 1623–1628, 1995.

[22]   M. Groover, *Fundamentals of Modern Manufacturing: Materials, Processes, and Systems*, 4th ed. John Wiley & Sons.

[23]   R. Singh, *Introduction to basic manufacturing processes and workshop technology*. New Delhi: New Age International Publishers, 2006.

[24]   M. C. Shaw, *Metal Cutting Principles*, 2nd ed. New York (USA): Oxford University Press, 2005.

[25]   W. A. Knight, *Fundamentals of Metal Machining and Machine Tools*, 3rd ed. CRC Press, 2005.

[26]   A. I. Azmi, R. J. T. Lin, and D. Bhattacharyya, "Machinability study of glass fibre-reinforced polymer composites during end milling," *Int. J. Adv. Manuf. Technol.*, vol. 64, no. 1–4, pp. 247–261, Mar. 2012.

[27]   J. P. Davim, P. Reis, and C. C. António, "A study on milling of glass fiber reinforced plastics manufactured by hand-lay up using statistical analysis (ANOVA)," *Compos. Struct.*, vol. 64, no. 3–4, pp. 493–500, Jun. 2004.

[28]   N. Rajesh Mathivanan, B. S. Mahesh, and H. Anup Shetty, "An experimental investigation on the process parameters influencing machining forces during milling of carbon and glass fiber laminates," *Meas. J. Int. Meas. Confed.*, vol. 91, pp. 39–45, 2016.

[29]   W. Hintze, M. Cordes, and G. Koerkel, "Influence of weave structure on delamination when milling CFRP," *J. Mater. Process. Tech.*, vol. 216, pp. 199–205, 2015.

[30]   J. S. Ahmad and A. H. Shahid, "Effect of edge trimming on failure stress of carbon fibre polymer composites," *Int. J. Mach. Mach. Mater.*, vol. 13, no. 2/3, p. 331, 2013.

[31]   I. S. Shyha, D. K. Aspinwall, S. L. Soo, and S. Bradley, "Drill geometry and operating effects when cutting small diameter holes in CFRP," *Int. J. Mach. Tools Manuf.*, vol. 49, no. 12–13, pp. 1008–1014, Oct. 2009.

[32]   C. C. Tsao and H. Hocheng, "Taguchi analysis of delamination associated with various drill bits in drilling of composite material," *Mach. Tools Manuf.*, vol. 44, pp. 1085–1090, 2004.

[33]   W. Chen, "Some experimental investigations in the drilling of carbon fiber-reinforced plastic (CFRP) composite laminates," *Int. J. Mach. Tools Manuf.*, vol. 37, no. 8, pp. 1097–1108, 1997.

[34]   A. I. Azmi, R. J. T. Lin, and D. Bhattacharyya, "Experimental Study of Machinability of GFRP Composites by End Milling," *Mater. Manuf. Process.*, vol. 27, no. 10, pp. 1045–1050, Oct. 2012.

[35]   P. Ghidossi, M. El Mansori, and F. Pierron, "Edge machining effects on the failure of polymer matrix composite coupons," *Compos. Part A Appl. Sci. Manuf.*, vol. 35, no. 7–8, pp. 989–999, 2004.

[36]   M. Slamani, J. F. Chatelain, and H. Hamedanianpour, "Influence of machining parameters on surface quality during high speed edge trimming of carbon fiber reinforced polymers," *Int. J. Mater. Form.*, pp. 1–23, 2018.

[37]   S. Gara and O. Tsoumarev, "Prediction of surface roughness in slotting of CFRP," *Meas. J. Int. Meas. Confed.*, vol. 91, pp. 414–420, 2016.

[38]   C. W. Wern, M. Ramulu, and K. Colligan, "A study of the surface texture of composite drilled holes," *J. Mater. Process. Technol.*, vol. 37, no. 1–4, pp. 373–389, Feb. 1993.

[39]   O. Çolak and T. Sunar, "Cutting Forces and 3D Surface Analysis of CFRP Milling with PCD Cutting Tools," *Procedia CIRP*, vol. 45, pp. 75–78, 2016.

[40]   K. Palanikumar, F. Mata, and J. P. Davim, "Analysis of surface roughness parameters in turning of FRP tubes by PCD tool," *J. Mater. Process. Technol.*, vol. 204, no. 1–3, pp. 469–474, 2008.

[41]   M. Nurhaniza, M. K. A. M. Ariffin, F. Mustapha, and B. T. H. T. Baharudin, "Analyzing the

Effect of Machining Parameters Setting to the Surface Roughness during End Milling of CFRP-Aluminium Composite Laminates," *Int. J. Manuf. Eng.*, vol. 2016, pp. 1–9, 2016.

[42]   A. Harun, H. Haron, J. A. Ghani, S. Mokhtar, and A. Sanuddin, "Fundamental Study on Delamination in Milling Kenaf Fiber Reinforced Plastic Composite (Unidirectional)," *Proc. ASME 2016 Int. Manuf. Sci. Eng. Conf.*, vol. 11, no. 7, pp. 4761–4766, 2016.

[43]   S. T. Kumaran, T. J. Ko, M. Uthayakumar, and M. M. Islam, "Prediction of surface roughness in abrasive water jet machining of CFRP composites using regression analysis," *J. Alloys Compd.*, vol. 724, pp. 1037–1045, 2017.

[44]   S. O. Ismail, H. N. Dhakal, E. Dimla, J. Beaugrand, and I. Popov, "Effects of drilling parameters and aspect ratios on delamination and surface roughness of lignocellulosic HFRP composite laminates," *J. Appl. Polym. Sci.*, vol. 133, no. 7, pp. 1–8, 2016.

[45]   S. O. Ismail, H. N. Dhakal, I. Popov, and J. Beaugrand, "Comprehensive study on machinability of sustainable and conventional fibre reinforced polymer composites," *Eng. Sci. Technol. an Int. J.*, vol. 19, no. 4, pp. 2043–2052, 2016.

[46]   U. C. Nwaogu, N. S. Tiedje, and H. N. Hansen, "A non-contact 3D method to characterize the surface roughness of castings," *J. Mater. Process. Technol.*, vol. 213, no. 1, pp. 59–68, Jan. 2013.

[47]   M. L. Herring, J. I. Mardel, and B. L. Fox, "The effect of material selection and manufacturing process on the surface finish of carbon fibre composites," *J. Mater. Process. Technol.*, vol. 210, no. 6–7, pp. 926–940, Apr. 2010.

[48]   X. Rimpault, J. F. Chatelain, J. E. Klemberg-Sapieha, and M. Balazinski, "Tool wear and surface quality assessment of CFRP trimming using fractal analyses of the cutting force signals," *CIRP J. Manuf. Sci. Technol.*, vol. 16, pp. 72–80, 2017.

[49]   J. P. Davim, *Surface Integrity in Machining*. London: Springer, 2010.

[50]   K. Palanikumar, "Application of Taguchi and response surface methodologies for surface roughness in machining glass fiber reinforced plastics by PCD tooling," *Int. J. Adv. Manuf. Technol.*, vol. 36, no. 1–2, pp. 19–27, Nov. 2006.

[51]   R. Leach, *Optical Measurement of Surface Topography*, vol. 53, no. 9. 2013.

[52]   R. Leach, "Surface topography measurement instrumentation," *Fundam. Princ. Eng. Nanometrology*, pp. 133–204, 2014.

[53]   M. Henerichs, C. Dold, R. Voss, and K. Wegener, "Performance of Lasered PCD-and CVD-Diamond Cutting Inserts for Machining Carbon Fiber Reinforced Plastics (CFRP)," pp. 1–8, 2014.

[54]   J. Zhang, X. Wang, B. Shen, and F. Sun, "Effect of boron and silicon doping on improving

the cutting performance of CVD diamond coated cutting tools in machining CFRP," *Int . J. Refract. Met. Hard Mater.*, vol. 41, pp. 285–292, 2013.

[55]   J. Zhang and B. Shen, "Fabrication and Drilling Tests of Chemical Vapor Deposition Diamond Coated Drills in Machining Carbon Fiber Reinforced Plastics," *J. Shanghai Jiaotong Univ.*, vol. 18, no. 4, pp. 394–400, 2013.

[56]   D. Che, I. Saxena, P. Han, P. Guo, and F. E. Kornel, "Machining of Carbon Fiber Reinforced Plastics/Polymers: A Literature Review," vol. 136, no. June, pp. 1–22, 2014.

[57]   A. Inspektor, E. J. Oles, and C. E. Bauer, "Theory and practice in diamond coated metal-cutting tools," *Int. J. Refract. Met. Hard Mater.*, vol. 15, no. 1–3, pp. 49–56, Jan. 1997.

[58]   J. Hu, Y. K. Chou, R. G. Thompson, J. Burgess, and S. Street, "Characterizations of nano-crystalline diamond coating cutting tools," *Surf. Coatings Technol.*, vol. 202, no. 4–7, pp. 1113–1117, Dec. 2007.

[59]   J. Paulo Davim, *Machining of Hard Materials*. London: Springer, 2011.

[60]   M. . Cook and P. . Bossom, "Trends and recent developments in the material manufacture and cutting tool application of polycrystalline diamond and polycrystalline cubic boron nitride," *Int. J. Refract. Met. Hard Mater.*, vol. 18, no. 2–3, pp. 147–152, Mar. 2000.

[61]   P. J. Heath, "Developments in applications of PCD tooling," *J. Mater. Process. Technol.*, vol. 116, pp. 31–38, 2001.

[62]   P. S. Sreejith, R. Krishnamurthy, S. K. Malhotra, and K. Narayanasamy, "Evaluation of PCD tool performance during machining of carbon/phenolic ablative composites," *J. Mater. Process. Technol.*, vol. 104, no. 1–2, pp. 53–58, Aug. 2000.

[63]   A. Faraz, D. Biermann, and K. Weinert, "Cutting edge rounding: An innovative tool wear criterion in drilling CFRP composite laminates," *Int. J. Mach. Tools Manuf.*, vol. 49, no. 15, pp. 1185–1196, 2009.

[64]   A. Kapadia, *Best Practise Guide Non-Destructive Testing of Composite Materials*. National Composites Network.

[65]   P. J. Schilling, B. R. Karedla, A. K. Tatiparthi, M. a. Verges, and P. D. Herrington, "X-ray computed microtomography of internal damage in fiber reinforced polymer matrix composites," *Compos. Sci. Technol.*, vol. 65, no. 14, pp. 2071–2078, Nov. 2005.

[66]   P. Wright, X. Fu, I. Sinclair, and S. M. Spearing, "Ultra High Resolution Computed Tomography of Damage in Notched Carbon Fiber--Epoxy Composites," *J. Compos. Mater.*, vol. 42, no. 19, pp. 1993–2002, Oct. 2008.

[67]   C. C. Tsao and H. Hocheng, "Computerized tomography and C-Scan for measuring delamination in the drilling of composite materials using various drills," *Int. J. Mach. Tools*

Manuf., vol. 45, no. 11, pp. 1282–1287, Sep. 2005.

[68]   L. Lasri, M. Nouari, and M. El Mansori, "Modelling of chip separation in machining unidirectional FRP composites by stiffness degradation concept," *Compos. Sci. Technol.*, vol. 69, no. 5, pp. 684–692, Apr. 2009.

[69]   D. Nayak, N. Bhatnagar, and P. Mahajan, "Machining Studies of Ud-Frp Composites Part 2: Finite Element Analysis," *Mach. Sci. Technol.*, vol. 9, no. 4, pp. 503–528, Dec. 2005.

[70]   G. V. G. Rao, P. Mahajan, and N. Bhatnagar, "Micro-mechanical modeling of machining of FRP composites – Cutting force analysis," *Compos. Sci. Technol.*, vol. 67, no. 3–4, pp. 579–593, Mar. 2007.

[71]   K. A. Calzada, S. G. Kapoor, R. E. DeVor, J. Samuel, and A. K. Srivastava, "Modeling and interpretation of fiber orientation-based failure mechanisms in machining of carbon fiber-reinforced polymer composites," *J. Manuf. Process.*, vol. 14, no. 2, pp. 141–149, Apr. 2012.

[72]   C. Santiuste, H. Miguélez, and X. Soldani, "Out-of-plane failure mechanisms in LFRP composite cutting," *Compos. Struct.*, vol. 93, no. 11, pp. 2706–2713, Oct. 2011.

[73]   J. Xu and M. El Mansori, "Numerical studies of frictional responses when cutting hybrid CFRP/Ti composite," *Int. J. Adv. Manuf. Technol.*, vol. 87, no. 1–4, pp. 657–675, 2016.

[74]   J. Xu and M. El Mansori, "Cutting modeling of hybrid CFRP/Ti composite with induced damage analysis," *Materials (Basel).*, vol. 9, no. 1, 2016.

[75]   C. Gao, J. Xiao, J. Xu, and Y. Ke, "Factor analysis of machining parameters of fiber-reinforced polymer composites based on finite element simulation with experimental investigation," *Int. J. Adv. Manuf. Technol.*, vol. 83, no. 5–8, pp. 1113–1125, 2016.

[76]   F. Kahwash, I. Shyha, and A. Maheri, "Modelling of cutting fibrous composite materials: Current practice," *Procedia CIRP*, vol. 28, pp. 52–57, 2015.

[77]   R. Danzl, F. Helmli, and S. Scherer, "Focus Variation – A Robust Technology for High Resolution Optical 3D Surface Metrology," *J. Mech. Eng.*, vol. 57, no. 03, pp. 245–256, Mar. 2011.

[78]   R. Danzl, F. Helmli, and S. Scherer, "Comparison of Roughness Measurements between a Contact Stylus Instrument and an Optical Measurement Device based on a Colour Focus Sensor," *Nanotech, Bost. Vol. III 284*, vol. 3, pp. 284–287, 2006.

[79]   N. Duboust *et al.*, "An optical method for measuring surface roughness of machined carbon fibre-reinforced plastic composites," *J. Compos. Mater.*, vol. 51, no. 3, pp. 289–302, 2017.

[80]   Minitab, "Minitab Support- What is a main effects plot?" [Online]. Available: http://support.minitab.com/en-us/minitab/17/topic-library/modeling-

300

statistics/anova/basics/what-is-a-main-effects-plot/. [Accessed: 21-Nov-2014].

[81]   M. Haddad, R. Zitoune, F. Eyma, and B. Castanie, "Study of the surface defects and dust generated during trimming of CFRP: Influence of tool geometry , machining parameters and cutting speed range," *Compos. Part A*, vol. 66, pp. 142–154, 2014.

[82]   O. Pecat, R. Rentsch, and E. Brinksmeier, "Influence of Milling Process Parameters on the Surface Integrity of CFRP," *Procedia CIRP*, vol. 1, pp. 466–470, Jan. 2012.

[83]   Hexply, "HexPly M21 Product Data," 2010. [Online]. Available: http://www.hexcel.com/Resources/DataSheets/Prepreg. [Accessed: 01-Feb-2017].

[84]   R. Voss, L. Seeholzer, F. Kuster, and K. Wegener, "Influence of fibre orientation, tool geometry and process parameters on surface quality in milling of CFRP," *CIRP J. Manuf. Sci. Technol.*, vol. 18, pp. 75–91, 2017.

[85]   W. Hintze, D. Hartmann, and C. Schütte, "Occurrence and propagation of delamination during the machining of carbon fibre reinforced plastics (CFRPs) – An experimental study," *Compos. Sci. Technol.*, vol. 71, no. 15, pp. 1719–1726, Oct. 2011.

[86]   K. Kerrigan and G. E. O'Donnell, "On the Relationship between Cutting Temperature and Workpiece Polymer Degradation during CFRP Edge Trimming," *Procedia CIRP*, vol. 55, pp. 170–175, 2016.

[87]   N. Nguyen-dinh, R. Zitoune, C. Bouvet, and S. Leroux, "Surface integrity while trimming of composite structures: X-ray tomography analysis," *Compos. Struct.*, vol. 210, no. December 2018, pp. 735–746, 2019.

[88]   J. Y. Sheikh-Ahmad, F. Almaskari, and F. Hafeez, "Thermal aspects in machining CFRPs: effect of cutter type and cutting parameters," *Int. J. Adv. Manuf. Technol.*, 2018.

[89]   N. Duboust *et al.*, "Machining of Carbon Fibre: Optical Surface Damage Characterisation and Tool Wear Study," *Procedia CIRP*, vol. 45, pp. 71–74, 2016.

[90]   P. Mallick, *Fiber-reinforced composites: materials, manufacturing, and design*, Third. CRC Press Taylor & Francis Group, 1993.

[91]   Hexply, "M91 Product Data & User Guide," 2010. [Online]. Available: http://www.hexcel.com/Resources/DataSheets/Prepreg. [Accessed: 01-Mar-2017].

[92]   J. R. Davis, *ASM Speciality Handbook: Tool Materials*. ASM International, 1995.

[93]   M. Petrovic, A. Ivankovic, and N. Murphy, "The mechanical properties of polycrystalline diamond as a function of strain rate and temperature," *J. Eur. Ceram. Soc.*, vol. 32, no. 12, pp. 3012–3017, 2012.

[94]   G. Chardon, O. Klinkova, J. Rech, S. Drapier, and J. Bergheau, "Characterization of friction properties at the work material / cutting tool interface during the machining of randomly

structured carbon fi bers reinforced polymer with Poly Crystalline Diamond tool under dry conditions," *Tribiology Int.*, vol. 81, pp. 300–308, 2015.

[95]   A. Mondelin, B. Furet, and J. Rech, "Characterisation of friction properties between a laminated carbon fibres reinforced polymer and a monocrystalline diamond under dry or lubricated conditions," *Tribol. Int.*, vol. 43, no. 9, pp. 1665–1673, Sep. 2010.

[96]   M. Hokka, D. Gomon, A. Shrot, T. Leemet, M. Bäker, and V. T. Kuokkala, "Dynamic Behavior and High Speed Machining of Ti-6246 and Alloy 625 Superalloys: Experimental and Modeling Approaches," *Exp. Mech.*, vol. 54, no. 2, pp. 199–210, 2014.

[97]   A. Abena, S. L. Soo, and K. Essa, "A finite element simulation for orthogonal cutting of UD-CFRP incorporating a novel fibre-matrix interface model," *Procedia CIRP*, vol. 31, pp. 539–544, 2015.

[98]   K. Kerrigan, J. Thil, R. Hewison, and G. E. O'Donnell, "An Integrated Telemetric Thermocouple Sensor for Process Monitoring of CFRP Milling Operations," *Procedia CIRP*, vol. 1, pp. 449–454, Jan. 2012.

[99]   K. Giasin, S. Ayvar-Soberanis, and A. Hodzic, "Evaluation of cryogenic cooling and minimum quantity lubrication effects on machining GLARE laminates using design of experiments," *J. Clean. Prod.*, vol. 135, pp. 533–548, 2016.

[100]   T. Xia, Y. Kaynak, C. Arvin, and I. S. Jawahir, "Cryogenic cooling-induced process performance and surface integrity in drilling CFRP composite material," *Int. J. Adv. Manuf. Technol.*, vol. 82, no. 1–4, pp. 605–616, 2016.

[101]   S. Basmaci, Gültekin, Yoruk , A, Koklu, Ugur, Morkavuk, "Impact of Cryogenic Condition and Drill Diameter on Drilling Performance of CFRP," *Appl. Sci.*, vol. 667, no. 7.

[102]   C. R. Cunningham, A. Shokrani, and V. Dhokia, "Edge trimming of carbon fibre reinforced plastic," *Procedia CIRP*, vol. 77, no. Hpc, pp. 6–10, 2018.

Appendix

Part A- Unidirectional Test

Table 10-1- Mean Fx Cutting forces from test, 45 degree fibre orientation, and un-worn tool.

Fibre Orientation	Feed Rate (mm/min)	RPM	Fx Sample 1	Fx Sample 2	Mean Fx (N)	STD
45	800	6000	67.7	79.6	**74.0**	**8.4**
45	1200	6000	80.7	78.1	**79.4**	**1.8**
45	800	8000	72.7	78.3	**75.0**	**4.0**
45	1200	8000	79.5	85.2	**82.3**	**4.0**

Table 10-2- Mean Fy Cutting forces from test, 45 degree fibre orientation, and un-worn tool.

Fibre Orientation	Feed Rate (mm/min)	RPM	Fy Sample 1	Fy Sample 2	Mean Fy (N)	STD
45	800	6000	60.2	56.5	**58.3**	**2.7**
45	1200	6000	75.7	76.7	**76.2**	**0.7**
45	800	8000	64.9	68.3	**66.6**	**2.4**
45	1200	8000	81.3	89.5	**85.4**	**5.7**

Table 10-3- Mean Fx Cutting forces from test, 90 degree fibre orientation, and un-worn tool.

Fibre Orientation	Feed Rate (mm/min)	RPM	Fx Sample 1	Fx Sample 2	Mean Fx (N)	STD
90	800	6000	81.3	78.9	**80**	**1.7**
90	1200	6000	98.9	100.1	**99.5**	**0.8**
90	800	8000	79.7	84.5	**82.1**	**3.4**
90	1200	8000	80.4	84.2	**82.3**	**2.7**

Table 10-4- Mean Fy Cutting forces, 90 degree fibre orientation, un-worn tool.

Fibre Orientation	Feed Rate (mm/min)	RPM	Fy Sample 1	Fy Sample 2	Mean Fy (N)	STD
90	800	6000	55.2	54.6	**54.9**	**0.4**
90	1200	6000	60.2	66.5	**63.4**	**4.5**
90	800	8000	57.0	60.4	**58.7**	**2.4**
90	1200	8000	57.3	63.4	**60.3**	**4.4**

Table 10-5- Mean Fx Cutting forces from test 45 degree fibre orientation worn tool.

Fibre Orientation	Feed Rate (mm/min)	RPM	Fx Sample 1	Fx Sample 2	Mean Fx (N)	STD
45	800	6000	116.6	109.2	**112.9**	**5.2**
45	1200	6000	130.4	126.0	**128.2**	**3.1**
45	800	8000	102.1	100.5	**101.3**	**1.1**
45	1200	8000	126.1	123.2	**124.7**	**2.1**

Table 10-6- Mean Fy Cutting forces from test 45 degree fibre orientation worn tool.

Fibre Orientation	Feed Rate (mm/min)	RPM	Fy Sample 1	Fy Sample 2	Mean Fy (N)	STD
45	800	6000	116.6	108.2	**112.1**	**5.9**
45	1200	6000	130.2	128.6	**129.2**	**1.1**
45	800	8000	103.6	104.4	**104**	**0.6**
45	1200	8000	130.2	127.8	**129**	**1.7**

Table 10-7- Mean Fx Cutting forces from test 90 degree fibre orientation worn tool.

Fibre Orientation	Feed Rate (mm/min)	RPM	Fx Sample 1	Fx Sample 2	Mean Fx (N)	STD
90	800	6000	109.1	105.0	**107.1**	**2.9**
90	1200	6000	119.3	120.7	**120.0**	**1.0**
90	800	8000	96.5	89.0	**92.7**	**5.3**
90	1200	8000	116.1	102.1	**109.1**	**9.9**

Table 10-8- Mean Fy Cutting forces from test 90 degree fibre orientation worn tool.

Fibre Orientation	Feed Rate (mm/min)	RPM	Fy Sample 1	Fy Sample 2	Mean Fy (N)	STD
90	800	6000	**131.4**	**131.0**	131.2	0.3
90	1200	6000	**148.7**	**154.3**	151.5	4.0
90	800	8000	**112.4**	**107.3**	109.9	3.6
90	1200	8000	**163.3**	**145.6**	154.5	12.5

Part B- Multidirectional Test

Table 10-9- Cutting Edge Radius from Alicona Scans (*Tool 2*).

Test Number	Feed	Cutting Speed	Tool 2 Edge Radius μm	Distance Machined (mm)
			2.89	0
3	1200	7000	2.89	80
4	1200	9000	2.89	160
5	1000	7000	3.75	240
6	1000	9000	3.75	320
11	1200	7000	4.80	400
12	1200	9000	4.80	480
15	1200	7000	5.31	560
16	1200	9000	5.31	640
17	1000	7000	5.35	720
18	1000	9000	5.35	800
23	1200	7000	5.53	880
24	1200	9000	5.53	960
25	1000	7000	5.57	1040
26	1000	9000	5.57	1120
31	1200	7000	5.91	1200
32	1200	9000	5.91	1280
35	1200	7000	6.21	1360
36	1200	9000	6.21	1440
37	1000	7000	6.38	1520
38	1000	9000	6.38	1600

Table 10-10- Average S$_a$ calculated from the test samples- Test 21-40.

Test Number	Feed (mm/min)	Cutting Speed (RPM)	Scan 1 Sa (µm)	Scan 2 Sa (µm)	Average Sa (µm)	Average skewness (µm)	Average kurtosis (µm)
21	1000	7000	1.73	1.74	1.73	-3.7	28.1
22	1000	9000	1.59	1.57	1.58	-3.6	29.1
23	1200	7000	1.83	1.82	1.83	-3.8	28.9
24	1200	9000	1.30	1.32	1.31	-3.6	29
25	1000	7000	1.65	1.52	1.59	-3.9	32.1
26	1000	9000	1.48	1.47	1.47	-2.8	25.4
27	1200	7000	2.13	2.11	2.12	-3.4	20.1
28	1200	9000	1.72	1.75	1.73	-3.6	26.6
29	1000	7000	1.68	2.01	1.84	-4.2	32
30	1000	9000	1.66	1.68	1.67	-3.8	28.1
31	1200	7000	2.04	2.00	2.02	-3.5	23.5
32	1200	9000	1.82	1.83	1.82	-3.5	26.4
33	1000	7000	1.81	1.96	1.89	-3.7	27
34	1000	9000	1.75	1.67	1.71	-4	33.4
35	1200	7000	1.97	1.83	1.90	-2.9	26.4
36	1200	9000	1.74	1.71	1.73	-3.4	27
37	1000	7000	1.88	1.89	1.88	-3.5	26.8
38	1000	9000	1.69	1.59	1.64	-2.5	20.7
39	1200	7000	2.28	2.26	2.27	-3.4	34
40	1200	9000	1.88	1.97	1.92	-3.8	38.1

Table 10-11- Average skewness and kurtosis (Test 1-20)

Test Number	Feed (mm/min)	Cutting Speed (RPM)	Skewness	Kurtosis
Test 1	1000	7000	-3.72	23.73
Test 2	1000	9000	-3.67	22.31
Test 3	1200	7000	-4.07	28.16
Test 4	1200	9000	-4.40	32.42
Test 5	1000	7000	-3.88	25.52
Test 6	1000	9000	-3.63	26.67
Test 7	1200	7000	-3.73	23.84
Test 8	1200	9000	-3.66	23.37
Test 9	1000	7000	-3.52	24.06
Test 10	1000	9000	-3.60	24.37
Test 11	1200	7000	-3.88	24.81
Test 12	1200	9000	-4.01	29.70
Test 13	1000	7000	-3.69	26.20
Test 14	1000	9000	-3.26	22.76
Test 15	1200	7000	-3.52	22.87
Test 16	1200	9000	-3.51	28.01
Test 17	1000	7000	-3.93	31.76
Test 18	1000	9000	-3.20	32.10
Test 19	1200	7000	-3.57	23.23
Test 20	1200	9000	-3.48	24.04

Table 10-12 Cutting Forces- Tests number 1-20.

Test	Feed Rate (mm/min)	Cutting Speed (RPM)	Mean Fx (N)	Mean Fy (N)	Min Fx (N)	Min Fy (N)	Max Fx (N)	Max Fy (N)
1	1000	7000	32.0	1.6	-108.2	132.1	191.9	121.4
2	1000	9000	33.2	9.3	-118.8	-82.7	200.6	127.9
3	1200	7000	36.1	1.8	-96.0	-106.1	188.2	123.2
4	1200	9000	38.4	10.6	-100.1	-91.3	191.9	130.5
5	1000	7000	42.6	13.5	-123.1	-92.8	206.8	172.5
6	1000	9000	43.5	22.2	-121.8	-66.7	217.9	180.4
7	1200	7000	45.1	21.7	-118.7	-86.3	222.6	167.4
8	1200	9000	45.0	17.0	-144.6	-73.5	252.7	161.4
9	1000	7000	45.9	21.9	-141.9	-71.7	247.9	208.5
10	1000	9000	48.2	26.8	-144.3	-45.4	252.6	215.0
11	1200	7000	56.0	22.3	-137.6	-100.1	246.2	216.4
12	1200	9000	52.6	28.9	-143.8	-57.6	254.5	225.5
13	1000	7000	54.4	29.8	-156.1	-81.1	259.5	242.6
14	1000	9000	51.2	32.6	-155.4	-50.4	268.2	238.1
15	1200	7000	56.7	25.2	-157.1	-94.9	264.7	241.0
16	1200	9000	52.7	32.0	-168.1	-105.1	261.6	265.4
17	1000	7000	57.5	33.5	-166.9	-65.3	277.5	254.5
18	1000	9000	53.8	39.4	-169.6	-124.6	261.1	325.4
19	1200	7000	60.6	28.2	-162.3	-115.8	275.1	257.3
20	1200	9000	59.7	34.6	-150.3	-48.6	292.7	235.8

Table 10-13- Cutting Forces- Test number 21-40.

Test	Feed Rate (mm/min)	Cutting Speed (RPM)	Mean Fx (N)	Mean Fy (N)	Min Fx (N)	Min Fy (N)	Max Fx (N)	Max Fy (N)
21	1000	7000	60.9	37.	-184.0	-78.2	283.4	282.3
22	1000	9000	56.5	41.8	-190.7	-75.1	304.3	265.4
23	1200	7000	65.9	37.7	-167.5	-70.4	289.5	285.1
24	1200	9000	64.1	43.3	-174.9	-75.4	295.7	284.8
25	1000	7000	65.7	44.4	-195.1	-77.8	304.8	330.1
26	1000	9000	61.2	49.	-186.2	-102.4	286.8	338.3
27	1200	7000	72.3	42.	-199.6	-111.1	323.1	334.8
28	1200	9000	69.8	46.8	-184.5	-68.5	323.1	301.3
29	1000	7000	64.4	46.9	-211.6	-80.4	312.6	336.1
30	1000	9000	60.2	48.	-211.0	-105.6	314.6	356.7
31	1200	7000	79.5	47.	-189.8	-120.8	323	344
32	1200	9000	77.1	54.4	-191.3	-81.9	313.4	363.3
33	1000	7000	70.8	51.7	-213.4	-90.7	-309.7	345.8
34	1000	9000	63.5	52.5	-214.7	-132.5	315.1	400.5
35	1200	7000	70.0	53.1	-223.4	-76.1	330	379.6
36	1200	9000	68.8	57.4	-214.4	-102.1	320.5	368.4
37	1000	7000	73.2	58.6	-209.3	-96.3	323.2	390.9
38	1000	9000	63.5	61.3	-200.4	-142.7	308.4	424.1
39	1200	7000	71.1	51.3	-219.7	-88.87	343.1	356.4
40	1200	9000	68.0	54.6	-205.2	-95.21	338.3	370.6

Part C- Subroutine

```fortran
      subroutine utimestep
     *( tstepc   ,tstepl   ,icall    ,timei    ,timelc   )
      implicit none
      include 'concom'
      include 'creeps'
      integer
     *   icall, iun6, ldebug, i, j, itype, ndof, icut, icnode, idum,
     *   maxnod, maxdof
      real*8
     *   tstepc, tstepl, timei, timelc, r0, r1, r2, r180, timeo,
     *   xcur, ycur, pi, tcut, coord, disp, tadj, radiuswp,
     *   ttime, xcurc, ycurc, rotadj, xtransc, radiuswp1, radiuswp2
      integer
     *   inclast, nnodes, nodes, ncut, nidle, nstept
      real*8
     *   xminw, xmaxw, yminw, ymaxw, gap, vtrans, vrot, radius,
     *   edepth, xmaxw0, angmin, angdef, rotfac, yminc
      parameter
     *(   maxnod = 20        ,maxdof = 6  )
      dimension
     *   coord(maxdof,maxnod)        ,disp(maxdof,maxnod)
      common
     *   xminw, xmaxw, yminw, inclast, nnodes, nodes(maxnod),
     *   ymaxw, gap, vtrans, vrot, ncut, nidle, radius, edepth,
     *   xmaxw0, angmin, angdef, rotfac, nstept, yminc
      data
     *   r0       ,r1       ,r2       ,r180     ,iun6     ,
     *   ldebug   ,pi       /
     *   0.0d0    ,1.0d0    ,2.0d0    ,180.0d0  ,6        ,
     *   1        ,3.1415926d0/
c----------------------------------------------------------------
c      user        subroutine        for        modifying        the        time        step
      called right after the time step has been updated
c
c*variables
c=tstepc - current time step as suggested by marc to be modified
c tstepl - current time step before it was modified by marc
c icall  - control flag describing when this routine is called
c          1 = setting the initial time step
c          2 = called during an increment
c          3 = called at the beginning of the increment
c timei  - time at the start of the current increment
c timelc - time period of the current load case
c nnodes - number of tip node numbers specified
c----------------------------------------------------------------
c initialisation
c----------------------------------------------------------------
c    flag to indicate cutting is occurring
      icut = 0
c
      timeo = tstepc
c
      ttime = cptim + timinc
c
c
      call scla
     *(   coord    ,r0       ,maxnod   ,maxdof   ,idum     )
c       check for presence of a cut-back this case we need to let Marc specify the time step
      if( inc .eq. inclast ) then
       icut = 3
      end if
c                   update last increment number
      inclast = inc
c
```

```
c------------------------------------------------------------------
c evaluate time adjustment needed for cutter to rotate between lowest
c cut position and top of workpiece
c------------------------------------------------------------------
c                      time for the next cutter to reach the next position
      tcut = (r2 * pi) / (ncut * vrot )
      rotadj = abs(abs(ymaxw)-abs(yminw)) / radius
c                        : here we check the angle (in degrees)
c                          and define a default typical value
c                         (radians)
      if( rotadj * r180/pi .lt. angmin ) then
       write(iun6,2800) rotadj
       rotadj = angdef * pi/r180
      end if
c
      rotadj = rotadj * rotfac
c                      then evaluate the time for  this rotational adjustment
      tadj = rotadj / vrot
c                     adjust the time so that the next cutter
c                     comes into the cutting zone at a lower
c                     position than the previous one left
      tcut = tcut - tadj
c
c------------------------------------------------------------------
c current node coordinates
c------------------------------------------------------------------
c                      loop over number of cutter tip nodes
c                      to extract the original
c                      coordinates and displacements as separate
c                      arrays
      do i = 1, nnodes
c                 original coordinates
        call nodvar
     *(   0       ,nodes(i)   ,coord(1,i) ,ndof       ,itype      )
        call nodvar
     *(   1       ,nodes(i)   ,disp(1,i)  ,ndof       ,itype      )
       end do
c                      loop over number of nodes to establish
c                      the new coordinate
      do i = 1, nnodes
c                 loop over number of DOFs
        do j = 1, ndof
c                   evaluate current cooordinate
         coord(j,i) = coord(j,i) + disp(j,i)
        end do
       end do
c
c------------------------------------------------------------------
c establish if any cutter node is close to workpiece
c                      loop over cutter nodes
      do i = 1, nnodes
c                 extract current x and y coordinates
       xcur = coord(1,i)
       ycur = coord(2,i)
       if( (ycur-ymaxw) .lt. r0 ) then
c                    check if any cutter nodes are close to
c                    the current cut face
        if( xcur-gap .lt. xmaxw ) then
         tstepc = tstepc
c                   set flag to indicate we are cutting:
c                      0 = not in cutting zone
c                      1 = very close to cutting zone
c                      2 = in cutting zone, but not likely to contact
c                      3 = use marc-calculated time step
c                      4 = in cutting zone, but not close enough
          icut = 3
c---------------------------alternatively, evaluate a time step based
```

312

```
c                        on the cutter passing through only a
c                        fraction of the typical workpiece element
c                        dimension by specifying a number of time
c                        steps
      tstepc = edepth / (radius * abs(vrot) * nstept)
c                        set flag to indicate we are cutting:
c                           0 = not in cutting zone
c                           1 = very close to cutting zone
c                           2 = in cutting zone, but not likely to contact
c                           3 = use marc-calculated time step
c                           4 = in cutting zone, but not close enough
      icut = 1
c----------------------------account for the case in which the cutter
c                        is close to the workpiece, but not close
c                        enough for small time steps yet
c                        : needs to account for feedrate since
c                           xcur is at end of last increment and
c                           xcur will actually be greater than seen
c                           here
      xtransc = abs(vtrans) * (5.0d0*edepth / (radius*abs(vrot)))
c                        now, check how close we are
      if( abs(abs(xcur) - xtransc - abs(xminw)) .gt.
     *    r2*edepth .and.
     *    (abs(xcur) - xtransc - abs(xminw) .lt. r0 )) then
        tstepc = 5.0d0*edepth / (radius*abs(vrot))
c                        set flag to indicate we are cutting:
c                           0 = not in cutting zone
c                           1 = very close to cutting zone
c                           2 = in cutting zone, but not likely to contact
c                           3 = use marc-calculated time step
c                           4 = in cutting zone, but not close enough
        icut = 4
      end if
      icnode = nodes(i)
      xcurc = xcur
      ycurc = ycur
     end if
    end if
   end do
c
c-----------------------------------------------------------------
c determine next time step, depending on whether the cutting is cutting or not
c-----------------------------------------------------------------
c                        if not cutting, then take bigger steps by
c                        dividing the time to rotate to the next
c                        cutter tip by a user-defined number
c----------------------------cutter far from workpiece so use large
c                        time step
      if( icut .eq. 0 ) then
        tstepc = tcut / float(nidle)
c                        inform user
        write(iun6, 2200) tstepc, timeo, xmaxw, ymaxw, gap, icut
c----------------------------cutter close to workpiece so use small
c                        time step
      else if( icut .eq. 1 ) then
c                        inform user
        write(iun6, 2300)
     *    tstepc, icnode, xcurc, ycurc, xmaxw, ymaxw, gap, icut
c----------------------------cutter close to workpiece but unlikely
c                        to contact - so use slightly larger time
c                        step
      else if( icut .eq. 2 ) then
c                        inform user
        write(iun6,2400) tstepc, icnode, radiuswp, radius, icut,
     *             xminw, yminc
c----------------------------cut-back detected, so use marc-calculated
c                        time step
```

313

```fortran
      else if( icut .eq. 3 ) then
c                       revert to the marc-calculated time step
         tstepc = timeo
c                       inform user
         write(iun6,2500) tstepc, icut
c----------------------------cutter close to workpiece, but not close
c                       enough yet - so adjust the time step
c                       to get us closer
      else if( icut .eq. 4 ) then
c                       inform user
         write(iun6, 2900)
     *    tstepc, icnode, xcurc, ycurc, xmaxw, ymaxw,
     *    abs(xcurc-xminw), icut, xcur, xtransc, xminw, edepth,
     *    radius, vrot
      end if
      return
      end
c---------------------------------------------------------------------
c extract original coordinate and current displacement for all nodes of current element
      call scla
     *( coord      ,r0        ,maxnod    ,maxdof    ,idum      )
c                       loop over number of nodes of current
c                       element
      do i = 1, nnods
c                       extract external/user node number
         nodec = nodext(nodlist(i))
c                       extract original coordinates
         call nodvar
     *( 0          ,nodec     ,coord(1,i) ,ndof     ,itype     )
c                       extract current displacements
         call nodvar
     *( 1          ,nodec     ,disp(1,i)  ,ndof     ,itype     )
      end do
c                       check for dimension mismatch
      if( ndof .gt. maxdof ) then
         write(6,1003) ndof, maxdof
      end if
c---------------------------------------------------------------------
c evaluate the current coordinate position for all nodes of current element
c---------------------------------------------------------------------
c                       loop over number of nodes of current
c                       element
      do i = 1, nnods
c                       loop over number of DOFs
         do j = 1, ndof
c                       evaluate current cooordinate
            coord(j,i) = coord(j,i) + disp(j,i)
         end do
      end do
c---------------------------------------------------------------------
c                       loop over number of nodes
      do i = 1, nnods
c                       extract external/user node number
         nodec = nodext(nodlist(i))
c                       update x-coordinate that represents the
c                       current depth of cut (axially) in the
c                       workpiece, along with corresponding
c                       y-coordinate value
         if( abs(coord(1,i)) .gt. abs(xmaxw) ) then
            xmaxw = coord(1,i)
c                       inform user
            write(iun6,1002) xmaxw, m(1), nodec
         end if
c                       update y-coordinate that represents the
c                       lowest point of the cut (vertically) in
c                       the workpiece
         if( coord(2,i) .lt. yminw ) then
```

314

```fortran
            yminw = coord(2,i)
c                       inform user
            write(iun6,1001) yminw, m(1), nodec
          end if
c                       update x-coordinate that represents the
c                       current front face of the workpiece
c                       (axially) in the area of the current cut
          if( abs(coord(1,i)) .lt. abs(xminw) ) then
            xminw = coord(1,i)
            yminc = coord(2,i)
c                       inform user
            write(iun6,1004) xminw, m(1), nodec
          end if
        end do
      end if
c     write(6,*) 'Exit UACTIVE'
      return
      end
c=====================================
c ncycle - iteration number
c-----------------------------------------------------------------
c initialise
c-----------------------------------------------------------------
c                       increment zero only
      if( inc .eq. 0 ) then
c                       closest initial x-coordinate of workpiece to the cutters
c                       : updated to measure depth of cut
        xmaxw = xmaxw0
        xminw = xmaxw
c                       minimum cut height of workpiece
        yminw = ymaxw
c                       last increment number
        inclast = -1
      end if
      return
      end


c=====================================

      subroutine ubginc
     *( inc      ,incsub    )
      implicit none
      integer
     *  inc, incsub, ios, nios, ilen1, i, maxnod, maxdof
      real*8
     *  r0
      integer
     *  inclast, nnodes, nodes, ncut, nidle, nstept
      real*8
     *  xminw, xmaxw, yminw, ymaxw, gap, vtrans, vrot, radius,
     *  edepth, xmaxw0, angmin, angdef, rotfac, yminc
c                       common block for file name
      include '../common/jacb'
      include '../common/jname'
      character*50
     *  datafile
      parameter
     *( nios = 1        )
      parameter
     *( maxnod = 20       ,maxdof = 6  )
      common
     *  /user_ab/
     *  xminw, xmaxw, yminw, inclast, nnodes, nodes(maxnod),
     *  ymaxw, gap, vtrans, vrot, ncut, nidle, radius, edepth,
     *  xmaxw0, angmin, angdef, rotfac, nstept, yminc
      dimension
     *  ios(nios)
```

```
      data
    *    r0          /
    *    0.0d0        /
c----------------------------------------------------------------
c----------------- read data from external file (PRM File)
      read(990,*) nnodes
c
      nnodes = int(nnodes)
c
      write(6,1002) nnodes
c                       number of cutting tip nodes
      if( nnodes .gt. maxnod ) then
       write(6,3001) nnodes, maxnod
       call quit(9000)
      end if
c                        cutter tip nodes
      do i=1,nnodes
       read(990,*) nodes(i)
       nodes(i) = int(nodes(i))
       write(6,1003) nodes(i)
c
       if( nodes(i) .eq. 0 ) then
        write(6,3000) i, nnodes
        call quit(9001)
       end if
      end do
c                   maximum y-coordinate of workpiece initially
c
      read(990,*) ymaxw
      ymaxw = real(ymaxw,8)
      write(6,1004) ymaxw
c                       distance in front of current cut face

      read(990,*) gap
      gap = real(gap,8)
      write(6,1005) gap
c                       cutter translational velocity
      read(990,*) vtrans
      vtrans = real(vtrans,8)
      write(6,1006) vtrans
c                       cutter rotation speed (rad/s)
      read(990,*) vrot
      vrot = real(vrot,8)
      write(6,1007) vrot
c                       number of cutters
      read(990,*) ncut
      ncut = int(ncut)
      write(6,1008) ncut
c                       number of load increments to cover the
      write(6,1009) nidle
c                       typical element length in workpiece in
c                       cutting zone
      read(990,*) edepth
      edepth = real(edepth,8)
      write(6,1011) edepth
c                       closest initial x-coordinate of workpiece
c                       to the cutters
      read(990,*) xmaxw0
      xmaxw0 = real(xmaxw0,8)
      write(6,1012) xmaxw0
c                       angle below which rotadj is given a
c                       typical default value (degrees)
      read(990,*) angmin
      angmin = real(angmin,8)
      write(6,1013) angmin
c                       typical default angle given to rotadj if
      read(990,*) angdef
```

```fortran
      angdef = real(angdef,8)
      write(6,1014) angdef
      read(990,*) rotfac
      rotfac = real(rotfac,8)
      write(6,1015) rotfac
c                     number of increments through which the
c                     cutter tip should traverse a typical
c                     workpiece element dimension
      read(990,*) nstept
      nstept = int(nstept)
      write(6,1016) nstept
c                     finished reading,
      goto 999
 900  call ioserr
   *( ios       ,nios        ,datafile   )
      end if
 999 continue
      return
      end
c===================================
      subroutine vcizer
   *( ivec      ,n        )
      implicit none
      integer
   *  ivec, n, i
      dimension
   *  ivec(n)
c-------------------------------------------------------------------
c*description
c initialises a vector with integer zeros
c-------------------------------------------------------------------
      do i = 1,n
       ivec(i) = 0
      end do
      return
      end
```